Order Number 9009732

Thermochemical-thermophysical data on phases in the Mg-Fe-Si-O system: A synthesis of theory and experimental data and computation of phase equilibrium

Fei, Yingwei, Ph.D.

City University of New York, 1989

U·M·I
300 N. Zeeb Rd.
Ann Arbor, MI 48106

THERMOCHEMICAL-THERMOPHYSICAL DATA ON PHASES IN THE Mg-Fe-Si-O SYSTEM: A SYNTHESIS OF THEORY AND EXPERIMENTAL DATA AND COMPUTATION OF PHASE EQUILIBRIUM

by

YINGWEI FEI

A dissertation submitted to the Graduate Faculty in Earth and Environmental Sciences in partial fulfillment of the requirements for the degree of Doctor of Philosophy, The City University of New York.

1989

This manuscript has been read and accepted for the Graduate Faculty in Earth and Environmental Sciences in satisfaction of the dissertation requirement for the degree of Doctor of Philosophy.

May 22, 1989
Date

S K Saxena
Chair of Examining Committee

August 10, 1989
Date

Daniel Habib
Executive Officer

Edward Schreiber

Alexander Nason

Robert L. Tillmann

Supervisory Committee

The City University of New York

Abstract

THERMOCHEMICAL-THERMOPHYSICAL DATA ON PHASES IN THE Mg-Fe-Si-O SYSTEM: A SYNTHESIS OF THEORY AND EXPERIMENTAL DATA AND COMPUTATION OF PHASE EQUILIBRIUM

by

Yingwei Fei

Adviser: Professor Surendra K. Saxena

Thermochemical and thermophysical data for phases in the Mg-Fe-Si-O system are critically evaluated by considering the available experimental phase equilibrium data, the calorimetric measurements, and measured thermophysical properties of solids. An internally consistent data base is thus established. A new equation of heat capacity (C_P) for solids is proposed for the extrapolation of C_P to high temperatures. The Birch-Murnaghan equation of state with temperature dependence of the bulk modulus is used to calculate the effect of pressure on the Gibbs free energy change of a reaction. Phases included in the data base are polymorphs of Fe (bcc-Fe, fcc-Fe and hcp-Fe), Fe_3O_4 (magnetite and high-pressure magnetite), Fe_2O_3 (hematite and high-pressure hematite), SiO_2 (quartz, coesite and stishovite), Mg_2SiO_4 (forsterite, β-phase, spinel and melt), Fe_2SiO_4 (fayalite, β-phase, spinel and melt), $MgSiO_3$ (pyroxene, ilmenite, garnet, perovskite and melt) and $FeSiO_3$ (pyroxene and perovskite), and MgO (periclase). Solid

solutions considered are MgO-FeO-$FeO_{1.5}$ (magnesiowustite), $(Mg,Fe)_2SiO_4$ (olivine, β-phase and spinel) and $(Mg,Fe)SiO_3$ (pyroxene and perovskite). The solid solutions are experimentally studied by determining the Mg and Fe partitioning between coexisting phases, magnesiowustite and olivine, magnesiowustite and β-phase, magnesiowustite and spinel, and magnesiowustite and perovskite, under various pressure and temperature conditions. The experiments are performed with the piston-cylinder apparatus, the multi-anvil device and the diamond-anvil cell technique at pressures between 2 and 28 GPa and temperatures between 1200 °C and 1500 °C. The solid solution parameters are obtained by fitting the experimental data simultaneously using the Margules formulation. They are consistent with solution calorimetry and phase equilibrium data.

The internally consistent data base can be used to reproduce the experimentally determined phase relations in the system at pressures up to 30 GPa and to melting temperatures. It is useful in generating phase diagrams for various different compositions for the purpose of planning new experiments and understanding the mineralogy and chemical composition of the Earth's mantle.

Acknowledgements

My thanks are due to my adviser Professor S. K. Saxena for his continueous encouragement and advice toward my Ph. D. degree. It benefited highly from suggestions and guidance by my supervisory committee members, Professors A. Navrotsky, R. C. Liebermann, C. E. Nehru and E. Schreiber. I am grateful to Dr. C. T. Prewitt for appointing me as a Predoctoral Fellow at the Geophysical Laboratory, Carnegie Institution of Washington. The chance to working with Dr. H-K. Mao and Dr. B. O. Mysen greatly improved my understanding of the relations between theory and experiments. I am also grateful to Dr. T. Gasparik and many graduate students in Mineral Physics Institute of SUNY at Stony Brook for their advice in operating the USSA-2000 multi-anvil apparatus, and to C. Bertka for her help in performing experiments in the piston-cylinder apparatus at the Geophysical Laboratory. Finally, my thanks are due to the Brooklyn graduate students, especially to J. Sykes, N. Chatterjee, Q. Fang and J. Zhang for their many helpful daily discussions.

My graduate school of the City University of New York made completion of my formal education possible, but the credits also go to those Institutes and Universities to which I closely related through personal contacts, especially to Mineral Physics Instite of State University of New York at Stony Brook, Geophysical Laboratory of Carnegie Institution of Washington, Princeton University, and Institute of Geochemistry of Academia Sinica.

Contents

Tables

Figures

CHAPTER 1

Introduction

The goal of this research is to obtain systematic thermochemical and thermophysical data with which we may describe the physical and chemical conditions of the Earth's mantle quantitatively through modeling of thermodynamic phase equilibria. Physical conditions imply the variation of pressure, temperature and density in the Earth's mantle. Seismic data provide critical physical constraints for the Earth's interior (e.g. for the density profile of the Earth). Chemical conditions imply the nature of the mineral assemblage and chemical composition of coexisting minerals. Information on chemical composition of the Earth may be derived either from meteorite data (e.g. chondritic Earth model) or from geological materials of supposedly mantle origin (e.g., peridotite nodules and xenoliths in kimberlites) intruded into the crust. The development of high pressure and high temperature techniques allows us to simulate mantle physical conditions in the laboratory. Experimental studies of phase equilibrium relations in systems which simulate planetary rocks at high pressure and high temperature provide important information on mineralogy and chemical composition of the mantle. Characterizing the physical properties of those "mantle" materials (e.g. determining the equation of state) by various techniques and comparing them with the observations from seismological studies form another approach to understanding the Earth's mantle. Thermodynamic modeling has the advantage that all the available information is taken into account in assessing possible physicochemical states of the mantle.

The calculations of this study are based on the principles of equilibrium thermodynamics as described in Chapter 2 and a thermochemical and thermophysical data set of proven internal consistency in the system discussed in Chapter 4. This work

includes (1) extrapolation of thermochemical and thermophysical properties to high pressure and high temperature by considering theoretical constraints, (2) systematization of existing thermochemical and thermophysical data on minerals in the Mg-Fe-Si-O system by checking the consistency among calorimetric measurements, phase equilibrium data and measured physical properties of minerals, (3) experimental determination of element partitioning in the Mg-Fe-Si-O system, and (4) calculation of phase equilibrium relations in the system at high pressure and high temperature and their implications for mantle constitution.

A thermochemical and thermophysical data set forms the basis of the model. It is essential in characterizing physical and compositional features of a system in equilibrium. Therefore, the emphasis of this work is to critically evaluate the available data to obtain an internally consistent set of thermochemical and thermophysical data. An internally consistent data set is one which permits the computation of phase equilibrium relations as established through experimental studies and is at the same time compatible with calorimetric and other measurements of thermophysical properties of the phases. Generating such a data base is complicated by the large uncertainties associated with the high pressure phase equilibrium relations, both because of the errors in pressure and temperature calibration and because the experiments generally represent unreversed reactions. In spite of these problems, it is important to review the present status of the existing thermochemical data set and its relation to the experimental phase studies. If a thermochemical data set produces calculated results which are reasonably consistent with experimental work, it can be used for computing possible phase equilibrium relations over a wide range of pressure, temperature and composition conditions. Such predictions are useful in planning future phase equilibrium experiments,which may then better constrain the preliminary data base. Conversely, if the attempt to create a data base exposes major inconsistencies, experiments to resolve

these discrepancies would be important. A complete thermodynamic analysis of the experimental phase diagrams in the system Mg-Fe-Si-O under mantle pressure and temperature conditions is presented in this work.

Ideally one should choose a system with all possible elements likely to appear in the Earth's mantle. Such a task is not possible at present because of a lack of experimental data. A simplified system, the Mg-Fe-Si-O system, is chosen in this study both because it has been most extensively studied at high pressure and high temperature and represents the major chemical composition of the Earth's mantle and because all the mineral structures proposed as likely in the mantle are included in the system. Phase equilibrium relations and element partitioning between coexisting minerals should provide essential information on mineralogy and chemical composition variations through out the mantle. A comparison of the calculated physical property profiles (e.g. the density profile) of the equilibrium assemblage simulating in the system of the mantle with the seismological observation may aid in understanding the chemistry of the mantle.

CHAPTER 2

Thermodynamics of Reactions at High Pressure and High Temperature

2.1 Temperature and Pressure Dependence of the Gibbs Free Energy

The change in Gibbs free energy (ΔG) as a function of temperature (T) and pressure (P) can be obtained from the relations:

$$\left(\frac{\partial^2 \Delta G}{\partial T^2}\right)_P = -\frac{C_P(T)}{T} \tag{2.1}$$

and

$$\left(\frac{\partial \Delta G}{\partial P}\right)_T = V(P,T) \tag{2.2}$$

where $C_P(T)$ is heat capacity at constant P and at a temperature T and V(P,T) is the molar volume at a temperature T and a pressure P. The free energy of a reaction is given by

$$\Delta G_{P,T} = \Delta H^0_T - T\Delta S^0_T + \int_1^P \Delta V(P,T)dP \tag{2.3}$$

where ΔH^0_T and ΔS^0_T are the standard enthalpy and entropy of a reaction, respectively, at temperature T and 1 atm. They are given by

$$\Delta \bar{H}^0_T = \Delta H^0_{298} + \int_{298}^T \Delta C_P dT \tag{2.4}$$

and

$$\Delta S_T^0 = \Delta S_{298}^0 + \int_{298}^{T} \frac{\Delta C_P}{T} dT \qquad (2.5)$$

where ΔH^0_{298} and ΔS^0_{298} are the standard enthalpy and entropy of reaction at 298.15 K, ΔC_P is the heat capacity difference between products and reactants, and $\Delta V(P,T)$ is the volume change for the reaction.

The extrapolation of temperature and pressure dependence of the Gibbs free energy of a solid or a liquid phase to high temperature and pressure is complicated by the nature of the heat capacity, C_P, and the behavior of molar volume, V(P,T). In order to obtain a suitable form of the Gibbs free energy for solids at high pressure and high temperature, it is necessary to discuss the heat capacity at high temperature, and the equation of state in detail.

Heat Capacity at High Temperature

The form of the heat capacity (C_P) for high temperature extrapolation has been discussed by Haas and Fisher (1976), Lane and Ganguly (1980), Holland (1981), Berman and Brown (1985) and Fei and Saxena (1987).

In general, C_P for a solid can be expressed as

$$C_p = C_v + \alpha^2 V K_T T + C'_P \qquad (2.6)$$

where C_V is the heat capacity of a crystal at constant volume. α is the coefficient of thermal expansion, V is the molar volume, and K_T is the isothermal bulk modulus, all at temperature T. C_P' is the contribution from cation disordering and anharmonicity (other than those corporated in the α^2VK_TT term).

Einstein (1907) and Debye (1912) derived equations for the temperature dependence of C_V, the heat capacity at constant volume, based on the assumption that atoms behave as harmonic oscillators in a crystal lattice. A reasonable expression for C_V can be derived by assuming that a crystal is composed of a system of atoms which vibrate as harmonic oscillators all with the same frequency, ν. In such a solid C_V is expressed by

$$C_V = 3Rn\left[\frac{x^2e^x}{(e^x-1)^2}\right] \tag{2.7}$$

where $x=\theta_E/T$. θ_E is the Einstein temperature given by $\theta_E=h\nu/k$. R, h, k and n are the gas constant, Planck constant, Boltzmann constant and the number of atoms in the chemical formula, respectively. A precise expression for C_V may be given by assuming that the crystal has a whole spectrum of frequencies from ν_1 to ν_m, where ν_m represents some maximum frequency for a particular crystal,

$$C_V = \frac{9Rn}{x^3}\int_0^x\left[\frac{x^4e^x}{(e^x-1)^2}\right]dx \tag{2.8}$$

where $x=h\nu_m/(kT)$. Equation (2.7) is difficult to use in fitting experimental data at

intermediate temperatures because of the assumption of a single oscillator frequency. Equation (2.8) is even more difficult to apply to thermodynamic calculations not only because of the complexity of the expression but also because of the difficulty in determining the frequency distribution. Kieffer's (1979a) review on the applicability of the Debye theory of lattice vibrations show that heat capacities of silicates show large deviations from the behavior expected from the theory.

For the purpose of fitting experimental data, a polynomial expression for C_V may be used

$$C_V = 3Rn(1 + k_1T^{-1} + k_2T^{-2} + k_3T^{-3}) \qquad (2.9)$$

where k_1, k_2 and k_3 are coefficients determined by fitting experimental data. Note that in equation (2.9) the terms in square bracket of equation (2.7) have been replaced with a polynomial expression in T. There are three coefficients in equation (2.9) as compared to one fixed Einstein temperature in equation(2.7). According to above considerations, a new C_P expression is given by

$$C_P = 3Rn(1 + k_1T^{-1} + k_2T^{-2} + k_3T^{-3}) + (A + BT) + C_P' \qquad (2.10)$$

where C_P' represents the departures from the 3Rn limit for some substances due to cation disordering, anharmonicity (other than those in corporated in the α^2VK_TT term) and electronic contributions. A and B are empirical coefficients derived by considering the anharmonicity contribution of α^2VK_TT to C_P.

The thermal expansion coefficient α may be expressed as

$$\alpha = \alpha_0 + \alpha_1 T + \alpha_2 T^{-2} \qquad (2.11)$$

where α_0, α_1, α_2 are coefficients determined by least squares analysis of volume expansion data. The molar volume at temperature, T, can be calculated by

$$V(1,T) = V^0_{298}(1 + \int_{298}^{T} \alpha dT) \qquad (2.12)$$

where V^0_{298} is the molar volume at 298 K and 1 atmosphere. The isothermal bulk modulus K_T may be expressed as

$$K_T = K_{T,0} + (\frac{\partial K_T}{\partial T})_P (T - 298) \qquad (2.13)$$

where $K_{T,0}$ and $(\partial K_T/\partial T)_P$ are the isothermal bulk modulus at 298 K and its temperature derivative at constant pressure, respectively.

Equation (2.10), unlike those proposed by Maier and Kelley (1932) and Haas and Fisher (1976), and recently by Holland (1981) and Berman and Brown (1985), has been found to comply with the requirement that the high temperature C_V would approach the 3Rn limit. It is formulated by taking into account the important role of the $\alpha^2 V K_T T$ term and, therefore, links the measured heat capacity with the measured physical properties of solids at high temperature. This provides additional constraint for evaluating an internally consistent thermochemical and thermophysical data set based on data from the calorimetric measurements, from the experimental phase equilibria and from the

measurements of solid physical properties. Figure 2.1 shows a comparison of the temperature dependence of the heat capacity of clinoenstatite calculated from different C_p equations. Several minerals for which the physical properties have been well studied were chosen to demonstrate the use of the proposed equation (see Fei and Saxena, 1986 for more detailed discussions).

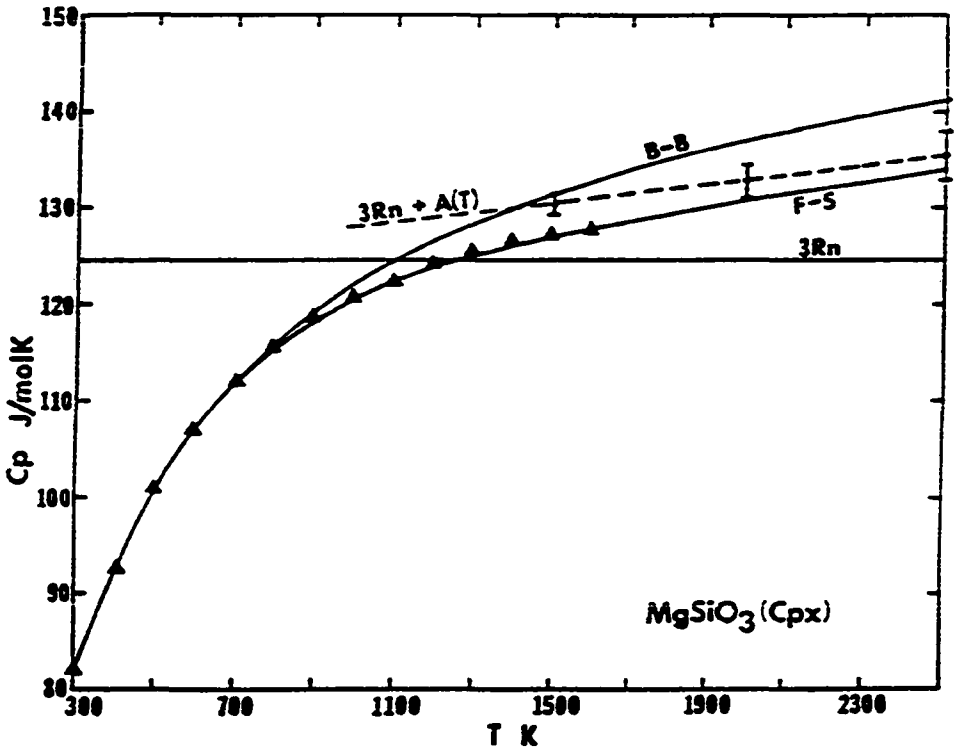

Figure 2.1 Comparison of C_p for clinoenstatite ($MgSiO_3$) calculated from three different C_p equations. The F-S equation is equation (2.10) proposed by Fei and Saxena (1987). The B-B equation is from Berman and Brown (1985) and the triangles are from Robie et al. (1978). The fitted temperature ranges are from 298 to 800 K for both F-S and B-B equations.

Molar Volume at High Pressure and High Temperature

The contribution of $\int VdP$ to Gibbs free energy becomes significant at high pressure. Therefore, the use of a suitable equation of state for the solids at high pressure and temperature is necessary for the phase equilibrium calculation. Experimental data on molar volumes are available either at high pressure and room temperature or at high temperature and 1 atm. The temperature dependence of molar volume can be represented by equation (2.12). The Murnaghan equation of state, which is based on the assumption that the bulk modulus changes linearly with pressure, and the Birch-Murnaghan equation of state, which is based on the finite-strain theory, are often used to represent experimental data on molar volume at high pressure. The Murnaghan equation of state is given by

$$P_M = \frac{K_{T,0}}{K'_{T,0}}\left[\left(\frac{V^0}{V}\right)^{K'_{T,0}} - 1\right] \qquad (2.14)$$

and the Birch-Murnaghan equation of state is

$$P_{B\text{-}M} = \frac{3}{2}K_{T,0}\left[\left(\frac{V^0}{V}\right)^{7/3} - \left(\frac{V^0}{V}\right)^{5/3}\right]\left\{1 - \frac{3}{4}(4 - K'_{T,0})\left[\left(\frac{V^0}{V}\right)^{2/3} - 1\right] + \ldots\right\} \qquad (2.15)$$

where and $K_{T,0}$. and $K_{T,0}'(= [\partial K_{T,0}/\partial P]_T)$ are the isothermal bulk modulus and its pressure derivative at 298 K, respectively. As discussed by Jeanloz and Knittle (1986), the Birch-Murnaghan equation of state may be considered as a better expression than the Murnaghan equation of state for the pressure-volume relation at very high pressures.

The method of extrapolation of the existing data to high P-T space is still controversial. Anderson and Zou (1989) and Heinz and Jeanloz (1984) have expounded on the relationships among the various thermochemical and thermophysical variables. In Anderson and Zou's model, the simultaneous effect of pressure and temperature on volume is taken care of by the thermal pressure (P_{th}), i.e.

$$P = P_{B\text{-}M} + P_{th} \tag{2.16}$$

where P_{th} is calculated by

$$P_{th} = \int_{298}^{T} \alpha K_T dT \tag{2.17}$$

Equation (2.17) has been simplified by assuming the product of α and K_T is constant.

In this study, $\int VdP$ is calculated by adopting the third order Birch-Murnaghan equation of state [equation (2.15)] where the temperature dependence of the isothermal bulk modulus is included and V^0/V is replaced by $V(1,T)/V(P,T)$. For computational convenience $\int PdV$ may be calculated from equation (2.15), instead of from $\int VdP$. The relation between $\int PdV$ and $\int VdP$ is given by

$$\int_{1}^{P} VdP = \int_{v(P,T)}^{v(1,T)} PdV + V(P - 1) \tag{2.18}$$

where

$$\int_{V(P,T)}^{V(1,T)} P dV = \frac{3}{2} K_T V(1,T) \{ \frac{3}{4}(1+2x)[Y^{4/3} - 1] - \frac{3}{2}(1+x)[Y^{2/3} - 1] - \frac{1}{2} x [Y^2 - 1] \} \qquad (2.19)$$

where

$$x = \frac{3}{4}\left[4 - \left(\frac{\partial K_T}{\partial P}\right)_T\right] \qquad \text{and} \quad Y = \frac{V(1,T)}{V(P,T)} \qquad (2.20)$$

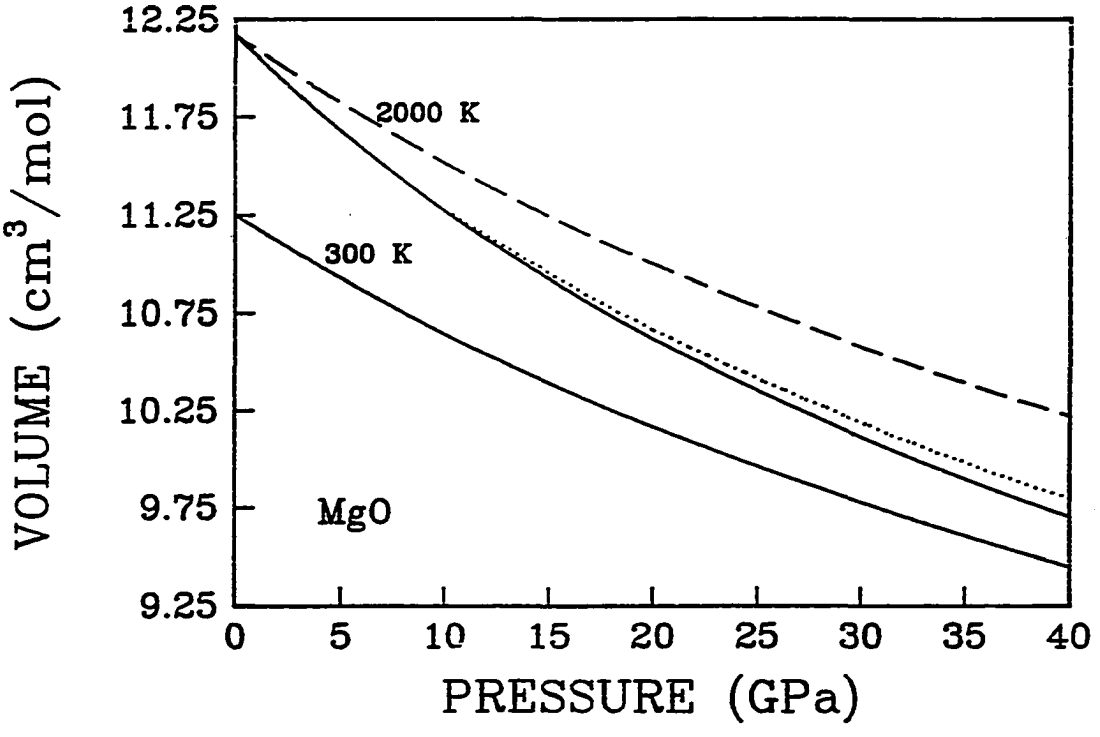

Figure 2.2 Comparison of P-V-T relations for MgO calculated by various models. The lower solid curve labeled as 300 K is calculated by Birch-Murnaghan (B-M) equation of state at 300 K. The upper solid curve is calculated at 2000 K using equation (2.15) where the temperature dependence of the bulk modulus is considered; and the dashed curve represents the result without considering the temperature dependence of the bulk modulus. Dotted curve is calculated from the thermal pressure model (Anderson and Zou, 1989).

The temperature dependence of the bulk modulus accounts for part of the simultaneous effect of pressure and temperature on volume. The calculated results for MgO are close to that calculated by Anderson and Zou's thermal pressure model (Fig. 2.2). However, the traditional method, in which the temperature dependence of the isothermal bulk modulus is not included, results in a significant overestimation of volume at high pressure and high temperature (Fig. 2.2). This modification does not significantly affect the phase equilibrium calculation where the phases in the reaction have similar thermal expansion and compression because only the volume change is concerned in the calculation, but it may play an important role in the reaction where the phases involved have very different thermophysical behavior.

2.2 Solid Solution Models

Various solid solution models were discussed by Fei et al. (1986). There are two different groups of solution models. The first group of models have their origin in the Flory-Huggins model (Flory, 1953), in which solutions are considered as athermal with zero excess enthalpy of mixing. The later refined versions, which are the Wilson model (Wilson, 1964), the quasi-chemical (Guggenheim, 1952) and the non-random two-liquids (NRTL) model (Renon and Prausnitz, 1968), do involve enthalpy of mixing and have been recently reviewed by Acree (1984). The second group of models simply express functions as power series in mole fraction. The Redlich-Kister and the two-constant Margules model fall in this category.

The Margules model for binary solution has been popularly used in geochemistry because of its simplicity of formulation, and is used in this study as well. For determining the properties of solid solutions from experimental data on compositions of

coexisting phases, the distribution of a component between two coexisting solid solutions e.g. (1,2)-M and (1,2)-N, where 1 and 2 are exchangeable components, may be considered as an ion-exchange reaction:

$$1\text{-}M + 2\text{-}N = 2\text{-}M + 1\text{-}N \tag{2.21}$$

At equilibrium, we have

$$RT\ln K = RT\ln K_D + RT\ln\left(\frac{\gamma_1}{\gamma_2}\right)^N - RT\ln\left(\frac{\gamma_1}{\gamma_2}\right)^M \tag{2.22}$$

where

$$K_D = \frac{(X_1/X_2)^N}{(X_1/X_2)^M} \tag{2.23}$$

and γ's are activity coefficients. We have used an asymmetric non-ideal solution model for binary solid solutions, for which the excess free energy of mixing (Margules formulation, see Thompson,1969) is defined as:

$$\Delta G^{ex} = X_1X_2(W_{12}X_2 + W_{21}X_1) \tag{2.24}$$

For the asymmetric model the activity coefficient of a component in a binary solution is given by

$$RT\ln\gamma_1 = X_2^2[W_{12} + 2X_1(W_{21} - W_{12})] \tag{2.25}$$

Note that the W_{ij} parameters represent adjustable constants. They are functions of both pressure and temperature. According to Thompson (1969) for W_{ij}, we may write:

$$W_{ij} = W^H_{ij} - TW^S_{ij} + PW^V_{ij} \tag{2.26}$$

where W^H_{ij}, W^S_{ij} and W^V_{ij} represent the excess entropy and excess volume contributions to the interaction energy W_{ij}. The Kohler model (see Bertrand et al. 1983) is used for ternary and multicomponent solutions. According to the model of Bertrand et al. (1983), an excess property of a multicomponent solution is given by

$$\Delta Z^{ex}_{12...N} = \sum_{i=1}^{N} \sum_{j>i}^{N} (X_i + X_j)(f_i + f_j)(\Delta Z^{ex}_{ij})^* \tag{2.27}$$

in which $(\Delta Z_{ij}^{ex})^*$ is the molar excess property (enthalpy, entropy, volume, free energy etc.) of the binary system with components at the same molar ratio as the multicomponent system and f_i and f_j are weighted mole fractions using weighting factors based on the excess properties of the binary systems. X_i is used as the mole fraction in the multicomponent system.

For activity coefficient of a component i, we have

$$\begin{aligned}(RT\ln\gamma_i)_{12...N} = &\sum_{j} (X_i + X_j)(f_i + f_j)(\Delta G^{ex}_{ij})^* \\ &- \sum_{j,k} (X_j + X_k)(f_j + f_k)(\Delta G^{ex}_{jk})^* \\ &+ \sum_{j} (f_i + f_j)(RT\ln\gamma_{ij})^* \qquad (i \neq j \neq k)\end{aligned} \tag{2.28}$$

where the binary functions are denoted by an asterisk. As discussed by Fei et al. (1986), the Kohler method of predicting the ternary solution properties is as good as the Wohl's formulation (see Saxena, 1973, Ganguly and Saxena, 1984) with the additional advantage of simplicity in extension to multicomponent solutions. In equation (2.22)

$$RT\ln K = -\Delta G_{P,T} \qquad (2.29)$$

We may substitute appropriately for the activity coefficients from the binary or multicomponent models noted above and depending on the nature of the observational data, equation (2.22) may be used to determine the unknowns, which may be $\Delta G_{P,T}$ or W_{ij} or a combination of these. Details of such calculations are discussed amply in the literature (e.g. Saxena,1973, Ganguly and Saxena,1984).

CHAPTER 3

Methods of Computation

3.1 Data Evaluation by Optimization Technique (MINUIT)

The problem of minimizing the difference (e.g. chi-square) between predictions from a theoretical form of an expression and the experimental data has been commonly solved in the geochemical literature through regression analyses which use the mid points of the error bars. Recently, however, the linear and non-linear programming techniques have been used to perform optimization procedure to obtain thermodynamic consistency of the optimized parameters with all valid experimental data (e.g. Halbach and Chatterjee, 1982 and Berman et al., 1986).

Today many optimization or minimization routines are available (e.g. in Numerical Recipes). The method adopted here is based on the minimizing subroutines (MINUIT) as discussed by James and Roos (1975). The first of these is the Monte Carlo search routine, in which all of the variable parameter values are chosen randomly according to uniform distributions centered at the best previous values with widths equal to the starting parameter errors. The routine is extremely useful for system with little information on parameters. The second is based on the SIMPLEX method which is one of the most successful stepping method to approach the minimum. The third MIGRAD is based on Fletcher's (1970) method which has the advantage of producing a full covariance matrix, whereas the SIMPLEX only gives estimates of the diagonal elements. Therefore, the MIGRAD minimizer can perform the error analysis and give both the individual and global correlation coefficients. The three methods successively lead to closer approach to the minimum. Combined use of these methods always gives

the best performance in function minimization.

The minimization may take the form of minimizing a chi-square function built from several different types of data. For example, we may define a function for ΔG^o of a heterogeneous reaction in which there are sub-functions corresponding to thermochemical and thermophysical properties of individual phases of the reaction, as discussed in Chapter 2. A typical problem may consist of minimizing the ΔG^o of a reaction with experimentally determined brackets for equilibrium pressures and temperatures and with some known and unknown thermodynamic properties of the reacting phases. Mainly two types of optimization procedure have been performed in this study, (1) optimizing thermodynamic properties of individual phase in the multi-reaction environment and (2) optimizing solution properties in the binary system.

To demonstrate the working of the method, following examples have been chosen:

EXAMPLE 1. To evaluate thermodynamic properties of Mg_2SiO_4 (β-phase) and SiO_2 (stishovite) from reactions:

Mg_2SiO_4 (olivine) = Mg_2SiO_4 (β-phase)

$2MgSiO_3$ (pyroxene) = Mg_2SiO_4 (β-phase) + SiO_2 (stishovite)

SiO_2 (coesite) = SiO_2 (stishovite)

Suppose that the thermochemical and thermophysical data for olivine, pyroxene and coesite have been well established from other evaluations; the thermophysical properties of β-phase and stishovite have been determined; the calorimetric measurements for β-phase and stishovite have been reported with some uncertainties; and the equilibrium

pressures and temperatures of three reactions above have been experimentally determined within certain brakets. If enthalpies and entropies of β-phase and stishovite are chosen to be optimizing parameters, the reported uncertainties of calorimetric data may be used as lower and upper limits of the parameters. The uncertainties in equilibrium pressure may be treated in similar way. The best values of enthalpies and entropies for both phases can be obtained through optimization procedure if there is no major inconsistency among the experimental data. On the other hand, in the case of multi-reaction optimization, any inconsistency may be easily detected by high chi-square values. When many parameters need to be optimized through a limited number of reactions, it is important to give lower and upper limits for the parameters, because several solutions may result with equally good fit to the experimental data.

EXAMPLE 2. To obtain solution parameters from equilibrium distribution data between coexisting phases, such as magnisiowustite (Mw) and olivine, Mw and β-phase, Mw and spinel, and Mw and perovskite.

Thermodynamic data of endmembers of all the solid solutions are assumed to be well evaluated. The distribution of Mg or Fe between two coexisting solid solution is considered as ion-exchange reaction, as discussed in Chapter 2. The equilibrium distribution data determined at various pressure and temperature conditions between various pairs of coexisting solutions may be simultaneously fitted with Margules formulation. If many ion-exchange reactions with one or more common solid solutions are taken into consideration, the optimized solution parameters should be well constrained. In addition, solution calorimetric data should also be used in the optimization.

It is also possible to optimize solution parameters and certain properties of endmembers

at the same time, but the optimized results should be carefully evaluated. In such a case the endmember data and the interaction parameters become mutually dependent.

3.2 Phase Equilibrium Calculation by SOLGASMIX

The multi-component and multi-reaction equilibrium calculations are best done by adopting the method of minimizing the total Gibbs free energy of a chosen system. The linear algebraic techniques were discussed by Eriksson (1975) and Smith and Missen (1982). They forms the basis of the computer program SOLGASMIX (Eriksson, 1975) which is used for all chemical equilibrium calculations in this study.

The total Gibbs free energy of a chemical system can be expressed as

$$G = \sum \mu_i n_i \tag{3.1}$$

where μ is chemical potential. Chemical potential and activity are interrelated by the expression

$$\mu = \mu^0 + RT\ln a \tag{3.2}$$

where μ^0 denotes the standard state potential. For an ideal gas phase species, a species in a non-ideal solution phase and a stoichiometric phase, respectively, we find

$$\mu_i = \mu_i^0 + RT\ln P + RT\ln x_i \tag{3.3}$$

$$\mu_i = \mu_i^0 + RT\ln\gamma_i + RT\ln x_i \tag{3.4}$$

$$\mu_i = \mu_i^0 \tag{3.5}$$

In these equations x is mole fraction and γ is activity coefficient.

The minimization of G in equation (3.1) at constant pressure and temperature is achieved with the constraints imposed by the mass balance relationships represented as

$$\sum a_{ij} n_i = b_j \; (j = 1, 2, \ldots\ldots l) \tag{3.6}$$

where a_{ij} is the number of atoms of the jth element in a molecule of the ith species, l is the total number of elements and b_j is the total amount of the jth element. This is a simple form of constrained optimization problem which may be solved by the Lagrange method of undetermined multipliers. For this, we define a function,

$$F = G + \sum_{j=1}^{l} \lambda_j (b_j - \sum a_{ij} n_i) \tag{3.7}$$

where λ_j denotes the Lagrangian multipliers, for which the necessary conditions, at an extremum of F, are

$$\left(\frac{\partial F}{\partial n_i}\right)_{n_{k \neq i}, \lambda} = \mu_i - \sum a_{ij} \lambda_j = 0 \tag{3.8}$$

$$\left(\frac{\partial F}{\partial \lambda_j}\right)_{\lambda_{k \neq j}, n} = b_j - \sum a_{ij} n_i = 0 \tag{3.9}$$

$$n_i \geq 0 \tag{3.10}$$

Combination of equations (3.3) to (3.5) with equation (3.8) gives

$$\mu_i^0 + RT\ln P + RT\ln x_i - \sum a_{ij} \lambda_j = 0 \tag{3.11}$$

$$\mu_i^0 + RT\ln\gamma_i + RT\ln x_i - \sum a_{ij}\lambda_j = 0 \qquad (3.12)$$

$$\mu_i^0 - \sum a_{ij}\lambda_j = 0 \qquad (3.13)$$

Equation (3.11) is valid for gas phase species while equations (3.12) and (3.13) hold for components of solution phases and stoichiometric phases respectively.

The system consisting of equations (3.6) and (3.11) to (3.13) with the unknowns n_i and λ_j is non-linear because of the logarithmic term in equations (3.11) and (3.12). The next step is therefore a linearization of these equations by expansion in a Taylor series around an estimated equilibrium composition up to and including the term of the first order. This is equivalent to making a quadratic approximation to the free-energy surface, and we can obtain an expression which relates n_i linearly to λ_j and the estimated equilibrium amounts. Incorporation of this expression into equation (3.6) gives then the final linear system of equations. The number of unknowns is reduced to the sum of elements and phases assumed to be present at equilibrium.

Parametrized activity-coefficient expressions to be inserted into equation (3.12) are supplied by the user. In order to avoid the need of also specifying derivatives, $\ln\lambda$ is treated as constant when calculating the partial derivative with respect to n_i in the Taylor expansion. The partial derivative is therefore approximate as long as the estimated equilibrium composition does not correspond to a free-energy minimum.

The approximation to the free-energy surface implies an iterative algorithm and, if

positive, the calculated n_i values are used as improved estimates in the subsequent iteration cycle. If some n_i values are negative, these are set to zero before being used as the starting-point for a new Taylor expansion. The iterative procedure ends when the calculated values coincide with the starting estimates.

The condensed phases included in the initial estimate are constrained by the Gibbs phase rule but need not necessarily be the correct ones of the final equilibrium state. Another phase combination might yield a lower free energy, and condensed phases need to be withdrawn from or added to the previous combination until the set of equilibrium phases is found. This set has the characteristic feature that the activity for an omitted stoichiometric phase must be less than one, as must the sum of mole fractions for an omitted solution phase.

For a more detailed description of the equations used in SOLGASMIX, see Eriksson and Rosén (1973).

CHAPTER 4

Experimental Determination of Element Partitioning in the Mg-Fe-Si-O System

Solid solutions in the Mg-Fe-Si-O system include (Mg,Fe)O (magnesiowustite), $(Mg,Fe)SiO_3$ (pyroxene and perovskite), and $(Mg,Fe)_2SiO_4$ (olivine, β-phase and spinel). They form four pairs of coexisting phases with magnesiowustite, magnesiowustite-olivine, magnesiowustite-β, magnesiowustite-spinel and magnesiowustite-perovskite (see Figure 4.1a,b). As discussed in Chapters 2 and 5, the solid solution properties may be derived from the element distribution data by considering the distribution of an element between two coexisting solid solution as exchangeable reaction. The purpose of this study is to determine the distribution of Mg and Fe between coexisting solid solutions mentioned above at various pressure and temperature conditions and to model the solid solutions by fitting the experimental data with the Margules formulation.

4.1 Techniques Used in the Experiments

The high pressure techniques used here are the piston-cylinder apparatus (up to pressure of 5 GPa), the multi-anvil device (up to pressure of 30 GPa) and the diamond-anvil cell technique. Chemical and structural analytical techniques such as X-ray diffraction, microprobe or SEM and Raman spectroscopy are used to characterize the structure and chemical composition of the samples.

A conventional 1/2-inch piston-cylinder apparatus was used for experiments at

pressures below 5 GPa. Details of the apparatus were described by Boyd and England (1960, 1963). Gold, platinum, molybdenum and graphite capsules were used depending on the nature of the experiments (see details below).

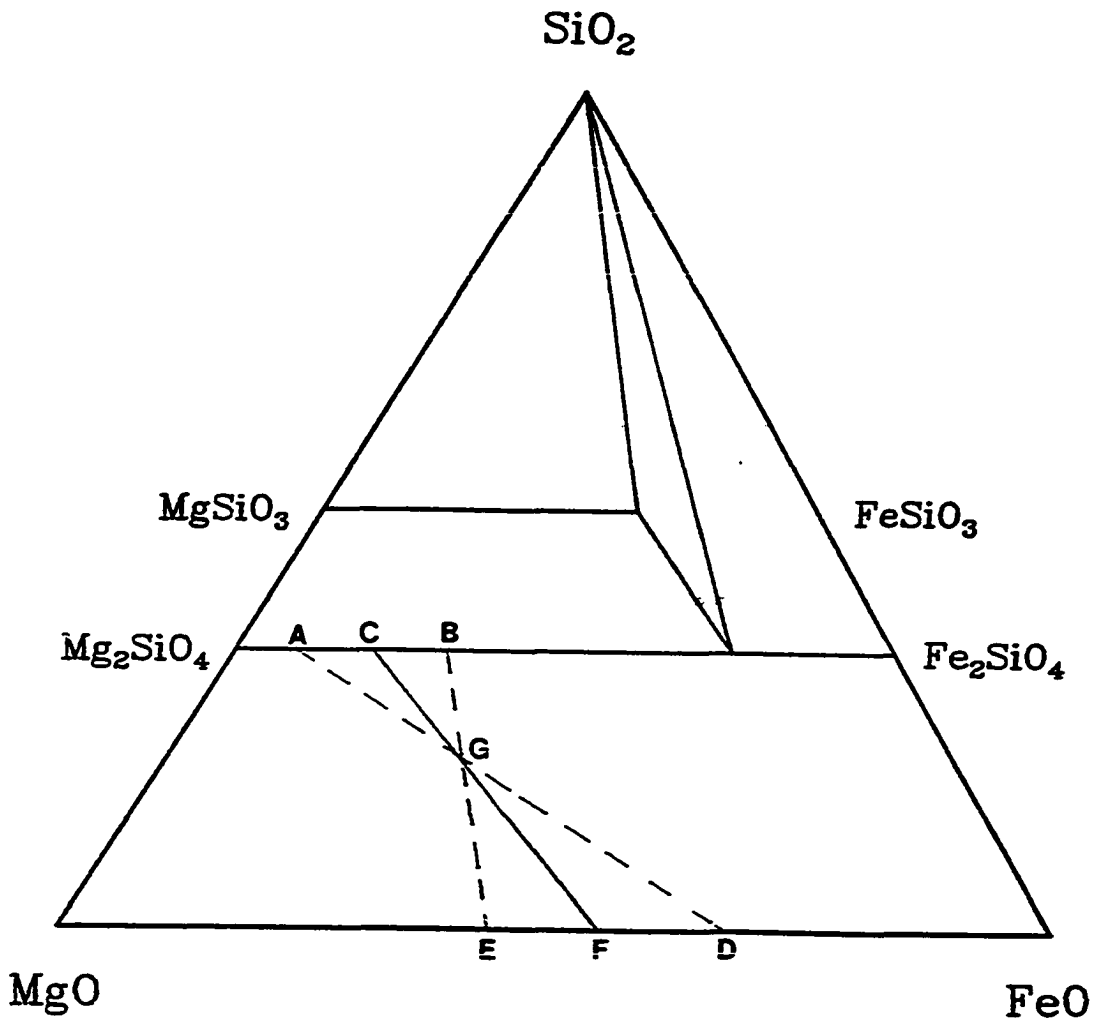

Figure 4.1a Schematic subsolidus isothermal section in the system MgO-FeO-SiO_2, showing the various phase assemblages present. The phase assemblages change accordingly when olivine transforms to β-phase and then to spinel, and quartz to coesite and then to stishovite with increasing pressure.

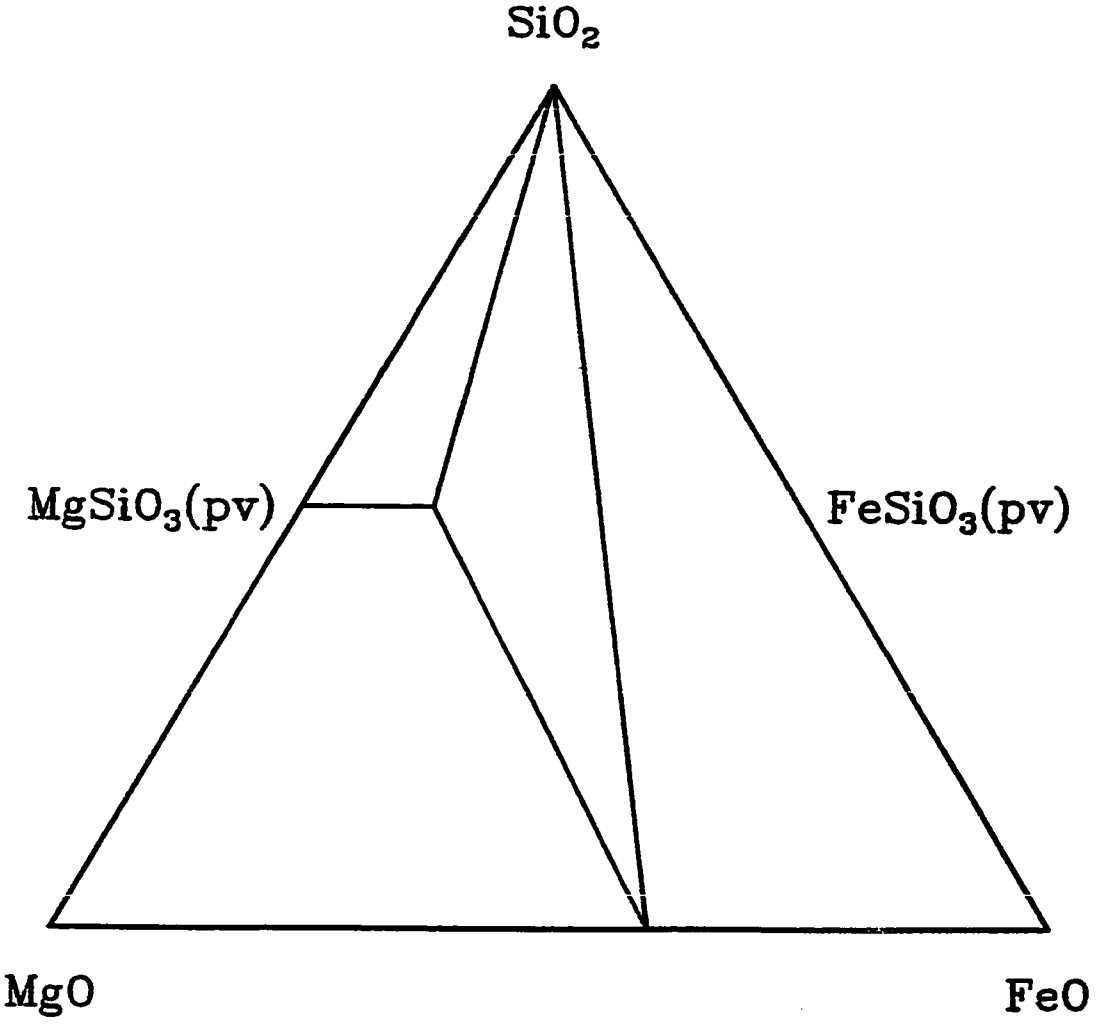

Figure 4.1b Schematic subsolidus isothermal section in the system MgO-FeO-SiO_2 at high pressure, showing only magnesiowustite, perovskite and stishovite stable.

The large-volume multi-anvil high-ressure device used here is a 2000-ton Uniaxial Split-Sphere Apparatus (USSA-2000) at SUNY Stony Brook. The detailed description of the apparatus is given by Liebermann et al. (1986) and Remsberg et al. (1988). The 10 mm octahedron cell-assembly which is capable of generating maximum pressure of 20 GPa was used in the experiments. A modification of the sample chamber, which was normally a cylinder of 1.7 mm diameter by 3 mm long, was made (Mao et al., 1988). Six counterbores of 0.5 mm diameter and 1.2 mm deep were drilled into a solid molybdenum cylinder. Each hole holds a seperate sample sealed by a cap. Therefore, six different samples can be run in one experiment at the same experimental condition. The modification has greatly improved the efficiency of using the multi-anvil apparatus for experimental petrologic studies at very high pressures.

The diamond-anvil cell technique used in this experiment was discussed by Mao and Bell (1978). The high temperature was achieved by the YAG laser heater. Pressure was calibrated with the ruby fluorescence technique.

4.2 Experimental Procedure

Synthetic olivines and magnesiowustites with different iron contents were used as starting materials in the distribution experiments. Magnesiowustite solid solutions were synthesized by Rosenhauer et al. (1976). Detailed chemical analyses of the samples are available (Rosenhauer et al., 1976). Olivine solid solutions were synthesized in the piston-cylinder apparatus, with oxide mixtures as starting material. The mixtures were prepared by weighing the heat-treated oxides, MgO, Fe_2O_3 and SiO_2, in olivine composition with different iron contents, followed by grinding under acetone in an agate mortar. The oxide mixtures were then placed in a CO_2-CO gas mixing furnace at

temperature of 1200 °C for 24 hours. To reduce the Fe^{3+} to Fe^{2+}, the oxygen fugacity (fO2) was controlled at about -10.50 between the IW (-11.91) and WM (-9.10) buffers at 1200 °C (Ulmer, 1971). The treated mixtures were reground and sealed in gold capsules with about 5% water. The capsules were then run in the piston-cylinder apparatus for 48 hours at 1000 °C and 15 kbar. The synthetic olivines were examined optically and with X-ray diffraction; no oxide remainder was present. The compositions were checked by electron microprobe.

To study the distribution of Mg and Fe between magnesiowustite and olivine, magnesiowustite and olivine of suitable compositions were mixed in appropriate proportions (e.g. 2 magnesiowustite to 3 olivine in most cases). The mixtures were ground to a grain size of less than 3 μm and well homogenized. Two different types of capsules, platinum capsule sealed inside with graphite capsule and molybdenum capsule, were used to test if there was iron loss in the runs. The equilibrium in Mg-Fe partitioning was checked by two methods. One method was to determine the distrubution coefficients as function of time. Figure 4.2 shows the distribution coefficients ($K_{Ol\text{-}Mw}$) determined from the samples run for 1, 2 and 10 hours at the same condition with starting material as mixture of forsterite and $(Mg_{.61}Fe_{.39})O$ magnesiowustite. The results indicate that equilibrium was achieved within 2 hours. Some samples were run for 24, 48 and 96 hours and they produced similar results (see Table 4.1). The other method was to mix magnesiowustite and olivine such that if two samples, mixture of olivine A and magnesiowustite D with bulk composition G and mixture of olivine B and magnesiowustite E with bulk composition G in Figure 4.1a, are run at the same time, both sample should have olivine C and magnesiowustite F at equilibrium.

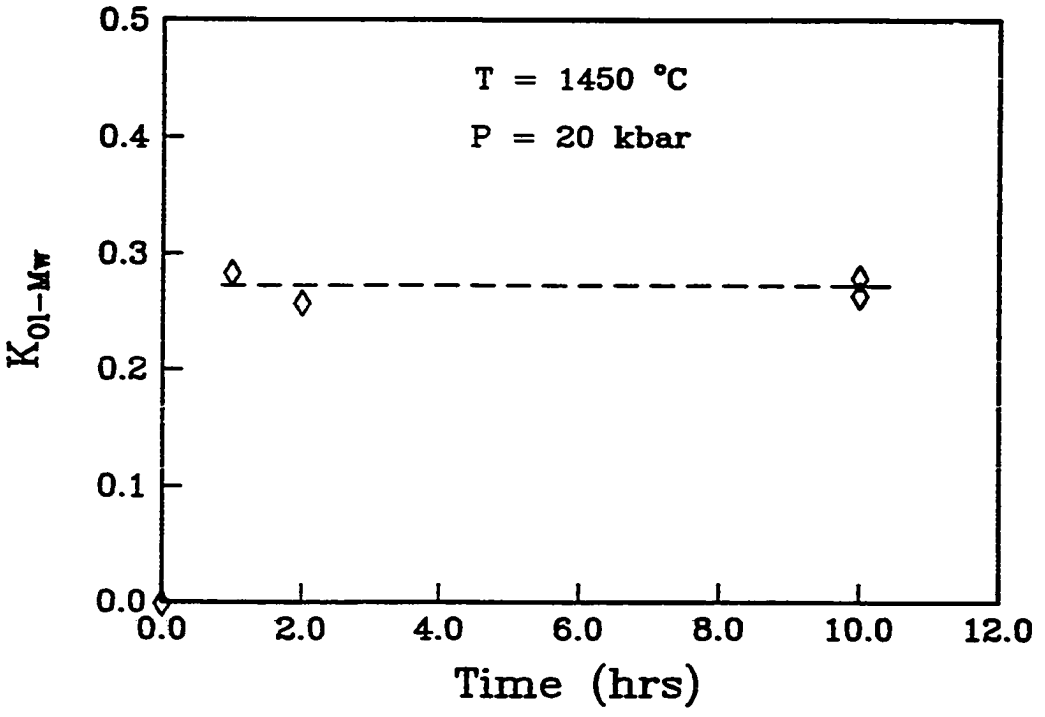

Figure 4.2 The relationship between $K_{Ol\text{-}Mw}$ [= $(X_{Fe}/X_{Mg})^{Ol}/(X_{Fe}/X_{Mg})^{Mw}$] and time at temperature of 1450 °C and pressure of 20 kbar. The starting material is mixture of forsterite and $(Mg_{0.61}Fe_{0.39})O$ magnesiowustite $(X_{Fe}/X_{Mg})^{Ol}/(X_{Fe}/X_{Mg})^{Mw} = 0$.

All experiments at pressures below 5 GPa were performed in the piston-cylinder apparatus. The multi-anvil device was used for determining distribution coefficients between magnesiowustite and olivine at 9 GPa and 1450 °C, between magnesiowustite and β-phase and between magnesiowustite and spinel at 15 GPa and 1500 °C. The multi-cell sample chambers described above were used in the experiments. Run products were examined optically. β-phase and spinel were identified by Raman spectroscopy (Figure 4.3). The compositions of coexisting phases were determined with electron microprobe and SEM.

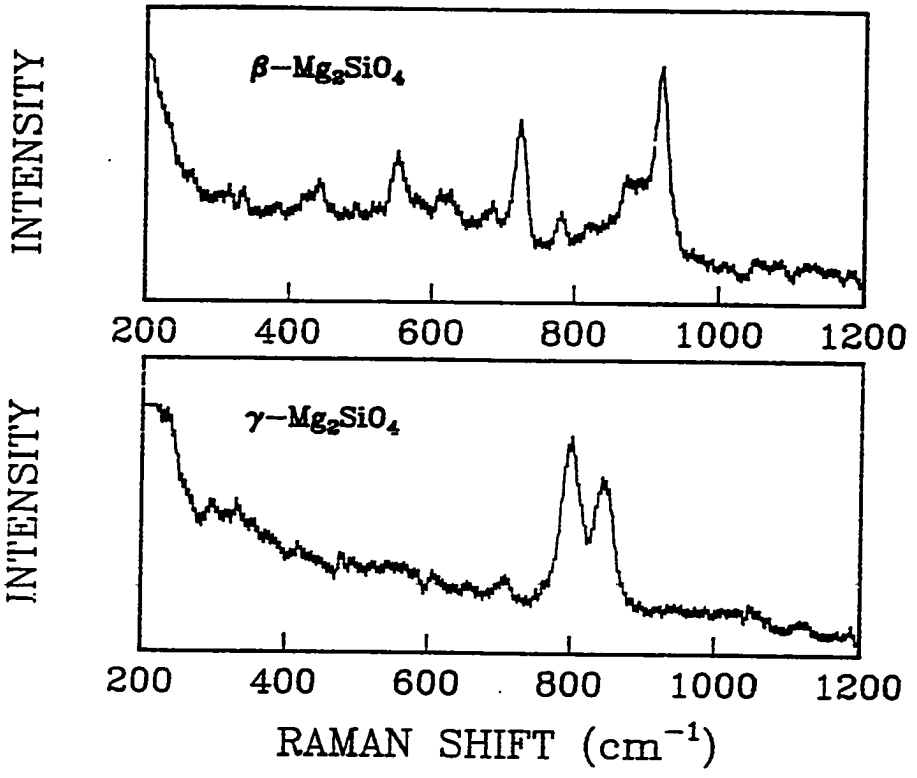

Figure 4.3 Raman spectrium of β-Mg_2SiO_4 and γ-Mg_2SiO_4.

To determine the distribution of Mg and Fe between magnesiowustite and perovskite, olivines (Fo85, Fo80 and Fo73) were used as starting materials. The powder olivine with small ruby grains was imbeded in a 250 μm hole drilled in a gasket. The sample was pressurized in the diamond-anvil cell and heated by YAG laser beam. Pressure in the ruby grains were measured with the fluorescence technique. The products were examined optically and by X-ray diffraction. The composition of each phase in the assemblage was determined both by X-ray diffraction (the relation between volume and composition) and by electron microprobe. The lattice parameters of each phase were

determined by X-ray diffraction, with gold as internal standard for calibration. The relation between volume and compostion for perovskite by Yagi et al. (1979) and that for magnesiowustite by Rosenhauer et al. (1976) were used for determining the compositions of perovskite and magnesiowustite. The results are consistent with those determined with electron microprobe. The grain size of each phase in the run products generally is small (less than 3 μm). It is not possible to determine the composition of each phase directly with electron microprobe. However, there is a correlation between the Fe/(Fe+Mg) and Si/(Fe+Mg) ratios. The composition of a pure phase was then obtained by extrapolation (Figure 4.4).

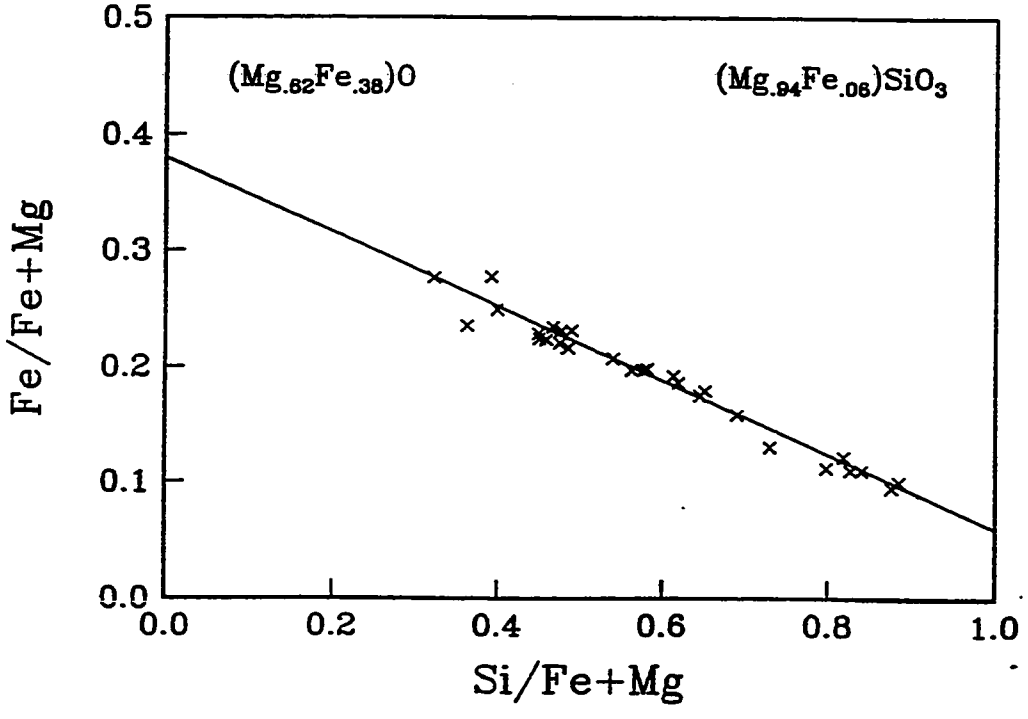

Figure 4.4 Compositions of coexisting phases of perovskite and magnesiowustite determined with microprobe plotted in the Fe/(Fe + Mg) - Si/(Fe + Mg) diagram. The compositions of perovskite and magnesiowustite were obtained by extrapolation.

4.3 Experimental Results

The experimental results are summarized in Tables 4.1 and 4.2 and plotted in Figures 5.7 to 5.10 (see Chapter 5 below).

Table 4.1 Experimental results on the Mg-Fe partitioning between magnesiowustite and olivine, magnesiowustite and β-phase, and magnesiowustite and spinel in the Mg-Fe-Si-O system

Run No.	Starting materials	P (kbar)	T (°C)	Time (hrs)	Capsule types	Coexisting phases A+B	Device	X_{Fe} in A	X_{Fe} in B
1.	Fo90+Mw20	20	1200	48	Pt+C	Mw+Ol	PCA	0.16	0.77
2.	Fo70+Mw40	20	1200	48	Pt+C	Mw+Ol	PCA	0.20	0.82
3a.	Fo78+Mw20	20	1200	96	Pt+C	Mw+Ol	PCA	0.21	0.85
3b.	Fo78+Mw20	20	1200	48	Pt+C	Mw+Ol	PCA	0.21	0.85
3c.	Fo78+Mw20	20	1200	24	Pt+C	Mw+Ol	PCA	0.21	0.83
4.	Fo100+Mw61	20	1200	48	Pt+C	Mw+Ol	PCA	0.06	0.23
5.	Fo57+Mw20	20	1200	48	Pt+C	Mw+Ol	PCA	0.41	0.93
6.	Fo78+Mw61	20	1200	48	Pt+C	Mw+Ol	PCA	0.14	0.68
7a.	Fo100+Mw61	20	1450	10	Pt+C	Mw+Ol	PCA	0.06	0.19
7b.	Fo100+Mw61†	20	1450	10	Pt+C	Mw+Ol	PCA	0.06	0.20
7c.	Fo100+Mw61	20	1450	2	Pt+C	Mw+Ol	PCA	0.06	0.21
7d.	Fo100+Mw61	20	1450	1	Pt+C	Mw+Ol	PCA	0.05	0.16
8.	Fo83+Mw20	20	1450	48	Pt+C	Mw+Ol	PCA	0.19	0.74
9.	Fo83+Mw20	20	1450	2	Mo	Mw+Ol	PCA	0.21	0.73
10.	Fo83+Mw61	20	1450	2	Mo	Mw+Ol	PCA	0.14	0.60
11.	Fo83+Mw61	40	1450	2	Pt+C	Mw+Ol	PCA	0.14	0.62
12.	Fo83+Mw20	40	1450	2	Mo	Mw+Ol	PCA	0.21	0.76
13.	Fo83+Mw20	40	1450	11	Mo	Mw+Ol	PCA	0.20	0.71
14.	Fo57+Mw20	40	1450	11	Mo	Mw+Ol	PCA	0.46	0.90
15.	Fo100+Mw61	40	1450	11	Mo	Mw+Ol	PCA	0.06	0.22
16.	Fo83+Mw20	20	1350	48	Pt+C	Mw+Ol	PCA	0.20	0.79

17.Fo57+Mw20	10	1200	48	Pt+C	Mw+Ol	PCA	0.42	0.92
18.Fo83+Mw20	90	1450	2	Mo	Mw+Ol	MAD	0.20	0.78
19.Fo83+Mw20	90	1450	2	Mo	Mw+Ol	MAD	0.22	0.83
20.Fo57+Mw20	90	1450	2	Mo	Mw+Ol	MAD	0.48	0.94
21.Fo83+Mw61	90	1450	2	Mo	Mw+Ol	MAD	0.15	0.67
22.Fo83+Mw61	90	1450	2	Mo	Mw+Ol	MAD	0.14	0.65
23.Fo83+Mw61	90	1450	2	Mo	Mw+Ol	MAD	0.14	0.66
24.Fo100+Mw61	150	1500	2	Mo	Mw+β	MAD	0.12	0.32
25.Fo83+Mw44	150	1500	2	Mo	Mw+β+Sp	MAD	0.26	0.45
26.Fo83+Mw44	150	1500	2	Mo	Mw+β+Sp	MAD	0.27	0.52
27.Fo57+Mw44	150	1500	2	Mo	Mw+Sp	MAD	0.51	0.75
28.Fo35+Mw20	150	1500	2	Mo	Mw+Sp	MAD	0.70	0.90
29.Fo100+Mw61	150	1500	2	Mo	Mw+β	MAD	0.10	0.25
30.Fo100+Mw61	150	1500	2	Mo	Mw+β	MAD	0.14	0.31
31.Fo83+Mw44	150	1500	2	Mo	Mw+Sp	MAD	0.37	0.59
32.Fo35+Mw20	150	1500	2	Mo	Mw+Sp	MAD	0.73	0.92
33.Fo35+Mw0	150	1500	2	Mo	Mw+Sp	MAD	0.84	0.95

Note: PCA = piston-cylinder apparatus; MAD = multi-anvil device; Mw = magnesiowustite; Ol = olivine; β = β-phase; Sp = spinel; Mo = molybdenum; Pt = platinum; C = graphite.

Table 4.2 Experimental results on the Mg-Fe partitioning between magnesiowustite and perovskite in the Mg-Fe-Si-O system at 260 kbar and about 1400 °C by diamond-anvil cell technique

Run No.	Starting materials	X-ray diffraction				Microprobe analysis	
		magnesiowustite		perovskite			
		a (Å)	X_{Fe}	V (Å^3)	X_{Fe}	$X_{Fe\ in\ Mw}$	$X_{Fe\ in\ Pv}$
19	Fo85	4.250	0.30	163.020	0.05	0.27	0.05
21	Fo80	4.260	0.39	163.144	0.08	0.38	0.07
23	Fo73	4.270	0.50	163.336	0.12	0.48	0.11

The distribution of Mg and Fe in the Mg-Fe-Si-O system has been systematically studied in this work. Temperature and pressure dependences of the Mg-Fe distribution coefficients between magnesiowustite and olivine have been determined. The experimental results show systematic variations of the distribution data with temperature and pressure (Figure 5.7). Various capsules were used in the experiments. There is no indication of iron loss during the run. Small amount of water (about 5%) when added to the sample showed no effect on the compositions of the coexisting phases (Table 4.1).

The distribution of Mg and Fe between magnesiowustite and β-phase or spinel were studied by using the multi-anvil device. The Mg-Fe distribution coefficients between magnesiowustite and spinel ($K_{Sp\text{-}Mw}$) determined in this study are systematically higher than those by Ito (1984) and Yagi et al. (1979). The differences may be partly due to the different pressure and temperature conditions. The results on the Mg-Fe partitioning between magnesiowustite and perovskite are consistent with those obtained by Ito (1984) and Yagi et al. (1979).

The combined use of the high pressure techniques, the piston-cylinder apparatus, the multi-anvil device and the diamond-anvil cell technique, allows us to study the system over broad ranges of pressure and temperature of interest. The results obtained in this study, combined with those by Ito (1984) and Yagi et al. (1979), provide rather complete information on the Mg-Fe partitioning between coexisting phases in the system. The experimental data are used to obtain solution properties of the solid solutions in the system (see Chapter 5 below).

CHAPTER 5

Thermodynamic Data Systematics

There are four major sources of data available for establishing an internally consistent data set: calorimetric measurements, phase equilibrium data, measured thermophysical properties of a phase, and heat capacities and entropies estimated from lattice vibrational models, see, for example, Akaogi et al. (1984). Ideally, we should be able to calculate the phase equilibrium relations from independently determined thermochemical and thermophysical data, and compare them with the results of high pressure experiments. The results are, in general, inconclusive because of uncertainties in calorimetric measurements, of problems in P, T calibrations, and because of the lack of reversals in experimental phase equilibrium studies. Therefore, it is necessary to evaluate and systematize the calorimetric data with the constraints provided by phase studies and vibrational calculations. The data base presented in this study is evaluated by considering all the available information in the system. The procedure of selection and evaluation of thermochemical and thermophysical data is discussed below.

5.1 System Fe-O:

Important minerals in this system are: iron polymorphs (bcc-Fe, fcc-Fe and hcp-Fe), wustite (variable Fe:O), magnetite polymorphs (Fe_3O_4 and high-pressure-Fe_3O_4) and hematite polymorphs (Fe_2O_3 and high-pressure-Fe_2O_3).

Polymorphism of Fe

Phase relations of Fe at high pressure and high temperature have been extensively studied (e.g. Bundy, 1965; Strong et al., 1973; Fukizawa, 1982; Manghnani et al., 1985; Mao et al., 1987; Akimoto et al., 1987; Manghnani et al., 1987; and Huang et al., 1987). Guillermet and Gustafson (1985) critically evaluated the thermochemical and thermophysical data for iron. Their data are adopted in this study to construct the phase digram of iron.

Wustite

Several phase equilibrium studies are available for this system (e.g. Goel et al., 1980, Björkman, 1984) and Kubaschewski (1982) has summarized the phase relations. Hazen and Jeanloz (1984) have discussed the crystal chemistry of wustite. As described by these authors, the structure of wustite is complex and difficult to determine. The variables which may affect the thermodynamic properties of wustite are a) degree of nonstoichiometry, b) the ratio of octahedral vacancies to tetrahedral ferric iron, and c) the size and shape of defect clusters, their periodicity and the extent of magnetite or iron exsolution. Each wustite sample may have its own structural peculiarities depending on the conditions of synthesis and thermal history; this makes measurements of thermochemical and physical properties a very difficult task. From the numerous phase equilibrium studies in the system Fe-O cited in Kubachewski (1982), it appears that certain phase boundary relationships are commonly accepted. However, details on various allotropic modifications of wustite are not well known (see Hazen and Jeanloz, 1984). Such modifications are the reflections of discontinuities in the thermochemical properties of the wustite solid solution.

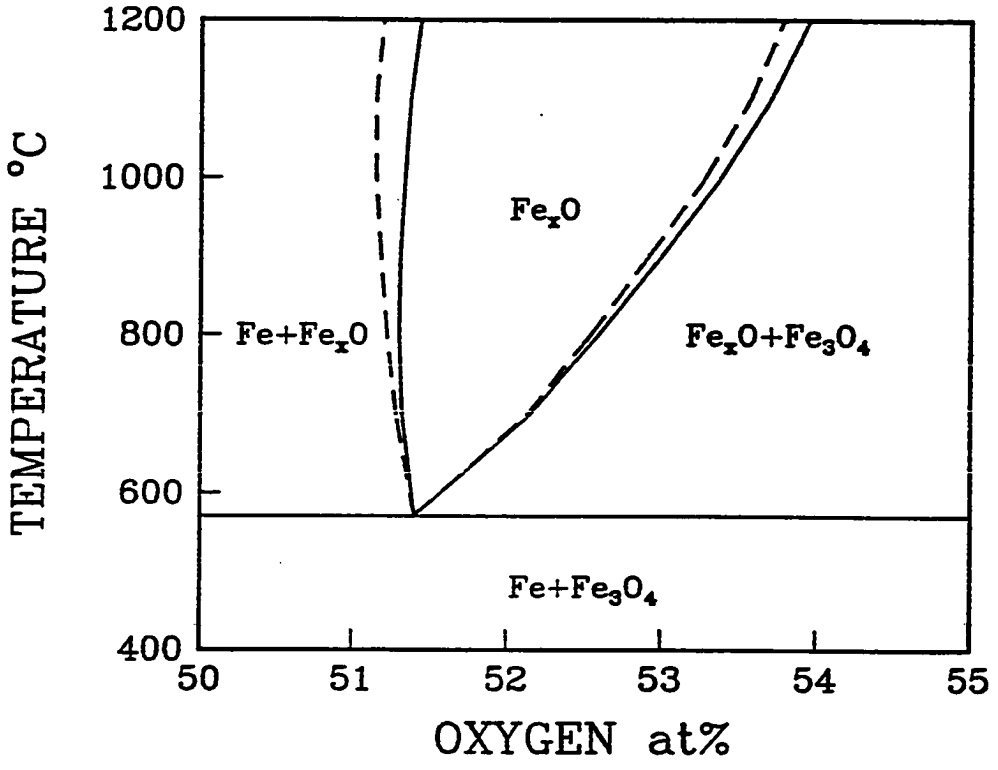

Figure 5.1 Equilibrium relations in the system Fe-O at a pressure of 1 bar. The dashed lines are from the review of Kubaschewski (1982). The solid lines represent the calculated curve using the data in Tables 5.2 to 5.5 and the wustite solution model as described in the text. The experimental data match the calculated data exactly where only one solid line appears.

Figure 5.1 shows part of the phase diagram for the Fe-O system at 1 bar. Wustite has a temperature-composition field within which its composition varies mainly between $Fe_{0.947}O$ and $Fe_{0.85}O$. The system may be modeled by considering wustite as a solid solution of two fictive, isostructural components FeO and $FeO_{1.5}$. Through such modeling one can hope to treat the thermodynamics of the hetereogeneous reactions (i.e. wustite reacting with other phases) generally within the errors in the thermochemical data

of the reacting phases. A precise model for the wustite solid solution particularly for modeling the crystal chemical behavior must include the effect of additional components (other than FeO and $FeO_{1.5}$) and other parameters discussed by Hazen and Jeanloz (1984). The reaction within the field of wustite solution is

$$\{FeO\} + 0.25O_2 = \{FeO_{1.5}\}$$

and in the field towards magnetite, the reaction may be conceived as

$$\{5FeO\} + O_2 = \{2FeO_{1.5}\} + Fe_3O_4$$

where the brackets denote the components in the wustite solution. The computed W_{ij} values for wustite are (FeO = 1, $FeO_{1.5}$ = 2):

W_{12} = -7229, W_{21} = -2142 (J/mol)

which are the same as in Bjorkman (1984). However, note that the thermochemical data on fictive endmember components used here are different. The enthalpy and entropy data on the two fictive end member components are determined simultaneously through these calculations and are listed in Table 5.2. The coefficients of C_P for fictive FeO and $FeO_{1.5}$ are the same as for the stoichiometric FeO and hematite respectively. Figure 5.1 shows the calculated phase boundaries using the data presented above and in Tables 5.2 to 5.5. The fit of the computed phase boundaries can be improved by using a ternary solution model for the wustite (Fe - FeO - $FeO_{1.5}$) as done by Goel et al. (1980) and Bjorkman (1984). However, in view of the uncertainties introduced at high pressures (discussed later) we have refrained from using the ternary model at present. The phase diagram of

the Fe-O system used here is based on several experimental results reviewed by Kubaschewski (1982), Goel et al. (1980) and Bjorkman (1984). References to the literature may be found in the above mentioned articles.

The errors in the W_{12} and W_{21} and in the ΔH^{o}_{f} and ΔS^{o}_{f} are related and cannot be independently evaluated. However, for fixed value of W_{ij}, a change of a few hundred joules in ΔH^{o}_{f} is enough to make the results on phase boundaries change beyond the quoted experimental uncertainty.

For calculations at high pressure, we need data on volume of mixing and on compressibility of the solid solution components FeO and $FeO_{1.5}$. Volume of mixing is assumed to be ideal with volume of the solution given by:

$$V_{FexO} = X_{FeO}V_{FeO} + X_{FeO1.5}V_{FeO1.5} = (3 - 2/X)V_{FeO} + (2/X - 2)V_{FeO}$$

Using the molar volume data of FeO as 12.25 cm^3 (extrapolated value from Rosenhauer et al., 1976) and the V_{FexO} data from Simons (1980) and Hentschel (1970), the molar volume of the fictive $FeO_{1.5}$ is determined to be 15.97 cm^3. For estimating the bulk modulus of Fe_xO (change in bulk modulus as a function of composition of wustite), there are two sets of data available (see review, Jeanloz and Hazen, 1983). The data from dynamic measurements indicate a $K_{T,0}$ of 180 GPa for FeO and a similar value for $FeO_{1.5}$. The static measurements of $K_{T,0}$ lead to values of 155 GPa and 137 GPa for FeO and $FeO_{1.5}$ respectively. Both data with their indicated limits have been used in the

phase equilibrium calculations.

Magnetite and Hematite

Magnetite transforms to its high-pressure polymorph at pressure of about 25 GPa at room temperature (Mao et al., 1974). The magnetite and high-pressure magnetite boundary was determined to have a negative slope (dT/dP = -45 K/GPa, Huang and Bassett, 1986). Shock-wave data indicate that hematite transforms to its high-pressure polymorph below pressure of 60 GPa. The transition also was not observed in the diamond-anvil cell below 30 GPa (Mao and Bell, 1977). Some physical properties of these phases are available (e.g. Mao et al., 1974; Ahrens et al., 1969; Finger et al., 1986; Wilburn et al., 1978; Sato and Akimoto, 1979; and Finger and Hazen, 1980). Thermochemical data for magnetite and hematite are from Haas (see Fei and Saxena, 1986).

There are several buffer reactions, wustite-iron (WI), magnetite-iron (MI), magnetite-wustite (MW) and hematite-magnetite (HM) buffers, in the system Fe-O. The phase equilibria in the system were experimentally determined by Eugster and Wones (1962). The computed phase equilibria, based on evaluated data for phases in the system, are in good agreement with the experimental data (Figure 5.2). The calculated QFM buffer, based on the evaluated data on quartz and fayalite (see below), is also shown in Figure 5.2.

5.2 System MgO-SiO_2

Phases in the MgO-SiO_2 system include all the mineral structures proposed as likely in

the mantle. These minerals are MgO (rocksalt), the polymorphs of SiO_2 (quartz, coesite and stishovite), Mg_2SiO_4 (olivine, β-phase and spinel) and $MgSiO_3$ (the pyroxene polymorphs, ilmenite, garnet and perovskite). The thermochemical and thermophysical data for periclase are well known (Robie et al., 1978; Suzuki, 1975; Jackson and Niesler, 1982; and Anderson and Zou, 1989). Data selections on other phases are discussed below. The results on the MgO-SiO_2 system included here are from Fei et al. (1989).

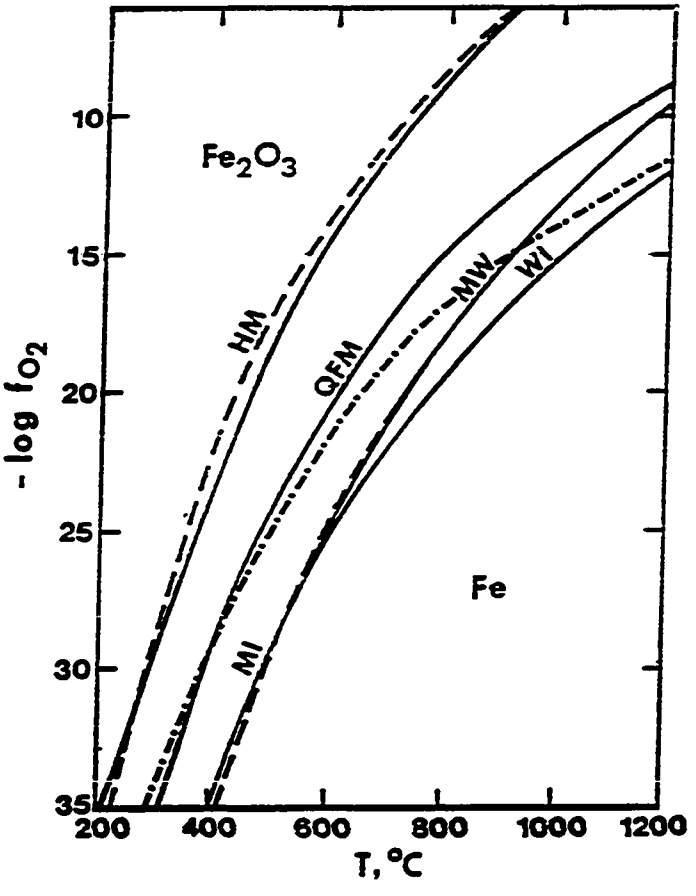

Figure 5.2 Computed phase equilibria in the system Fe-O at a pressure of 1 bar. The solid lines represent calculated results; the dashed lines experimental data of Eugster and Wones (1962). The missing part of the dashed lines match the calculated lines. I = iron; W = wustite; H = hematite; M = magnetite; Q = quartz; F = fayalite.

Polymorphism of SiO_2

The polymorphism of SiO_2 is quite complicated. Here we only focus on three high pressure polymorphs (quartz, coesite and stishovite). Weaver et al. (1979) and recently Kuskov and Fabrichnaya (1987) compared the thermochemical-thermophysical data with phase equilibrium data for the quartz-coesite-stishovite transformations. Akaogi and Navrotsky (1984), using new calorimetric data, calculated phase relations in the three polymorphs. Fei and Saxena (1986) started with the thermochemical data on quartz from Robie et al. (1978), and evaluated the thermochemical data on coesite and stishovite; these data were then combined with the phase equilibrium data for the quartz-coesite transformation (Bohlen and Boettcher, 1982), for the coesite-stishovite transformation (Yagi and Akimoto, 1976) and with the calorimetric data from Akaogi and Navrotsky (1984). There are several high pressure reactions involving stishovite (e.g. pyroxene = β-phase + stishovite in the Mg-Si-O system, pyroxene = spinel + stishovite and spinel = wustite + stishovite in the Fe-Si-O system, and perovskite = magnesiowustite + stishovite in the Mg-Fe-Si-O system). The physical properties of stishovite play an important role in those phase equilibrium relations. The thermal expansion of stishovite was determined by Ito et al. (1974) in a temperature range of 291 - 873 K. The compression of stishovite has been extensively studied by various methods, namely, the static compression, the ultrasonic, the shock wave, the brillouin scattering and theoretical calculation. The reported values of bulk modulus for stishovite range from 250 GPa (Liebermann et al., 1976) to 343 GPa (Akimoto, 1975) The choice of bulk modulus of 316 GPa for stishovite (Weidner et al., 1982) in this study is supported by a global optimization in which all high pressure reactions involving stishovite are included. The data on stishovite were evaluated by simultaneously fitting several phase

boundaries involving stishovite (Fei and Saxena, 1986).

Polymorphism of Mg_2SiO_4

The phase relations for the three Mg_2SiO_4 polymorphs (olivine, β-phase and spinel) have been experimentally investigated by Ringwood and Major (1970), Suito (1972), Kawada (1977), Suito (1977), Ohtani (1979), Fukizawa (1982), Sawamoto (1986b), Katsura and Ito (1989), and Ito and Takahashi (1989). For pressure calibration at high temperatures, Suito (1977) used the data of Yagi and Akimoto (1976) who determined the coesite-stishovite boundary by the in-situ X-ray diffraction method. The pressures for the α-β transition determined by Suito (1977) were higher than that determined by Ringwood and Major (1970), Suito (1972) and Kawada (1977). Suito argued that the discrepancies were due to different starting materials, pressure media, apparatus and pressure scale (Suito, 1977). Fukizawa (1982) determined the α-β transition pressure using the in-situ X-ray diffraction method based on a gold internal pressure standard. The preliminary result (dashed line labeled as F(82) in Figure 5.3) is about 1 GPa lower in pressure than that determined by Suito (1977) (dashed line labeled as SU(77) in Figure 5.3) Very recently, Katsura and Ito (1989) have precisely determined the α-β transition pressures at 1473 and 1873 K to be 14 and 15 GPa, respectively. Their result is close to Suito's at 1273 K and to Fukizawa's at 1873 K. On the other hand, the calorimetric data for the α-β transition obtained by Akaogi et al. (1984) are consistent with Suito's results when the entropy change value of -10.5 J/mol.K for the α-β transition is used. The calorimetric data are also consistent with Katsura and Ito's results if the entropy change of -7.7 J/mol.K is chosen (Akaogi et al., 1989). The optimized data in this study favor Katsura and Ito's results (see discussion below).

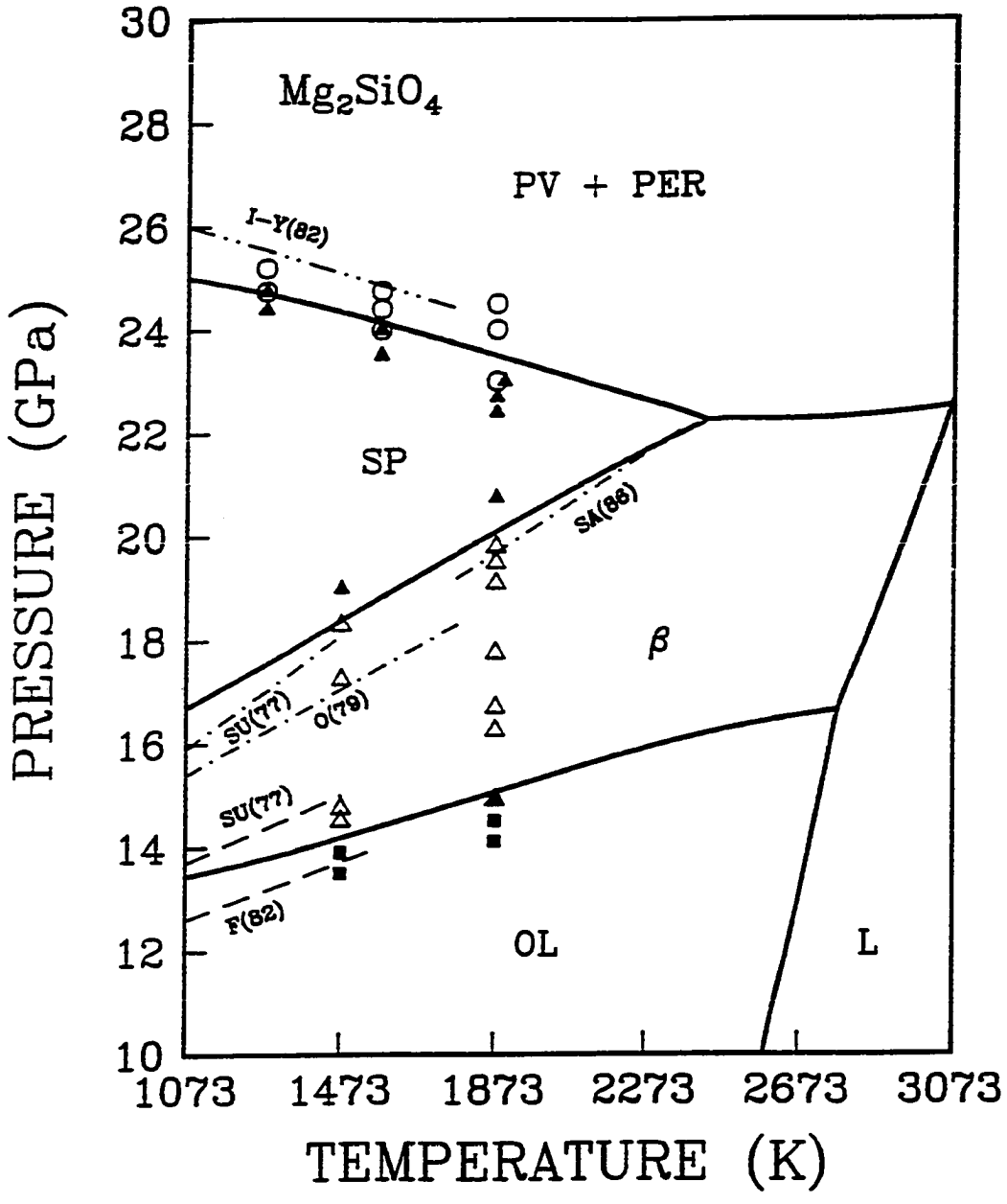

Figure 5.3 Comparison of calculated phase boundaries in Mg_2SiO_4 with experimental phase equilibrium data. Solid lines are calculated results based on Tables 5.2 to 5.5. Experimental data: Katsura and Ito (1989) (■ Ol, ▵ β, ▲ SP); Ito and Takahashi (1989) (▲ SP, ○ PV+PER); F(82) = Fukizawa (1982); SU(77) = Suito (1977); O(79) = Ohtani (1979); SA(86) = Sawamoto (1986); and I-Y(82) = Ito and Yamada (1982). OL = olivine, β = β-phase, SP = spinel, L = liquid, PER = periclase and PV = perovskite.

Figure 5.3 shows that pressures for the β-γ transition determined by Ohtani (1979) (dot-dashed line labeled as O(79) in Figure 5.3) are about 0.8 GPa lower than those determined by Suito (1977) (dot-dashed line labeled as SU(79) in Figure 5.3). The disagreement could be totally due to the pressure calibration. Ohtani determined the phase boundary of pyroxene-ilmenite transition in ZnSiO3 as P(GPa) = 8.0(±0.5) + 0.0018T(K) and used it for comparing the pressure calibration. Such pressures are about 0.6 GPa lower than those determined with the in-situ X-ray diffraction experiments [P(GPa) = 8.6 + 0.002T(K), Akimoto et al., 1977]. When the pressures for the β-γ transition determined by Ohtani (1979) are calibrated using the experimental results of Akimoto et al. (1977), they agree with Suito's data. Recently, additional data on the β-γ transition at high temperatures were reported by Sawamoto (1986b) (dot-dashed line labeled as SA(86) in Figure 5.3). The data provided an important constraint on the slope of the β-γ transition boundary. Precise determination of the β-γ transition boundary has been made by Katsura and Ito (1989). Their results are generally consistent with that of Suito (1977) and Sawamoto (1986b). The pressures for decomposition of spinel into perovskite and periclase were determined by Ito and Yamada (1982) (double dot-dashed line labeled as I-Y(82) in Figure 5.3). The pressure calibration at high temperature is based on the pyroxene-ilmenite transition in $ZnSiO_3$ (Akimoto et al., 1977) and decomposition of $MgAl_2O_4$ (Liu, 1980) and γ-Ni_2SiO_4 (Navrotsky et al., 1979) into the constituent oxide mixtures. Recently, Ito and Takahashi (1989) reported a new result on the spinel = perovskite + periclase transformation [P(GPa) = 28.4 - 0.0028T(K)].

After examining the experimental equilibrium data in the system Mg_2SiO_4, the following data were selected for evaluating an internally consistent data set: the α-β transition by Katsura and Ito (1989) and β-γ transition by Katsura and Ito (1989) (1473 - 1873 K) and

by Sawamoto (1986b) (1873 - 2373 K) and, the decomposition of spinel into perovskite and periclase by Ito and Takahashi (1989). This choice of phase equilibrium data in the system Mg_2SiO_4 is also supported by the calorimetric data and the phase equilibrium data in the system $MgSiO_3$ (see discussion below).

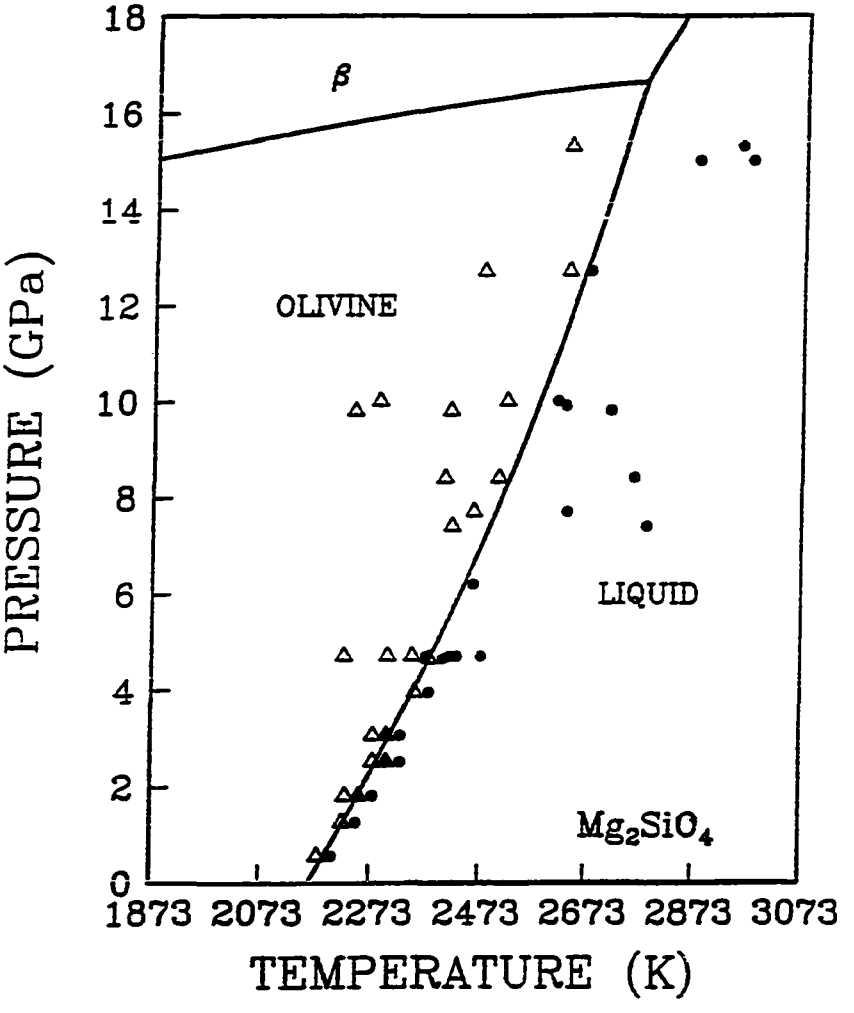

Figure 5.4 Melting curve of Mg_2SiO_4. Solid line is calculated result and symbols represent experimental data. ● (melt) and △ (solid) are from Davis and England (1964) and Ohtani and Kumazawa (1981).

Sumino et al. (1977), Sawamoto et al. (1984) and Weidner et al. (1984) studied the physical properties of the three Mg_2SiO_4 polymorphs. The heat capacity and the thermophysical data of the three Mg_2SiO_4 polymorphs are listed in Tables 5.2 to 5.6. The enthalpy and entropy of olivine are from Saxena and Chatterjee (1986) and Robie et al. (1982). The enthalpies and entropies of β-phase and spinel have been evaluated by accepting the phase transition boundaries in the Mg_2SiO_4 system as determined by Katsura and Ito (1989) and Sawamoto (1986b). The calculated transition parameters (ΔH^o, ΔS^o and ΔV) at 1000 K are found to be consistent with the calorimetric data reported by Akaogi et al. (1984), and by a recent refinement of the enthalpy of the β-γ transition (Akaogi et al., 1989). A systematic comparison of the parameters is shown in Table 5.7. The thermochemical and thermophysical data for periclase are well known (Robie et al., 1978; Suzuki, 1975; Jackson and Niesler, 1982; and Anderson and Zou, 1989). The thermochemical data for perovskite are evaluated from transformation data on decomposition of spinel into perovskite and periclase and on the ilmenite-perovskite transition as determined by Ito and Takahashi (1989). They are consistent with the data set for the $MgSiO_3$ system, see below.

The melting curve of Mg_2SiO_4 was determined by Davis and England (1964) (to pressure of 5 GPa) and recently by Ohtani and Kumazawa (1981) (to pressure of 15 GPa). The entropy of fusion is from Navrotsky et al. (1988) and the initial slope of the fusion curve $[(\partial P/\partial T_m)_{P=0} = 0.0192$ GPa/K] from Davis and England (1964) The molar volume of the melt at zero pressure is calculated by the Clausius-Clapeyron equation, $dP/dT_m = \Delta S_m/\Delta V_m$, where ΔV_m and ΔS_m are the volume and entropy changes on melting. The bulk modulus of the melt and its pressure derivative were calculated to be

43.8 GPa and 6.5 at melting temperature. respectively, from the melting curve (Figure 5.4). Ghiorso and Carmichael (1980)'s enthalpy of fusion (170.2 kJ/mol) is considered to be too high as compared to the value of 114 kJ/mol reported by Navrotsky et al. (1989). If the value of 170.2 kJ/mol were used for the enthalpy of fusion, the calculated bulk modulus would be 54.9 GPa at melting temperature. It is also noted that the change in slope of the melting curve with pressure depends strongly on the pressure derivative of the bulk modulus, especially at very high pressure.

Polymorphism of $MgSiO_3$

The phase relations in $MgSiO_3$ are quite complex. There are six $MgSiO_3$ polymorphs (protoenstatite, orthoenstatite, clinoenstatite, non-cubic garnet, ilmenite and perovskite) and possibly a seventh (cubic garnet). Two-phase regions separate the phase fields of pyroxene and ilmenite in polymorphic transitions. The phase relations among ortho, clino, and protoenstatite are still the subject of considerable controversy. These transitions are difficult to study because the enthalpy, entropy, and volume changes are extremely small and the transitions tend to be sluggish and susceptible to the influence of impurities and shear stresses. From the point of view of high pressure transitions to non-pyroxene phases, the differences among the thermodynamic properties of the pyroxene polymorphs exert only a minimal influence. Accordingly, Fei et al. (1989) have generated a thermodynamic description of a pyroxene based on orthoenstatite as evaluated in the system CaO-MgO-Al_2O_3-SiO_2 by Saxena and Chatterjee (1986). The bulk modulus of orthoenstatite is from Weidner et al. (1978). Heat capacities are from Krupka et al. (1985a,b), supported also by DSC measurements by Ashida et al. (1988). At 173 to 1073 K the difference in heat capacity between ortho and clino-enstatite is

small (Krupka et al., 1985a,b; Haselton, 1979; Watanabe, 1982; Ashida et al., 1988).

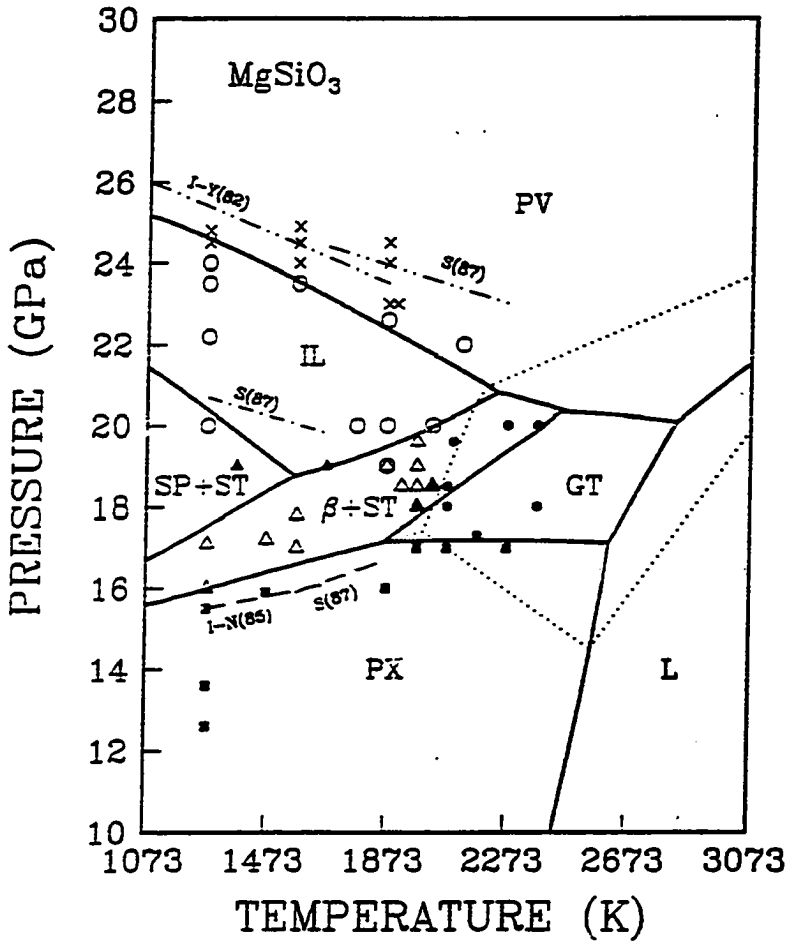

Figure 5.5 Phase relations in $MgSiO_3$ in the pressure range between 10 and 30 GPa: a comparison detween the calculated and the experimental results. Solid lines are calculated phase boundaries. Dotted lines represent the calculated results when the optimized data on garnet are based on phase equilibriun data for the β+ST = GT transformation (see text). Experimental data: Akaogi and Akimoto (1977) (■ PX, △ β+ST); Sawamoto (1987) (■ PX, ● GT, △ β+ST, ○ IL); Ito and Navrotsky (1985) (▲ SP+ST, ○ IL); Ito and Takahashi (1989) (○ IL, × PV); I-N(85) = Ito and Navrotsky (1985); S(87) = Sawamoto (1987); and I-Y(82) = Ito and Yamada (1982). PX = pyroxene, β = β-phase, SP = spinel, ST = stishovite, IL = ilmenite, PV = perovskite, GT = garnet and L = liquid.

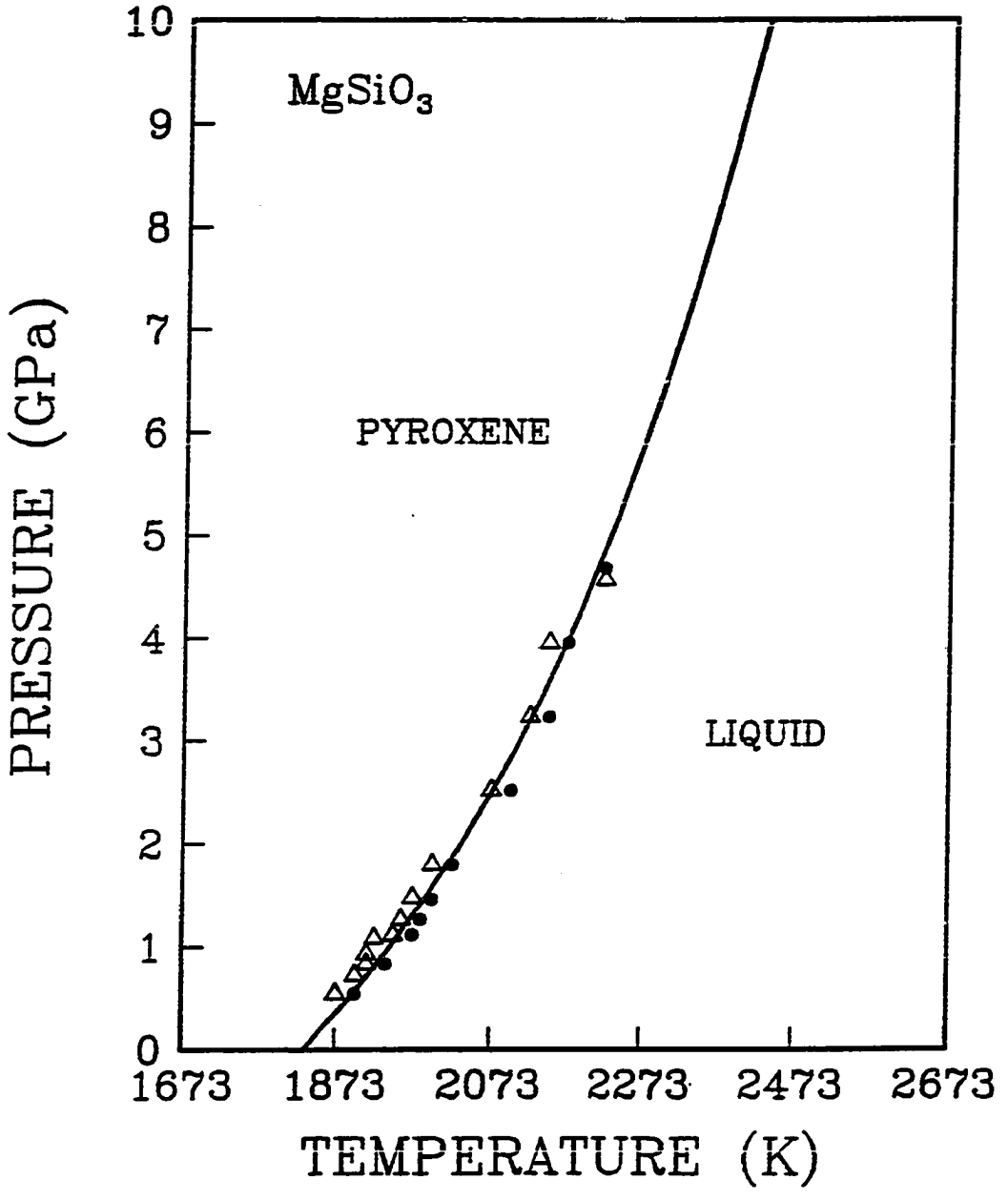

Figure 5.6 Melting curve of $MgSiO_3$. Solid line is calculated result and symbols represent experimental data. ● (melt) and △ (solid) are from Boyd et al. (1964).

The data for pyroxene evaluated above and the data for β-phase and stishovite, which are consistent with the values derived from Mg_2SiO_4 and SiO_2, were used in calculating the transformation boundary for decomposition of pyroxene into β-phase and stishovite. The result agrees with the experimentally determined transformation boundary by Akaogi and Akimoto (1977), Ito and Navrotsky (1985) and Sawamoto (1987) (dashed line labeled as I-N(85) and S(87) in Figure 5.5). Once again, for the present discussion it is unimportant whether the pyroxene is ortho (as suggested by Ito, based on orthopyroxene starting material and a few reversals) or clino, as would be consistent with other high pressure data (Akimoto, 1977; Kato and Kumazawa, 1985 and Kato and Kumazawa, 1986).

The data for garnet are more fragmentary. Recently, Kato and Kumazawa (1985, 1986) reported that garnet phase of $MgSiO_3$ is stable at very high temperature. It is tetragonal, presumably because of ordering of Mg and Si on octahedral sites, but a cubic form may also exist and cubic (majorite) garnet solid solution between $Mg_4Si_4O_{12}$ ($4MgSiO_3$) and $Mg_3Al_2Si_3O_{12}$ (pyrope) are reasonably well documented (Ringwood, 1967; Akaogi and Akimoto, 1977; Liu, 1977; Akaogi et al, 1987). Akaogi et al. (1987) estimated the enthalpy of the pyroxene-cubic garnet transition as 36.5 kJ (per mole $MgSiO_3$) and the bulk modulus of cubic garnet as 154 GPa (assuming $K' = 4.0$) from enthalpies of solution and volume compression along the $Mg_4Si_4O_{12}$-$Mg_3Al_2Si_3O_{12}$ join. Their extrapolated molar volume for cubic garnet is 28.50 cm3/mole ($MgSiO_3$), slightly larger than volumes near 28.1 to 28.2 cm^3/mole for tetragonal garnet (Kato and Kumazawa, 1985, 1986). Because the enthalpy of the cubic-tetragonal transition are unknown, we shall use data for the cubic phase in subsequent calculations. Lacking thermal expansion

data, we assume α the same as for pyrope (Leitner et al., 1980). Heat capacities for $MgSiO_3$ garnet are unavailable. One can either use values estimated from vibrational calculations (see below) or those for pyrope; they are similar. Using the former gives the values for coefficients given in Table 5.3. Kato and Kumazawa (1985) and Sawamoto (1986a) found that at temperatures above 1973 K at approximately 17 GPa, pyroxene transforms directly to garnet. From these data and their enthalpy, Akaogi et al. (1987) calculated ΔS^o (pyroxene = garnet) of -3.65±0.73 J/K mol. This entropy change is a little more negative than our value (ΔS_{1000} = -2.13 J/K.mol) but their calculated phase boundaries are not very different from ours. The unavailability of thermochemical data for tetragonal garnet adds an unknown (but presumably small) uncertainty to these calculations. Some data are available for $MgSiO_3$ ilmenite. The bulk modulus and elasticity have been reported by Weidner and Ito (1985) and heat capacity at 300 - 600 K has been measured by Watanabe (1982). Recently Ashida et al. (1988) have measured heat capacity over a somewhat wider range (160 - 550 K) and the thermal expansion at 295 - 875 K. McMillan and Ross (1987) calculated the entropy and heat capacity at 0 - 1800 K using vibrational models. All these estimates of C_P are in close agreement. We evaluated the enthalpy and entropy of ilmenite from phase equilibrium data for the reaction, spinel + stishovite = ilmenite (Ito and Navrotsky, 1985) and for the ilmenite-perovskite transition by Ito and Takahashi (1989), P(GPa) = 27.5 - 0.0025 T(K), a slightly lower curve than previously determined (Ito and Yamada, 1982). Since the data for ilmenite have to be consistent with both transformations, very little adjustment can be done to the ilmenite data. The calculated enthalpy of the pyroxene-ilmenite transition at 298 K (59.9 kJ/mol) is in good agreement with the new calorimetric value of 59.03±4.26 kJ/mol (Ashida et al., 1988) which revises the earlier prilimenary calorimetric value of 71.8 kJ/mol (Ito and Navrotsky, 1985). Indeed the

calculations identified this discrepancy between earlier calorimetric and phase equilibrium data at the same time as further calorimetric studies independently revised the value of ΔH^o so as to remove the discrepancy.

Data for $MgSiO_3$ perovskite include estimates of compression by X-ray diffraction (Yagi et al., 1982; Kudoh et al., 1987) and from elasticity (Yeganeh-Haeri et al., 1989) and of thermal expansion (Knittle et al., 1986). The reactions ilmenite = perovskite and spinel = perovskite + periclase have been studied by Ito and Yamada (1982) and recently by Ito and Takahashi (1989). Both these transitions appear to have negative P-T slopes. No heat capacity measurements have been reported but see below for an estimate of C_p from vibrational models. Recently Ito, Akaogi and Navrotsky (Navrotsky, pers. comm.) attempted to measure the enthalpy of the perovskite by drop solution calorimetry. They obtained a value of ΔH^o (ilmenite = perovskite) in the range 40 - 60 kJ/mol; the large uncertainty reflecting the presence of significant amounts of other phases in the sample. Vibrational calculations (see Fei et al., 1989) support that the entropy of the ilmenite-perovskite transition is positive, implying a negative dP/dT, but they suggest that ΔS^o may depend quite strongly on temperature. The parameters shown in Tables 5.2 and 5.3 generally satisfy all the above observations.

The melting relations of $MgSiO_3$ at one atmosphere are complicated by incongruent melting. The incongruency disappears with increasing pressure (within the first GPa) (Chen and Presnall, 1975). The enthalpy of fusion has not been measured but an estimate is available (Ghiorso and Carmichael, 1980). The C_p of the liquid has also been estimated (Carmichael et al., 1977). The bulk modulus of the $MgSiO_3$ melt and its pressure derivative are evaluated from the melting curve determined by Boyd et al.

(1964). Although the data evaluated here are only based on melting up to 5 GPa, the calculated melting curve at high pressure also agrees well with experiments up to 9 GPa (Kato and Kumazawa, 1983) (see Figure 5.6).

5.3 System FeO-SiO_2:

Stable iron silcates in this system include fayalite, spinel and orthoferrosillite. β-phase and perovskite are not stable and will be discussed as fictive components in solid solutions.

Polymorphism of Fe_2SiO_4

Fe_2SiO_4, unlike Mg_2SiO_4, directly transforms from olivine (α) to spinel (γ) at high pressure. The transformation has been experimentally studied using the quench technique (Akimoto et al., 1965, 1967) and using the in-situ X-ray diffraction method (Inoue, 1975; Sung and Burns, 1976; and Furnish and Bassett, 1983). Very recently, Yagi et al. (1987) accurately determined the equilibrium phase boundary between 1073 and 1473 K using a cubic anvil type of high-pressure and high temperature X-ray diffraction apparatus combined with synchrotron radiation. The transition pressure P(GPa) = 3.43 + 0.0025T(K). The in-situ observation also provides information on thermal expansion at high pressure. The thermophysical properties, such as molar volume, thermal expansion and bulk modulus, for α-Fe_2SiO_4 and γ-Fe_2SiO_4 have been studied by many geophysicists (e.g. Akimoto et al., 1976; Suzuki et al., 1979, 1981; Sumino, 1979; Marumo et al., 1977; and Sato, 1977). Those data have been used to calculate the volumes at high pressure and high temperature using the equation of state

discussed in Chapter 2. The calculated results are in good agreement with that observed in in-situ X-ray diffraction experiments (Yagi et al., 1987). The thermochemical data, such as enthalpy, entropy and heat capacity, for α-Fe_2SiO_4 are from Robie et al. (1982). Heat capacity for γ-Fe_2SiO_4 was determined by Watanabe (1982). The enthalpy and entropy for γ-Fe_2SiO_4 are evaluated from the phase equilibrium data (Yagi et al., 1987), constrained by the calorimetric data on ΔH^o_{1000} and ΔS^o_{1000} of the α-γ transition as obtained by Akaogi et al. (1989). The calculated boundary is shown in Figure 5.7. The evaluated data on γ-Fe_2SiO_4 along with the data on FeO (wustite) and stishovite are consistent with the experimental data on reaction, γ-Fe_2SiO_4 = FeO (wustite) + SiO_2 (stishovite), determined by Yagi et al. (1979) and Ohtani (1979). β-Fe_2SiO_4 is treated as a fictive component in the ststem. Its thermochemical and thermophysical properties are either extrapolated from limited solution data or estimated by using analogy (Fei and Saxena, 1986). The calorimetric data on ΔH^o_{1000} and ΔS^o_{1000} of the α-β transition as estimated by Akaogi et al. (1989) are used as additional constraints in the calculations.

The melting curve of Fe_2SiO_4 was determined by Akimoto et al. (1967) (to pressure of 8 GPa) and by Ohtani (1979) (to pressure of 20 GPa). The entropy of fusion and C_P of liquid are from Ghiorso and Carmichael (1980).The bulk modulus and its pressure derivative of Fe_2SiO_4 melt are derived from the melting curve.

Polymorphism of $FeSiO_3$

Perovskite, garnet (cubic and non-cubic) and ilmenite in $FeSiO_3$ are not stable and can

be treated as fictive components. Garnet and ilmenite in $FeSiO_3$ are not considered in this study because of the small iron solubility in both garnet and ilmenite solutions and because of lack of thermochemical and thermophysical data on these fictive components. The data on Fe-perovskite are estimated from limited solution data and from analog with other related phases (Fei and Saxena, 1986).

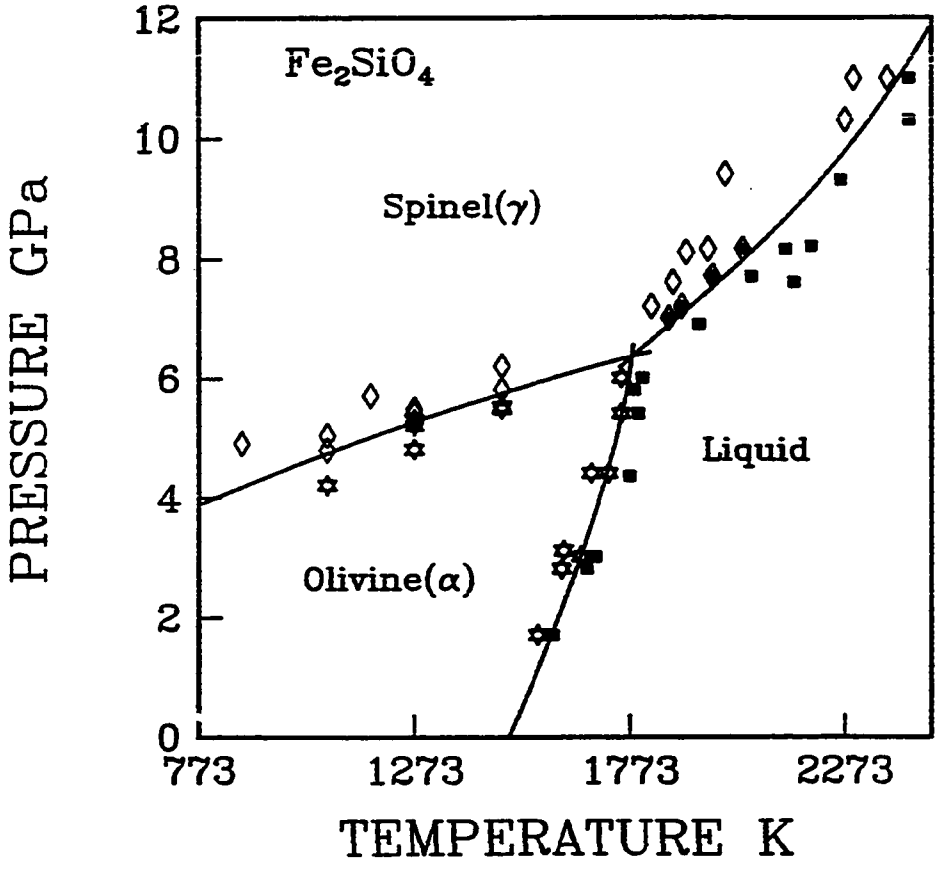

Figure 5.7 Phase relations in Fe_2SiO_4. Solid lines are calculated phase boundaries. Experimental data on the olivine - spinel transition are from Yagi et al. (1987) (olivine and spinel). The equilibrium data on melting are from Akimoto et al. (1967) and Ohtani (1979) (olivine, spinel and melt).

For ferrosillite ($FeSiO_3$), the data are based on the data of orthoferrosillite (Bohlen and Boettcher,1981; Syono et al., 1971; and Akimoto, 1972). These data alongy with the data on spinel (Fe_2SiO_4) and stishovite evaluated from the systems Fe_2SiO_4 and SiO_2 are consistent with the experimental data on reaction, $2FeSiO_3$ (ferrosillite) = Fe_2SiO_4 (spinel) + SiO_2 (stishovite), determined by Akimoto and Syno (1970).

5.4 System MgO-FeO-SiO$_2$

There are seven possible solid solutions, (Mg,Fe)O (magnesiowustite), $(Mg,Fe)_2SiO_4$ (olivine, β-phase, spinel) and $(Mg,Fe)SiO_3$ (pyroxene, ilmenite, perovskite), in the system. For the magnesiowustite solid solution, MgO (periclase) may be chosen to mix as a third component with FeO and $FeO_{1.5}$. However, both experiments (Simons, 1980) and thermodynamic calculation (Fei and Saxena, 1986) indicate that the stoichiometric FeO composition is approached closely above 5 GPa. Therefore, the magnesiowustite solid solution is simply treated as a binary solution with endmembers, MgO and stoichiometric FeO, in all high pressure equilibrium calculations.

The solution properties may be derived from three types of experimental data: (1) direct measurements of mixing properties, such as mixing volume and mixing enthalpy, (2) element distribution between coexisting phases, and (3) phase equilibrium data.

As discussed in Chapter 2, the solution properties may be represented by interaction energy parameters, W_{ij}, in Margules model. The W_{ij} parameters are considered to be a function of pressure and temperature (Equation 2.26). W^H_{ij} represents the excess

enthalpy contribution to the interaction energy W_{ij} and may be directly determined by solution calorimetry. Wood and Kleppa (1981) measured the enthalpies of solution of Mg_2SiO_4-Fe_2SiO_4 olivine solid solutions in $Pb_2B_2O_5$ melt at 970 K. The data were fitted with the Margules formulation with $W^H_{Mg\text{-}Fe}$ and $W^H_{Fe\text{-}Mg}$ of 8.4 and 4.2 kJ/mol respectively. Recently, Akaogi et al. (1989) measured the enthalpies of solution of Mg_2SiO_4-Fe_2SiO_4 spinel solid solutions. The spinel solid solution showed a positive deviation from ideal mixing and can be fitted with a symmetric model with W^H of 3.9 kJ/mol.

The excess volume contribution (W^V_{ij}) to the interaction energy W_{ij} may be independently derived from measurements of mixing volumes of the solution. However, the excess volume in solid solutions generally is very small and may not be detected in most cases because it is less than the uncertainties in experiments. An alternative way to determine such contribution is to determine activity-composition relationships over a wide pressure range and to fit the excess free energy as a function of pressure (see discussion below).

The excess entropy cannot be directly measured by experiments, but may be derived either from the difference between the measured excess enthalpy and the excess free energy obtained from activity-composition determinations or from the excess free energies obtained from activity-composition relationships at various temperatures.

To establish the temperature and pressure dependences of the W_{ij} parameters of the solid solutions, one has to know activity-composition relations at various temperature and pressure conditions. The activity-composition relations may be established from

determination of element distribution between coexisting minerals, as discussed in Chapter 2. Nafziger and Muan (1967) determined the Mg-Fe distribution between coexisting magnesiowustite and olivine at 1473 K and 1 bar. In this study the Mg-Fe distributions have been determined over a temperature range of 1473 - 1723 K and pressure up to 9 GPa (Chapter 4). The Mg-Fe distribution between coexisting magnesiowustite and silicate spinel was studied by Yagi et al. (1979) using the diamond-anvil cell technique and by Ito (1984) and Ito et al. (1984) using the multi-anvil device. The Mg-Fe distributions between coexisting magnesiowustite and b-phase at Mg-rich side ($X^{\beta}_{Fe} < 0.25$) and between coexisting magnesiowustite and silicate spinel at $X^{Sp}_{Fe} > 0.25$ have been determined at temperature of 1773 K and pressure of 15 GPa in this study (see Chapter 4). Perovskite forms limited solid solution with some maximum content of $FeSiO_3$. Ito (1984), Ito et al. (1984) and Yagi et al. (1979) determined the compositions of coexisting magnesiowustite and perovskite. The data obtained by the diamond-anvil cell technique (Yagi et al., 1979) and by multi-anvil device (Ito, 1984) are consistent in Mg-Fe distribution, but different in the maximum solubility of $FeSiO_3$ in perovskite. The data of Ito (1984) showed that the maximum solubility of $FeSiO_3$ in perovskite is about 10 mole percent and increases slightly with increasing temperature. Similarly Yagi et al. (1979) made the important observation that at high pressure up to 70 GPa the solubility of $FeSiO_3$ does not exceed 20 mole percent. Recently, Guyot et al. (1988) also concluded that pressure does not significantly affect the Mg-Fe distribution. Silimar results are obtained in this study (see Chapter 4). These data provide important constraints on the thermochemical properties of Fe-perovskite.

All the Mg-Fe distribution data discussed above have been used to determine solid solution properties of magnesiowustite, olivine, β–phase, spinel and perovskite solid

solutions. Note that magnesiowustite is a common solid solution for all the determined Mg-Fe distribution data. Simultaneously fitting these data with the Margules formulation provide a set of consistent solution parameters. The optimized results are shown in Table 5.6. In the optimization procedure the solution calorimetric data for olivine and spinel solid solution have been taken into consideration. The optimized W_{ij} parameters for olivine solid solution are also consistent with those evaluated from olivine-pyroxene and olivine-garnet equilibria (Chatterjee, 1987). Various calculated Roozeboom diagrams for the exchange of Mg^{2+} and Fe^{2+} between coexisting solid solutions are shown in Figures 5.8, 5.9, 5.10 and 5.11.

Phase equilibrium relations in a binary system provide independent information on solid solution properties. In the system Mg_2SiO_4-Fe_2SiO_4, Akimoto and Fujisawa (1968) determined the phase equilibrium relations in an Fe-rich region up to $(Mg_{0.73}Fe_{0.27})_2SiO_4$. The complete phase diagrams in the system were determined by Kawada (1977) at temperatures of 1073, 1273 and 1473 K and presented by Akimoto (1987) with revised pressure calibration. Recently, Katsura and Ito (1989) determined the phase digrams in a Mg-rich region up to $(Mg_{0.45}Fe_{0.55})_2SiO_4$ at temperatures of 1473 and 1873 K. With increasing pressure, $(Mg,Fe)_2SiO_4$ spinel breaks down into perovskite and magnesiowustite in a Mg-rich region and into magnesiowustite and stishovite in an Fe-rich region. The phase diagrams were first proposed by Yagi et al. (1979) based on the experiments with diamond-anvil cell technique and recently determined by Ito and Takahashi (1989) in a Mg-rich region up to $(Mg_{0.4}Fe_{0.6})_2SiO_4$ at temperatures of 1373 and 1873 K. These phase diagrams may be used either to derive solution parameters or to compare with those calculated from evaluated thermodynamic data (see Chapter 6 for discussion).

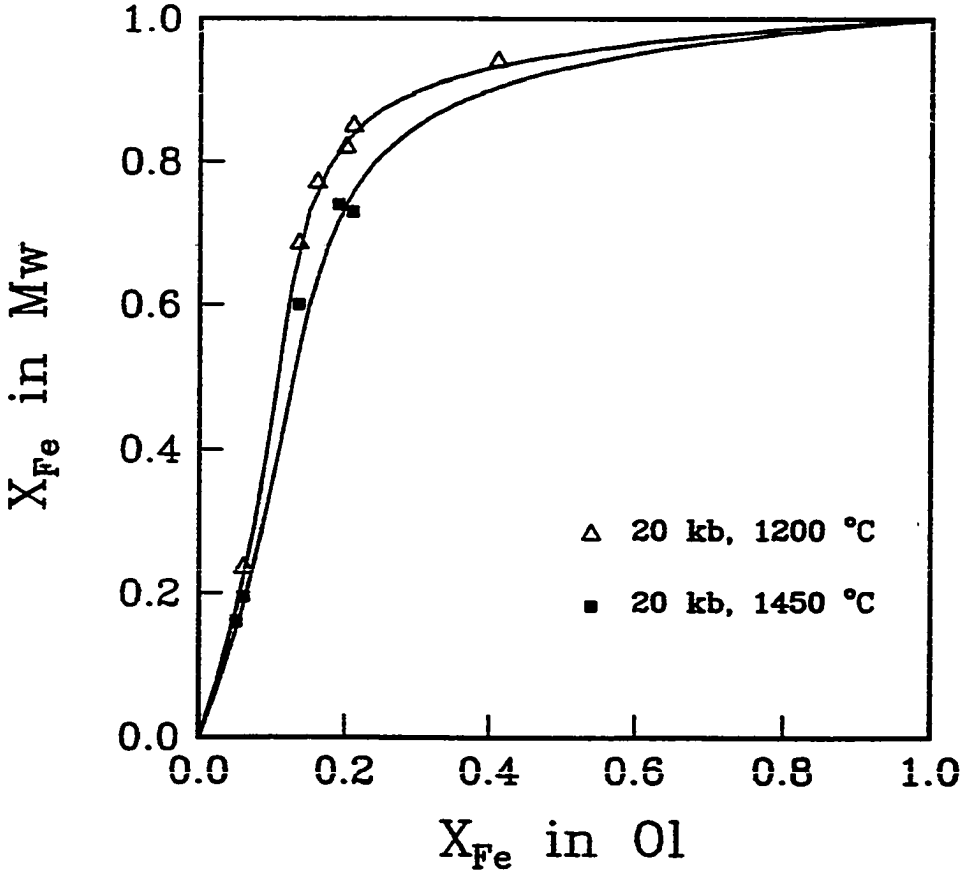

Figure 5.8a Distribution of Mg and Fe between coexisting magnesiowustite (Mw) and olivine (Ol) at a pressure of 20 kbar and at temperatures of 1200 °C (upper curve) and 1450 °C (lower curve). Experimental data are from this study (see Chapter 4).

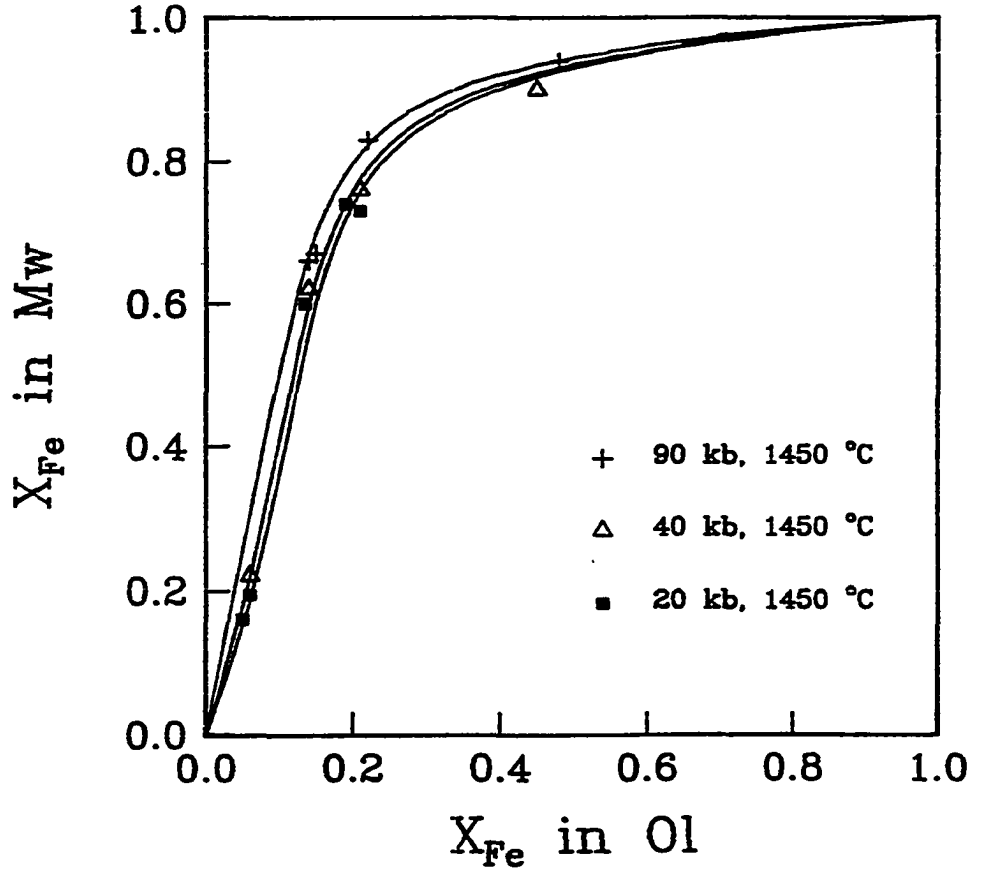

Figure 5.8b Distribution of Mg and Fe between coexisting magnesiowustite (Mw) and olivine (Ol) at a temperatures of 1450 °C and at pressures of 20 kbar (lower curve), 40 kbar (middle curve) and 90 kbar (upper curve). Experimental data are from this study (see Chapter 4).

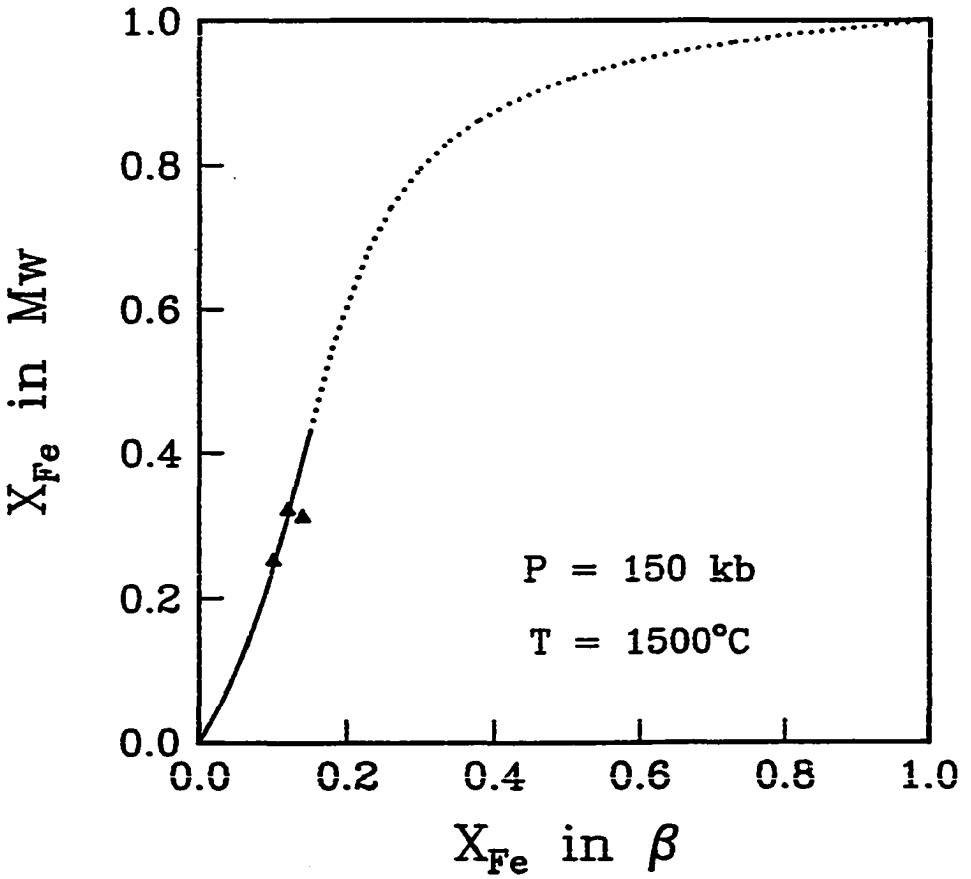

Figure 5.9 **Distribution of Mg and Fe between coexisting magnesiowustite (Mw) and β-phase (β) at pressure of 150 kbar and at temperature of 1500 °C. Experimental data are from this study (see Chapter 4).**

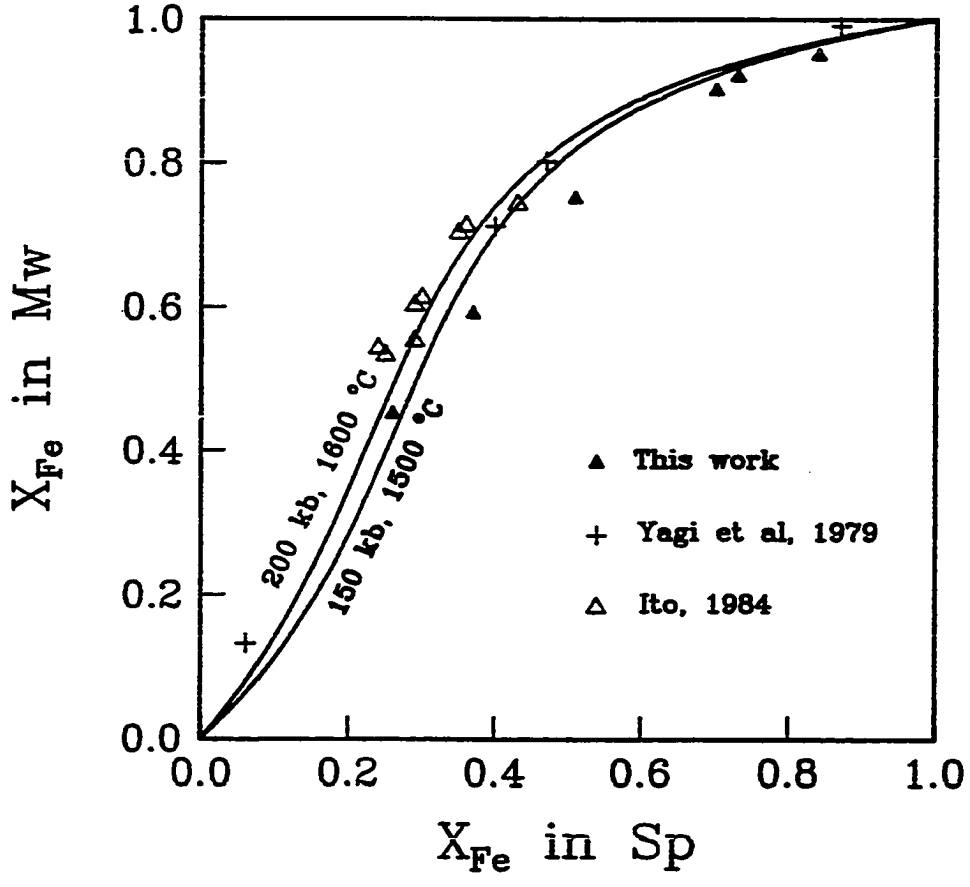

Figure 5.10 Distribution of Mg and Fe between coexisting magnesiowustite (Mw) and spinel (Sp) at temperature of 1500 °C and pressure of 150 kbar (lower curve), and at temperature of 1600 °C and pressure of 200 kbar (upper curve). Experimental data are from this study (see Chapter 4), Ito et al. (1984) and Yagi et al. (1979).

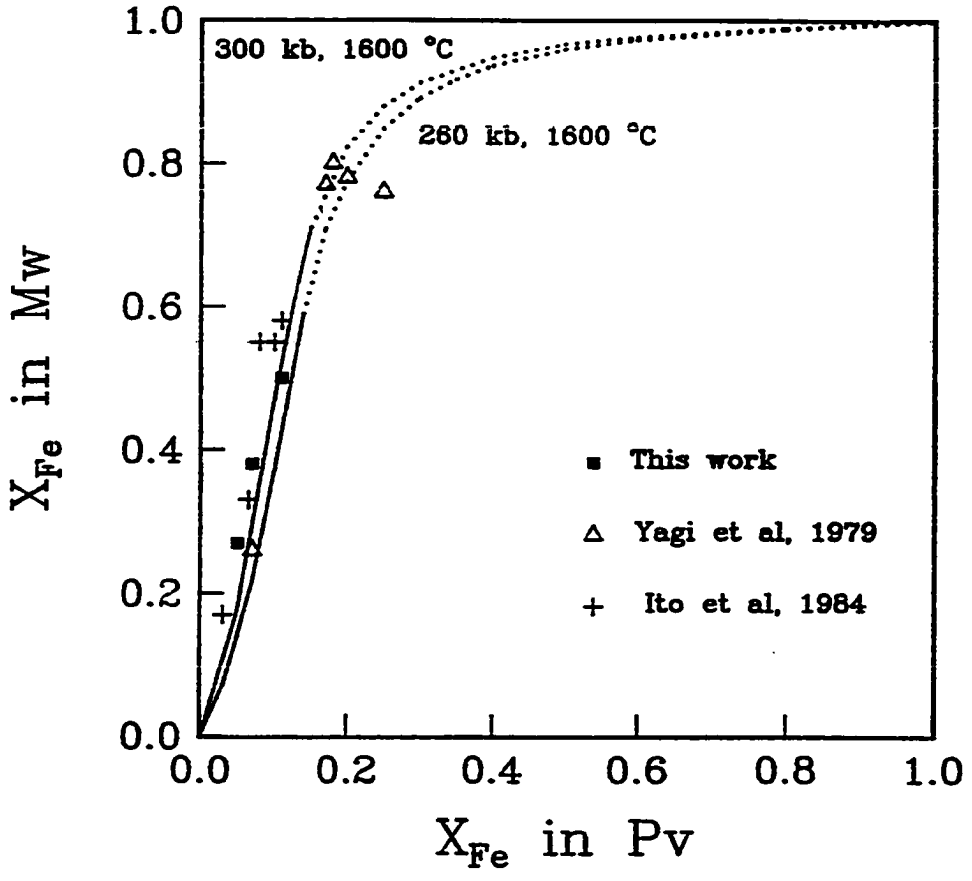

Figure 5.11 Distribution of Mg and Fe between coexisting magnesiowustite (Mw) and perovskite (Pv) at a temperature of 1600 °C and pressures of 260 kbar (lower curve), and 300 kbar (upper curve). Experimental data are from this study (see Chapter 4), Ito et al. (1984) and Yagi et al. (1979).

5.5 Discussion

The present data set (Tables 5.2 to 5.6) has been critically evaluated by performing a global optimization in which all the phase equilibrium data of possible reactions in the system (Table 5.1) have been considered and the enthalpies and entropies of reacting phases have been optimized by taking the reported uncertainties of experimental data as lower and upper limits of the optimizing parameters. Details of the optimization technique have been discussed in Chapter 3. The method of minimizing the total Gibbs free energy of a chosen system, as discussed in Chapter 3, is used to calculate the phase relations.

It is perhaps remarkable, given the wide range of data used and their rather large uncertainties, that one set of thermochemical and thermophysical parameters can be found which satisfy, at least in a general sense, the phase equilibria, calorimetry, and vibrational calculations. Although there are still considerable uncertainties, especially in parameters for the Mg-garnet, Mg-perovskite, and fictive components (β-Fe_2SiO_4 and $FeSiO_3$ perovskite), the phase relations in the system are constrained. Most experimental phase equilibrium data are reproduced as shown in Figures 5.1 to 5.11.

Phase equilibrium data included in this study cover wide range of pressure (up to 30 GPa) and temperature (up to 2473 K). The contribution of $\int VdP$ to Gibbs free energy is large at high pressure and one must know the volume at simultaneous high P and T. Therefore, the use of a suitable equation of state for solids at high pressure and temperature is necessary for the phase equilibrium calculation. Experimental data on molar volume are generally available either at high pressure and room temperature or at high temperature and 1 atm. The method of exptrapolation of the existing data to high

P-T space is still controversial. In this study we have adopted the Birch-Murnaghan equation of state where the temperature dependence of the isothermal bulk modulus is included (see Chapter 2). Unfortunately, data on the temperature dependence of isothermal bulk modulus are generally not available for most high pressure phases. The data for β-phase, spinel, ilmenite and perovskite were optimized through phase equilibrium relation. An optimized $(\partial K_T/\partial T)_P$ value of -0.055 GPa/K, for perovskite agrees with that predicted by self-consistent quasiharmonic lattice dynamics (Wolf and Bukowinski, 1987).

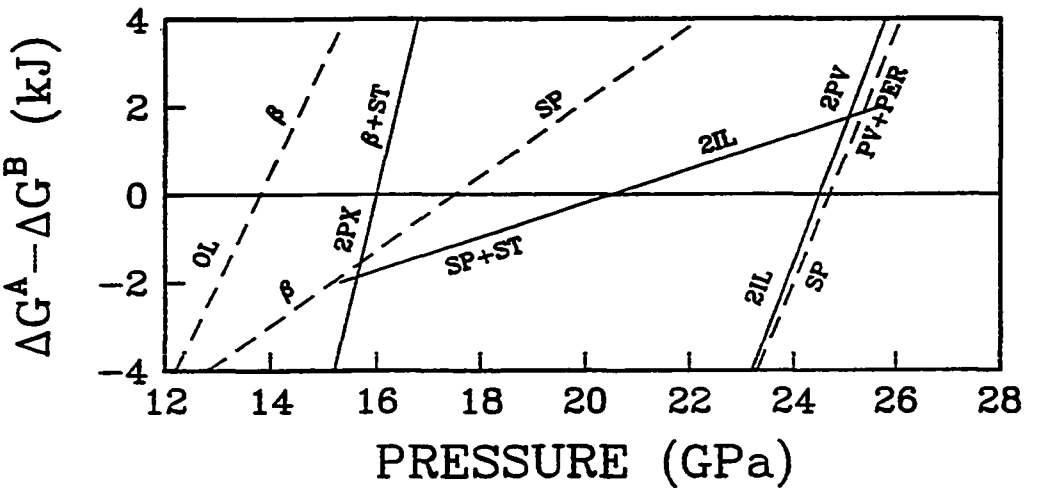

Figure 5.12 Effect of ±4 kJ/mol in ΔG_{1273} of transition on phase transition pressure at temperature of 1273 K. Phase transitions in the systems $MgSiO_3$ and Mg_2SiO_4 are represented by solid and dashed lines, respectively. The phase phase transitions are OL = β, β = SP, SP = PV + PER, 2PX = β + ST, SP +ST = 2IL, and 2IL = 2PV, where the left side of the reactions is defined as A and the right side as B. The abbreviations are same as in Figures 5.3 and 5.5.

Anderson and Zou (1989) have shown that K_T (at atmospheric pressure) for MgO changes from 161 GPa at 300 K to 110 GPa at 2000 K, with an average value of -0.030 GPa/K. The optimized values for β-phase, spinel, ilmenite, and perovskite generally fall in a comparable range. Anderson and Zou (1989) also point out that the product αK_T is approximately constant for MgO as a function of temperature. It is found, from the optimization, that the largest magnitude of $(\partial K_T/\partial T)_P$ is for phases with high bulk modulus and high thermal expansion.

Some discussion is appropriate of the effect of uncertainties in calculated value of ΔG° on the calculated phase equilibria. Figure 5.12 shows the effect of ±4 kJ/mol uncertainty in ΔG°_{1273} of transition on phase transition pressure at a temperature of 1273 K in the Mg_2SiO_4 and $MgSiO_3$ systems. Because the pressure-temperature field, especially in the $MgSiO_3$ system (Figure 5.5), is divided into many fields of stable assemblages, the margin for error in ΔG° values for individual phases is small and the system is well constrained. If one changes the ΔG° of a phase by more than 300 J/mol, the calculated stability fields of several related minerals can be completely upset. For example, if the enthalpy of garnet is decreased by 350 J/mol, the garnet phase will be calculated to form directly from pyroxene at 1273 K. Decrease of about 1000 J/mol in ΔH°_{298} of ilmenite would eliminate the two-phase region between enstatite and ilmenite; and an increase of about 1000 J/mol would totally eliminate the ilmenite stability field between spinel plus stishovite and perovskite (Figure 5.12). Thus we conclude that the calculated free energies of transition are generally constrained to ±500 J/mol or better. The uncertainties in ΔG° are difficult to attribute to uncertainties in individual thermochemical and thermophysical parameters unless one has compelling specific evidence. Data evaluated

both from phase equilibrium reactions and from calorimetric measurements generally are within the limits of the calorimetric data as listed in Table 5.7. In the systems Mg_2SiO_4 and $MgSiO_3$ several phases, β-phase, spinel and perovskite, are common. Therefore, data on β-phase have to be evaluated by simultaneously fitting the phase equilibrium data of the α-β and β-γ transitions in Mg_2SiO_4 and the pyroxene = β + stishovite transition in $MgSiO_3$. Since data on stishovite, pyroxene and olivine (α) are well established from other systems (Fei and Saxena, 1986 and Saxena and Chatterjee, 1986), evaluated data on β-phase are tightly constrained in such global optimization. Similar considerations apply to evaluation of data for perovskite and ilmenite. From the derived data for perovskite and ilmenite we may closely reproduce the phase equilibrium relations of the spinel + stishovite = ilmenite, ilmenite = perovskite and spinel = perovskite + periclase reactions. The Gibbs free energy for ilmenite evaluated from phase equilibrium data is more negative than that calculated from lattice vibrational model. If the entropy and heat capacity of ilmenite calculated from vibrational model were used, ilmenite stability field would be eliminated from the $MgSiO_3$ phase diagram. Therefore, the thermochemical and thermophysical data set derived here is generally adequate for calculating phase equilibria with uncertainties of 0.5 GPa or so in the location of phase boundaries.

Table 5.1 Summary of reactions in the Mg-Fe-Si-O system

Reactions	*References*
1. Fe (*bcc*) = Fe (*fcc*)	Bundy (1965)
2. Fe (*bcc*) = Fe (*hcp*)	Bundy (1965)
3. Fe (*fcc*) = Fe (*hcp*)	Bundy (1965)
4. $4\{FeO\} + O_2 = 4\{FeO_{1.5}\}$	Kubaschewski (1982)
5. $5\{FeO\} + O_2 = 2\{FeO_{1.5}\} + Fe_3O_4$	Kubaschewski (1982)
6. $7\{FeO\} + O_2 = 6\{FeO_{1.5}\} + Fe$	Kubaschewski (1982)
7. Fe_3O_4 (*mgt*) = Fe_3O_4 (*high-pressure mgt*)	Mao et al. (1974) Huang and Bassett (1986)
8. Fe_2O_3 (*hmt*) = Fe_2O_3 (*high-pressure hmt*)	Mao and Bell (1977)
9. SiO_2 (*qz*) = SiO_2 (*coe*)	Bohlen and Boettcher (1982)
10. SiO_2 (*coe*) = SiO_2 (*st*)	Yagi and Akimoto (1976)
11. Mg_2SiO_4 (α) = Mg_2SiO_4 (β)	Katsura and Ito (1989) Fukizawa (1982) Suito (1977)
12. Mg_2SiO_4 (β) = Mg_2SiO_4 (γ)	Katsura and Ito (1989) Sawamoto (1986) Ohtani (1979) Suito (1977)
13. Mg_2SiO_4 (γ) = $MgSiO_3$ (*pv*) + MgO (*per*)	Ito and Takahashi (1989) Ito and Yamada (1982)
14. Mg_2SiO_4 (α) = Mg_2SiO_4 (*melt*)	Davis and England (1964) Ohtani and Kumazawa(1981)
15. $2MgSiO_3$ (*px*) = Mg_2SiO_4 (β) + SiO_2 (*st*)	Akaogi and Akimoto (1977) Sawamoto (1987) Ito and Navrotsky (1985)
16. $MgSiO_3$ (*px*) = $MgSiO_3$ (*gt*)	Sawamoto (1987)

17. $2MgSiO_3$ (*gt*) = Mg_2SiO_4 (β) + SiO_2 (*st*)	Sawamoto (1987)
18. $2MgSiO_3$ (*il*) = Mg_2SiO_4 (γ) + SiO_2 (*st*)	Ito and Navrotsky (1985)
19. $MgSiO_3$ (*il*) = $MgSiO_3$ (*pv*)	Ito and Takahashi (1989) Ito and Yamada (1982) Sawamoto (1987)
20. $MgSiO_3$ (*px*) = $MgSiO_3$ (*melt*)	Boyd et al. (1964) Kato and Kumazawa (1983)
21. Fe_2SiO_4 (α) = Fe_2SiO_4 (γ)	Yagi et al. (1987) Akimoto et al. (1965, 1967)
22. $2FeSiO_3$ (*px*) = Fe_2SiO_4 (γ) + SiO_2 (*st*)	Akimoto and Syno (1970)
23. Fe_2SiO_4 (γ) = FeO (mw) + SiO2 (st)	Yagi et al. (1979) Ohtani (1979)
24. $(Mg,Fe)_2SiO_4$ (α) = $(Mg,Fe)_2SiO_4$ (γ)	Akimoto and Fujisawa(1968) Kawada (1977) Akimoto (1987)
25. $(Mg,Fe)_2SiO_4$ (α) = $(Mg,Fe)_2SiO_4$ (β)	Katsura and Ito (1989) Akimoto (1987)
26. $(Mg,Fe)_2SiO_4$ (β) = $(Mg,Fe)_2SiO_4$ (γ)	Katsura and Ito (1989) Akimoto (1987)
27. $(Mg,Fe)_2SiO_4$ (γ) = $(Mg,Fe)SiO_3$ (*pv*) + (Mg,Fe)O	Ito and Takahashi (1989)
28. $(Mg,Fe)_2SiO_4$ (γ) = 2(Mg,Fe)O (*mw*) + SiO2 (*st*)	Ito and Takahashi (1989)
29. $(Mg,Fe)SiO_3$ (*pv*) = (Mg,Fe)O (*mw*) + SiO2 (*st*)	Ito and Takahashi (1989)
30. Mg-α + Fe-*mw* = Mg-*mw* + Fe-α	This study Nafziger and Muan (1967)
31. Mg-β + Fe-*mw* = Mg-*mw* + Fe-β	This study
32. Mg-γ + Fe-*mw* = Mg-*mw* + Fe-γ	This study Ito (1984) Yagi et al. (1979)

33. Mg-*pv* + Fe-*mw* = Mg-*mw* + Fe-*pv*	This study Ito (1984) Yagi et al. (1979)
34. Mg-α + Fe-*px* = Mg-*px* + Fe-α	Matsui and Nishizawa (1974)
35. Fe_2SiO_4 (α) + SiO_2 (*qz*) = $2FeSiO_3$ (*px*)	Lindsley et al. (1964)
36. $(Mg,Fe)_2SiO_4$ (α) + SiO_2 (*qz*) = $2(Mg,Fe)SiO_3$ (*px*)	Bohlen and Boettcher (1981)

Abbreviations: mgt = magnetite, hmt = hematite, qz = quartz, coe = coesite, st = stishovite, α = olivine, β = β-phase, γ = spinel, pv = perovskite, per = periclase, px = pyroxene, gt = garnet, il = ilmenite, and mw = magnesiowustite.

Table 5.2 Data on standard enthalpy and entropy of formation from elements at 298.15 K for phases in the Mg-Fe-Si-O system

Phases	$\Delta H°_{298}$ J/mol	$\Delta S°_{298}$ J/mol·K	References
1. O_2(oxygen)	0	205.150	Robie et al. (1978)
2. 1/2$Mg_2SiO_4(\alpha)$	-1087160	47.055	Robie et al. (1982)
3. 1/2$Fe_2SiO_4(\alpha)$	-739085	75.500	Robie et al. (1982)
4. 1/2$Mg_2SiO_4(\beta)$	-1070600	45.862	Fei et al. (1989)
5. 1/2$Fe_2SiO_4(\beta)$	-734000	70.900	Akaogi et al. (1989)
6. 1/2$Mg_2SiO_4(\gamma)$	-1065600	44.010	Fei et al. (1989)
7. 1/2$Fe_2SiO_4(\gamma)$	-735750	70.516	Akaogi et al. (1989)
8. $MgSiO_3$(px)	-1545552	66.170	Brousse et al. (1984)
9. $FeSiO_3$(px)	-1195200	94.560	Chatterjee (1987)
10. $MgSiO_3$(pv)	-1442500	63.577	Fei et al. (1989)
11. $FeSiO_3$(pv)	-1090100	100.770	see text
12. MgO(mw)	-601490	26.940	Robie et al. (1978)
13. FeO(mw)	-267270	57.590	Fei and Saxena (1986)
14. $FeO_{1.5}$(mw)	-380900	54.900	Fei and Saxena (1986)
15. Fe(bcc)	0	27.280	Robie et al. (1978)
16. Fe(fcc)	9476	37.570	see text
17. Fe(hcp)	6200	31.310	see text
18. 1/4Fe_3O_4(mgt)	-278887	37.660	Haas (1984)
19. 1/4Fe_3O_4(hp mgt)	-236500	45.000	Fei and Saxena (1986)
20. 1/2Fe_2O_3(hmt)	-412391	43.700	Haas (1984)
21. 1/2Fe_2O_3(hp hmt)	-374600	43.700	Fei and Saxena (1986)
22. SiO_2(qz)	-910700	41.460	Robie et al. (1978)
23. SiO_2(coe)	-907771	38.730	Fei and Saxena (1986)
24. SiO_2(st)	-858818	34.380	Fei and Saxena (1986)

25. $MgSiO_3$(il)	-1485700	60.371	Fei et al. (1989)
26. $MgSiO_3$(gt)	-1510400	64.180	Fei et al. (1989)
27. 1/2Mg_2SiO_4(melt)	-1030160	73.405	Navrotsky et al. (1989)
28. 1/2Fe_2SiO_4(melt)	-692998	106.430	see text
29. $MgSiO_3$(melt)	-1463646	110.880	see text

NOTE: The abbreviations are same as in Table 5.1.

Table 5.3 Data on heat capacity of phases in the Mg-Fe-Si-O system

Phases	$C_P = a + bT + cT^{-2} + eT^{-3} + gT^{-1}$ a	b	c	e	g
1. O_2(oxygen)	39.450	5.6090E-4	9.0670E+5	6.0390E+05	-6.1010E+3
2. 1/2Mg_2SiO_4(α)	83.496	7.8185E-3	-5.5745E+6	8.8266E+08	9.6193E+2
3. 1/2Fe_2SiO_4(α)	83.498	1.3559E-2	-6.5624E+5	-1.2827E+08	-2.7808E+3
4. 1/2Mg_2SiO_4(β)	84.268	6.5380E-3	8.8230E+4	-3.1137E+08	-6.1128E+3
5. 1/2Fe_2SiO_4(β)	84.391	1.2017E-2	-8.5874E+6	1.5766E+09	5.2759E+3
6. 1/2Mg_2SiO_4(γ)	84.751	5.8540E-3	3.3038E+6	-9.4132E+08	-1.0453E+4
7. 1/2Fe_2SiO_4(γ)	85.609	1.3559E-2	-3.2322E+6	5.6422E+08	-2.7355E+3
8. $MgSiO_3$(px)	126.665	1.9414E-3	-6.2505E+6	8.5349E+08	-2.2049E+3
9. $FeSiO_3$(px)	131.890	6.2140E-5	-4.9470E+6	1.4250E+07	2.3190E+2
10. $MgSiO_3$(pv)	125.080	6.3329E-3	-7.3634E+6	9.1187E+08	8.4838E+2
11. $FeSiO_3$(pv)	142.210	1.5410E-3	-1.1860E+6	2.7440E+08	-1.4540E+4
12. MgO(mw)	49.654	3.8410E-3	-1.3898E+6	1.2720E+08	-7.9166E+2
13. FeO(mw)	68.435	1.1940E-3	1.6970E+6	1.3480E+08	-1.1880E+4
14. $FeO_{1.5}$(mw)	39.874	4.6440E-2	-1.6420E+6	1.4020E+08	3.5750E+3
(955 K, 335 J/mol)	-69.915	7.2450E-2	7.8240E+7	-7.2840E+06	-1.7580E+2
(1250 K, 0 J/mol)	197.400	4.3230E-2	6.1970E+7	2.4040E+11	-4.3270E+5
15. Fe(bcc)	-28.567	5.3340E-2	-5.8930E+6	4.7540E+08	2.5630E+4
(800 K, 499 J/mol)	-248.280	2.4920E-1	6.6090E+7	-5.0110E+08	-1.2310E+4
(1000 K, 0 J/mol)	-639.740	6.9540E-1	6.6700E+5	-8.3700E+07	-1.8640E+3
(1042 K, 0 J/mol)	1917.200	-1.7750E+0	-8.4950E+6	1.0430E+09	2.4370E+4
(1060 K, 0 J/mol)	-553.630	3.3200E-1	2.9300E+8	-2.2360E+08	-4.7740E+3
(1184 K, 899 J/mol)	23.819	8.4160E-3	-7.2950E+4	1.0050E+07	1.7860E+2
(1665 K, 836 J/mol)	52.121	3.2840E-3	4.8000E+6	8.4260E+09	-3.3290E+4
16. Fe(fcc)	41.357	1.0540E-3	1.5470E+6	5.2260E+07	-1.0720E+4
17. Fe(hcp)	-28.567	5.3340E-2	-5.8930E+6	4.7540E+08	2.5630E+4
(800 K, 499 J/mol)	41.357	1.0540E-3	1.5470E+6	5.2260E+07	-1.0720E+4
18. 1/4Fe_3O_4(mgt)	18.343	5.6670E-2	2.3840E+5	1.7470E+06	3.8690E+1
(848 K, 391 J/mol)	-2.828	2.4510E-2	3.1140E+7	1.8610E+07	3.8340E+2

	(1300 K, 0 J/mol)	86.812	1.5820E-2	1.9740E+7	8.8960E+10	-1.4480E+5
19.	1/4Fe_3O_4(hp mgt)	18.343	5.6670E-2	2.3840E+5	1.7470E+06	3.8690E+1
	(848 K, 391 J/mol)	-2.828	2.4510E-2	3.1140E+7	1.8610E+07	3.8340E+2
	(1300 K, 0 J/mol)	86.812	1.5820E-2	1.9740E+7	8.8960E+10	-1.4480E+5
20.	1/2Fe_2O_3(hmt)	39.874	4.6440E-2	-1.6420E+6	1.4020E+08	3.5750E+3
	(955 K, 335 J/mol)	-69.915	7.2450E-2	7.8240E+7	-7.2840E+06	-1.7580E+2
	(1250 K, 0 J/mol)	197.400	4.3230E-2	6.1970E+7	2.4040E+11	-4.3270E+5
21.	1/2Fe_2O_3(hp hmt)	39.874	4.6440E-2	-1.6420E+6	1.4020E+08	3.5750E+3
	(955 K, 335 J/mol)	-69.915	7.2450E-2	7.8240E+7	-7.2840E+06	-1.7580E+2
	(1250 K, 0 J/mol)	197.400	4.3230E-2	6.1970E+7	2.4040E+11	-4.3270E+5
22.	SiO_2(qz)	101.490	2.7820E-3	4.3530E+6	-1.9130E+08	-2.9610E+4
	(848 K, 476 J/mol)	78.812	1.2050E-3	1.7310E+6	1.2020E+08	-1.2130E+4
23.	SiO_2(coe)	74.428	8.1500E-4	-7.4182E+6	1.3073E+09	1.4606E+3
24.	SiO_2(st)	65.535	9.5711E-3	-5.2702E+6	7.7873E+08	1.0674E+3
25.	$MgSiO_3$(il)	90.412	1.9401E-2	7.7246E+6	-2.7890E+09	-4.3397E+2
26.	$MgSiO_3$(gt)	126.741	2.3338E-3	-6.3302E+6	8.6451E+08	-2.3030E+3
27.	1/2Mg_2SiO_4(melt)	83.496	7.8185E-3	-5.5745E+6	8.8266E+08	9.6193E+2
	(2163 K, 0 J/mol)	133.950	0.0000E+0	0.0000E+0	0.0000E+00	0.0000E+0
28.	1/2Fe_2SiO_4(melt)	83.498	1.3559E-2	-6.5624E+5	-1.2827E+08	-2.7808E+3
	(1490 K, 0 J/mol)	119.872	0.0000E+0	0.0000E+0	0.0000E+00	0.0000E+0
29.	$MgSiO_3$(melt)	126.665	1.9414E-3	-6.2505E+6	8.5349E+08	-2.2049E+3
	(1832 K, 0 J/mol)	177.443	0.0000E+0	0.0000E+0	0.0000E+00	0.0000E+0

REFERENCES: 1, 2, 3. Robie et al. (1978); 4.Watanabe (1982); 5. Fei and Saxena (1986); 6, 7. Watanabe (1982); 8. Krupka et al. (1985a,b); 9. Watanabe (1982); 10, 11. Fei et al. (1989); 12. Robie et al. (1978); 13. see Fei and Saxena (1986); 14. Haas (see Fei and Saxena, 1986); 15. Barin and Knacke (1978); 16, 17. Guillermet and Gustafson (1985); 18, 19, 20, 21. Haas (see Fei and Saxena, 1986); 22, 23, 24. Robie et al. (1978); 25. Watanabe (1982); 26. see Fei et al. (1989); 27, 28, 29. Carmichael et al. (1977). The abbreviations are same as in Table 5.1.

Table 5.4 Data on molar volume and thermal expansion coefficients of phases in the Mg-Fe-Si-O system

	$\alpha = \alpha_0 + \alpha_1 T + \alpha_2 T^{-2}$ ¶				
Phases	V^o_{298} cm^3/mol	α_0 (10^4)	α_1 (10^8)	α_2	**References**
2. $1/2Mg_2SiO_4(\alpha)$	21.835	0.3052	0.8504	-0.5824	J & T (1983) ¶Suzuki et al. (1981)
3. $1/2Fe_2SiO_4(\alpha)$	23.140	0.2660	0.8736	-0.2487	Akimoto et al.(1976) ¶Suzuki et al. (1981)
4. $1/2Mg_2SiO_4(\beta)$	20.270	0.2711	0.6885	-0.5767	Akimoto et al.(1976) ¶Suzuki et al. (1980)
5. $1/2Fe_2SiO_4(\beta)$	21.575	0.2319	0.7117	-0.2430	F & S (1986)
6. $1/2Mg_2SiO_4(\gamma)$	19.825	0.2367	0.5298	-0.5702	Ito et al. (1974) ¶Suzuki et al. (1979)
7. $1/2Fe_2SiO_4(\gamma)$	21.010	0.2455	0.3591	-0.3703	Marumo et al.(1977) ¶Suzuki et al. (1979)
8. $MgSiO_3$(px)	31.330	0.2947	0.2694	-0.5588	J & T (1983) ¶Skinner (1966)
9. $FeSiO_3$(px)	32.950	0.2947	0.2694	-0.5588	Syono et al. (1971) ¶Skinner (1966)
10. $MgSiO_3$(pv)	24.500	0.2627	1.5198	-0.0429	Yagi et al. (1978) ¶Knittle et al. (1986)
11. $FeSiO_3$(pv)	25.599	0.2627	1.5198	-0.0429	F & S (1986)
12. MgO(mw)	11.250	0.3681	0.9283	-0.7445	Robie et al. (1978) ¶Suzuki (1975)
13. FeO(mw)	12.250	0.1688	0.2040	0.0190	see text
14. $FeO_{1.5}$(mw)	15.970	0.2453	1.6702	0.0020	see text
15. Fe(bcc)	7.150	0.5055	-1.0483	0.0128	Mao et al. (1967)

					¶Clark (1966)
16. Fe(fcc)	6.840	0.7310	0.0000	0.0000	see G & G (1985)
17. Fe(hcp)	6.740	0.7360	0.0000	0.0000	see G & G (1985)
18. 1/4Fe_3O_4(mgt)	11.130	0.2611	3.2602	0.0040	Mao et al. (1974)
					¶F & S (1986)
19. 1/4Fe_3O_4(hp mgt)	9.110	0.2611	3.2602	0.0040	Mao et al. (1974)
20. 1/2Fe_2O_3(hmt)	15.130	0.2453	1.6702	0.0020	F & H (1980)
					¶F & S (1986)
21. 1/2Fe_2O_3(hp hmt)	13.430	0.2453	1.6702	0.0020	Mao and Bell (1977)
22. SiO_2(qz)	22.688	0.3100	2.6780	0.0000	Robie et al. (1978)
					¶Skinner (1966)
23. SiO_2(coe)	20.640	0.0543	0.8315	-0.0605	Robie et al. (1978)
					¶Skinner (1962)
24. SiO_2(st)	14.010	0.1023	1.3500	-0.0000	Robie et al. (1978)
					¶Ito et al. (1974)
25. $MgSiO_3$(il)	26.350	0.2439	0.0000	0.0000	Ito and Matsui(1977)
					¶Ashida et al. (1988)
26. $MgSiO_3$(gt)	28.500	0.2966	0.2381	-0.5865	Akaogi et al. (1987)
					¶see text
27. 1/2Mg_2SiO_4(melt)	21.414	0.9500	0.0000	0.0000	Fei et al. (1989)
28. 1/2Fe_2SiO_4(melt)	26.008	0.9800	0.0000	0.0000	see text
29. $MgSiO_3$(melt)	35.000	0.6400	0.0000	0.0000	Fei et al. (1989)

J & T = Jeanloz and Thompson; F & S = Fei and Saxena; F & H = Finger and Hazen; and G & G = Guillermet and Gustafson. Other abbreviations are same as in Table 5.1.

Table 5.5 Data on bulk modulus, its pressure and temperature derivatives of phases in the Mg-Fe-Si-O system

Phases	$K_{T,0}$§ GPa	K_T'	$\partial K_T/\partial T$¶ GPa/K	References
2. $1/2Mg_2SiO_4(\alpha)$	128.0	5.32	-0.0224	Sumino et al. (1977) ¶Anderson and Zou (1989)
3. $1/2Fe_2SiO_4(\alpha)$	137.9	4.00	-0.0258	Sumino (1979)
4. $1/2Mg_2SiO_4(\beta)$	172.0	4.27	-0.0323	Sawamoto et al. (1984) ¶Fei et al. (1989)
5. $1/2Fe_2SiO_4(\beta)$	166.0	4.00	-0.0215	Fei and Saxena (1986)
6. $1/2Mg_2SiO_4(\gamma)$	183.0	4.27	-0.0348	Weidner et al. (1984) ¶Fei et al. (1989)
7. $1/2Fe_2SiO_4(\gamma)$	197.0	4.00	-0.0375	Sato (1977)
8. $MgSiO_3$(px)	107.0	4.20	-0.0200	Weidner et al. (1978) ¶Watanabe (1982)
9. $FeSiO_3$(px)	101.0	4.20	-0.0200	Akimoto (1972)
10. $MgSiO_3$(pv)	247.0	4.00	-0.0550	Yagi et al. (1982) ¶Fei et al. (1989)
11. $FeSiO_3$(pv)	287.2	4.00	-0.0596	Fei and Saxena (1986)
12. MgO(mw)	160.3	4.07	-0.0272	Jackson and Niesler (1982) ¶Anderson and Zou (1989)
13. FeO(mw)	180.0	4.00	-0.0200	see Fei and Saxena (1986)
14. $FeO_{1.5}$(mw)	180.0	4.00	-0.0200	see Fei and Saxena (1986)
15. Fe(bcc)	164.0	5.00	-0.0200	Mao et al. (1967)
16. Fe(fcc)	156.0	5.40	-0.0200	Mao and Bell (1977)
17. Fe(hcp)	156.0	5.40	-0.0200	Mao and Bell (1977)
18. $1/4Fe_3O_4$(mgt)	183.0	4.00	-0.0200	Mao et al. (1974)
19. $1/4Fe_3O_4$(hp mgt)	448.0	4.00	-0.0200	Ahrens et al. (1969)

20. $1/2Fe_2O_3$(hmt)	225.0	4.00	-0.0200	Finger and Hazen (1980)
21. $1/2Fe_2O_3$(hp hmt)	399.0	4.00	-0.0200	Ahrens et al. (1969)
22. SiO_2(qz)	37.4	6.40	-0.0040	Soga (1968)
23. SiO_2(coe)	96.0	8.40	-0.0200	Levien and Prewitt (1981)
				¶Watanabe (1982)
24. SiO_2(st)	314.0	6.00	-0.0470	Weidner et al. (1982)
				¶Watanabe (1982)
25. $MgSiO_3$(il)	210.0	4.00	-0.0100	Weidner and Ito (1985)
				¶Fei et al. (1989)
26. $MgSiO_3$(gt)	154.0	4.00	-0.0220	Akaogi et al. (1987)
				¶Fei et al. (1989)
27. $1/2Mg_2SiO_4$(melt)	98.7†	6.50	-0.0235	Fei et al. (1989)
28. $1/2Fe_2SiO_4$(melt)	10.5†	6.50	-0.0000	see text
29. $MgSiO_3$(melt)	20.6†	6.50	-0.0000	Fei et al. (1989)

§ The conversion from the adibatic bulk modulus K_S to the isothermal bulk moduluds K_T is: $K_T = K_S/(1 + T\alpha\gamma_{th})$, where γ_{th} is the thermal Gruneisen constant (see Watanabe,1982; Carmichael, 1982; and Lees et al., 1983 for data sources).

† $K_{T,0}$ at melting temperatures.

The abbreviation are same as in Table 5.1.

Table 5.6 Nonideal mixing parameters of solid solutions in the Mg-Fe-Si-O system

Solid solutions	W_{Mg-Fe} (J/mol)	W_{Fe-Mg} (J/mol)
Magnesiowustite	16100	26300 - 5.56T
Olivine (α)	4500 + 0.013P	6500 + 0.013P
β-phase	1000	2000
Spinel (γ)	3900 - 1.10T	3900
Pyroxene	0	0
Perovskite	4130 - 1.37T + 0.011P	-4050 - 2.45T + 0.015P

Table 5.7 Comparison of enthalpies and entropies of phase transitions

Reactions	ΔH° (J/mol)		ΔS° (J/mol·K)	
	298 K	1000 K	298 K	1000 K
SiO_2				
Qz = Coe	2929[A1]	1330[A1]	-2.73[A1]	-4.97[A1]
	2929±293[B9]	1339±293[B9]	-2.93±0.84[C9]	-5.02±0.42[C9]
Coe = St	48953[A1]	48572[A1]	-4.35[A1]	-5.36[A1]
	48953±1715[B9]		-4.18±1.67[C9]	
Mg_2SiO_4				
α = β	33120[A1]	30330[A1]	-2.39[A1]	-6.82[A1]
		29970±2840[B3]		-7.70±1.9[C3]
		29958±2846[B3]		-10.46±2.1[C2]
				-11.72±2.5[D2]
β = γ	10000[A1]	8240[A1] -3.70[A1]		-6.40[A1]
		9080±2120[B3]		-7.30±1.4[C3]
		6820±3766[B2]		-6.28±3.8[C2]
				-5.44±3.8[D2]
Fe_2SiO_4				
α = β	10170[A1]	9650[A1]	-9.20[A1]	-10.81[A1]
		9620±1260[B3]		-10.90±0.8[C3]
β = γ	-3500[A1]	-4940[A1]	-0.77[A1]	-3.28[A1]
		-5790±2730[B3]		-3.10±2.1[C3]
$MgSiO_3$				
Px = Gt	35150[A1]	35140[A1]	-1.99[A1]	-2.13[A1]
		36500[B4]	-2.40[D8]	-3.65±0.7[C4]
				-2.44[D8]
Px = Il	59850[A1]	58740[A1]	-5.80[A1]	-6.23[A1]
	59030±4260[B6]		-13.88[D8]	-16.48[D8]

	71800^{B5}			
Il = Pv	43200^{A1}	46580^{A1}	$+3.21^{A1}$	$+7.00^{A1}$
	51000^{D7}		-2.84^{D8}	$+3.97^{D8}$
$FeSiO_3$				
Px = Pv	105100^{A1}	104030^{A1}	$+6.21^{A1}$	$+8.11^{A1}$

A = consistent value from phase equilibria, calorimetry and vibrations

B = calorimetry

C = calorimetry and phase equilibria

D = vibrational calculations

1 = Fei et al. (1989)

2 = Akaogi et al. (1984)

3 = Akaogi et al. (1989)

4 = Akaogi et al. (1987)

5 = Ito and Navrotsky (1985). This value now considered to be in error.

6 = Ashida et al. (1988)

7 = Navrotsky (1988, pers. comm.)

8 = Navrotsky (1989)

9 = Akaogi and Navrotsky (1984)

CHAPTER 6

Phase Diagrams and Applications

A major goal of this study is to establish a thermochemical and thermophysical data set which may be used to compute experimentally determined phase equilibrium as closely as possible. These data should at the same time be compatible with all evaluated calorimetric data and measurements of physical properties of each phase. The data in Tables 5.2 to 5.6 meet these criteria well and may be used to explore possible phase equilibrium in systems of varying compositions at pressures up to and exceeding 30 GPa. Such computations should be deemed essential in planning experimental studies relevant to mantle mineralogy, in pointing out major inconsistencies in the existing data and in understanding the mineralogy and chemical composition of the mantle.

6.1 Calculation of Phase Diagrams

Once an internally consistent data set on phases in the system is established, phase diagrams for geochemically and geophysically interesting compositions can be generated by using the method of free energy minimization (see Chapter 3). For the purpose of reproducing experimentally determined phase equilibria, the P-T phase diagrams of pure phases in the Mg-Fe-Si-O system may be constructed. Figures 5.3, 5.5 and 5.7 show the calculated phase relations in the systems Mg_2SiO_4, $MgSiO_3$ and Fe_2SiO_4, respectively. Similar phase diagrams for the polymorphs of Fe, SiO_2 and $FeSiO_3$ can be generated.

In the Mg_2SiO_4-Fe_2SiO_4 binary system, the phase relations have been calculated by

using the present data set and the solid solution model established by the calorimetric and Mg-Fe distribution data (Tables 5.2 to 5.6). Olivine (α) structure transforms to β-phase and spinel (γ) with increasing pressure. The α-γ loop is metastable at the Mg-rich end, interrupted by the stability of β-phase. Figures 6.1a and 6.1b show the isothermal phase relations at 1473 and 1873 K, respectively, in the Mg_2SiO_4-Fe_2SiO_4 binary system. The calculated diagrams are in good agreement with those determined by Katsura and Ito (1989) in the Mg-rich region and by Akimoto (1987) in the Fe-rich region. Note that the calculated results are also consistent with solution calorimetry and element partitioning data in the system. At higher pressure, spinel (γ) breaks down into perovskite and magnesiowustite in the Mg-rich region or into magnesiowustite and stishovite in the Fe-rich region. The calculated isothermal phase diagrams at 1373 and 1873 K in the Mg_2SiO_4-Fe_2SiO_4 binary system are shown in Figures 6.2a and 6.2b, respectively. They are in agreement with recent experimental results reported by Ito and Takahashi (1989). Note that Figures 6.2a and 6.2b are calculated from the present data base where the solid solution model was established from the solution calorimetric and element partitioning data in the system.

The data base can be used not only for reproducing the existing experimental results, but also for interpolation and even extrapolation with caution. Thermodynamic modeling with a well evaluated data base allows us to explore phase relations in the system in various ways. For instance, one may construct phase relations in pressure-temperature space or in pressure-composition space. It is also possible to produce phase relations for which experiments have not yet been conducted. Figure 6.3 shows phase equilibrium relations in the Mg-Fe-Si-O system with olivine composition $(Mg_{0.88}Fe_{0.12})_2SiO_4$ up to pressure of 30 GPa. One may also calculate phase relations by varying olivine composition, or by mixing olivine and pyroxene or olivine and magnesiowustite in

desired proportions. Such phase relation computation can provide critical information on geotherm and density profile through the mantle (see discussion below).

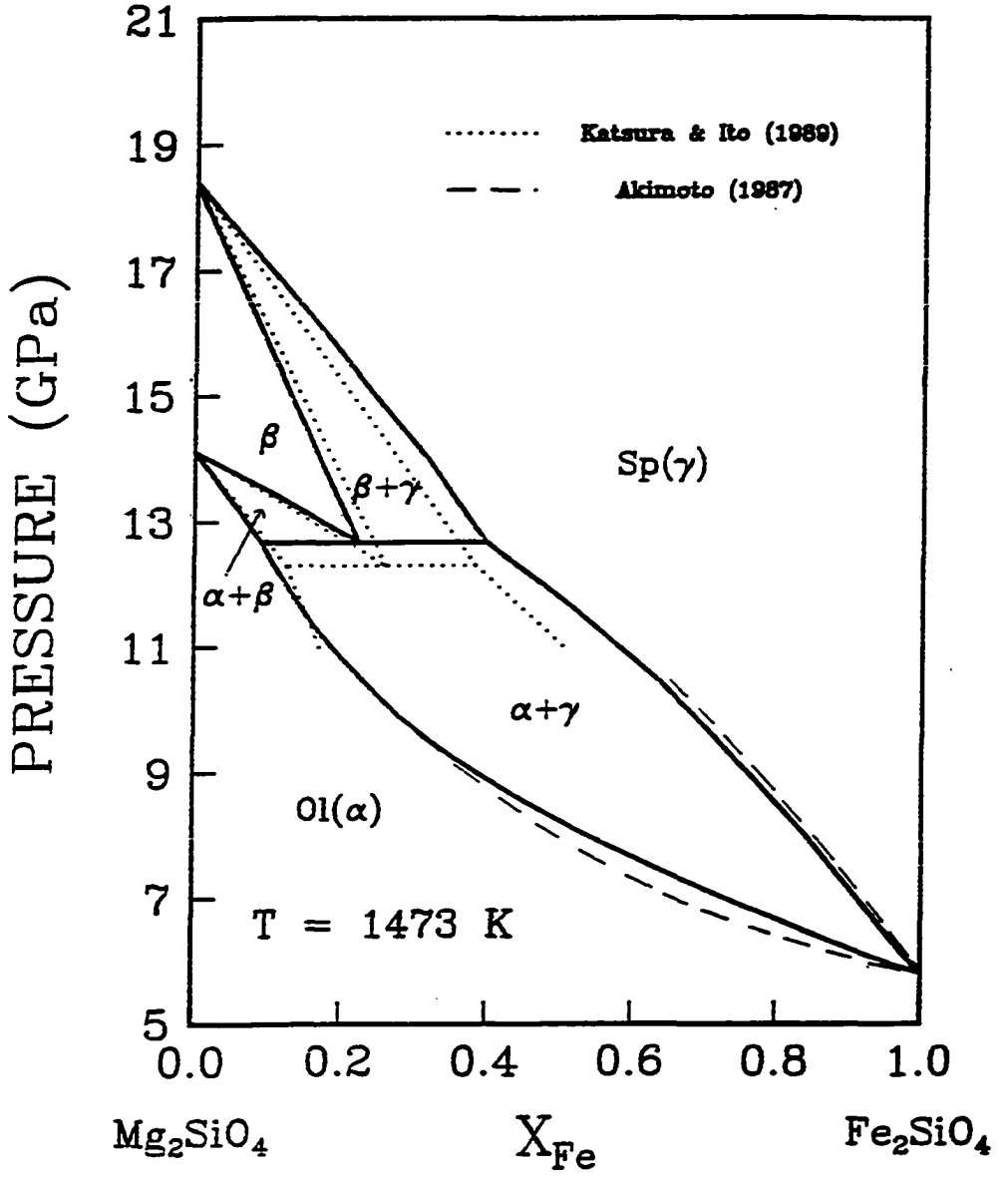

Figure 6.1a Isothermal phase relations at 1473 K in the binary system Mg_2SiO_4 and Fe_2SiO_4. The solid curves are calculated from the present data set shown in Tables 5.2 to 5.6. The experimental data by Katsura and Ito (1989) (the dotted curves) and by Akimoto (1987) (the dashed curves) were plotted for the comparisons.

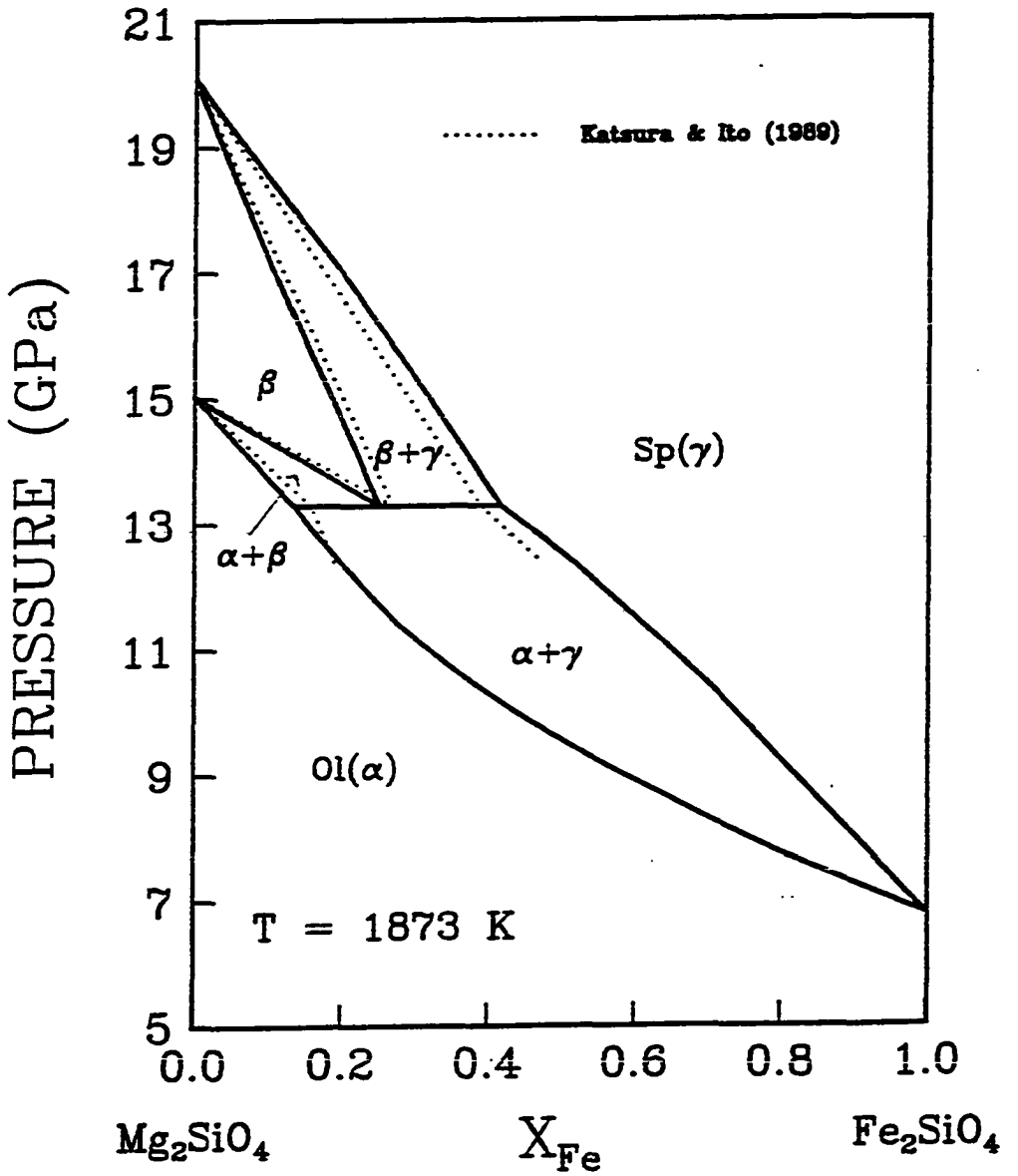

Figure 6.1b Isothermal phase relations at 1873 K in the binary system Mg_2SiO_4 and Fe_2SiO_4. The solid curves are calculated from the present data set shown in Tables 5.2 to 5.6. The dotted curves represent the experimental data by Katsura and Ito (1989).

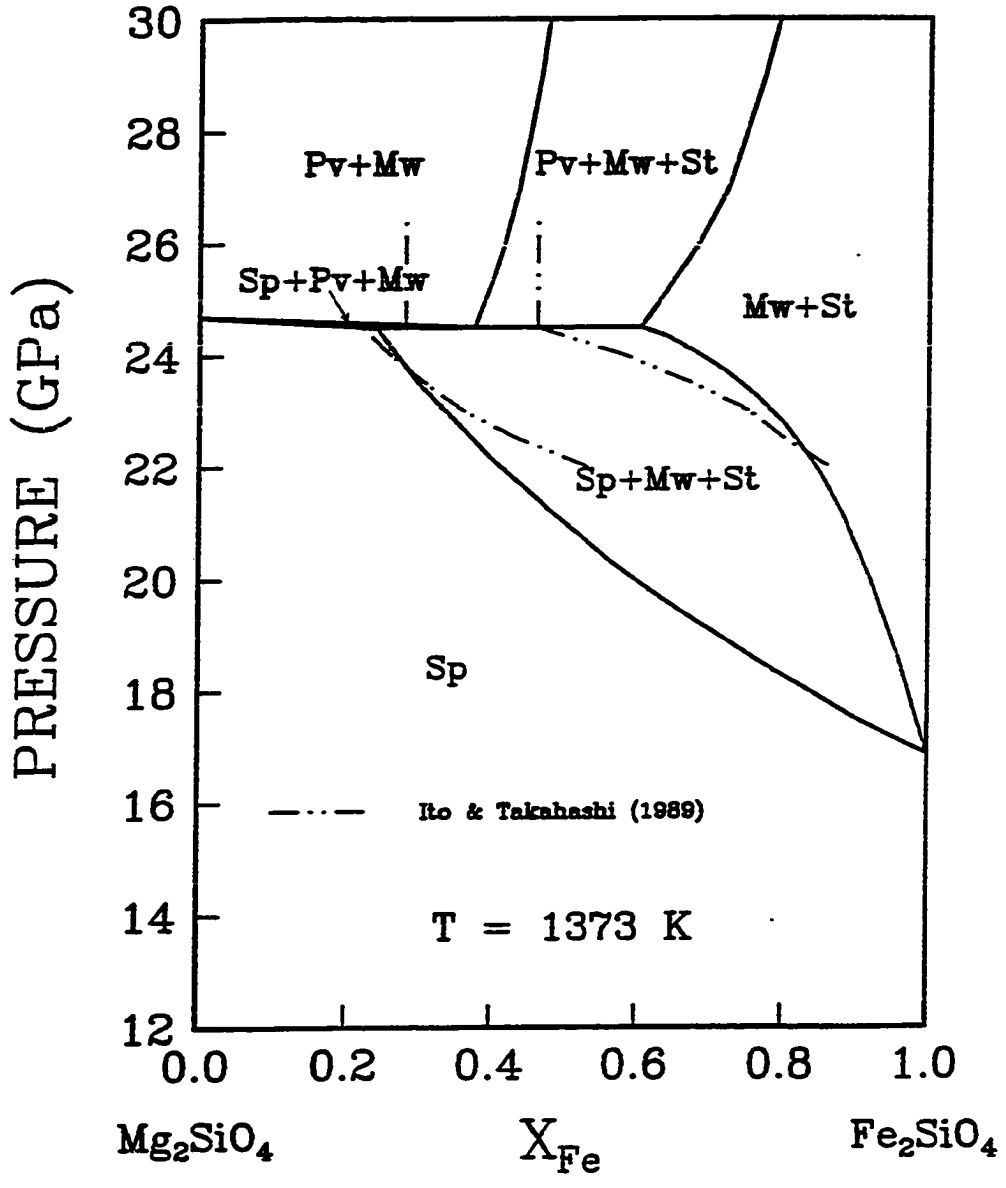

Figure 6.2a Isothermal phase relations at 1373 K in the binary system Mg_2SiO_4 and Fe_2SiO_4. The solid curves are calculated from the present data set shown in Tables 5.2 to 5.6. The dotted curves represent the experimental data by Ito and Takahashi (1989).

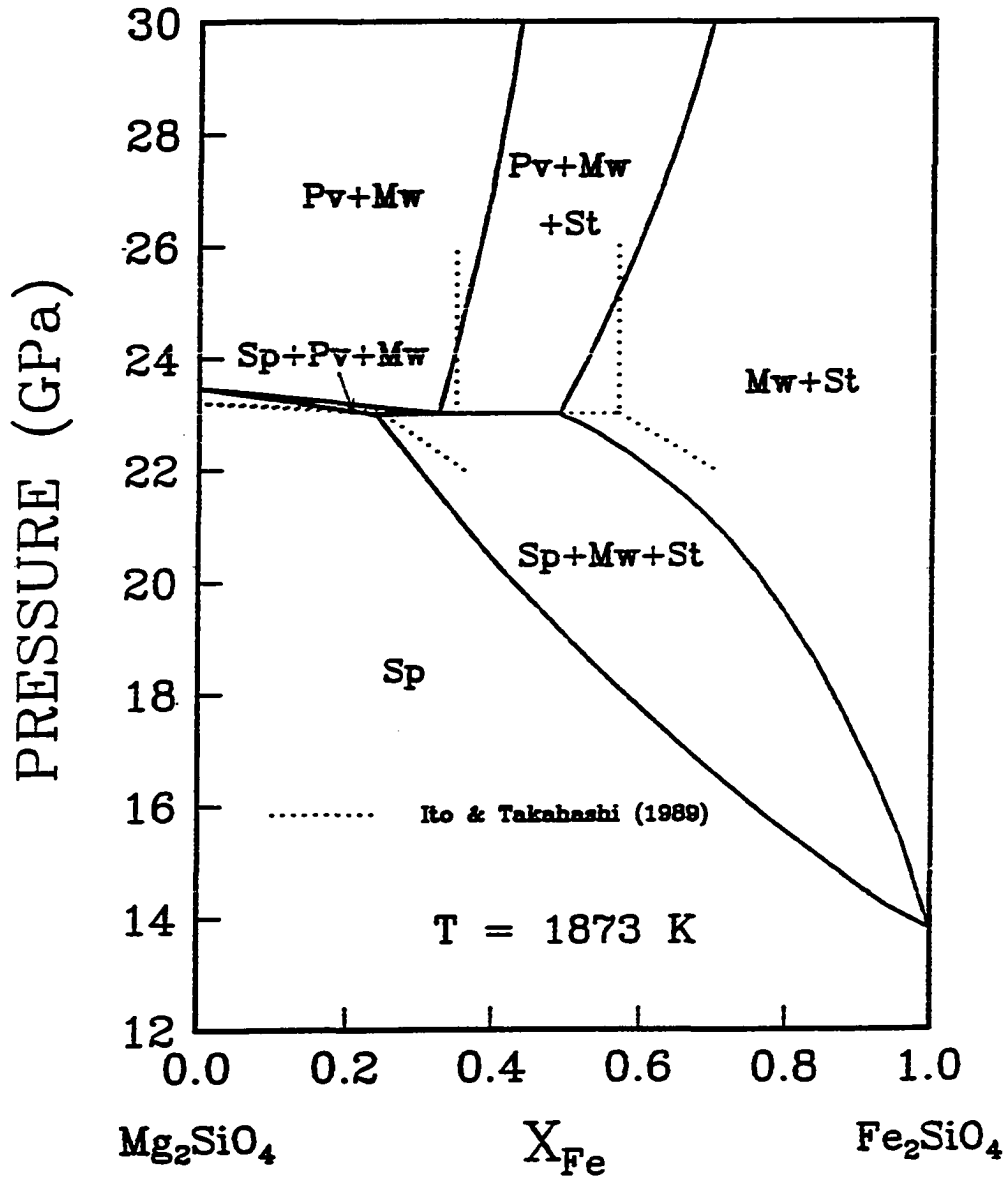

Figure 6.2b Isothermal phase relations at 1873 K in the binary system Mg_2SiO_4 and Fe_2SiO_4. The solid curves are calculated from the present data set shown in Tables 5.2 to 5.6. The dotted curves represent the experimental data by Ito and Takahashi (1989).

6.2 Applications

MgO, FeO and SiO_2 are considered the dominant components of the Earth's mantle. Phase relations in the Mg-Fe-Si-O system are of great interest to geochemists and geophysicists because both the 400 km and the 670 km seismic discontinuities may reflect the phase transformations of olivine (α) to β-phase and of spinel (γ) to perovskite plus magnesiowustite, respectively.

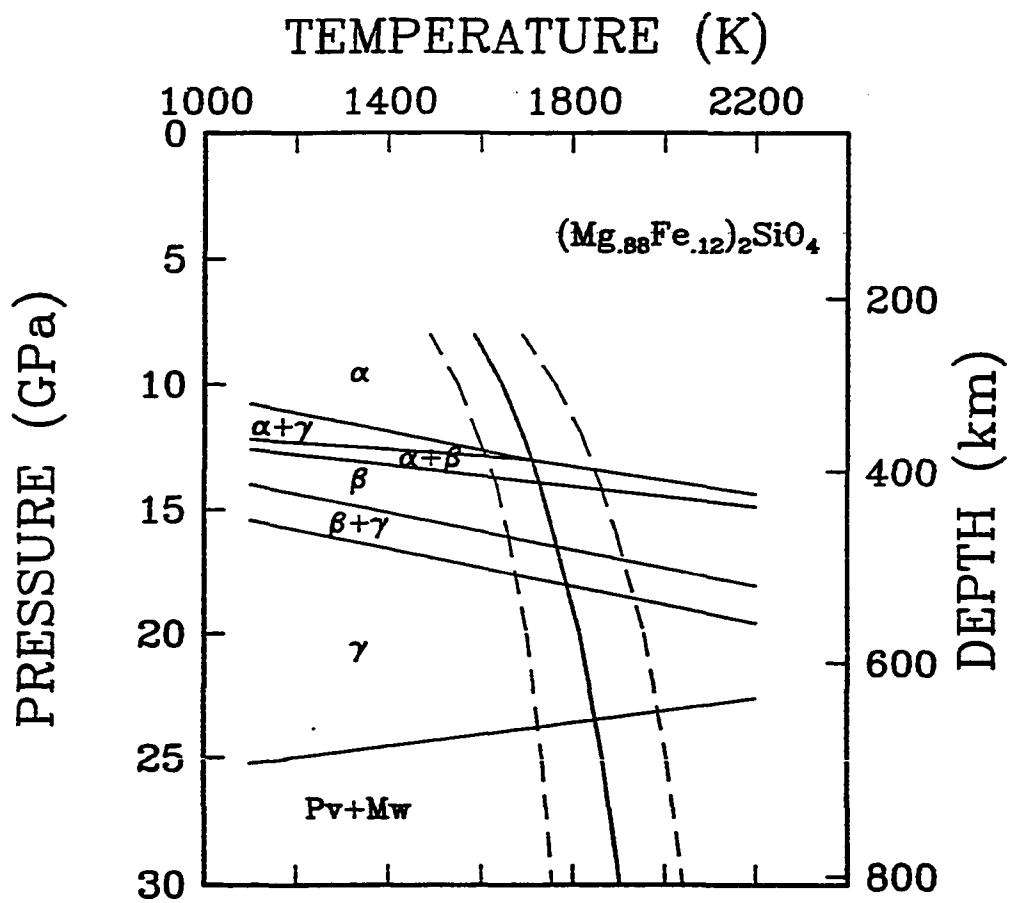

Figure 6.3 Phase equilibrium relations in the Mg-Fe-Si-O system with composition of $(Mg_{0.88}Fe_{0.12})_2SiO_4$. The estimated geotherm (see text) is shown by heavy line and its upper and lower limits are shown by dashed lines.

In the mantle model of peridotitic composition (Ringwood, 1975), olivine $(Mg_{0.88}Fe_{0.12})_2SiO_4$ is the major component. Phase diagram for this olivine is shown in Figure 6.3. The depth and width of the α-β transformation are a function of temperature. If the 400 km discontinuity is attributed to the α-β transformation of $(Mg_{0.88}Fe_{0.12})_2SiO_4$ olivine in the depth range of 380 - 420 km (e.g. Wiggins and Helmberger, 1973; Given and Helmberger, 1980; and Grand and Helmerger, 1984), the corresponding temperature ranges from 1650 to 1750 K. The width of the α+β assemblage at that temperature is about 17 km (0.8 GPa). The $(Mg_{0.88}Fe_{0.12})_2SiO_4$ spinel breaks down into $(Mg_{0.94}Fe_{0.06})SiO_3$ perovskite and $(Mg_{0.82}Fe_{0.18})O$ magnesiowustite within a very small pressure interval (less than 0.15 GPa), as shown in Figures 6.2a,b and 6.3. The sharpness of this boundary is compatable with the seismic observation of the 670 km discontinuity where the velocity increase is sharp. If this transformation is the dominant cause of the 670 km discontinuity, the temperature required for the transformation at that depth is about 1850 K. The depth of the α-β transformation increases with increasing temperature and the depth of the transformation of spinel to perovskite and magnesiowustite decreases with increasing temperature (Figure 6.3). Therefore, the separation of these two transformations may be used for constraining the geotherm of the mantle if the 400 and 670 km discontinuities are the reflections of the two phase transformations. The geotherm derived from this study is close to that by Brown and Shankland (1981). Although there are uncertainties in both the experimental pressure and the depth of the discontinuity, it is possible to provide the lower and upper limits for the geotherm by taking such uncertainties into consideration. The lower and upper limits of the geotherm shown in Figure 6.3 are derived by considering the uncertainties of ±1GPa in pressure, ±20 km for the 400 km discontinuity and ±15 km for the 670 km discontinuity.

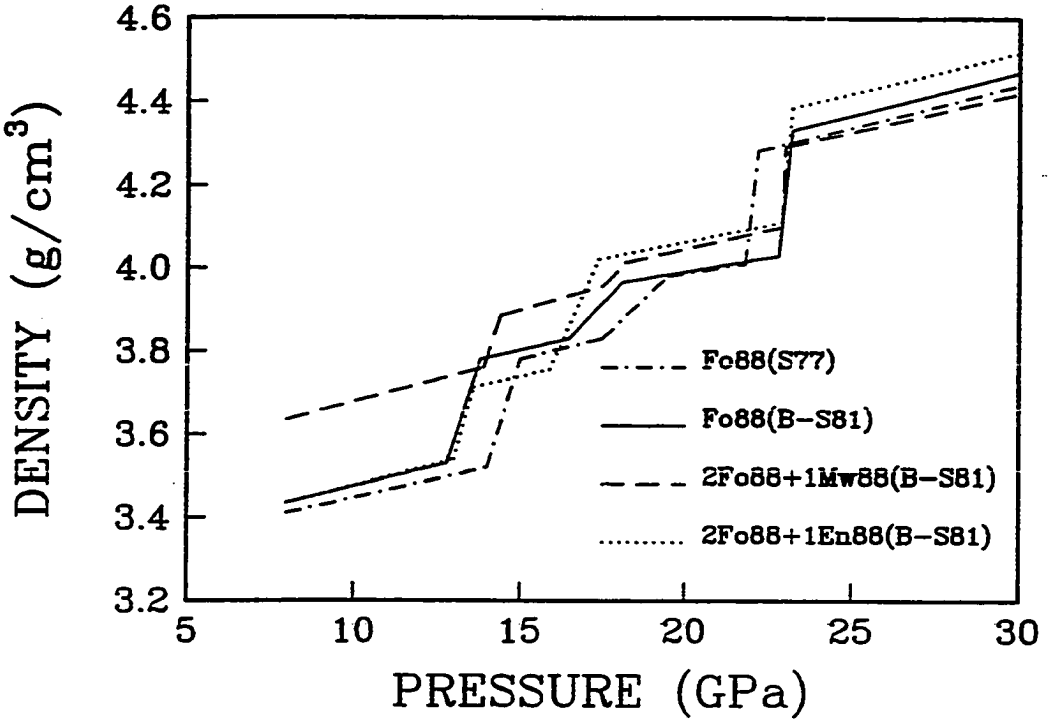

Figure 6.4 Density profiles calculated from the stable mineral assemblages in the Mg-Fe-Si-O system under various conditions. Solid line, labeled as Fo88(B-S81), is the calculated density profile with composition of $(Mg_{.88}Fe_{.12})_2SiO_4$ (Fo88) along Brown and Shankland (1981)'s geotherm (B-S81); dot-dashed line with Fo88 along Stacey (1977)'s geotherm (S77); dashed line with mixture of 2 Fo88 + 1 $(Mg_{.88}Fe_{.12})O$ (Mw88) along B-S81; and dotted line with mixture of 2 Fo88 + 1 $(Mg_{.88}Fe_{.12})SiO_3$ (En88) along B-S81.

Composition variation within a reasonable range [e.g. $(Mg_{0.93}Fe_{0.07})_2SiO_4$ to $(Mg_{0.85}Fe_{0.15})_2SiO_4$] does not have significant effect on the depth of the two transformations. The density profile may reflect some compositional change. It is possible to generate various density profiles by varying the molar ratios of FeO/(MgO +

FeO) and $(MgO + FeO)/SiO_2$ along the assumed geotherm or by adopting different geotherms. Figure 6.4 shows the density profiles with bulk chemical composition of $(Mg_{0.88}Fe_{0.12})_2SiO_4$ along geotherms by Brown and Shankland (1981) and by Stacey (1977). The density profiles for 2 olivine + 1 pyroxene and 2 olivine + 1 magnesiowustite with the FeO/(MgO + FeO) ratio of 0.12 are also calculated along the geotherm by Brown and Shankland (1981). The calculations are just for demonstrating how one may apply the thermodynamic model to solve some geophysical problems. The present data base is inadequate for comparing the calculated density profile with that derived from the seismic data. In order to make the comparison, at least Ca and Al should be included in the system. However, if the calculated results, which are based on somewhat simplified chemical composition of the mantle, are used to compare with the density profile derived from the seismic data, the deviation of the calculated profile from the realistic one may provide information on the direction of variation in the chemical composition of the mantle.

To simulate the density profile of the mantle, at least two factors, chemical composition and geothermal gradient, can be simultaneously varied within certain reasonable ranges. A number of possible combinations of these factors may yield similar result on the density profile. The limited experimental data on phase equilibria and physical properties of materials can be used to explore these possibilities only when they are fitted into a predictive model such as this equilibrium thermodynamic model. If the present data set were extended by introducing other elements in the system such as Ca, Al, Ni and Na which are likely in the mantle, we could then simulate the density profile of the mantle.

Adiabatic rise of diapirs is a useful concept and geophysical models require calculations of adiabatic gradients. The data base can be used to calculate the enthalpy of a mineral

assemblage at given pressure and temperature. Therefore, one can calculate the adiabatic path for diapirs ascending from the starting position (e.g. 300 km and 1600 K) by satisfying the condition, $\Delta H(P,T) = 0$. The applications of such calculation to geochemistry and geophysics were discussed by Saxena and Eriksson (1985).

The calculation of phase equilibrium relations in the system extended to the Mg-Fe-Si-C-H-O system has some implications for early mantle-fluid composition and the oxidation state of the mantle. The study of fluids in the C-H-O system at high pressure and temperature forms a separate study by itself and will not be discussed in this thesis, The detailed information may be found from several my publications with S. K. Saxena. Those papers are attached as Appendix.

APPENDIX

List of published papers:

1. A thermochemical data base for phase equilibria in the system Fe-Mg-Si-O at high pressure and temperature.

2. An equation for the heat capacity of solids.

3. Some binary and ternary silicate solution models.

4. Fluids at crustal pressures and temperatures: I. pure species.

5. High pressure and high temperature fluid fugacities.

6. The pressure-volume-temperature equation of hydrogen.

7. Fluid mixtures in the C-H-O system at high pressure and high temperature.

8. Phase equilibrium in a system of chondritic composition: implications for early mantle-fluid compositions.

9. Internally consistent thermodynamic data and equilibrium phase relations for compounds in the system MgO-FeO-SiO_2 at high pressure and high temperature.

10. Experimental determination of element partitioning and calculation of phase relations in the Mg-Fe-Si-O system at high pressure and high temperature.

Phys Chem Minerals (1986) 13:311–324

PHYSICS AND CHEMISTRY OF MINERALS

A Thermochemical Data Base for Phase Equilibria in the System Fe–Mg–Si–O at High Pressure and Temperature

Yingwei Fei and Surendra K. Saxena

Department of Geology, Brooklyn College, Brooklyn, N.Y. 11210 and Department of Earth and Environmental Science, Graduate Center, CUNY, New York, N.Y. 10036, USA

Abstract. A thermochemical data base for phases in the system Fe–Mg–Si–O at high pressures up to 300 kbar is established by supplementing the available calorimetric data with data calculated from experimental high pressure synthesis studies. Phases included in the data base are the SiO_2 polymorphs, rock salt solid solutions (Fe–Mg–O), Fe_2O_3, Fe_3O_4, (Mg, Fe)$_2SiO_4$ olivine, spinel, modified spinel and (Mg, Fe)SiO_3 perovskite and pyroxene. Phases not included are the $MgSiO_3$-ilmenite and -garnet. Fe–Mg solution properties of olivine, spinel, perovskite and wustite (rock salt) are estimated. The wüstite solid solution has been modeled as a nonideal solution of three end members: FeO, $FeO_{1.5}$ and MgO. The new data base is made consistent with most of the available information on high pressure phase studies.

The data base is useful in generating phase diagrams of various different compositions for the purpose of planning new experiments and analysing existing phase synthesis data.

Introduction

Equilibrium relations in the system Mg–Fe–Si–O with minerals iron, quartz, coesite, stishovite, magnesiowüstite (rock salt), hematite, magnetite, clinopyroxene, olivine, modified spinel, spinel, ilmenite, garnet ($MgSiO_3$), and perovskite are of particular importance in understanding the mineralogy of the mantle. Recent studies of the Fe–Si–O system by Meyer and Eugster (1983), Bjorkman (1984), Hazen and Jeanloz (1984) and Haas (1985, pers. comm.), of the system Mg–Si–O by Akaogi et al. (1984), Ito and Yamada (1982) and of the Mg–Fe–Si–O system by Navrotsky and Akaogi (1984), Yagi et al. (1979) and Ito et al. (1984) and Ito (1984) have resulted in important phase diagrams and thermochemical data. However, these results and the results of several other studies have not been used to obtained an internally consistent set of thermochemical-thermophysical data. An internally consistent data set is one which permits the computation of phase equilibrium relations as established through experimental studies and is at the same time compatible with calorimetric and other measurements of thermochemical properties of the phases. Similar studies have been conducted previously by Wood and Holloway (1984) and Saxena and Chatterjee (1986) for the CaO–MgO–Al_2O_3–SiO_2 system. Generating such a data base is complicated by the large uncertainties associated with the high pressure phase equilibrium relations, both because of the errors in pressure and temperature calibration and because the experiments generally represent unreversed reactions. In spite of these problems, it is important to review the present status of the existing thermochemical data set and its relation to the experimental phase studies. If a thermochemical data set produces calculated results which are reasonably consistent with experimental work, it can be used for computing possible phase equilibrium relations over a wide range of pressure, temperature and composition conditions. Such predictions are useful in planning future phase equilibrium experiments, which may then be used to better constrain the preliminary data base. Conversely, if the attempt to create a data base exposes major inconsistencies, experiments to resolve these discrepencies would be important. The purpose of this paper is to present a thermodynamic analysis of the experimental phase diagrams in the system Mg–Fe–Si–O under mantle pressure and temperature conditions.

The mineral names are abbreviated as shown below: Stishovite: St, perovskite: Pv, spinel: Sp, olivine: Ol, ilmenite: Ilm, wüstite: Fe_xO, magnesiowüstite: MgO or Mw, magnetite: Mgt, clinopyroxene: Cpx. Magnesiowüstite (Mw) has been used as a name for the ternary MgO–FeO–$FeO_{1.5}$ solid solution. High pressure magnetite is referred to as high-P-Mgt.

Since there is only meagre experimental information available on $MgSiO_3$-ilmenite and -garnet, these phase are not included in this study.

Thermodynamics of Reactions at High Pressure and High Temperature

The standard free energy of a reaction is given by

$$\Delta G^0(P, T) = \Delta H^0_T - T\Delta S^0_T + \int_1^P \Delta V(P, T)\, dP \qquad (1)$$

where ΔH^0_T and ΔS^0_T are the enthalpy and entropy of reaction, respectively, at temperature T and are given by:

$$\Delta H^0_T = \Delta H^0_{298} + \int_{298}^{T} \Delta C_p\, dT \qquad (2)$$

and

$$\Delta S^0_T = \Delta S^0_{298} + \int_{298}^{T} (\Delta C_p/T)\, dT \qquad (3)$$

where ΔH^0_{298} and ΔS^0_{298} are the standard enthalpy and entropy of reaction at 298 K, and ΔC_p is the heat capacity difference between products and reactants.

Berman and Brown (1985) argued that at very high temperatures the value of C_p per gram atom should approach the theoretical Petit and Dulong (1819) limit of 3R (R = gas constant) with the limit for C_p given by

$$C_p \simeq 3R + \alpha^2 V T/\beta$$

where α and β are the coefficients of thermal expansion and compressibility, respectively, and V the molar volume. Berman and Brown (1985) studied the available C_p data and found the following empirical expressions which would bring the high temperature extrapolation closer to theory than other equations used previously. These expressions are given by

$$C_p = k_0 + k_1 T^{-0.5} + k_2 T^{-2} + k_3 T^{-3} (k_1, k_2 < 0) \quad (4)$$

and

$$C_p = k_0 + k_1 T^{-0.5} + k_2 T^{-2} + k_3 T^{-3} + C_p(\lambda) \quad (5)$$

where

$$C_p(\lambda) = T(l_1 + l_2 T)^2 \quad (6)$$

Equation (6) is for phases with lambda transformations. For $T > T_\lambda$, heat capacity is calculated using the first four terms of equation (5). The coefficients of C_p for many minerals were tabulated by Berman and Brown (1985).

In equation (1), $\Delta V(P, T)$ is the volume change for a reaction. The molar volume of the phase at the pressure and temperature of interest is calculated from the Murnaghan equation

$$V(P, T) = V(1, T)(1 + K_0' / K_0 \, P)^{-1/K_0'} \quad (7)$$

where K_0 and K_0' are the bulk modulus and it's pressure derivative respectively. $V(1, T)$ is the molar volume at T and 1 atmosphere given by

$$V(1, T) = V_0 \left(1 - \int_{298}^{T} \alpha(T)\, dT\right). \quad (8)$$

V_0 is the molar volume at 298 K and 1 atmosphere and $\alpha(T)$ is a temperature dependant coefficient of thermal expansion

$$\alpha(T) = \alpha_0 + \alpha_1 T + \alpha_2 T^{-2} \quad (9)$$

where α_0, α_1 and α_2 are coefficients determined by least sqares analysis of the volume expansion data. Combining equations (7), (8) and (9) and integrating we obtain

$$\int_1^P V(P, T)\, dP = V_0[1 + \alpha_0(T - 298) + \alpha_1/2(T^2 - 298^2) - \alpha_2(1/T - 1/298)] \cdot \{K_0/(K_0' - 1)[(1 + K_0'/K_0 P)^{((K_0' - 1)/K_0')} - 1]\}. \quad (10)$$

Equation (10) does not include the temperature dependence of the bulk modulus. Such data are available for very few substances. It is expected that in computing ΔG, such effects will largely be cancelled.

Method of Computation

Although many of the computations presented in the following text are easily performed, the multicomponent-multireaction equilibrium calculations are best done by adopting the method of minimizing the total Gibbs free energy of a chosen system. The linear algebraic techniques were discussed by Eriksson (1975) and Smith and Missen (1982). A brief description is included in the Appendix.

In certain cases, it is necessary to determine the properties of solid solutions from experimental data on compositions of coexisting phases. The distribution of a component between two coexisting solid solutions e.g. (1, 2)−M and (1, 2)−N, where 1 and 2 are exchangeable components, may be considered as an ion-exchange reaction:

$$1\text{−M} + 2\text{−N} = 2\text{−M} + 1\text{−N} \quad (11)$$

At equilibrium, we have

$$RT \ln K = RT \ln K_D + RT \ln(\gamma_1/\gamma_2)^N - RT \ln(\gamma_1/\gamma_2)^M \quad (12)$$

where $K_D = (X_1/X_2)^N/(X_1/X_2)^M$

and γ's are activity coefficients. We have used an asymmetric nonideal solution model for binary solid solutions, for which the excess free energy of mixing (Margules formulation, see Thompson 1969) is defined as:

$$\Delta G^{ex} = X_1 X_2 (W_{12} X_2 + W_{21} X_1) \quad (13)$$

For the asymmetric model the activity coefficient of a component in a binary solution is given by

$$RT \ln \gamma_1 = X_2^2 [W_{12} + 2X_1 (W_{21} - W_{12})] \quad (14)$$

Note that the W_{ij} parameters represent adjustable constants. They are functions of both pressure and temperature. According to Thompson (1969) for W_{ij}, we may write:

$$W_{ij} = W_{ij}^H - T W_{ij}^S + P W_{ij}^V \quad (14.a)$$

where W_{ij}^H, W_{ij}^S and W_{ij}^V represent the excess enthalpy, excess entropy and excess volume contributions to the interaction energy W_{ij}. The Kohler model (see Bertrand et al. 1983) is used for ternary and multicomponent solutions. According to the model of Bertrand et al., an excess property of a multicomponent solution is given by

$$\Delta Z^{ex}_{12\ldots N} = \sum_{i=1}^{N} \sum_{j>i}^{N} (X_i + X_j)(f_i - f_j)(\Delta Z^{ex}_{ij})^* \quad (15)$$

in which $(\Delta Z^{ex}_{ij})^*$ is the molar excess property (enthalpy, entropy, volume, free energy etc.) of the binary system with components at the same molar ratio as the multicomponent system and f_i and f_j are weighted mole fractions using weighting factors based on the excess properties of the binary systems. X_i is used as the mole fraction in the multicomponent system.

For activity coefficient of a component i, we have

$$(RT \ln \gamma_i)_{12\ldots N} = \sum_j (X_i + X_j)(1 - f_i - f_j)(\Delta G^{ex}_{ij})^* - \sum_{j,k} (X_j + X_k)(f_j + f_k)(\Delta G^{ex}_{jk})^* + \sum_j (f_i + f_j)(RT \ln \gamma_i)^*_{ij} \quad (i \neq j \neq k) \quad (16)$$

where the binary functions are denoted by an asterisk.

As discussed by Fei, Saxena and Ericsson (1986), the Kohler method of predicting the ternary solution properties is as good as the Wohl's formulation (see Saxena 1973, Ganguly and Saxena 1984) with the additional advantage of simplicity in extension to multicomponent solutions. In equation (12)

$$RT \ln K = -\Delta G(P, T)$$

We may substitute appropriately for the activity coefficients from the binary or multicomponent models noted above and depending on the nature of the observational data, equation (12) may be used to determine the unknowns, which may be $\Delta G^0(P, T)$ or W_{ij} or a combination of these. Details of such calculations are discussed amply in the literature (e.g. Saxena 1973, Ganguly and Saxena 1984).

Selection and Calculation of Thermochemical Data

For several phases, thermochemical data are available in the literature (see Tables 1 to 3). For other phases the data are computed using experimental phase equilibrium relations as discussed below.

Fe–O

Important minerals in this system are: iron (Fe), wüstite (variable Fe:O), magnetite (Fe_3O_4) and hematite (Fe_2O_3). Several phase equilibrium studies are available for this system (e.g. Goel et al. 1980, Bjorkman 1984) and Kubaschewski (1982) has summarized the phase relations. Hazen and Jeanloz (1984) have discussed the crystal chemistry of wüstite. As described by these authors, the structure of wüstite is complex and difficult to determine. The variables which may affect the thermodynamic properties of wüstite are a) degree of nonstoichiometry, b) the ratio of octahedral vacancies to tetrahedral ferric iron, and c) the size and shape of defect clusters, their periodicity and the extent of magnetite or iron exsolution. Each wüstite sample may have its own structural peculiarities depending on the conditions of synthesis and thermal history; this makes measurements of thermochemical and physical properties a very difficult task. From the numerous phase equilibrium studies in the system Fe–O cited in Kubaschewski (1982), it appears that certain phase boundary relationships are commonly accepted. However, details on various allotropic modifications of wüstite are not well known (see Hazen and Jeanloz 1984). Such modifications are the reflections of discontinuities in the thermochemical properties of the wüstite solid solution.

Figure 1 shows part of the phase diagram for the Fe–O system at 1 bar. Wüstite has a temperature-composition field within which its composition varies mainly between $Fe_{0.947}O$ and $Fe_{0.85}O$. The system may be modeled by considering wüstite as a solid solution of two fictive, isostructural components FeO and $FeO_{1.5}$. Through such modeling we can hope to treat the thermodynamics of the hetereogeneous reactions (i.e. wüstite reacting with other phases) generally within the errors in the thermochemical data of the reacting phases. A precise model for the wüstite solid solution particularly for modeling the crystal chemical behavior must include the effect of additional components (other than FeO and $FeO_{1.5}$) and other parameters discussed by Hazen and Jeanloz (1984). The reaction within the field of wüstite solution is

$$\{FeO\} + 0.25\ O_2 = \{FeO_{1.5}\} \qquad (17)$$

and in the field towards magnetite, the reaction may be conceived as

$$\{5FeO\} + O_2 = \{2FeO_{1.5}\} + Fe_3O_4 \qquad (18)$$

where the brackets denote the components in the wüstite solution. The computed W_{ij} values for wüstite are (FeO = 1, $FeO_{1.5}$ = 2): $W_{12} = -7.229$, $W_{21} = -2.142$ (J/mol) which

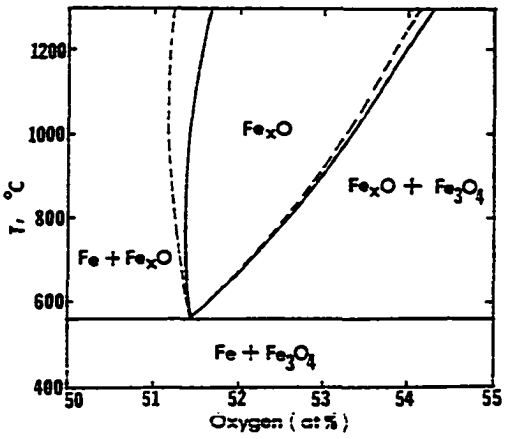

Fig. 1. Equilibrium relations in the system Fe–O at a pressure of 1 bar. The dashed lines are from the review of Kubaschewski (1982). The solid lines represent the calculated curve using the data in Tables 1 and 2 and the wüstite solution model as described in the text. The experimental data match the calculated data exactly where only one solid line appears

are the same as in Bjorkman (1984). However, note that the thermochemical data on fictive end member components used here are different. The enthalpy and entropy data on the two fictive end member components are determined simultaneously through these calculations and are listed in Table 1. The C_p coefficients for fictive FeO and $FeO_{1.5}$ are the same as for the stoichiometric FeO and hematite respectively. Figure 1 shows the calculated phase boundaries using the data presented above and in Table 1. The fit of the computed phase boundaries can be improved by using a ternary solution model for the wüstite (Fe–FeO–$FeO_{1.5}$) as done by Goel et al. (1980) and Bjorkman (1984). However, in view of the uncertainties introduced at high pressures (see later) we have refrained from using the ternary model at present. The phase diagram of the Fe–O system used here is based on several experimental results reviewed by Kubaschewski (1982), Goel et al. (1980) and Bjorkman (1984). References to the literature may be found in the above mentioned articles.

The errors in the W_{12} and W_{21} and in the ΔH_f^0 and ΔS_f^0 are related and cannot be independently evaluated. However, for fixed value of W_{ij}, a change of a few hundred joules in ΔH_f^0 is enough to make the results on phase boundaries change beyond the quoted experimental uncertainty.

For calculations at high pressure, we need data on volume of mixing and on compressibility of the solid solution components FeO and $FeO_{1.5}$. Volume of mixing is assumed to be ideal with volume of the solution given by:

$$V_{Fe_xO} = X_{FeO} V_{FeO} + X_{FeO_{1.5}} V_{FeO_{1.5}} = (3 - 2X) V_{FeO} + (2X - 2) V_{FeO_{1.5}} \qquad (19)$$

Using the molar volume data of FeO as 12.25 cm^3 (stoichiometric FeO, Robie et al. 1978) and the V_{Fe_xO} data from Simons (1980) and Hentschel (1970), the molar volume of the fictive $FeO_{1.5}$ is determined to be 15.97 cm^3. For estimating the bulk modulus of Fe_xO (change in bulk modulus

Table 1. Data on standard enthalpy of formation and entropy of formation from elements at 298.15 K

No	Name	Formula	ΔH°_{298} (J/mol)	ΔS°_{298} (J/Kmol)	T_r (K)	H_{T_r} (J/mol)
1	Oxygen	O_2	0± 0	205.15±0.04		
2	Forsterite	$MgSi_{0.5}O_2$	−1,088,600± 700	47.06±0.42		
3	Fayalite	$FeSi_{0.5}O_2$	− 739,085± 650	75.50±0.10		
4	β−Fo	$MgSi_{0.5}O_2$	−1,072,450±1,000	44.53±1.00		
5	β−Fa	$FeSi_{0.5}O_2$	− 736,473±2,000	70.93±1.50		
6	γ−Fo	$MgSi_{0.5}O_2$	−1,069,300±1,800	42.75±1.50		
7	γ−Fa	$FeSi_{0.5}O_2$	− 738,334±1,500	68.44±1.50		
8	Clinoenstatite	$MgSiO_3$	−1,544,010±1,000	67.23±1.00		
9	Clinoferrosilite	$FeSiO_4$	−1,193,590±1,000	95.40±1.00		
10	Perovskite	$MgSiO_3$	−1,436,000±2,000	69.86±1.50		
11	Perovskite	$FeSiO_3$	−1,094,000±5,000	95.86±2.00		
12	Ilmenite	$MgSiO_3$	−1,489,600±2,000	58.00±2.50		
13	Wüstite (1)	MgO	− 601,490± 290	26.94±0.17		
14	Wüstite (2)	$FeO_{1.5}$	− 380,900± 200	54.90±0.20		
15	Wüstite (3)	FeO	− 267,270± 200	57.59±0.20		
16	Magnetite	$Fe_{0.75}O$	− 278,887± 148	37.66±0.10	848	391
					1,300	0
17	High-P-Mgt	$hFe_{0.75}O$	− 236,500±2,000	45.00±1.00		
18	Hematite	$FeO_{1.5}$	− 412,391± 404	43.70±0.33	956	335
					1,250	0
19	High-P-Hem	$hFeO_{1.5}$	− 374,600±2,000	43.70±1.00		
20	Iron	α−Fe	0± 0	27.28±0.13	**	
21	Quartz	SiO_2	− 910,700±1,000	41.46±0.20	848	499
22	Coesite	SiO_2	− 907,771±2,000	38.73±2.50		
23	Stishovite	SiO_2	− 858,818±2,000	34.38±1.50		

Notes on Tables 1, 2 and 3. These tables show an internally consistent data set which has been used in this work. Alternate values of some of the parameters particularly for coefficients of thermal expansion and bulk modulus. In most cases the differences are minor. A detailed list of the alternate data are available in the hand book edited by Carmichael (1982).

1. Oxygen: Robie et al. (1978). 2. Forsterite: Enthalpy and entropy. See text. C_p. Watanabe (1982). V_0. Matsui and Syono (1968). $\alpha(T)$, Suzuki (1975) and Suzuki et al. (1981). K_0. Sumino et al. (1977). 3. Fayalite: Enthalpy, entropy and C_p. Robie et al. (1982). V_0. Akimoto et al. (1976). $\alpha(T)$, Suzuki et al. (1981). K_0. Sumino (1979). 4. β-Forsterite: Enthalpy, and entropy. Akaogi et al. (1984). C_p. Watanabe (1982). V_0. Akimoto et al. (1976). $\alpha(T)$. Suzuki et al. (1980). K_0. Mizukami et al. (1975). 5. β-Fayalite: Estimated in this study. 6. γ-Forsterite: Enthalpy and entropy, Akaogi et al. (1984). C_p. Watanabe (1982). V_0. Ito et al. (1974). $\alpha(T)$. Suzuki et al. (1979). K_0. Mizukami et al. (1975). 7. γ-Fayalite: Enthalpy and entropy determined in this study. C_p. Watanabe (1982). V_0. Marumo et al. (1977). $\alpha(T)$. Suzuki et al. (1979). K_0. Sato (1977). 8. Clinoenstatite: Enthalpy and Entropy of ortho clino transition. Lindsley et al. (1981). C_p. Watanabe (1982). V_0. Syono et al. (1971). $\alpha(T)$. Skinner (1966) and Touloukian et al. (see Watanabe 1982). K_0. Estimated from orthenstatite. Weidner et al. (1978). 9. Clinoferrosillite: Enthalpy and Entropy of ortho-clino transition. Lindsley (1981). C_p. Watanabe (1982). V_0. Syono et al. (1971). $\alpha(T)$. Estimated from Skinner (1966). K_0. Orthoferrosillite from Akimoto (1972) 10. Mg-Perovskite: Enthalpy, entropy and C_p determined in this study. V_0. Yagi et al. (1978). $\alpha(T)$. Jeanloz (Pers. Comm. 1985). K_0. Yagi et al. (1982). 11. Fe-Perovskite: All data determined in this study. 12. Ilmenite: Enthalpy and entropy, this study. C_p. Watanabe (1982). V_0. Ito et al. (1982). $\alpha(T)$. this study. K_0. Liebermann (1976). 13. Wüstite (MgO): Enthalpy, entropy and C_p. Robie et al. (1978). V_0. Robie et al. (1978). $\alpha(T)$. Suzuki (1975). K_0. Mao et al. (1979). 14. Wüstite (FeO): see text. 15. Wüstite ($FeO_{1.5}$): see text. 16. Magnetite: Enthalpy, entropy and C_p. Haas (Pers. Comm. 1984). V_0. Mao et al. (1974). $\alpha(T)$. Hass (Pers. Comm. 1984). K_0. Mao et al. (1974). 17. High-*P*-Magnetite: Enthalpy, entropy and C_p. this study. V_0. Mao et al. (1974). K_0. Ahrens et al. (1969). 18. Hematite: Enthalpy, entropy and C_p. Haas (Pers. Comm. 1984). V_0 and K_0. Liebermann (1968). 19. High-*P*-Hematite: Enthalpy, entropy and C_p, this study. V_0. Mao et al. (1974). K_0. Ahrens et al. (1969). 20. Iron: Enthalpy, entropy and C_p. Barin and Knacke (1978). V_0. Mao et al. (1967). $\alpha(T)$, Clark (1966). K_0. Mao et al. (1967). ** The transitions temperatures are 800, 1,000, 1,042, 1,060, 1,184 and 1,665 K. 21. Quartz: Enthalpy, entropy, C_p and V_0. Robie et al. (1978). $\alpha(T)$. Skinner (1966). K_0. Soga (1968). 22. Coesite: Enthalpy and entropy, this study. C_p and V_0, Robie et al. (1978). $\alpha(T)$. Skinner (1962). K_0. Levien (1981). 23. Stishovite: Enthalpy and entropy, see text. C_p and V_0. Robie et al. (1978). $\alpha(T)$. Ito et al. (1974). K_0. Striefler et al. (1976).

as a function of composition of wüstite), there are two sets of data availabie (see review. Jeanloz and Hazen 1983). The data from dynamic measurements indicate a K_0 of 1.80 Mb for FeO and a similar value for $FeO_{1.5}$. In Figure 2 the data are shown as model A with limits shown by curves A1 and A2. The static measurements of K_0 lead to values of 1.55 Mb and 1.37 Mb for FeO and $FeO_{1.5}$ respectively. In Figure 2 such data are shown in model B. Both models with their indicated limits have been used in our phase equilibrium calculations.

Magnesiowüstite, Olivine and Spinel Solid Solutions

For the magnesiowüstite solid solution, MgO (periclase) is chosen to mix as a third component with FeO and $FeO_{1.5}$. Ito et al. (1984), Ito (1984) and Yagi et al. (1979) determined the distribution of iron and magnesium between coexisting silicate spinel and magnesiowüstite at high temperatures and high pressures and Nafziger and Muan (1967) on Fe−Mg distribution between coexisting magnesiowüstite and olivine at 1,200 °C and 1 bar. These data may be

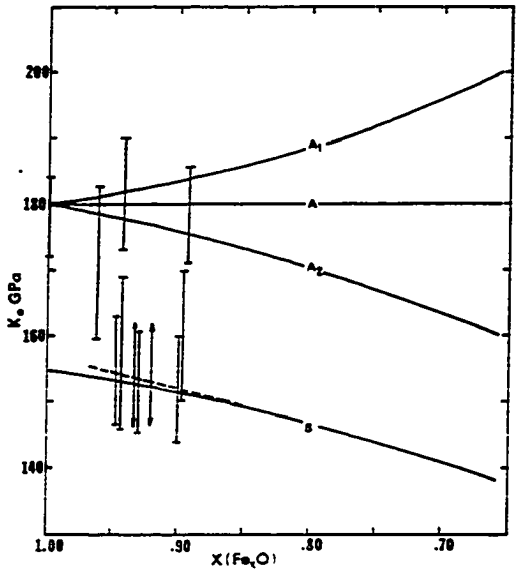

Fig. 2. Isothermal bulk modulus of wüstite as a function of composition or nonstoichiometry. Figure modified from Jeanloz and Hazen (1983). The three curves A, A_1 and A_2 show the effect of extrapolating the results of dynamic measurements. The B curve shows bulk modulus according to the static measurements

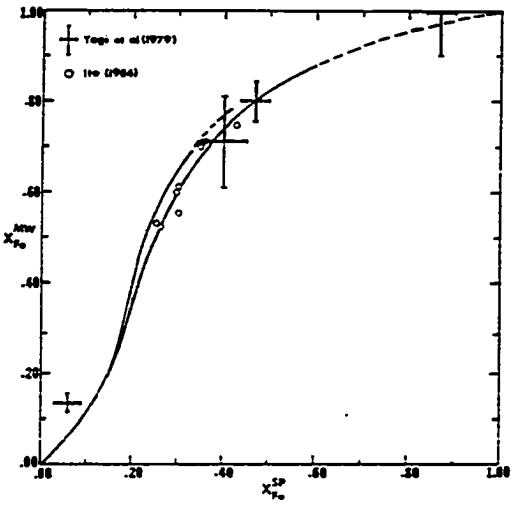

Fig. 3. Distribution of Fe and Mg between wüstite and spinel at a temperature of 1,100 °C and at pressures of 190 kbar (lower curve) and 230 kbar (upper curve). The experimental data are from Ito (1984) and Yagi et al. (1979)

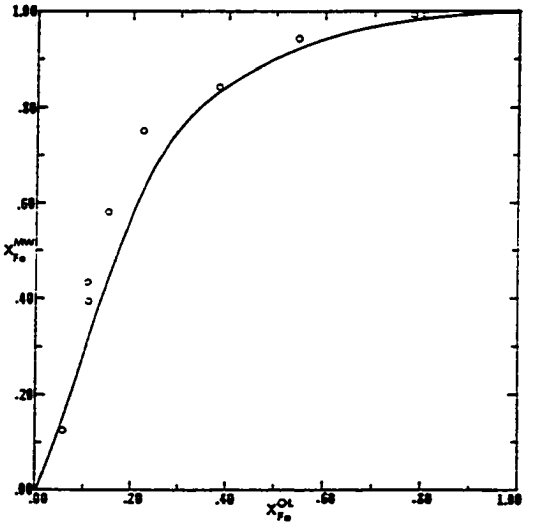

Fig. 4. Distribution of Fe and Mg between coexisting wüstite and olivine at 1,200 °C and a pressure of 1 atm. The experimental data are from Nafziger and Muan (1967). The distribution data in the middle compositional range do not fit well with the calculated curve. This is a consequence of the constraints on solution properties from the other high pressure distribution data (see Figs. 3 and 6)

used to determine solid solution properties of the ternary magnesiowüstite, and of the binary spinel and olivine solid solutions. There are additional data on coexisting pairs of olivine-spinel, olivine-β-phase and β-phase-spinel (see Jeanloz and Thompson 1979 and Fig. 6 later), which should be considered simultaneously in calculating the solution parameters. The computed and observed results on compositions of coexisting phases are shown in Figures 3 and 4.

The calculated data on W_{ij} for the three solutions are (J/mol):

Olivine: $W_{Mg-Fe} = -8{,}314$: $W_{Fe-Mg} = -8{,}314$;
Spinel: $W_{Mg-Fe} = -9{,}977$: $W_{Fe-Mg} = -9{,}977$;
Magnesiowüstite: $W_{Mg-Fe} = -4{,}157$: $W_{Fe-Mg} = 16{,}628$;
β-phase: $W_{Mg-Fe} = -11{,}210$: $W_{Fe-Mg} = -11{,}210$.

For olivine, β-phase and spinel the negative W_{ij} indicate a negative deviation from ideal behavior. For olivine, Wood and Kleppa's (1982) results indicate a positive enthalpy of mixing at 1 bar and 970 K. Their results do not imply a positive W (free energy parameter) and are not necessarily in contradiction with the present results. The negative free energy of mixing as found here may be the combined result of a negative excess volume of mixing and a positive excess entropy of mixing. But this would require that the W_{ij} be a function of pressure and temperature and not constant as given above. In fact the misfit of the calculated curve to the distribution data in the middle compositional range as shown in Figure 4 disappears if we use 0 and 16,628 J/mol as W_{Mg-Fe} and W_{Mg-Fe}, respectively, for olivine. The present data set is not sufficient for evaluating the solution properties in detail and the W_{ij} should be regarded merely as an adjustable constant without any physical significance. These constants cannot be usually changed by more than 10 percent without causing significant misfit of the computed curves to the observed data. If the data on W_{ij} are determined using one pair of coexisting phases (e.g. spinel and wüstite), spurious results may be obtained because of

Table 2. Data on heat capacity of phases in the system Fe–Mg–Si–O

No	$Cp=k_0+k_1T^{-0.5}+k_2T^{-2}+k_3T^{-3}+L_1T+L_2T^2+L_3T^3$						
	k_0	k_1 (10^{-3})	k_2 (10^{-7})	k_3 (10^{-8})	L_1 (10^{2})	L_2 (10^{4})	L_3 (10^{7})
1	44.948	−0.3231	0.0000	0.8331	0.0000	0.0000	0.000
2	108.897	−0.7041	0.0000	−2.6318	0.0000	0.0000	0.000
3	127.665	−1.0617	0.0000	0.8315	0.0000	0.0000	0.000
4	108.218	−0.7362	0.0000	−2.7895	0.0000	0.0000	0.000
5	136.332	−1.3198	0.0000	2.2412	0.0000	0.0000	0.000
6	100.096	−0.5184	−0.0660	−2.4582	0.0000	0.0000	0.000
7	130.986	−1.2014	0.0000	1.3419	0.0000	0.0000	0.000
8	169.701	−1.3667	0.0000	−2.7811	0.0000	0.0000	0.000
9	166.572	−0.9876	−0.0224	−4.3628	0.0000	0.0000	0.000
10	159.423	−1.1776	−0.2979	6.0543	0.0000	0.0000	0.000
11	156.294	−0.7986	−0.3203	4.4726	0.0000	0.0000	0.000
12	204.423	−2.3570	0.0000	3.3958	0.0000	0.0000	0.000
13	58.633	−0.1888	−0.1669	2.3524	0.0000	0.0000	0.000
14	44.399	0.0000	−0.0455	0.0000	4.4413	0.0000	0.000
	−70.121	0.0000	7.8182	0.0000	7.2534	0.0000	0.000
	603.613	−23.3797	0.0000	2,458.9000	0.0000	0.0000	0.000
15	79.625	−0.6432	0.0000	2.8439	0.0000	0.0000	0.000
16, 17	18.389	0.0000	0.0252	0.0000	5.6655	0.0000	0.000
	−2.428	0.0000	3.1281	0.0000	2.4351	0.0000	0.000
	229.436	−8.0196	0.0000	906.2500	0.0000	0.0000	0.000
18, 19	44.399	0.0000	−0.0455	0.0000	4.4413	0.0000	0.000
	−70.121	0.0000	7.8182	0.0000	7.2534	0.0000	0.000
	603.613	−23.3797	0.0000	2,458.9000	0.0000	0.0000	0.000
20	28.175	0.0000	−0.0290	0.0000	−0.7318	0.2504	0.000
	−263.454	0.0000	6.1920	0.0000	25.5800	0.0000	0.000
	−641.905	0.0000	0.0000	0.0000	69.6300	0.0000	0.000
	1,946.250	0.0000	0.0000	0.0000	−178.7000	0.0000	0.000
	−561.932	0.0000	29.1200	0.0000	33.4100	0.0000	0.000
	23.991	0.0000	0.0000	0.0000	0.8360	0.0000	0.000
	83.164	−1.7925	0.0000	88.5332	0.0000	0.0000	0.000
21	128.470	−1.5769	0.0000	2.0212	0.0000	0.0000	0.000
	109.270	−1.4083	0.0000	40.4960	0.0000	0.0000	0.000
22	85.186	−0.3663	−0.3893	6.6563	0.0000	0.0000	0.000
23	88.621	−0.3047	−0.6587	12.4313	0.0000	0.0000	0.000

the possible cancellation of nonideality effect. However, with the employment of three coexisting pairs of phases (olivine-wüstite, wüstite-spinel and olivine-spinel), the chances of the calculated set of constants being unique are much improved.

$MgO-SiO_2$

Phase relations in the SiO_2 system were discussed recently by Akaogi and Navrotsky (1984). Adopting the equilibrium pressure and temperature for the reaction

$$\text{Quartz} = \text{Coesite} \qquad (20)$$

as calculated by them and the thermochemical data on quartz from Robie et al. (1978), the $\Delta H^0_{f,298}$ and $\Delta S^0_{f,298}$ for coesite are calculated (Table 1). Akaogi and Navrotsky (1984) also evaluated the data on coesite-stishovite transition. Their recommended $P-T$ curve is adopted by us and used in calculating $\Delta H^0_{f,298}$ and $\Delta S^0_{f,298}$ for stishovite. However, we find that a number of data is available for K_0 (and the choice must be constrained by considering the reactions listed in Table 4). The K_0 listed in Table 3 for stishovite matches closely with the determination by Striefler and Barsch (1976). If this approach is not followed, certain inconsistencies result. For example, if a K_0 of 2.49 Mb is used, we find that in the pressure range of 235–280 kbar and at a temperature of 1,273 K, the following reaction takes place:

$$Mg_2SiO_4\ (\text{spinel}) = 2MgO\ (\text{Periclase}) + SiO_2\ (\text{St}) \qquad (21)$$

instead of

$$Mg_2SiO_4\ (\text{spinel}) = MgSiO_3\ (\text{Pv}) + MgO\ (\text{Periclase}) \qquad (22)$$

as observed in the experiments of Ito and Yamada (1982) and Yagi et al. (1979). The data on various other phases involved in the reactions with stishovite are listed in Tables 1 to 3 and their derivations when related to the stishovite data are fully discussed in the following sections.

For magnesian silicates, the evaluation of the data is begun with the data on forsterite which have appeared recently (Robie et al. 1982, Brousse et al. 1984). These data were evaluated by Saxena and Chatterjee (1986) in the system $CaO-MgO-Al_2O_3-SiO_2$.

Navrotsky et al. (1979) and Akaogi et al. (1984) have determined thermochemical data on $\alpha-$, $\beta-$ and $\gamma-Mg_2SiO_4$ by high temperature oxide melt solution calorimetry. Akaogi et al. (1984) critically evaluated the existing thermochemical data and listed the transition parameters (ΔH, ΔS, and ΔV) at 1,000 K for the $\alpha-\beta$, $\alpha-\gamma$ and $\beta-\gamma$ transitions. We are interested in $\Delta H_{f,298}$, ΔS_{298} and C_p

Table 3. Data on molar volume, coefficients of thermal expansion and compressibility

No	V_0 (cm³/mol)	α_0 (10^5)	α_1 (10^8)	α_2	K_0 (Mb)	K_0'
2	21.835	0.3052	0.8504	−0.5824	1.292	4.88
3	23.140	0.2660	0.8736	−0.2487	1.379	4.00
4	20.270	0.2711	0.6885	−0.5767	1.600	4.00
5	21.575	0.2319	0.7117	−0.2430	1.660	4.00
6	19.765	0.2367	0.5298	−0.5702	2.130	4.00
7	21.010	0.2455	0.3591	−0.3703	1.970	4.00
8	31.270	0.1391	2.5440	0.1282	1.000	4.00
9	33.040	0.1391	2.5440	0.1282	1.160	4.00
10	24.500	0.1100	2.5440	0.1282	2.580	4.00
11	25.500	0.1100	2.5440	0.1282	2.780	4.00
12	26.350	0.1100	2.5440	0.1282	2.100	4.00
13	11.250	0.3681	0.9283	−0.7445	1.599	4.56
14	15.970	0.2453	1.6702	0.0020	1.800	4.00
15	12.250	0.1688	0.2040	0.0190	1.800	4.00
16	11.131	0.2611	3.2602	0.0040	1.830	4.00
17	9.115	0.2611	3.2602	0.0040	4.488	4.00
18	15.137	0.2453	1.6702	0.0020	2.066	4.53
19	13.430	0.2453	1.6702	0.0020	3.991	4.00
20	7.150	0.5055	−1.0483	0.0128	1.640	5.00
21	22.690	0.3100	2.6780	0.0000	0.374	6.40
22	20.640	0.0543	0.8315	−0.0605	0.960	8.40
23	14.010	0.1023	2.0000	0.0000	3.160	6.00

Table 4. Reactions used in estimating the compressibility data on stishovite

Reactions	References
1. $2MgSiO_3$(Cpx) $=2MgSi_{0.5}O_2(\beta)+SiO_2$(St)	Akaogi and Akimoto (1977)
2. $2FeSiO_3$(Cpx) $=2FeSi_{0.5}O_2$(Sp)$+SiO_2$(St)	Akimoto and Syno (1970)
3. $2Mg_{0.5}SiO_2$(Sp) $=2MgO$(rock salt)$-SiO_2$(St)	See text
4. SiO_2(Coes)$=SiO_2$(St)	See text
5. $2FeSi_{0.5}O_2=2FeO$(MW)$+SiO_2$(St)	Yagi et al. (1979)
6. $2Mg_{0.5}SiO_2$(Sp) $=MgSiO_3$(Per)$+MgO$(rock salt)	Ito and Yamada (1982) Yagi et al. (1979)

data which may be used to calculate ΔG over a broad temperature range. Since Suito's (1977) experiments on the transition covers a broad range of temperature and appear consistent with thermochemistry, his data are used in calculating these quantities. ΔH^0_{1000} and ΔS^0_{1000} data as determined by Akaogi et al. (1984) are used as additional constraints. Uncertainties in these calculated data are large and are of the same magnitude (see Tables 1 to 3) as discussed by Akaogi et al. (1984).

The data on clinoenstatite are based on the data on orthoenstatite (Brousse et al. 1984) with the ortho/clino transition data from Lindsley et al. (1981). This combination along with the data on the β-phase and on stishovite reproduce the pressure-temperature relations for reaction (1) in Table 4 as determined by Akaogi and Akimoto (1977).

For $MgSiO_3$-perovskite and ilmenite, the unavailable thermochemical data (see Tables 1 to 3) are estimated from the data of Ito and Yamada (1982) and Navrotsky and Akaogi (1984).

$FeO-SiO_2$

Heat capacity for $\gamma-Fe_2SiO_4$ is determined by Watanabe (1982). At equilibrium for the $\alpha-\gamma$ transition, we have

$$\Delta G(P, T)=0$$

To calculate ΔG for the reaction, we need ΔH^0_{298} and ΔS^0_{298} in addition to the already available data on heat capacity and molar volumes. Akimoto (1965, 1967) determined the equilibrium pressure and temperature for the $\alpha-\gamma$ transition. If these data are used with the additional constraints provided by the data on ΔH^0_{1000} and ΔS^0_{1000} as obtained by Navrotsky and Akaogi (1984), we may calculate ΔH^0_{298} and ΔS^0_{298} for $\alpha-\gamma$ transition and therefore the $\Delta H^0_{f,298}$ and $\Delta S^0_{f,298}$ for $\gamma-Fe_2SiO_4$. The calculated data are listed in Table 1. Figure 5 shows the equilibrium pressure-temperature curve calculated from these data.

For clinoferrosillite ($FeSiO_3$), the data are based on the data of orthoferrosillite (Bohlen and Boettcher 1982) with ortho/clino transition data from Lindsley (1981). These data along with the data on Fe-spinel are consistent with the experimental data on reaction (2) in Table 4. $FeSiO_3$-perovskite is considered later.

$Mg_2SiO_4-Fe_2SiO_4$

Figure 6 shows phase relations in the binary $Mg_2SiO_4-Fe_2SiO_4$ system. The $\alpha-\gamma$ loop is metastable at the Mg-rich end, interrupted by the stability of β-phase. Thermochemical data are available (Tables 1–3) for $\beta-Mg_2SiO_4$ but not for $\beta-Fe_2SiO_4$ because the latter is a fictive component occurring only in solution and not as a pure phase. To

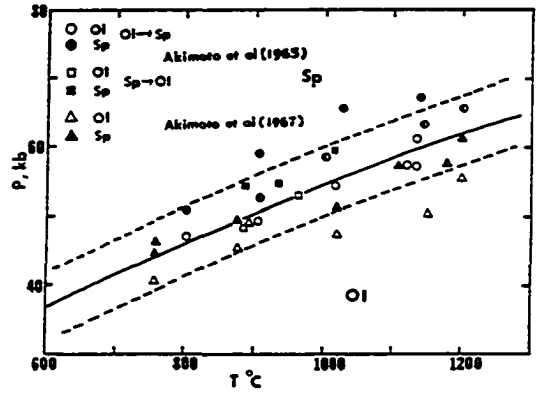

Fig. 5. Equilibrium data on the fayalite-spinel transition. The curve is fitted using the adjusted thermochemical data in Tables 1 to 3

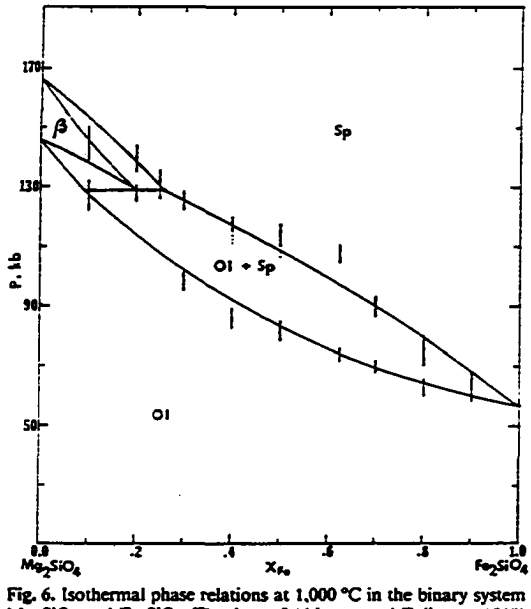

Fig. 6. Isothermal phase relations at 1,000 °C in the binary system Mg_2SiO_4 and Fe_2SiO_4. The data of Akimoto and Fujisawa (1968) and Kawad (1977) are presented as short vertical bars. The curves are fitted using the thermochemical data in Tables 1 to 3. See text for other details

estimate its thermochemical properties, the C_p is first estimated from the relation:

$$C_p(\beta-Fe_2SiO_4)=C_p(\beta-Mg_2SiO_4)-C_p(\alpha-Mg_2SiO_4)+C_p(\alpha-Fe_2SiO_4) \quad (23)$$

The estimated C_p may then be combined with the data on $\alpha-\beta$ and $\beta-\gamma$ transitions as determined by Navrotsky and Akaogi (1984) to obtain $\Delta H_{f,298}$ and ΔS_{298} for the $\beta-Fe_2SiO_4$ phase. The phase relations calculated by using these data are shown in Figure 6.

$MgSiO_3-FeSiO_3$

$FeSiO_3$-perovskite appears as a component of the perovskite solid solution. It has not been synthesized and from the available data as discussed below, it is unstable. Therefore the thermochemical data have to be estimated from the available synthesis experimental data. Ito (1984), Ito et al. (1983) and Yagi et al. (1979) have determined the compositions of coexisting magnesiowüstite and perovskite. These data indicate that the maximum content of $FeSiO_3$ in perovskite when it becomes unstable, breaking down to magnesiowüstite and stishovite is a function of pressure. The data of Ito et al. (1983) show that increasing temperature from 1,100 °C to 1,600 °C does not increase the solubility of $FeSiO_3$ in perovskite significantly. Similarly Yagi et al. (1979) make the important observation that high pressure upto 700 kbar does not raise the solubility of $FeSiO_3$ to significantly beyond 20 mole percent. These data provide important constraints on the thermochemical properties of Fe-perovskite. As the coefficient of Fe–Mg distribution between coexisting magnesiowüstite and perovskite changes little with pressure or temperature, only the compositional dependence of the distribution need be modeled. The W_{ij} parameters for magnesiowüstite having already been determined, the W_{ij} parameters for perovskite are determined using the experimental distribution data discussed above. These are:

$$W_{Mg,\,Fe}=W_{Fe,\,Mg}=-2{,}494\ \text{J/mol}.$$

Since the stability of Fe-perovskite is highly dependent on the pressure effect, it is important to discuss the molar volume and bulk modulus data on Fe-perovskite. Yagi et al. (1979) suggested 25.06 cm^3 and 2.58 as the values for molar volume and bulk modulus respectively. One approach we adopt in determination of the Fe end member of a solid solution is to calculate starting values of enthalpy, entropy and heat capacity by comparing the differences in these properties as revealed in the available data on Mg and Fe end members. Table 5 shows such a comparison for many pairs of different crystal structures. The starting values of enthalpy and entropy are then refined by comparing the

Table 5. Determination of data for perovskite ($FeSiO_3$) by comparison

Formula	Structure	$\Delta H_{298,Mg}-\Delta H_{298,Fe}$ (J/mol)	$\Delta S_{298,Mg}-\Delta S_{298,Fe}$ (J/kmol)	$V_{0,Mg}-V_{0,Fe}$ (cm^3/mol)
$MgSi_{0.5}O_2-FeSi_{0.5}O_2$	Olivine	−349.515	−28.44	−1.30
$MgSi_{0.5}O_2-FeSi_{0.5}O_2$	Spinel	−330.966	−25.69	−1.24
$MgAl_2O_4-FeAl_2O_4$	Spinel	−350.599	−25.87	−1.04
$MgSiO_3-FeSiO_3$	Opx	−351.780	−28.29	−1.67
$MgSiO_3-FeSiO_3$	Cpx	−350.420	−28.17	−1.57
$MgSiO_3-FeSiO_3$	Perovskite	−350.000 ± 15.000	−26.00 ± 2.00	−1.00 ± 0.50

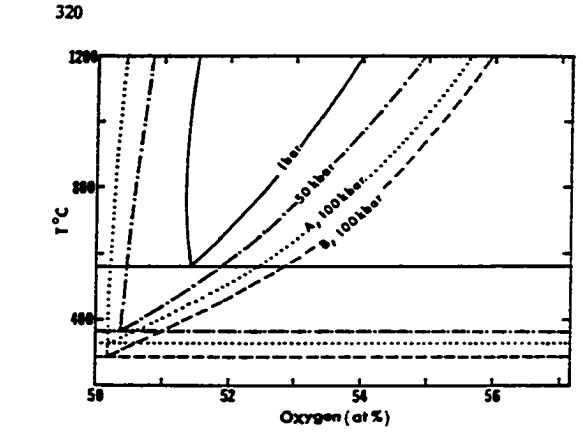

Fig. 8. Effect of pressure on the stability of wüstite in the system Fe–O. Models A and B represent the bulk modulus for wüstite shown in Figure 2

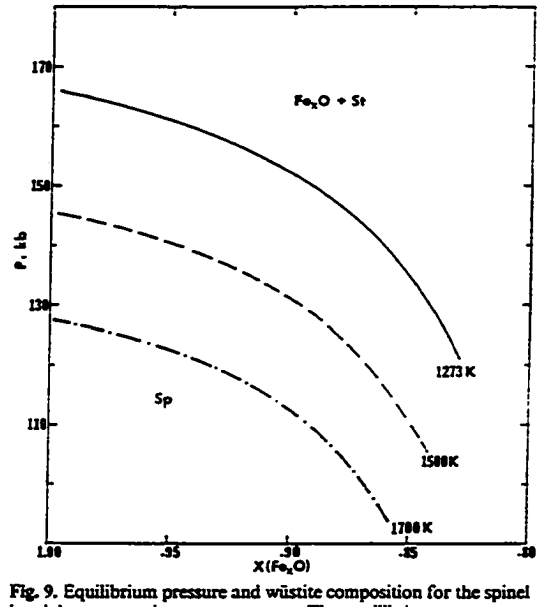

Fig. 9. Equilibrium pressure and wüstite composition for the spinel breakdown at various temperatures. The equilibrium pressure at a given temperature varies as a function of the wüstite composition determined by the Fe/O ratio of the system

The System Fe–O–Si

With the addition of Si to the system, fayalite (Fe_2SiO_4), ferrosillite ($FeSiO_3$), coesite (SiO_2), stishovite (SiO_2), β- and γ-spinel (Fe_2SiO_4), perovskite ($FeSiO_3$) and quartz are added to the list of possible phases.

Figure 9 shows the calculated relations for the divariant reaction:

$$Fe_2SiO_4 = \{2\ FeO\} + SiO_2 \qquad (24)$$

where {FeO} is a component in the wüstite solid solution ($FeO-FeO_{1.5}$). The pressure of the equilibrium reaction

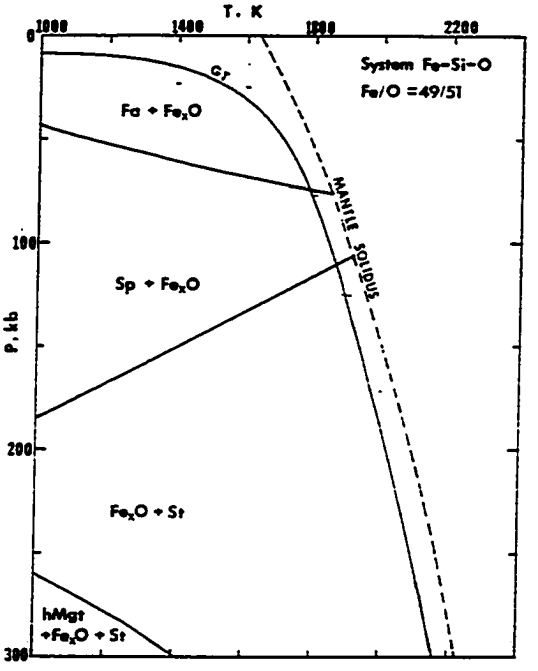

Fig. 10. Phase equilibrium relations in the system with Fe:O as 49:51 and some SiO_2. With increasing pressure fayalite changes to spinel and spinel to wüstite and stishovite. The oxide, wüstite, starts disproportionating first to wüstite and high-*P*-magnetite and finally to iron and high-*P*-magnetite. The solid curve labeled *GT* represents approximate oceanic geothermal gradient and the dashed curve the mantle solidus (Stacey 1977)

at a given temperature will be a function of the Fe:O ratio and the composition of the wüstite solid solution. Thus at 1,000 °C, the equilibrium pressure for the above reaction may vary from nearly 130 kbar to 170 kbar as shown in Figure 9. This pressure is shown as a single value in figures drawn by Yagi et al. (1979) and Jeanloz (1983). These diagrams refer to a fixed, albeit unspecified, value of oxygen fugacity and of Fe_xO in wüstite. Oxygen is involved in the reaction only indirectly; its variation being represented by the two end members FeO and $FeO_{1.5}$ of the wüstite solid solution.

Figure 10 shows phase equilibrium relations in the Fe–Si–O system with an Fe/O ratio of 49/51. The calculations are done using the Gibbs free energy minimization technique (Saxena and Eriksson 1985) which permits the inclusion of all phases possible in the system. In the temperature range from 1,000 K to mantle solidus, the mineralogical changes are mainly due to increasing pressure. At pressures up to 40 to 70 kbar, fayalite is in equilibrium with a wüstite of somewhat varying composition. In fact, such a wüstite is stable all through the range of pressure of this study (300 kbar). Fayalite changes to γ-spinel which breaks down to wüstite and stishovite with increasing pressure. Finally, a high pressure assemblage with high-*P*-magnetite, wüstite and stishovite appears. The data on molar volume of high-*P*-magnetite is the same as that of Mao and Bell (1977)

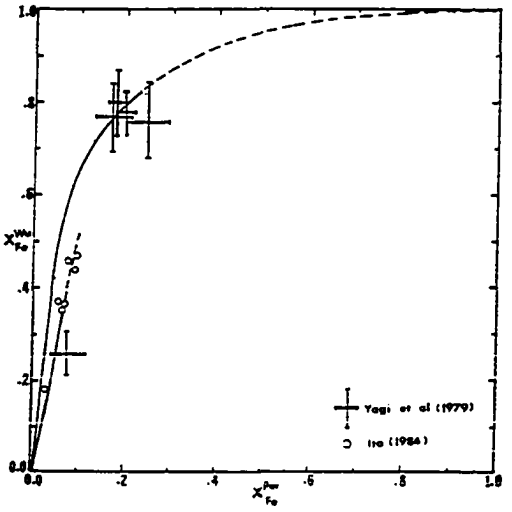

Fig. 7. Distribution of Fe and Mg between coexisting perovskite and magnesiowüstite. The distribution data are from Yagi et al. (1979) and Ito (1984). The solid curves are computed distributions at temperature of 1,100 °C and pressure of 260 kbar (lower curve) at temperature of 1,000 °C and pressure of 450 kbar (upper curve)

calculated compositions of coexisting phases with the observed compositions. When this approach is used for Fe-perovskite with volume data of Yagi et al. (1979), the observed compositions could not be matched even after using the maximum range of variation in the enthalpy and entropy data permitted by crystal-chemical considerations. Therefore, it is found necessary to reestimate the molar volume and bulk modulus data. The estimated data are listed in Table 3 and are somewhat different than those calculated by Yagi et al. (1979). Figure 7 shows the distribution of Fe and Mg in coexisting magnesiowüstite and perovskite at a temperature of 1,000 °C and at pressures of 260 and 450 kbar. The computed results at 450 kbar are quite consistent with the results of Yagi et al. (1979), with about 20 mole per cent $FeSiO_3$. With decreasing pressure the molar concentration of $FeSiO_3$ decreases as it should according to Ito's (1984) results. The ternary phase topology is compatible with all the phase relations at 260 kbar as presented by Ito et al. (1984), Ito (1984) and Yagi et al. (1979). However, at 230 kbar, these results are consistent only with the results of Ito (1984) and do not show a stable solution of perovskite as found by Yagi et al. (1979) (see discussion later).

Discussion of Errors in the Estimated Data

If measured calorimetric and thermophysical data on certain phases are not available, these data should be derived from experimental phase equilibrium studies as discussed in previous sections. There may be considerable errors of pressure and temperature in the experimental data, especially at high pressures, which could cause large errors in the estimated thermochemical-thermophysical data. Some of the experimental data may be unreversed. In general, if the phase equilibrium data were reliable, we adjusted those thermochemical data that were considered as least reliable. Some missing data were also estimated this way. Since there are errors in pressure and temperature in the experimental phase equilibrium data, the estimated thermochemical data involve uncertainties which could be different over different temperature and pressure ranges. The error in ΔG of the equilibrium reaction should also be distributed among the various parameters. For example, the transition pressure between $\alpha-Mg_2SiO_4$ and $\beta-Mg_2SiO_4$ is around 140 kbar in the temperature range between 700 to 1,300 °C for the polymorphs. If there is an error of ±10 kbar for this transition, the error in ΔG is ±1,300 J/mol. This error can be assigned to any of the thermochemical or physical parameters of the phase or phases involved. For example if assigned to enthalpy, we have an error of ±1,300 J/mol. Similiarly we could have ±1.3 J/Kmol on entropy, ±0.06 cm^3/mol on molar volume or ±0.23 Mb on bulk modulus. For the decomposition of $\gamma-Mg_2SiO_4$ to periclase and perovskite at about 255 kbar in the temperature range of 700 to 1,400 °C, an error of ±20 kbar in equilibrium pressure reflects an error of ±6,000 J/mol in ΔG, which could be equivalent to ±6,000 J/mol error on enthalpy, ±6.0 J/Kmol on entropy, ±0.22 cm^3/mol on molar volume or ±0.40 Mb on bulk modulus. The error assignment need not be arbitrary if most of the parameters are independently well measured.

Thermochemical data calculated from experimental phase equilibrium may not be the global value for the phase if the calculation is done only with one set of equilibrium data. The use of multireaction equilibrium calculation as done here through the method of minimization of free energy prevents such problems. This point was well demonstrated in the derivation of the data on stishovite. The thermochemical and physical data estimated for stishovite reproduce the phase transition between coesite and stishovite as well as for those stishovite involving reactions listed in Table 4.

Phase Equilibrium Calculations

The System Fe—O at High Pressures

The following work is based on the experimental data of Mao et al. (1979) and the theoretical interpretation of Mao and Bell (1977). Bell et al. (1979) and Hazen and Jeanloz (1984).

Figure 8 shows calculated phase relations in the Fe—O system at various P, T and compositions. Two models A and B of bulk modulus, as discussed before, are used in the calculations. There is virtually no effect of bulk modulus differences up to 50 kbar. The effect becomes significant at 100 kbar. In general the effect of pressure on the phase relations is to lower the temperature of the triple point (coexisting Fe, Fe_xO and Fe_3O_4) and increase the size of the compositional field of stability of Fe_xO. According to these calculations, the stoichiometric FeO composition is approached closely at 100 kbar at low temperature. Simons (1980) found a similar behavior in wüstite at 45 kbar. However, Liu (1976) reports that at pressures greater than 100 kbar, the iron content of wüstite decreases somewhat. It has not been possible to reproduce this effect in this study.

and Mao et al. (1974). The latter found it difficult to reverse the magnetite/high-*P*-magnetite reaction in their experiments and therefore the thermochemical data for this phase transformation is uncertain. The data used here are in conformity with the estimated phase diagram of Mao and Bell (1977).

All boundaries between assemblages shown as solid lines in Fig. 8 are divariant fields because of the Fe_xO solution. The effect on equilibrium *P* and *T*, however, is small and cannot be shown in the figure.

The System Fe–Mg–Si–O

A detailed description of the phase relations in this system would require a consideration of oxygen fugacity at various pressures and temperatures and will be discussed in future publications. The present data, however, do permit the calculations in the stability field of magnesiowüstite. Some representative mineral assemblages at 2,000 °K and at various pressures are:

150 kbar: β-phase + Cpx + Mw
185 kbar: β-phase + Mw + St
200 kbar: β-phase + Mw + St
220 kbar: Sp + Mw + St
250 kbar: Mw + St
300 kbar: Pv + Mw + St
320 kbar: Pv + Mw

Discussion and Conclusions

A major goal of this study is to establish a thermochemical data set which may be used to compute experimentally determined phase equilibrium as closely as possible. These data should at the same time be compatible with all evaluated calorimetric and volume (molar volume, thermal expansion and compressibility) data which are available to date. The data in Tables 1 to 3 and the solution data presented in this study meet these criteria well and may be used to explore possible phase equilibrium in systems of varying compositions at pressures upto and exceeding 300 kbar. Such computations should be deemed essential in planning experimental studies relevant to mantle mineralogy and in pointing out major inconsistencies in the existing data.

Two sets of somewhat different phase synthesis data are available in the system Mg–Fe–Si–O. The data of Ito (1984) differ in one major respect from the data of Yagi et al. (1979). While the phase synthesis data on the stability of pure $MgSiO_3$-perovskite are similar in both studies, perovskite solution with a few mole percent of $FeSiO_3$ appears below 200 kbar in the study of Yagi et al. (1979), compared to a pressure of about 250–260 kbar in the study of Ito (1984). Although the Fe–Mg distribution data in coexisting pairs of phases (magnesiowüstite-perovskite, magnesiowüstite-olivine, olivine-spinel, magnesiowüstite-spinel) strongly support the choice of the solution model for perovskite, it is important that new experimental be obtained on coexisting perovskite-magnesiowüstite in the pressure range of 200–300 kbar.

The experimental data reviewed in this study have made it possible to establish the framework of a thermochemical data base but several of the data presented here require refinement. Many possibilities for experimental studies may be noted. For example, magnesiowüstite solid solution is calculated to be stable over a broad pressure range with one or more of all the other Fe–Mg solid solutions (olivine, spinel, clinopyroxene, perovskite and ilmenite). The properties of this solid solution as presented here are tentative and must be refined through data on compositions of coexisting phases. Clinopyroxene and magnesiowüstite coexist over a broad temperature and pressure range and the compositional data on this pair should be extremely useful in constraining the magnesiowüstite solution properties. Further constraints could be provided with the data on coexisting olivine and magnesiowüstite at 100 kbar; at present data are available only at 1 bar. A well-established data set for magnesiowüstite could then be used to determine the solution properties of other phases, e.g. spinel, ilmenite, and perovskite.

Appendix

The method of minimizing the total Gibbs free energy employing linear algebraic techniques as discussed by Eriksson (1975) and Smith and Missen (1982) is particularly suitable for computers. It forms the basis of the computer program SOLGASMIX (Eriksson 1975) which is used for all chemical equilibrium calculations in this book.

The total Gibbs free energy of a chemical system can be expressed as

$$G=\Sigma \mu_i n_i \tag{1}$$

where μ is chemical potential. Chemical potential and activity are interrelated by the expression

$$\mu=\mu^0+RT\ln a \tag{2}$$

where μ^0 denotes the standard state potential. For an ideal gas phase species, a species in a non-ideal solution phase and a stoichiometric phase, respectively, we find

$$\mu_i=\mu_i^0+RT\ln P+RT\ln x_i \tag{3}$$

$$\mu_i=\mu_i^0+RT\ln\gamma_i+RT\ln x_i \tag{4}$$

$$\mu_i=\mu_i^0 \tag{5}$$

In these equations *x* is mole fraction and γ is activity coefficient.

The minimization of *G* in equation (1) at constant pressure and temperature is achieved with the constraints imposed by the mass balance relationships represented as

$$\Sigma a_{ij} n_i=b_j (j=1, 2,\ldots l) \tag{6}$$

where a_{ij} is the number of atoms of the jth element in a molecule of the ith species, l is the total number of elements and b_j is the total amount ot the jth element. This is a simple form of constrained optimization problem which may be solved by the Lagrange method of undetermined multipliers. For this, we define a function,

$$F=G+\sum_{j=1}^{l}\lambda_j\left(b_j-\sum a_{ij} n_i\right) \tag{7}$$

where λ_j denotes the Lagrangian multipliers, for which the necessary conditions, at an extremum of F, are

$$\left(\frac{\partial F}{\partial n_i}\right)_{n_{i\neq},\lambda}=\mu_i-\sum a_{ij}\lambda_j=0. \tag{8}$$

$$\left(\frac{\partial F}{\partial \lambda_j}\right)_{\lambda_{k\neq j},n} = b_j - \sum a_{ij} n_i = 0. \quad (9)$$

$$n_i \geq 0 \quad (10)$$

Combination of equations (3) to (5) with equation (8) gives

$$\mu_i^0 + RT \ln P + RT \ln X_i - \Sigma a_{ij} \lambda_j = 0 \quad (11)$$

$$\mu_i^0 + RT \ln \gamma_i + RT \ln X_i - \Sigma a_{ij} \lambda_j = 0 \quad (12)$$

$$\mu_i^0 - \Sigma a_{ij} \lambda_j = 0 \quad (13)$$

Equation (11) is valid for gas phase species while equations (12) and (13) hold for components of solution phases and stoichiometric phases respectively.

The system consisting of equations (6) and (11) to (13) with the unknowns n_i and λ_j is non-linear because of the logarithmic term in equations (11) and (12). The next step is therefore a linearization of these equations by expansion in a Taylor series around an estimated equilibrium composition up to and including the term of the first order. This is equivalent to making a quadratic approximation to the free-energy surface, and we can obtain an expression which relates n_i linearly to λ_j and the estimated equilibrium amounts. Incorporation of this expression into equation (6) gives then the final linear system of equations. The number of unknowns is reduced to the sum of elements and phases assumed to be present at equilibrium.

Parametrized activity-coefficient expressions to be inserted into equation (12) are supplied by the user. In order to avoid the need of also specifying derivatives, $\ln \gamma_i$ is treated as constant when calculating the partial derivative with respect to n_i in the Taylor expansion. The partial derivative is therefore approximate as long as the estimated equilibrium composition does not correspond to a free-energy minimum.

The approximation to the free-energy surface implies an iterative algorithm and, if positive, the calculated n_i values are used as improved estimates in the subsequent iteration cycle. If some n_i values are negative, these are set to zero before being used as the starting-point for a new Taylor expansion. The iterative procedure ends when the calculated values coincide with the starting estimates.

The condensed phases included in the initial estimate are constrained by the Gibbs phase rule but need not necessarily be the correct ones of the final equilibrium state. Another phase combination might yield a lower free energy, and condensed phases need to be withdrawn from of added to the previous combination until the set of equilibrium phases is found. This set has the characteristic feature that the activity for an omitted stoichiometric phase must be less than one as must the sum of mole fractions for an omitted solution phase.

For a more detailed description of the equations used in SOLGASMIX, see Eriksson and Rosén (1973).

Acknowledgements. The writers had valuable help from A. Navrotsky in the evaluation of the experimental data and in the many revisions of the original manuscript. Financial support for the research was provided by the National Science Foundation (grant # EAR 8415800) and the CUNY-PSCBHE (grant # 6-65191).

References

Ahrens TJ, Anderson DL, Ringwood AE (1969) Equations of state and crystal structure of high-pressure phases of shocked silicates and oxides. Rev Geophys 7:667–707

Akaogi M, Akimoto S (1977) Pyroxene-garnet solid solution equilibria in the system $Mg_4Si_4O_{12}-Mg_3Al_2Si_3O_{12}$ and $Fe_4Si_4O_{12}-Fe_3Al_2Si_3O_{12}$ at high pressures and temperatures. Phys Earth Planet Inter 15:90–106

Akaogi M, Navrotsky A (1984) The quartz-coesite-stishovite transformations: New calorimetric measurements and calculation of phase diagrams. Phys Earth Planet Inter 36:124–134

Akaogi M, Ross NL, McMillan P, Navrotsky A (1984) The Mg_2SiO_4 polymorphs (olivine, modified spinel and spinel) thermodynamic properties from oxide melt solution calorimetry, phase relations and models of lattice vibrations. Am Mineral 69:499–512

Akimoto S (1972) The system $MgO-FeO-SiO_2$ at high pressures and temperatures – Phase equilibria and elastic properties. Tectonophysics 13:161–187

Akimoto S, Fujisawa H, Katsura T (1965) Olivine-spinel transition in Fe_2SiO_4 and Ni_2SiO_4. J Geophys Res 66:1969–1977

Akimoto S, Fujisawa H (1968) Olivine-spinel solid solution equilibria in the system $Mg_2SiO_4-Fe_2SiO_4$. J Geophys Res 73:1467–1473

Akimoto S, Komada E, Kushiro I (1967) Effect of pressure on the melting of olivine and spinel polymorphs of Fe_2SiO_4. J Geophys Res 68:679–686

Akimoto S, Matsui Y, Syono Y (1976) High pressure crystal chemistry in orthosilicates and formation of the mantle transition zone, in the Physics and Chemistry of Minerals and Rocks, R J Strens (ed), John Wiley, London, pp 327–363

Akimoto S, Syono Y (1970) High-pressure decomposition of the system $FeSiO_3-MgSiO_3$. Phys Earth Planet Inter 3:186–188

Barin I, Knacke O (1973) Thermochemical properties of inorganic substances. Springer, Berlin Heidelberg New York

Bell PM, Yagi T, Mao HK (1979) Iron-magnesium distribution coefficients between spinel [(Mg, Fe)$_2$SiO$_4$], magnesiowüstite [(Mg, Fe)O] and perovskite [(Mg, Fe)SiO$_3$]. Carnegie Inst Washington Yearb 78:618–621

Berman RG, Brown TH (1985) Heat capacity of minerals in the system $Na_2O-K_2O-CaO-MgO-FeO-Fe_2O_3-Al_2O_3-SiO_2-TiO_2-H_2O-CO_2$: representation, estimation and high temperature extrapolation. Contrib Mineral Petrol 89:168–183.

Bertrand GL, Acree WE Jr, Burchfield T (1983) Thermochemical excess properties of multicomponent systems: representation and estimation from binary mixing data. J Solution Chem 12:327–340

Bjorkman B (1984) Quantitative equilibrium calculations on systems with relevance to copper melting and converting. Ph D Thesis, Univ of Umea, Sweden

Bohlen SR, Boettcher AL (1982) Experimental investigations and geological applications of olivine-orthopyroxene geobarometry. Am Mineral 66:951–964

Brousse C, Newton RC, Kleppa OJ (1984) Enthalpy of formation of forsterite, enstatite, akermanite, monticellite and merwinite at 1,073 K determined by alkali borate solution calorimetry. Geochim Cosmochim Acta 48:1081–1088

Carmichael RS (1982) Handbook of physical properties of rocks. CRC Press

Clark SP Jr (1966) Handbook of physical constants. Mem Geol Soc Am 97

Eriksson G (1975) Thermodynamic studies of high temperature equilibria. XII.SOLGASMIX a computer program for calculation of equilibrium compositions in multiphase systems. Chem Scr 8:100–103

Fei Y, Saxena SK, Eriksson GE (1986) Silicate solution models. Contrib Mineral Petrol (in press)

Ganguly J, Saxena SK (1984) Mixing properties of aluminosilicate garnets: constraints from natural and experimental data and application to geothermobarometry. Am Mineral 69:88–97

Goel RP, Kellogg HH, Larrain J (1980) Mathematical description of the thermodynamic properties of the system iron-oxygen and iron-oxygensilica. Metall Trans B 11B:107–117

Guggenheim EA (1967) Thermodynamics. North-Holland Publ Co, Amsterdam

Hazen RM, Jeanloz R (1984) Wüstite ($Fe_{1-x}O$): A review of its defect structure and physical properties. Rev Geophys Space Phys 22:37–46

Helgeson HC, Delany JM, Nesbitt HW, Bird DK (1978) Summary and critique of the thermodynamic properties of rock-forming minerals. Am J Sci 278-A:221

Hentschel B (1970) Stoichiometric FeO as metastable intermediate of the decomposition of wüstite at 225 C. Z Naturforsch A-25:1996–1997

Ito E (1984) Ultra-high pressure phase relations of the system $MgO-FeO-SiO_2$ and their geophysical implications. Materials Science of the Earth's Interior, edited by I Sunagawa, pp 387–394

Ito E, Yamada H (1982) Stability relations of silicate spinel ilmenites and perovskites. In: Akimoto S and Manghnani MH (eds) High pressure research in geophysics, pp 405–419

Ito E, Takahashi E, Matsui Y (1984) The mineralogy and chemistry of the lower mantle: an implication of the ultrahigh-pressure phase relations in the system $MgO-FeO-SiO_2$. Earth Planet Sci Lett 67:238–248

Ito H, Kawada K, Akimoto S (1974) Thermal expansion of stishovite. Phys Earth Planet Inter 8:277–281

Jeanloz R, Thompson AB (1983) Phase transitions and mantle discontinuities. Rev Geophys Space Phys 21:51–74

Jeanloz R, Hazen RM (1983) Compression, nonstoichiometry and bulk viscosity of wüstite. Nature 304:620–622

Kawada K (1977) System $Mg_2SiO_4-Fe_2SiO_4$ at high pressures and temperatures and the earth's interior. Ph D Thesis, Univ of Tokyo, Tokyo, pp 187

Kubaschewski O (1982) Iron-binary phase diagrams. Springer, Berlin Heidelberg New York, pp 185

Kuskov DL (1979) Equations of state for some substances at very high pressures. Geokhimiya 7:963–983

Lindsley DH (1981) The formation of pigeonite on the join hedenbergite-ferrosillite at 11.5 and 15 kbar: experiments and a solution model. Am Mineral 66:1175–1182

Lindsley DH, Grover JE, Davidson PM (1981) The thermodynamics of the $Mg_2Si_2O_6-CaMgSi_2O_6$ join: a review and an improved model. Adv Phys Geochem 1:149–176

Liu L (1976) The high-pressure phases of $FeSiO_3$ with implications for Fe_2SiO_4 and FeO. Earth Planet Sci Lett 33:101–106

Levien L, Prewitt CT (1981) High-pressure crystal structure and compressibility of coesite. Am Mineral 66:324–333

Liebermann RC (1976) Elasticity of ilmenite. Phys Earth Planet Inter 12:5–10

Liebermann RC, Ringwood AE, Major A (1976) Elasticity of polycrystalline stishovite. Earth Planet Sci Lett 32:127–

Liebermann RC, Schreiber E (1968) Elastic constants of polycrystalline hematite as a function of pressure to 3 kbar. J Geophys Res 73:65–86

Mao HK (1974) A discussion of the iron oxides at high pressure with implications for the chemical and thermal evolution of the earth. Carnegie Inst Washington Yearb 73:510–518

Mao HK, Bell PM (1979) Equations of state of MgO and εFe under static pressure conditions. J Geophys Res 84:4533–4536

Mao HK, Bell PM (1977) Disproportionation equilibrium in iron-bearing systems at pressures above 100 kbar with applications to chemistry of the earths mantle. In: Saxena SK and Bhattacharji S (eds) Energetics of geological processes. Springer, Berlin Heidelberg New York, pp 236–249

Mao HK, Takahashi T, Bassett WA, Kinsland GL, Merrill L (1974) Isothermal compression of magnetite to 320 kbar and pressureinduced phase transformation. J Geophys Res 79:1165–1170

Marumo F, Isobe M, Akimoto S (1977) Electron density distributions in crystals for $\gamma-Fe_2SiO_4$ and $\gamma-CO_2SiO_4$. Acta Crystallogr Sect B33:713–716

Matsui Y, Syano Y (1968) Unit cell dimensions of some synthetic olivine group solid solutions. Geochem J 2:51–59

Mizukami S, Ohtani A, Kawai N (1975) High pressure x-ray diffraction studies on $\beta-$ and $\gamma-Mg_2SiO_4$. Phys Earth Planet Inter 10:177–182

Myers J, Eugster HP (1983) The system $Fe-Si-O$: Oxygen buffer calibrations to 1,500 K. Contrib Mineral Petrol 82:75–90

Nafziger RH, Muan A (1967) Equilibrium phase compositions and thermodynamic properties of olivines and pyroxenes in the system $MgO-$"FeO"$-SiO_2$. Am Mineral 52:1364–1385

Navrotsky A, Akaogi M (1984) The phase relations in systems $Fe_2SiO_4-Mg_2SiO_4$ and $CO_2SiO_4-Mg_2SiO_4$: calculation from thermochemical data and geophysical applications. J Geophys Res 89:10135–10140

Navrotsky A, Pintchovsky F, Akimoto S (1979) Calorimetric study of the stability of high pressure phases in the system $CaO-SiO_2$ and "FeO"$-SiO_2$ and calculation of phase diagrams in $MO-SiO_2$ systems. Phys Earth Planet Inter 19:275–292

Ostrovsky IA (1979) The thermodynamics of substances at very high pressures and temperatures and some mineral reactions in the earths mantle. Phys Chem Minerals 5:105–118

Petit AT, Dulong PL (1819) Recherches sur quelques points important de la theorie de la chaleur. Ann Chim Phys 10:395–413

Ringwood AE (1969) Phase transformations in the mantle. Earth Planet Sci Lett 5:401–412

Ringwood AE (1975) Composition and petrology of the earth's mantle. McGraw-Hill, New York

Robie RA, Finch CB, Hemingway BS (1982) Heat capacity and entropy of fayalite (Fe_2SiO_4) between 5.1 and 383 K: comparision of calorimetric and equilibrium values for the QFM buffer reaction. Am Mineral 67:463–469

Robie RA, Hemingway BS, Takei H (1982) Heat capacities and entropies of Mg_2SiO_4, Mn_2SiO_4 and CO_2SiO_4 between 5 and 380 K. Am Mineral 67:470–482

Robie RA, Hemingway BS, Fisher JR (1978) Thermodynamic properties of minerals and related substances at 298.15 K and 1 bar (10^5 pascals) pressure and at higher temperatures. US Geol Survey Bull 1452

Ryzhenko BN, Volkov VP (1971) Fugacity coefficients of some gases in a broad range of temperatures and pressures. Geokhimiya 7:760–773

Sato Y (1977) Equation of state of mantle minerals determined through high-pressure x-ray study in highpressure research: Applications in Geophysics, Manghnani MH and Akimoto S (eds), Academic Press, New York, pp 307–323

Saxena SK (1973) Thermodynamics of rock-forming crystalline solutions. Springer, Berlin Heidelberg New York, p 189

Saxena SK, Eriksson GE (1985) Anhydrous phase equilibria in earth's upper mantle. J Petrol 26:378–390

Saxena SK, Chatterjee N (1986) Thermochemical data on mineral phases. 1. The system $CaO-MgO-Al_2O_3-SiO_2$. J Petrol (in press)

Simons B (1980) Composition-lattice parameter relationship of the magnesiowüstite solid solution series. Carnegie Inst Washington Yearb 79:376–380

Skinner BJ (1962) Thermal expansion of ten minerals. US Geol Surv Prof Paper 450D:109–112

Skinner BJ (1966) Thermal expansion. In: Clark SP Jr (ed) Handbook of physical constants. Geol Soc Am Mem, pp 75–95

Smith WR, Missen RW (1982) Chemical reaction equilibrium analysis. Wiley-Interscience, New York, pp 364

Soga N (1963) The temperature and pressure deriveratives of isotropic sound velocities of α-quartz. J Geophys Res 73:827–829

Stacey FD (1977) Physics of the earth. Wiley, New York, pp 414

Striefler ME, Barsch GR (1976) Elastic and optical properties of stishovite. J Geophys Res 81:2453

Suito K (1977) Phase relations of pure Mg_2SiO_4 up to 200 kilobars. In: Manghnani MH and Akimoto S (eds) High pressure research, Academic Press, New York, pp 365

Sumino Y, Nishizawa O, Goto T, Ohno I, Ozima (1977) Temperature variation of elastic constants of single-crystal forsterite between 190 and 400 C. J Phys Earth 28:273–280

Sumino Y (1979) The elastic constants of Mn_2SiO_4, Fe_2SiO_4 and

CO_2SiO_4 and the elastic properties of olivine group minerals at high temperature. J Phys Earth 27:209–238
Suzuki I (1975) Thermal expansion of periclase and olivine and their anharmonic properties. J Phys Earth 23:145–159
Suzuki I, Ohtani E, Kumazama M (1979) Thermal expansion of $\gamma-Mg_2SiO_4$. J Phys Earth 27:53–61
Suzuki I, Ohtani E, Kumazawa M (1980) Thermal expansion of modified spinel, $\beta-Mg_2SiO_4$. J Phys Earth 28:273–280
Suzuki I, Seya K, Takei H, Sumino Y (1981) Thermal expansion of fayalite, Fe_2SiO_4. Phys Chem Mineral 7:60–63
Syono Y, Akimoto S, Matsui Y (1971) High pressure transformations in zinc silicates. J Solid State Chem 3:369–380
Thompson JB Jr, Waldbaum DR (1969) Mixing properties of sanidine crystalline solutions: Calculations based on two-phase data. Am Mineral 54:811–838
Watt JP, Ahrens TJ (1982) The role of iron partitioning in mantle composition evolution and scale of convection. J Geophys Res 87:5631–5644
Weidner DJ, Wang H, Ito J (1978) Elasticity of orthoenstatite. Phys Earth Planet Inter 17:7
Wood BJ, Kleppa OJ (1981) Thermochemistry of forsterite-fayalite olivine solutions. Geochim Cosmochim Acta 45:529–534
Watanabe H (1982) Thermochemical properties of synthetic high-pressure compounds relevant to the earths mantle. In: Akimoto S and Manghnani MH (eds) High pressure research in geophysics, pp 441–464
Weaver JS, Chipman DW, Takahashi T (1979) Comparison between thermochemical and phase stability data for the quartz-coesite-stishovite transformations. Am Mineral 64:604–614
Yagi T, Mao HK, Bell PM (1982) Hydrostatic compression of perovskite type $MgSiO_3$. In: Advances in Phys Geochem Vol 2, Springer, Berlin Heidelberg New York
Yagi T, Akimoto S (1976) Direct determination of coesite-stishovite transition by in-situ x-ray measurements. Tectonophysics 35:259–270
Yagi T, Bell PM, Mao HK (1979) Phase relations in the system $MgO-FeO-SiO_2$ between 150 and 700 kbar at 1,000 °C. Carnegie Inst Washington Yearb 78:614–618
Yagi T, Mao HK, Bell PM (1978a) Effect of iron on the stability and unit-cell parameters of ferromagnesian silicate perovskite. Carnegie Inst Washington Yearb 77:837–841
Yagi T, Mao HK, Bell PM (1978b) Structure and crystal chemistry of perovskite-type $MgSiO_3$. Phys Chem Minerals 3:97–110

Received January 1, 1986

Contrib Mineral Petrol (1986) 94:221–229

Contributions to Mineralogy and Petrology

Some binary and ternary silicate solution models

Y. Fei[1], S.K. Saxena[1], and G. Eriksson[2]

[1] Department of Geology, Brooklyn College, Brooklyn, NY, 11210, USA
[2] Department of Inorganic Chemistry, University of Umeå, S-901 87 Umeå, Sweden

Abstract. Four different solution models, the two-parameter Margules, the quasi-chemical (QC), the Wilson and the non-random two-liquid (NRTL) model, have been used for fitting the calorimetric excess enthalpy of solution for the following four binary silicate systems: anorthite-albite, pyrope-grossular, diopside-enstatite and diopside-Ca-Tschermak. All models except the Wilson model yield a satisfactory fit to the data but the NRTL model generally results in the lowest residuals. The use of NRTL and QC facilitates the study of the configurational and non-configurational parts of the excess entropy of mixing.

Three different methods, namely those of Kohler, Wohl, and Hillert, have been used to combine binary solution properties to predict ternary solution properties. Comparison of computed excess free energy of mixing in a hypothetical solution shows that all the three methods are viable but the Kohler and Wohl methods are similar to each other and are significantly different from the Hillert method. The Kohler method with one or a combination of different binary models is recommended for predicting multicomponent solution properties.

Introduction

Geochemists have mainly used the Margules model for binary solid solutions, partly due to its detailed discussion by Thompson (1967, 1969) and partly due to its simplicity of formulation. Other solution models such as the quasi-chemical model and those described here have largely been ignored (Green 1970; Saxena 1973; Powell 1983). The purpose of this paper is firstly to compare the capabilities of some binary solution models, popular in chemical and metallurgical literature, in predicting the excess functions of mixing in several binary silicates and secondly to study the various methods available for computing multicomponent solution properties from the data on binary solutions. For ternary or multicomponent solutions the paper will be mainly concerned with the empirical methods and there will be no discussion on the physical significance. The work will exclude mixing on more than one site in multisite solids.

Abbreviations. G^{ex}, excess free energy of mixing; H^{ex}, excess enthalpy of mixing; S^{ex}, total excess entropy of mixing; S^{cx}, configurational excess entropy of mixing; W_{ij}, interaction energy parameter between species i and j; X_i, mole fraction of species i; QC, quasi-chemical; NRTL, non-random two-liquid; M, Margules formulation; W, Wohl's formulation; RK, Redlich-Kister; K, Bertrand-Kohler; H, Hillert; Di, diopside ($CaMgSi_2O_6$); En, enstatite ($Mg_2Si_2O_6$); Py, pyrope ($Mg_3Al_2Si_3O_{12}$); Gr, grossular ($Ca_3Al_2Si_3O_{12}$); CaTs, Ca-Tschermak ($CaAl_2SiO_6$); Ab, albite ($NaAlSi_3O_8$); An, anorthite ($CaAl_2Si_2O_8$). Other abbreviations and symbols in the text.

Offprint requests to: Y. Fei

Binary solution models

We shall divide the models to be discussed under two different groups. The first group of models have their origin in the Flory-Huggins model (Flory 1953), in which solutions are considered as athermal with zero excess enthalpy of mixing. The later refined versions, which are the Wilson model (Wilson 1964), the quasi-chemical (Guggenheim 1952) and the non-random two-liquids (NRTL) model (Renon and Prausnitz 1968), do involve enthalpy of mixing and have been recently reviewed by Acree (1984). The second group of models simply express functions by a power series in mole fraction. The Redlich-Kister and the two-constant Margules model amply discussed in geochemical literature (Thompson 1967; Saxena 1973) fall in this category.

Flory-Huggins and Wilson models

Solutions with zero enthalpy of mixing are referred to as athermal solutions. The entropy of mixing for such solutions was discussed by Flory (1953). In the Flory-Huggins model, it is assumed that m sites are occupied consecutively by the same species and if there are n_2 moles of this species and n_1 moles of the solvent, the volume fraction of the solvent and the solute are given by

$$\xi_1 = n_1/(n_1 + n_2 m)$$

and

$$\xi_2 = n_2 m/(n_1 + n_2 m). \quad (1)$$

For athermal solution then

$$G^{mix}_{12} = -T S^{mix}_{12} = RT(n_1 \ln \xi_1 + n_2 \ln \xi_2). \quad (2)$$

Equation (2) is expected to be useful when the mixing species have identical molar volumes. Wilson (1964) considered mixing of species which differ in volume and in their intermolecular forces.

The free energy of mixing in the Wilson model is given by

$$G^{mix} = RT(X_1 \ln\phi_1 + X_2 \ln\phi_2) \quad (3)$$

where ϕ_i is the volume fraction of a component i about a central cation of the same type. The volume fraction of a component is determined by considering the probability of cation distributions. The probability of finding a cation of type 2 relative to type 1 around a central cation of type 1 is given by

$$X_{21}/X_{11} = X_2 \exp(-w_{12}/RT)/X_1 \exp(-w_{11}/RT) \quad (4)$$

where X_{ij} is the local mole fraction component of i in the immediate vicinity of component j, and w_{ij} is proportional to the interaction energy between components i and j. Similarly for the reverse probability, we have

$$X_{12}/X_{22} = X_1 \exp(-w_{12}/RT)/X_2 \exp(-w_{22}/RT). \quad (5)$$

The volume fraction ϕ is defined as

$$\begin{aligned}\phi_1 &= X_{11}V_1/(X_{11}V_1 + X_{21}V_2) \\ &= X_1 V_1 \exp(-w_{11}/RT)/[X_1 V_1 \exp(-w_{11}/RT) \\ &\quad + X_2 V_2 \exp(-w_{12}/RT)].\end{aligned} \quad (6)$$

Similarly

$$\begin{aligned}\phi_2 = X_2 V_2 \exp(-w_{22}/RT)/[&X_1 V_1 \exp(-w_{12}/RT) \\ &+ X_2 V_2 \exp(-w_{22}/RT)]\end{aligned} \quad (7)$$

where V_1 and V_2 are molar volumes of components 1 and 2 respectively. The excess of free energy of mixing is then given by

$$G^{ex} = -RT[X_1 \ln(X_1 + X_2 W_{21}) + X_2 \ln(X_2 + X_1 W_{12})] \quad (8)$$

where

$$W_{21} = (V_2/V_1)\exp[-(w_{12} - w_{11})/RT] \quad (9)$$

$$W_{12} = (V_1/V_2)\exp[-(w_{12} - w_{22})/RT]. \quad (10)$$

One of the major problems with the Wilson models that it cannot be used to predict unmixing. According to the model, a system will be close to separation into two phases when the parameters W_{ij} are close to zero. In this limit the excess free energy of mixing cancels with the ideal free energy of mixing, requiring that the free energy of mixing to equal zero at all binary compositions. This in turn means a high excess enthalpy which would increase with temperature because H^{ex} equals TS^{ex}.

The non-random two-liquids (NRTL) model

To remedy the defect in the Wilson model, Renon and Prausnitz (1968) introduced the NRTL model where they developed further the concept of non-random mixing of two liquid sub-mixtures. Each sub-mixture may be comparable to a domain (or a cell) in which the central molecule (1 or 2) is surrounded by a definite order of the two types of molecules. This order determines the mole fractions X_1 and X_2. The total Gibbs free energy of mixing (G^{mix}) of the solution is

$$G^{mix} = X_1 G^{(1)} + X_2 G^{(2)} \quad (11)$$

where $G^{(1)}$ and $G^{(2)}$ are related to local mole fraction compositions through

$$G^{(1)} = X_{11} w_{11} + X_{21} w_{12} \quad (12)$$

$$G^{(2)} = X_{12} w_{12} + X_{22} w_{22} \quad (13)$$

where w_{ij} represents a binary interaction parameter and X_{ij} refers to the mole fraction of component i in the immediate vicinity of component j. According to Renon and Prausnitz (1968) the excess free energy of mixing is given by

$$G^{ex} = X_1(G^{(1)} - G^{(1)}_{pure}) + X_2(G^{(2)} - G^{(2)}_{pure}). \quad (14)$$

Combining Eqs. (11)–(14), they obtained

$$G^{ex} = X_1 X_{21}(w_{12} - w_{11}) + X_2 X_{12}(w_{12} - w_{22}). \quad (15)$$

In analogy with the Wilson model, the local mole fractions are related to the overall mole fractions as follows:

$$X_{21}/X_{11} = X_2 \exp(-\alpha w_{12}/RT)/X_1 \exp(-\alpha w_{11}/RT) \quad (16)$$

and

$$X_{12}/X_{22} = X_1 \exp(-\alpha w_{12}/RT)/X_2 \exp(-\alpha w_{22}/RT) \quad (17)$$

where α is a correction factor. The excess free energy of mixing is given by

$$\begin{aligned}G^{ex} = RTX_1X_2\{&[\tau_{21}W_{21}/(X_1 + X_2W_{21})] \\ &+ [\tau_{12}W_{12}/(X_2 + X_1W_{12})]\}\end{aligned} \quad (18)$$

where

$\tau_{12} = (w_{12} - w_{22})/RT$;
$\tau_{21} = (w_{12} - w_{11})/RT$;
$W_{12} = \exp(-\alpha\tau_{12})$;
$W_{21} = \exp(-\alpha\tau_{21})$.

Other excess functions are

$$\begin{aligned}H^{ex} = RTX_1X_2\{&[(X_1 + X_2W_{21})\tau_{21}W_{21} \\ &- X_1\alpha\tau_{21}^2W_{21}]/(X_1 + X_2W_{21})^2 \\ &+ [(X_2 + X_1W_{12})\tau_{12}W_{12} \\ &- X_2\alpha\tau_{12}^2W_{12}]/(X_2 + X_1W_{12})^2\}\end{aligned} \quad (19)$$

$$\begin{aligned}S^{ex} = -RX_1X_2[&X_1\alpha\tau_{21}^2W_{21}/(X_1 + X_2W_{21})^2 \\ &+ X_2\alpha\tau_{12}^2W_{12}/(X_2 + X_1W_{12})^2].\end{aligned} \quad (20)$$

For activity coefficients, we have

$$\begin{aligned}RT\ln\gamma_1 = RTX_2^2[&\tau_{21}W_{21}^2/(X_1 + X_2W_{21})^2 \\ &+ \tau_{12}W_{12}/(X_2 + X_1W_{12})^2].\end{aligned} \quad (21)$$

The expression for γ_2 is obtained by exchanging the subscripts 1 and 2.

Quasi-chemical model

In the zeroth approximation, Guggenheim (1952) considered a random mixing of two components. Thus, the average number of AB pairs in a particular configuration is given by

$$X = N_A N_B/(N_A + N_B) \quad (22)$$

where N_A and N_B refer to the number of moles of the species A and B respectively. The quasi-chemical model replaces the physically unrealistic random value of X with

$$X^2 = (N_A - X)(N_B - X)\exp(-2w/ZkT) \quad (23)$$

where k is Boltzmann constant and $2w/Z$ is the energy required to change an AA pair and a BB pair into two AB pairs and X. $1/2(N_A - X)$ and $1/2(N_B - X)$ are proportional to the number of AB, AA and BB pairs respectively. It is possible to directly compare the quasi-chemical model with the zeroth approximation by defining a parameter β, such that

$$X = [N_A N_B/(N_A + N_B)][2(\beta + 1)]. \quad (24)$$

If $\beta = 1$, we obtain the zeroth approximation. If β is greater than unity, there would be a tendency for clustering. A

less than unity value of β indicates a trend towards compound formation. From (23), one may obtain

$$\beta=\{1+4X_1X_2[\exp(2W/ZRT)-1]\}^{1/2}. \quad (25)$$

In order to consider mixing of molecules of different sizes, Guggenheim (1952) introduced the concept of polymers occupying the sites. A monomer occupies one site, a dimer two and a r-mer occupies r sites. A volume fraction ϕ is defined as the fraction of sites occupied by a polymer. For non-athermal solutions, Guggenheim (1952) argued that the configurational potential energy may be expressed as a sum of contributions from pairs of neighboring elements, the contribution from each pair depending on the nature of both elements forming the pair. He used the word *contact* to denote the geometrical relation of an element to the element of some other molecule in a neighboring site. Thus an open-chain r-mer containing r elements has Zq contacts where q is related to r by

$$(1/2)Z(r-q)=r-1. \quad (26)$$

The following equations of the QC model are adopted from Guggenheim (1952). They have also been discussed by Green (1970) and Saxena (1973). The excess functions of mixing are given by (Saxena 1973):

$$G^{ex}=(1/2)ZRT\{X_1q_1\ln[(\beta+\Phi_1-\Phi_2)/\Phi_1(\beta+1)] + X_2q_2\ln[(\beta+\Phi_2-\Phi_1)/\Phi_2(\beta+1)]\} \quad (27)$$

$$H^{ex}=[4X_1X_2W/\beta(\beta+1)]\exp(2W/ZRT) \cdot[X_1q_1\Phi_2/(\beta+\Phi_1-\Phi_2)+X_2q_2\Phi_1/(\beta+\Phi_2-\Phi_1)] \quad (28)$$

$$S^{ex}=(H^{ex}-G^{ex})/T \quad (29)$$

where Z is coordination number, Φ_1 and Φ_2 are contact fractions, q_1 and q_2 contact factors, and W is the interaction parameter. The quantities q and Φ are related as

$$\Phi_1=X_1q_1/(X_1q_1+X_2q_2)$$

and

$$\Phi_2=X_2q_2/(X_1q_1+X_2q_2) \quad (30)$$

and β is given by (25). Differentiation of (27), gives:

$$RT\ln\gamma_1=RT\ln[1+\Phi_2(\beta-1)/\Phi_1(\beta+1)]^{Zq_1/2}. \quad (31)$$

To obtain $RT\ln\gamma_2$, exchange the subscripts 1 and 2.

Margules model

This model has been discussed extensively by Thompson (1969) and therefore, no new reviews is necessary. The excess free energy of mixing (Saxena 1973) is given by

$$G^{ex}=X_1X_2(X_2W_{12}^G+X_1W_{21}^G). \quad (32)$$

Other excess functions may be expressed similarly:

$$H^{ex}=X_1X_2(X_2W_{12}^H+X_1W_{21}^H) \quad (33)$$
$$S^{ex}=X_1X_2(X_2W_{12}^S+X_1W_{21}^S). \quad (34)$$

Activity coefficients are given by

$$RT\ln\gamma_1=X_2^2[W_{12}^G+2X_1(W_{21}^G-W_{12}^G)] \quad (35)$$
$$RT\ln\gamma_2=X_1^2[W_{21}^G+2X_2(W_{12}^G-W_{21}^G)]. \quad (36)$$

Redlich-Kister model

Guggenheim (1937) suggested that G^{ex} can be expressed as a polynomial in X as

$$G^{ex}=X_1X_2[A_0+A_1(X_1-X_2)+A_2(X_1-X_2)^2+\ldots] \quad (37)$$

where A_0, A_1 and A_2 are constants. The activity coefficients using the Redlich-Kister method are given by

$$RT\ln\gamma_1=X_2^2[A_0+A_1(3X_1-X_2) +A_2(X_1-X_2)(5X_1-X_2)+\ldots] \quad (38)$$

$$RT\ln\gamma_2=X_1^2[A_0+A_1(3X_2-X_1) +A_2(X_2-X_1)(5X_2-X_1)+\ldots]. \quad (39)$$

Note that the two-parameter Margules formulation is a special case of the polynomial model with two constants A_0 and A_1 which are related to W^G by

$$A_0=(W_{21}^G+W_{12}^G)/2 \quad (40)$$
$$A_1=(W_{21}^G-W_{12}^G)/2 \quad (41)$$

If temperature dependence of the constants A_0, A_1, A_2, etc., is known, H^{ex} and S^{ex} can be calculated as follows:

$$H^{ex}=X_1X_2\{A_0-T(\partial A_0/\partial T)+[A_1-T(\partial A_1/\partial T)](X_1-X_2) +[A_2-T(\partial A_2/\partial T)](X_1-X_2)^2+\ldots\} \quad (42)$$

$$S^{ex}=-X_1X_2[(\partial A_0/\partial T)+(\partial A_1/\partial T)(X_1-X_2) +(\partial A_2/\partial T)(X_1-X_2)^2+\ldots]. \quad (43)$$

Ternary models

Excellent reviews of empirical methods of predicting ternary solution properties from binary solution data have appeared recently (Hillert 1980; Bertrand et al. 1983; Acree 1984). On the basis of these reviews and our own experience with ternary models (Saxena 1973; Ganguly and Saxena 1984), we have selected three models of combining the binary data to predict ternary properties. These are the Wohl model, the Bertrand-Kohler model, and the Hillert model. There are few ternary data available on solid solutions and there is no way the different predictive behaviour of the models. However, several studies of phase equilibrium in experimental and natural systems require the ternary models for inter- and extra-polation. It is, therefore, important to document the predictions of these models.

Wohl's model

According to Wohl (1953) the excess free energy of mixing is given by

$$G^{ex}=X_1X_2[W_{12}X_2+W_{21}X_1]+X_2X_3[W_{23}X_3+W_{32}X_2] +X_1X_3[W_{13}X_3+W_{31}X_1] +X_1X_2X_3[0.5(W_{12}+W_{21}+W_{13} +W_{31}+W_{23}+W_{32})-C] \quad (44)$$

where C is a ternary constant to be determined from the ternary solution data (Ganguly and Saxena 1984 for estimation). For activity coefficient of component 1, we have

$$RT\ln\gamma_1=X_2^2[W_{12}+2X_1(W_{21}-W_{12})] +X_3^2[W_{13}+2X_1(W_{31}-W_{13})] +X_2X_3[0.5(W_{21}+W_{12}+W_{31}+W_{13}-W_{23}-W_{32}) +X_1(W_{21}-W_{12}+W_{31}-W_{13}) +(X_2-X_3)(W_{23}-W_{32})-(1-2X_1)C]. \quad (45)$$

For γ_2 replace 1 by 2, 2 by 3 and 3 by 1. Similarly, for γ_3 replace 1 by 3, 2 by 1 and 3 by 2.

Table 1. Excess enthalpy of mixing at 970° K for four binary silicate solid solutions

Di-CaTs		Di-En		Py-Gr		An-Ab	
X_{Di}	H^{ex}/kJ	X_{Di}	H^{ex}/kJ	X_{Py}	H^{ex}/kJ	X_{An}	H^{ex}/kJ
0.900	4.058±1.136	0.900	3.556±1.741	0.910	5.983±1.698	0.900	3.891±0.880
0.800	5.858±1.089	0.800	6.443±0.969	0.820	6.527±1.335	0.830	2.427±1.426
0.650	5.941±1.193	0.700	9.916±1.386	0.725	8.494±1.458	0.770	3.807±1.545
0.500	4.017±1.442	0.600	12.050±0.953	0.530	7.113±1.424	0.700	5.397±0.728
0.300	3.096±1.249	0.500	12.678±1.146	0.200	3.515±1.598	0.650	5.230±0.841
		0.400	12.678±0.809	0.100	4.017±1.669	0.600	4.602±0.781
		0.300	12.468±1.349			0.500	4.728±1.762
		0.220	10.000±1.628			0.420	3.724±1.764
						0.400	3.891±2.198
						0.330	2.720±0.698
						0.300	2.634±1.588
						0.250	3.180±0.804
						0.200	3.138±0.762
						0.150	2.176±1.124
						0.110	0.293±1.399
						0.100	0.293±1.123
						0.050	0.084±0.923

Abbreviations. Ab, albite ($NaAlSi_3O_8$); Di, diopside ($CaMgSi_2O_6$); Gr, grossular ($CaAl_{2/3}SiO_4$); CaTs, Ca-Tschermak ($CaAl_2SiO_6$); Py, pyrope ($MgAl_{2/3}SiO_4$); En, enstatite ($Mg_2Si_2O_6$); An, anorthite ($CaAL_2Si_2O_8$)
Data sources. Newton et al. (1977), Newton et al. (1979), and Newton et al. (1980)
The *errors in excess enthalpy of mixing* were computed from the formula

$$\delta H^{ex} = \sqrt{(X_1\delta H_1)^2 + (X_2\delta H_2)^2 + (\delta H^{mix})^2}$$

where δH_1, δH_2 and δH^{mix} are the errors in the enthalpies of the two end-members and of the mixing, respectively, and X_1 and X_2 are mole fractions

Bertrand-Kohler model

Bertrand et al. (1983) proposed a general model of which the Kohler formulation becomes a special case. According to the model of Bertrand et al., an excess property of a multicomponent solution is given by

$$Z^{ex}_{12\ldots N} = \sum_{i=1}^{N}\sum_{j>i}^{N}(X_i - X_j)(f_i - f_j)(\Delta Z^{ex}_{ij})^* \quad (46)$$

in which $(\Delta Z^{ex}_{ij})^*$ is the molar excess property (enthalpy, entropy, volume, free energy, etc.) of the binary system with components at the same molar ratio as in multicomponent system and f_i and f_j are weighted mole fractions using weighing factors based on the excess properties of the binary systems. X_i is used as the mole fraction in the multicomponent system.

For the activity coefficient of compound i, we have

$$\begin{aligned}(RT\ln\gamma_i)_{12\ldots N} = &\sum_j (X_i + X_j)(1 - f_i - f_j)(\Delta G^{ex}_{ij})^* \\ &- \sum_{j,k}(X_j + X_k)(f_j + f_k)(\Delta G^{ex}_{jk})^* \\ &+ \sum_j (f_i + f_j)(RT\ln\gamma_i)^*_{ij} \quad (i \neq j \neq k)\end{aligned} \quad (47)$$

where the binary functions denoted by an asterisk, represent the excess property of the binary system.

The Hillert model

Hillert (1980) suggested a modification of Toop's (1965) method. The excess free energy of mixing for a ternary mixture is given by

$$\begin{aligned}G^{ex} = &[X_2(1 - X_1)][X_1^0 X_2^0][A^0_{12} - A^1_{12}(X_1^0 - X_2^0)] \\ &+ [X_3(1 - X_1)][X_1^0 X_3^0][A^0_{13} - A^1_{13}(X_1^0 - X_3^0)] \\ &+ (X_2 X_3)[A^0_{23} + A^1_{23}(X_{23} - X_{32})]\end{aligned} \quad (48)$$

where

$$V_{23} = (1 + X_2 - X_3)/2$$
$$V_{32} = (1 + X_3 - X_2)/2.$$

X_i^0 is used as the mole fraction in the binary system. The constants A^0_{12}, A^1_{12} etc. are similar to the constants A_0 and A_1 in the Redlich-Kister formulation.

A note on entropy of mixing

For a binary simple mixture (Guggenheim 1967), we have

$$G^{ex} = X_1X_2W^G \quad (49)$$

where W is the interaction energy parameter. Partial differentiation of Eq. (49) yields

$$H^{ex} = X_1X_2[W^G - T(\partial W^G/\partial T)] \quad (50)$$
$$S^{ex} = -X_1X_2[\partial W^G/\partial T]. \quad (51)$$

The square bracketed terms are defined by Thompson (1967) as W^H and W^S, leading to the popularly used relation

$$W^G = W^H - TW^S. \quad (52)$$

Since $\partial W^G/\partial T$ is usually negative, W^S becomes a positive quantity which when substituted in Eq. (51) yields a positive excess entropy of mixing. Such S^{ex} implies a total entropy of mixing greater than the random mixing configurational entropy. Note that the excess entropy of mixing consists of S^{ex} arising due to unequal temperature dependence of the pairpotential energy of interactions in the solution and the excess configurational entropy, S^{ex}_c, which should always be less than zero.

From the above discussion, it is apparent that the only part of the excess entropy of mixing the models can predict (Eqs. 15 and 19) from isothermal heat of solution data is

Table 2. Calculated solution parameters at 970° K for four binary silicate solid solutions. All units in kJ

Solution model		Di-CaTs (1)	Di-CaTs (2)	Di-En (1)	Di-En (2)	Py-Gr (1)	Py-Gr (2)	An-Ab (1)	An-Ab (2)
Margules	W_{12}	0.000		65.923		5.494		8.272	
	W_{21}	41.242		37.091		16.912		28.706	
	D	0.908		0.370		0.569		0.756	
Redlich-Kister	A_0	17.280		51.798		8.694		18.117	
	A_1	17.355		−16.636		5.996		10.389	
	A_2	24.945		− 2.272		11.247		2.414	
	D	0.335		0.398		0.371		0.779	
Quasi-chemical	W	74.417		106.905		30.932		44.455	
	Z	8		11		8		8	
	q_1	0.3		1.2		0.2		0.3	
	q_2	1.7		0.8		1.8		1.7	
	D	0.513		1.097		0.473		0.773	
Wilson	$w_{12}-w_{11}$	9.694		10.883		9.184		4.184	
	$w_{12}-w_{22}$	12.874		10.912		13.836		13.082	
	V_2/V_1	0.962		0.946		1.106		0.498	
	D	3.889		9.890		0.768		1.916	
NRTL	$w_{12}-w_{22}$	53.559		13.703		30.280		34.100	
	$w_{12}-w_{11}$	14.498		59.894		13.100		3.703	
	α	0.15		0.05		0.30		0.15	
	D	0.614		0.423		0.335		0.770	

D is the standard deviation computed from the formula

$$D=\sqrt{\frac{\sum(Y_i-X_i)^2}{n-p}}$$

where Y_i are the calculated data, X_i are the averages of the observations, n is the number of experimental points and p is the number of parameters

the configurational part. For the remaining S^{ex}, it is essential to obtain the temperature dependence of the solution parameters. In this work, we shall refer to the *model* (NRTL and QC) *calculated* excess entropy of mixing as the configuration excess entropy of mixing S_c^{ex}.

Method of study

Heat of solution measurements are available for the following binary systems: plagioclase ($NaAlSi_3O_8$-$CaAl_2Si_2O_8$; Newton et al. 1980), garnet ($Mg_3Al_2Si_3O_{12}$-$Ca_3Al_2Si_3O_{12}$; Newton et al. 1977), pyroxene ($CaMgSi_2O_6$-$CaAl_2SiO_6$; Newton et al. 1977), and pyroxene ($Mg_2Si_2O_6$-$CaMgSi_2O_6$; Newton et al. 1979). Using these data, excess enthalpy of mixing were calculated (Table 1). The data were then processed with a non-linear multiple regression technique employing the various model equations listed in the previous section to calculate solution parameters (Table 2). All the experimental data evaluated by the experimenters themselves have been used in the fitting procedures. We found no basis to reject any of the data or to use weighting factors. For the NRTL model a value of α was chosen between 0.05 to 0.5 (*see* discussion on significance of α later) and a search for the best fitting W parameters was made by manually scanning through the range of α values by minimizing the standard deviation (see Table 2). In each case, the residuals and the standard error (BMD statistical package) are minimized. The comparison among different models is based on the standard deviations. In calculating the standard deviation the residuals, the number of datum as well as degrees of freedom are considered (Table 2). Similarly, for the quasi-chemical model, several

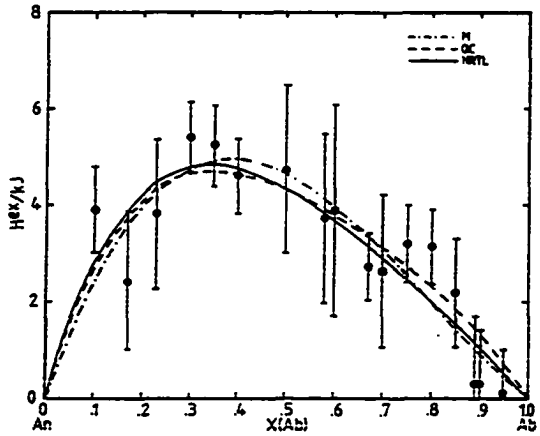

Fig. 1. Calculated excess enthalpy of mixing for the anorthite-albite join at 970° K. Experimental data from Newton et al. (1980)

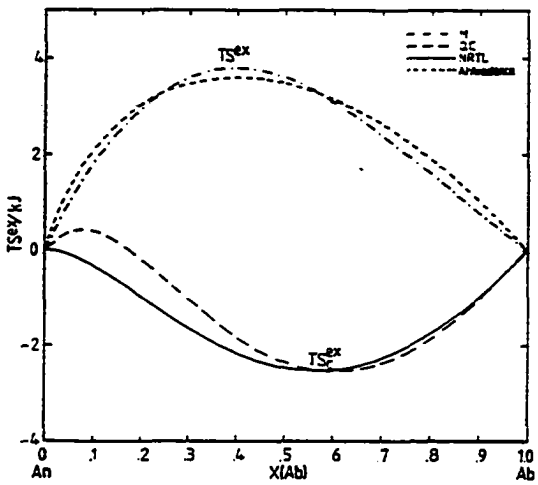

Fig. 2. Calculated excess entropy of mixing for the anorthite-albite join at 970° K according to the Margules and Al-avoidance models and excess configurational entropy of mixing according to the QC and NRTL models

combinations of the coordination number Z and the contact factors q_1 and q_2 ($q_1+q_2=2$) were tried (for the significance of Z, q_1 and q_2 *see* Green 1970; Saxena 1973; Guggenheim 1952).

Excess free energy of mixing for a ternary solid solution was calculated using the Kohler formulation (Bertrand-Kohler model), the Wohl model, and the Hillert model.

Results and discussion

1. Binary solutions

Table 2 shows the results of the regression analysis of data on four binary solutions employing five different models.

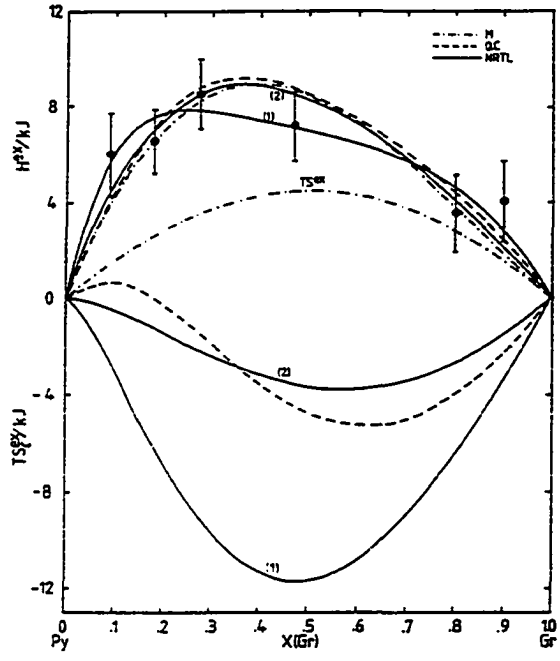

Fig. 3. Calculated excess functions of mixing for the pyrope-grossular join at 970° K. Solid curves 1 and 2 are calculated from the NRTL model. The solution parameters are given in Table 2 for curve 1. The parameters for curve 2 are $(w_{12}-w_{22})=18.277$ kJ, $(w_{12}-w_{11})=2.823$ kJ, $\alpha=0.25$. Experimental data are from Newton et al. (1977)

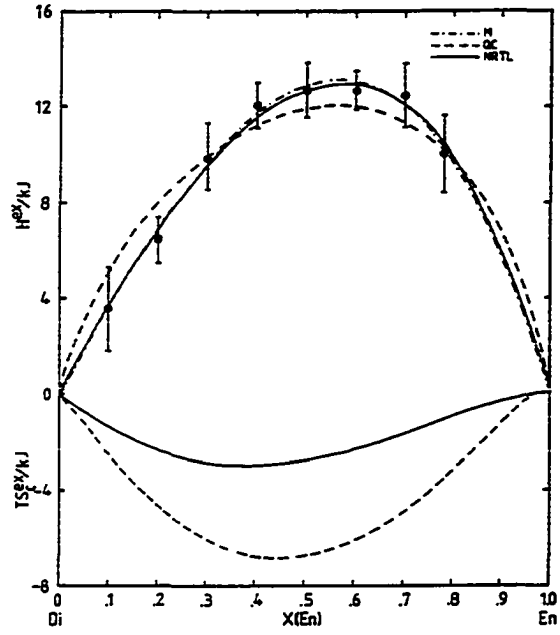

Fig. 4. Calculated excess functions of mixing for the join $CaMgSi_2O_6$-$Mg_2Si_2O_6$ at 970° K. Experimental data are from Newton et al. (1979)

Since the Redlich-Kister model with three or more constants is bound to be the better fitting than the two-constant Margules, we shall not discuss it separately. With increasing number of constants, the Redlich-Kister model, although superior for calculating phase diagrams, is not readily interpretable in terms of crystal-chemical parameters.

Anorthite-albite. Except for the Wilson model, all four models can be fit with similar residuals. Figure 1 shows the excess enthalpy of solution at 970° K calculated according to the three models, Margules quasi-chemical and the non-random two-liquid (referred to as M, QC and NRTL respectively). As noted before, the QC and NRTL models also yield the configurational excess entropy of mixing (S^{ex}_c) (*see* Eqs. 20 and 29). The term $-TS^{ex}_c$ is shown in Fig. 2 for the two models. For the M model, $S^{ex}_{(total)}$ has been derived from Eq. (34) where

$$W^S_{12}=-(W^G_{12}-W^H_{12})/T \tag{53}$$

and similarly for W^S_{21}. The values for W^G_{ij} are from Saxena and Ribbe (1972) who used Orville's (1972) phase equilibrium data. The Saxena-Ribbe formulation was used because Ganguly and Saxena (1984) found it to be consistent with data on garnet-plagioclase phase equilibria. There would be little difference if Ghiorso's (1984) formulation is used. In addition, we have also plotted $-TS^{ex}$ calculated with the Al-avoidance model of Kerrick and Darken (1975) as:

$$-TS^{ex}=RT[X_{Ab}\ln[A_{Ab}(2-X_{Ab})] + X_{An}\ln[(1-X_{An})^2/4]]. \tag{54}$$

Note that $-TS^{ex}$ derived from the combination of phase equilibrium data of Orville (1972) and enthalpy of solution data should be comparable if the model of Al-avoidance is appropriate. As demonstrated by Newton et al. (1980) and shown in Fig. 2, the model produces a close approximation of S^{ex}. Comparison of TS^{ex} and TS^{ex}_c as predicted by the NRTL and QC models gives an indication of the magnitude of the non-configurational part of the excess entropy.

Pyrope-grossular. For this binary solution, Table 2 and Fig. 3 show that all models reproduce the data on excess enthalpy of solution rather well. The fit with the NRTL model is best, followed by the QC and by the Margules model. For the NRTL model, we calculated two sets of solution parameters by changing α. Both reproduce the data on excess enthalpy of solution rather well, but the configurational excess entropies of mixing predicted by the two sets of parameters are significantly different. This may imply that the factor α has some connotation with crystal chemical parameters. To predict a reliable configurational entropy, one might determine the factor α separately in terms of crystal chemical parameters. Figure 3 shows plots of $-TS^{ex}_c$ for the QC and NRTL models and $-TS^{ex}$ for the M model, for which a W^G of 6.276 J/cation has been taken from Haselton and Newton (1980). Again, we may

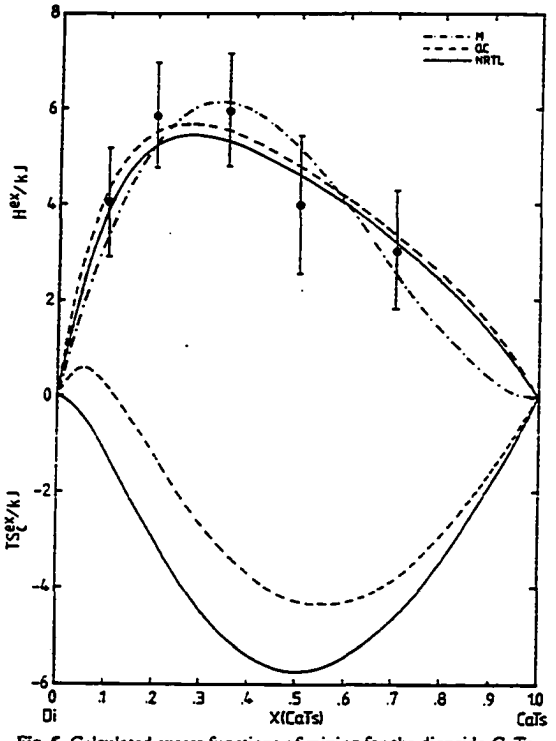

Fig. 5. Calculated excess functions of mixing for the diopside-CaTs join at 970° K. Experimental data are from Newton et al. (1977)

consider the difference between S_c^{ex} and S^{ex} as representing the non-configurational part of S^{ex}.

Diopside-enstatite. The NRTL and M models fit the enthalpy data better than the QC model. For the QC model, a high coordination number (Z) of 11 was needed. The M2 site is nominally 8-coordinated. When a value of 8 was used for Z, the results of the fit were quite unacceptable, the fitted curve totally missed several data points. Figure 4 shows that the QC model tends to produce a less symmetric curve than required by the data. Figure 4 also shows a plot of $-TS_c^{ex}$ as calculated by the NRTL and QC models. According to Lindsley et al. (1981), W^G for this system is zero, which would require a S^{ex} (non-configurational) of similar magnitude to S_c^{ex}, but opposite in sign.

Diopside-Ca-Tschermak. Figure 5 and Table 2 show that both the QC and NRTL models are equally well suited to the solution data and result in lower residuals than the Margules model. From Gasparik and Lindsley's (1980) analysis of the phase equilibrium data, and the heat of solution data of Newton et al. (1977), the solution has a $W^G_{21} = 30.90$ and $W^G_{12} = 12.25$. Figure 5 shows $-TS_c^{ex}$ for the NRTL and QC models and $-TS^{ex}$ for the Margules model. For this solution there is a substantial difference between the two quantities, suggesting a large non-configurational excess entropy of mixing.

General discussion. The nature of excess functions predicted by the two-parameter Margules model have been discussed amply in literature (Newton et al. 1977, 1980; Lindsley et al. 1981). Therefore, we shall concentrate on understanding the applicability of QC and NRTL models. The QC parameters q_1 and q_2 known as "contact factors" are supposed to be related to the geometry and size of the mixing units, with the property that $q_1/q_2 \to 1$ as either becomes unity (Guggenheim 1952; Green 1970). In our case we have used $q_1 + q_2 = 2.0$ which satisfies the above requirement. However, to obtain the desired asymmetric fit q_1 and q_2 had to be made considerably different. There is no relationship between q_1/q_2 and a size property, e.g., molar volume ratio of the mixing units. In view of Green's (1970) success in using the QC model, the results from this model are disappointing, particularly if we consider that the q_1/q_2 ratio seems to bear no relation to the volume differences of the mixing species. In addition to the physically meaningless contact factors, the coordination numbers z used, also seem unsatisfactory. Similarly, for the NRTL model, which fits data for all the solutions very well, the factor α does not show any correlation with volume ratio of the species. The parameter α characterizes the tendency of the components to mix in a nonrandom manner (*see* Acree 1984). When α equals zero, the local mole fractions (X_{ij}, see Eq. 2) become equal to the overall mole fractions (X_i) and mixing is completely random. Therefore it is disturbing to note that the Di-En solution has the smallest α and Py-Gr the largest indicating that no physical meaning can be attached to α. A comparison of the various plots of $-TS_c^{ex}$ against mole fraction shows that for all the solutions, the quantity $-TS_c^{ex}$ is high for the compositional side with high H^{ex}. Thus for the pyrope-grossular solution the models NRTL and in particular QC predict $-TS_c^{ex}$ which is closer to zero for pyrope-rich compositions than for those rich in grossular. In this regard $-TS_c^{ex}$ behaves similarly to (but with opposite sign) the excess volume of mixing (Haselton and Newton 1980). This implies that volume of mixing can be better modelled employing the NRTL or QC model than by Margules formulation.

2. *Ternary solution models*

As explained earlier, three methods of combining binary model parameters to predict ternary solution properties are chosen. As an example, let us consider a ternary solution with the following data: $W_{12} = 10.460$, $W_{21} = 837$, $W_{13} = 3.617$, $W_{31} = 9.132$, $W_{23} = 11.529$ and $W_{32} = 10.437$. The solution parameters are partly those used by Ganguly and Saxena (1984) for garnet. The calculations are not necessarily for garnet since all the data on garnet solution are not yet available. Figure 6 shows excess free energy of mixing calculated according to Kohler formulation. The G^{ex} data resulting from the use of Wohl's formulation are very similar and, therefore, have not been plotted separately. However, the data from the Hillert model are significantly different. These data are plotted in Fig. 7 which shows that the G^{ex} tends to be higher for some of the ternary compositions than those computed by either the Kohler or Wohl formulation. Remembering that a simple summation of the binary G^{ex} would yield the highest values of the ternary G^{ex}, the Kohler and Wohl formulations depart most and the Hillert model least of the three from predicting such values. The question as to which model is most appropriate can be

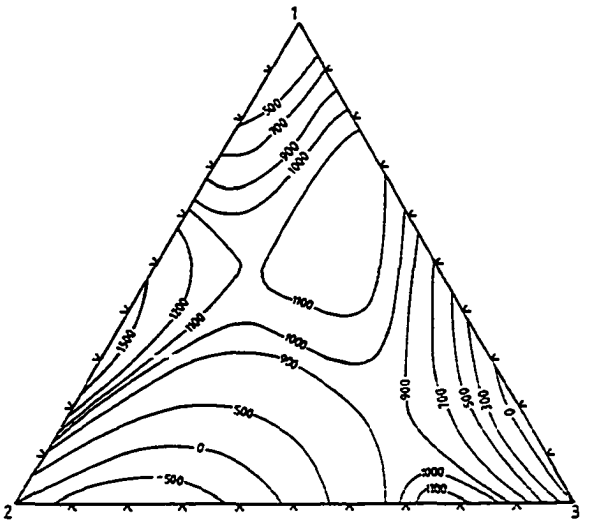

Fig. 6. Calculated excess free energies in a hypothetical ternary system according to the Kohler model

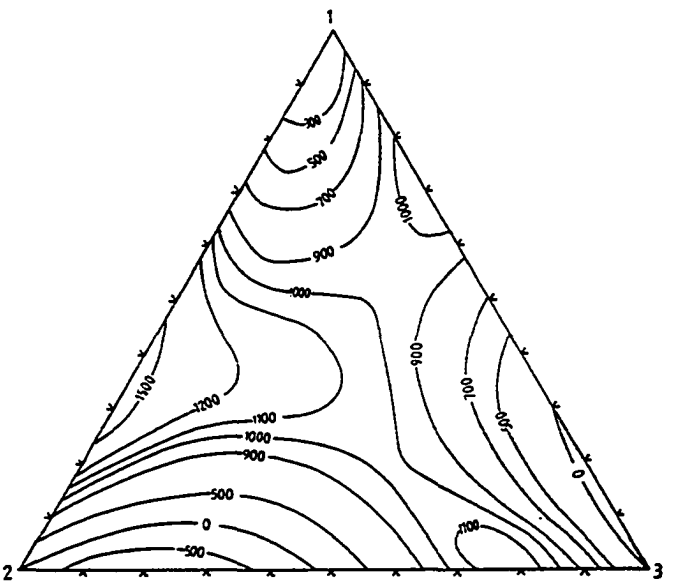

Fig. 7. Calculated excess free energies in a hypothetical ternary system according to the Hillert model

answered only with additional data on ternary solutions. It is possible to consider addition of ternary or higher constants to any of the above models if suitable data are available. Ganguly and Saxena (1984) discussed empirical estimate of such constants to any of the above models if suitable data are available. Ganguly and Saxena (1984) discussed empirical estimate of such constants for Wohl's model.

Conclusions

For the purpose of calculating phase diagrams and reproducing experimental equilibria, it is obvious that the best model is the polynomial expression as proposed by Guggenheim (1937) which has now come to be popularly known as Redlich-Kister model after the authors who wrote the expression for the activity coefficients. The polynomial when truncated after two constants is equivalent to the two-parameter Margules model which may be used in many cases. It is easy to handle computationally. The QC model, even after unrealistic adjustments in the physical parameters, does not work well. The NRTL model also is not an improvement over the Redlich-Kister model because, although it is functionally useful in data representation, it appears to have coefficients that are physically meaningless.

Purely as a method for fitting solution data, the NRTL model has been found to be as useful as the Margules model for two solutions and somewhat better for the remaining two. Its direct use with the phase equilibrium data should be possible wherever separate estimates of H^{ex} and S^{ex} are not needed. The model is easily extended to a multicomponent system as follows (Acree 1984, p 99):

$$\Delta G^{ex}_{12\ldots n} = RT\sum_{i=1}^{N}[X_i(\sum_{j=1}^{N}X_j\tau_{ji}W_{ji})/(\sum_{m=1}^{N}W_{mi}X_m)]. \quad (55)$$

The combination of the binary data to predict ternary or multicomponent data may be done using any of the three models discussed in the text. We recommend the Kohler formulation because of the easy formulation. Any binary model Margules, Redlich-Kister, QC or NRTL or any combination thereof can be used in this formulation.

Acknowledgements. The research has been supported by a NSF grant (EAR #8415800) and by a PSC-BHE grant (#6-64191). Eriksson acknowledges the research support from the Swedish Natural Science Council (NFR).

References

Acree WE Jr (1984) Thermodynamic properties of nonelectrolyte solutions. Academic Press, New York, p 308

Bertrand GL, Acree WE Jr, Burchfield T (1983) Thermodynamical excess properties of multicomponent systems: representation and estimation from binary mixing data. J Solution Chem 12:327–340

Flory PJ (1953) Molecular configuration of polyelectrolytes. J Chem Phys 21:162–163

Ganguly J, Saxena SK (1984) Mixing properties of aluminosilicate garnets: constraints from natural and experimental data, and applications to geothermo-barometry. Am Mineral 69:88–97

Gasparik T, Lindsley DH (1980) Phase equilibria at high pressure of pyroxenes containing monovalent and trivalent ions. Rev Mineral 7:309–340

Ghiorso MS (1984) Activity/composition relations in the ternary feldspars. Contrib Mineral Petrol 85:186–196

Green EJ (1970) Predictive thermodynamic models for mineral systems. I. Quasi-chemical analysis of the halite-sylvite subsolidus. Am Mineral 55:1692–1713

Guggenheim EA (1937) Theoretical basis of Raoult's law. Trans Faraday Soc 33:151–159

Guggenheim EA (1952) Mixtures. Clarendon Press, Oxford, p 365

Guggenheim EA (1967) Thermodynamics. North Holland Publishing Co., Amsterdam, p 437

Haselton HT, Newton RC (1980) Thermodynamics of pyrope-grossular garnets and their stabilities at high temperatures and pressures. J Geophys Res 85:6973–6982

Hillert M (1980) Empirical methods of predicting and representing thermodynamic properties of ternary solution phases. CALPHAD 4:1–12

Kerrick DM, Darken LS (1975) Statistical thermodynamic models for ideal oxide and silicate solid solutions, with application to plagioclase. Geochim Cosmochim Acta 39:1431–1442

Lindsley DH, Grover JE, Davidson PM (1981) The thermodynamics of the $Mg_2Si_2O_6-CaMgSi_2O_6$ join: a review and an improved model. Adv Phys Geochem 1:149–176

Newton RC, Charlu TV, Kleppa OJ (1977) Thermochemistry of high pressure garnets and clinopyroxenes in the system $CaO-MgO-Al_2O_3-SiO_2$. Geochim Cosmochim Acta 41:369–377

Newton RC, Charlu TV, Kleppa OJ (1980) Thermochemistry of the high structural state plagioclases. Geochim Cosmochim Acta 44:933–941

Newton RC, Charlu TV, Anderson PAM, Kleppa OJ (1979) Thermochemistry of synthetic clinopyroxenes on the join $CaMgSi_2O_6$-$Mg_2Si_2O_6$. Geochim Cosmochim Acta 43:55–60

Orville PM (1972) Plagioclase cation equilibria with aqueous chloride solution: Results of 700° C and 2,000 bars in the presence of quartz. Am J Sci 272:234–272

Powell R (1983) Thermodynamics of complex phases. Adv Phys Geochem 3:241–266

Renon H, Prausnitz JM (1968) Local compositions in thermodynamic excess functions for liquid mixtures. Am Inst Chem Eng J 14:135–144

Saxena SK (1973) Thermodynamics of rock-forming crystalline solutions. Springer Heidelberg Berlin New York, p 189

Saxena SK, Ribbe PH (1972) Activity-composition relations in feldspars. Contrib Mineral Petrol 37:131–138

Thompson JB Jr (1967) Thermodynamic properties of simple solutions. In: Abelson PH (ed) Researches in geochemistry, vol 11. John Wiley, Inc, New York, pp 340–361

Thompson JB Jr, Waldbaum DR (1969) Mixing properties of sanidine crystalline solutions. III. Calculation based on two-phase data. Am Mineral 54:811–838

Toop GW (1965) Predicting ternary activities using binary data. Trans Am Inst Min Eng 223:850–855

Wilson GM (1964) A new expression for the excess free energy of mixing. J Am Chem Soc 86:127–130

Wohl K (1953) Thermodynamic evaluation of binary and ternary liquid systems. Chem Eng Prog 49:218–219

Received December 17, 1985; Accepted June 13, 1986

Geochimica et Cosmochimica Acta Vol. 51, pp. 251–254
© Pergamon Journals Ltd. 1987. Printed in U.S.A.

0016-7037/87/$3.00 + .00

An equation for the heat capacity of solids

YINGWEI FEI and S. K. SAXENA

Department of Geology, Brooklyn College, Brooklyn, NY 11210, U.S.A., and Department of Earth and Environmental Sciences, Graduate School, CUNY, New York, NY 10036, U.S.A.

(*Received April* 14, 1986; *accepted in revised form November* 11, 1986)

Abstract—A new expression for the heat capacity of solids is proposed: a) for fitting the measured low-temperature heat capacity data on crystals, and b) for estimating heat capacity at high temperatures without violating the limit set by PETIT and DULONG (1819).

$$C_p = 3Rn(1 + k_1T^{-1} + k_2T^{-2} + k_3T^{-3}) + (A + BT) + C_p'$$

where R and n are the gas constant and the number of atoms in the chemical formulae, respectively. A and B are calculated from thermal expansion coefficient and isothermal bulk modulus data. The k_i's are determined by fitting the measured low-temperature heat capacity data. C_p' is the departures from the $3Rn$ limit for some substances due to cation disordering, anharmonicity and electronic contributions.

The five constants in the proposed equation were determined for six minerals for which the physical properties have been well studied. The errors possibly resulting from experimental measurements or extrapolations of the thermal expansion coefficient and bulk modulus were carefully examined.

INTRODUCTION

TEMPERATURE DEPENDENCE OF the heat capacity can be measured by various calorimetric techniques over rather limited temperature ranges. The most popularly used empirical equations for the representation of the temperature dependence of the heat capacity of solids, proposed by MAIER and KELLEY (1932) and HAAS and FISHER (1976), only provide for interpolation between the temperatures of the calorimetric measurements, and not for the extrapolation to high temperature. Applications of thermodynamic calculations to natural systems such as the Earth's mantle require an equation for the heat capacity of minerals which can be extrapolated to very high temperatures. A number of equations have been proposed for extrapolation of the heat capacity to high temperature (LANE and GANGULY, 1980; HOLLAND, 1981; and BERMAN and BROWN, 1985). In those extrapolations of heat capacity, the behavior of heat capacity at high temperatures is very much dependent on the fits of the measured low-temperature heat capacity data. Such extrapolated data, therefore, may lead to erroneous results. In this paper, an equation for the heat capacity of solids is proposed. The equation not only reproduces the measured low-temperature heat capacity data as well as other existing equations but also provides for the extrapolation of the heat capacity to high temperature. This study was prompted by the stimulating discussion of the problems with heat capacity equations by HOLLAND (1981) and recently by BERMAN and BROWN (1985).

THEORETICAL CONSIDERATIONS

The theory of the heat capacity of solids was established by EINSTEIN (1907) and DEBYE (1912) who derived equations for the temperature dependence of C_v, the specific heat capacity at constant volume, based on the assumption that atoms behave as harmonic oscillators in a crystal lattice.

The relation between specific heat capacity at constant pressure, C_p, and specific heat capacity at constant volume, C_v, is given by

$$C_p = C_v + \alpha^2(T)V(T)K_T(T)T \quad (1)$$

where $\alpha(T)$ is a temperature-dependent coefficient of thermal expansion. $V(T)$ and $K_T(T)$ are molar volume and isothermal bulk modulus, respectively, at temperature T. In Eqn. (1), a reasonable expression for C_v can be derived by assuming that a crystal is composed of a system of atoms which vibrate as harmonic oscillators all with the same frequency, ν. In such a solid C_v is expressed by

$$C_v = 3Rn[x^2e^x/(e^x - 1)^2] \quad (2)$$

where $x = \theta_E/T$. θ_E is the Einstein temperature given by $\theta_E = h\nu/k$. R, h, k and n are the gas constant, Planck constant, Boltzmann constant and the number of atoms in the chemical formula, respectively. A precise expression for C_v may be given by assuming that the crystal has a whole spectrum of frequencies from ν_1 to ν_m, where ν_m represents some maximum frequency for a particular crystal.

$$C_v = (9Rn/x^3)\int_0^x [x^4e^x/(e^x - 1)^2]dx \quad (3)$$

where $x = h\nu_m/(kT)$. Equation (2) is difficult to use in fitting experimental data at intermediate temperatures because of the assumption of a single oscillator frequency. Equation (3) is even more difficult to apply to thermodynamic calculations not only because of the complexity of the expression but also because of the difficulty in determining the frequency distribution. KIEFFER's (1979) review on the applicability of the Debye theory of lattice vibrations show that heat capacities of silicates show large deviations from the behavior expected from the theory.

For the purpose of fitting experimental data, a polynomial expression for C_v may be used

$$C_v = 3Rn[1 + k_1T^{-1} + k_2T^{-2} + k_3T^{-3}] \quad (4)$$

where k_1, k_2 and k_3 are coefficients determined by fitting experimental data. Note that in Eqn. (4) the terms in square

bracket of Eqn. (2) have been replaced with a polynomial expression in T. There are three coefficients in Eqn. (4) as compared to one fixed Einstein temperature in Eqn. (2). According to above considerations, a new C_p expression is given by

$$C_p = 3Rn[1 + k_1T^{-1} + k_2T^{-2} + k_3T^{-3}] + A(T) + C_p' \quad (5)$$

where

$$A(T) = \alpha^2(T)V(T)K_T(T)T \quad (6)$$

and C_p' represents the departures from the $3Rn$ limit for some substances due to cation disordering, anharmonicity and electronic contributions. Obviously, $C_p' = 0$ if atoms behave as harmonic oscillators and there is no cation disordering effect in a crystal lattice. The thermal expansion coefficient $\alpha(T)$ may be expressed as

$$\alpha(T) = \alpha_0 + \alpha_1T^{-1} + \alpha_2T^{-2} + \alpha_3T^{-3} \quad (7)$$

where α_0, α_1, α_2 and α_3 are coefficients determined by least squares analysis of volume expansion data. The molar volume can be calculated by

$$V(T) = V_0 \exp\left[\int_{298}^{T} \alpha(T)dT\right] \quad (8)$$

where V_0 is the molar volume at 298 K and 1 atmosphere. The isothermal bulk modulus $K_T(T)$ may be expressed as

$$K_T(T) = K_{T0} + (\partial K_{T0}/\partial T)_p(T - 298) \quad (9)$$

where K_{T0} and $(\partial K_{T0}/\partial T)_p$ are the isothermal bulk modulus at 298 K and its temperature derivative at constant pressure, respectively. By computing $A(T)$ from Table 1 for many substances, we found that $A(T)$ at high temperature is approximately linear (see dashed lines in Figs. 1–3). To simplify Eqn. (7), $A(T)$ may be expressed as

$$A(T) = A + BT \quad (10)$$

A and B are constants determined by Eqn. (6). Finally, a five-coefficient C_p equation is given by

$$C_p = 3Rn(1 + k_1T^{-1} + k_2T^{-2} + k_3T^{-3}) + (A + BT) + C_p' \quad (11)$$

where A and B are independently determined through thermal expansion, molar volume and bulk modulus data. k_1, k_2 and k_3 are determined by least squares analysis of the measured low-temperature heat capacity data. Obviously, at high temperature, C_p' for a crystal in which atoms behave as harmonic oscillators, approaches the PETIT and DULONG (1819) limit given by

$$C_p = 3Rn + A(T). \quad (12)$$

RESULTS AND DISCUSSION

In a recent paper BERMAN and BROWN (1985) made an important contribution by estimating the heat capacity of several silicates. They reviewed the theory on heat capacity and the heat capacity data on several minerals, and proposed the following expression for reproducing the low temperature data and estimating the high temperature data:

$$C_p = k_0 + k_1T^{-.5} + k_2T^{-2} + k_3T^{-3}$$

$$(\text{where } k_1, k_2 < 0). \quad (13)$$

This equation, unlike those used by HAAS and FISHER (1976) and ROBIE *et al.* (1978) and the Maier-Kelley equation, was found to comply with the requirement that the estimated heat capacity at high temperature approaches the high temperature limit predicted by lattice vibrational theory.

The essential difference between Eqn. (11) of this study and the Berman-Brown equation is as follows. Equation (13) is formulated without taking into account the important role of the "$A(T)$" term of Eqn.

Table 1. Data on molar volume, coefficients of thermal expansion, bulk modulus and its temperature derivative, and number of atoms in the chemical formula.

No.	Minerals	V_o cm^3/mol	a_0 (10^4)	a_1 (10^1)	a_2	a_3 (10^{-3})	Md. Temp. ranges(K)	K kb	$(\partial K/\partial T)_p$ kb/K	n
1.	Mg_2SiO_4(Olivine)	43.67	.6151	-.3441	12.9139	-1.6564	298-1200	1279	-.224	7
2.	$MgAl_2O_4$(Spinel)	39.71	.3735	-.1072	3.0722	-0.4433	298-1273	1952	-.222	7
3.	$MgSiO_3$(Cpx)	31.27	.5607	-.3470	13.5820	-1.8088	298-1473	1071	-.200	5
4.	$Mg_3Al_2Si_3O_{12}$(Py)	113.26	.3661	-.1082	3.2070	-0.4464	298-1073	1754	-.220	20
5.	MgO(Rocksalt)	11.25	.6167	-.2285	7.7917	-1.1002	298-1273	1605	-.272	2
6.	SiO_2(Coesite)	20.64	.2770	-.2047	7.5834	-0.9852	298-1273	1136	-.200	3

1. V_o: Matsui and Syono (1968); $\alpha(T)$: Suzuki (1975) and Suzuki et al. (1981); K and $(\partial K/\partial T)_p$: Carmichael (1982).
2. V_o: Robie et al. (1978); $\alpha(T)$: Suzuki et al. (1979); K: Carmichael (1982); $(\partial K/\partial T)_p$: Watanabe (1982).
3. V_o: Syono et al. (1971); $\alpha(T)$: Skinner (1966); K: Carmichael (1982); $(\partial K/\partial T)_p$: Watanabe (1982).
4. V_o: Robie et al. (1978); $\alpha(T)$: Skinner (1966); K and $(\partial K/\partial T)_p$: Carmichael (1982).
5. V_o: Robie et al. (1978); $\alpha(T)$: Suzuki (1975); K and $(\partial K/\partial T)_p$: Carmichael (1982).
6. V_o: Robie et al. (1978); $\alpha(T)$: Skinner (1966); K and $(\partial K/\partial T)_p$: Carmichael (1982).

* The conversion from the isothermal bulk modulus K_T and its temperature derivative $(\partial K_T/\partial T)_p$ to the adiabatic bulk modulus K_s and its temperature derivative $(\partial K_s/\partial T)_p$ are:

$K_T = K_s/(1 + T\alpha\gamma_{th})$

and

$(\partial K_T/\partial T)_p = |(\partial K_s/\partial T)_p - (\alpha\gamma_{th}K_T)(1+(T/\alpha)(\partial\alpha/\partial T))|/(1+T\alpha\gamma_{th})$

where γ_{th} is the thermal Grueneisen constant.

** Abbreviations: Cpx = Clinopyroxene; Py = Pyrope.

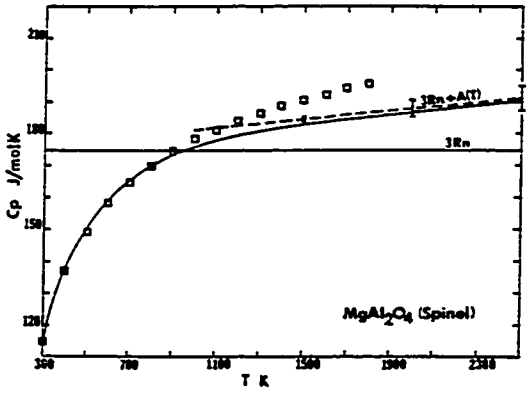

FIG. 1. Data on C_p for spinel plotted against temperature. The squares represent data from ROBIE *et al.* (1978). All the points up to 1900 K are from the experimentally determined heat content data. The error bars show the errors in the function ($3Rn + A(T)$) due to the errors in the measurements of thermal expansion and compressibility. The solid line represents C_p calculated from Eqn. (11) which was fitted to the low-temperature (298–800 K) C_v data. See text for discussion.

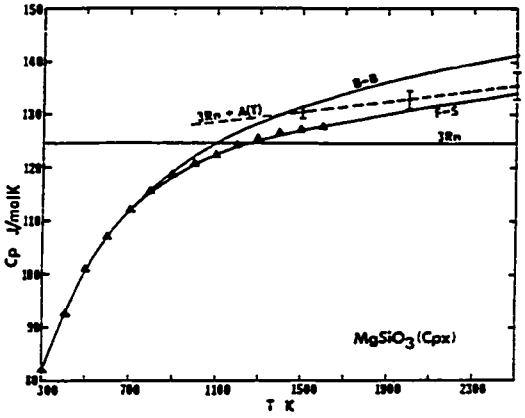

FIG. 3. Data on C_p for clinoenstatite ($MgSiO_3$) as calculated using three different methods. The F-S equation is Eqn. (11) of this study. The B-B equation is from BERMAN and BROWN (1985) and the triangles are from ROBIE *et al.* (1978). The fitted temperature ranges are from 298 K to 800 K for both F-S and B-B equations. See text for discussion.

(11). The Berman-Brown equation was determined empirically making sure that the formulation did comply with the high temperature limit. Similarly, there is nothing in the formulation which ensures that the limit set by Eqn. (12) will not be exceeded. Both these problems are taken care of in Eqn. (11) of this study. First, we have linked the high- and low-temperature relations, which BERMAN and BROWN (1985) treated as independent and second, we have included the $3Rn$ term to ensure that the high temperature C_v would approach the appropriate limit. In these respects, Eqn. (11) is unlike any formulation presented before. Note that the heat capacities of minerals have been calculated in this work by subtracting the "$A(T)$" contribution (based on the most recent data, Table 1) from C_p and then determining the k_i constants in the C_v equation.

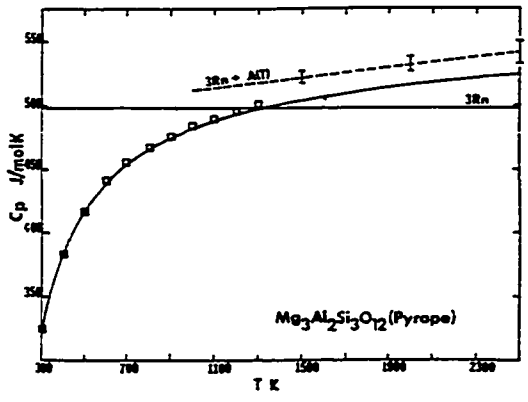

FIG. 2. Data on C_p for pyrope plotted against temperature. The squares represent experimental C_p data from HASELTON (1979). The computed curve is calculated using data up to 800 K to show the effect of extrapolation. In this case the discrepancy at 1300 K is negligible. If all the data to 1300 K were used in the analysis, the computed curve does not change significantly even at high temperature (*e.g.* 2500 K).

Figures 1 to 3 show the C_p data on three silicates plotted against temperature. Here, we have accepted that the C_p data obtained by using the equations of ROBIE *et al.* (1978) and HASELTON (1979) represent the low-temperature experimental measurements faithfully. These data are plotted in all figures for comparison. The solid curve represents data calculated by using the C_p Eqn. (11) of this study. The C_v constants k_i are determined from the regression analysis of the low-temperature data on $[C_p - A(T)]$. Note that the sources of error in these calculations are: a) departures from the $3Rn$ limit for some substances due to anharmonicity and electronic contributions, and b) the errors in extrapolating the thermal expansion and compressibility data. To show the magnitude of the latter errors on $3Rn + A(T)$ term, we use the equation:

$$\delta C_p = [(\partial C_p/\partial\alpha)^2(\delta\alpha)^2 + (\partial C_p/\partial K_T)^2(\delta K_T)^2]^{1/2}$$

where we adopt somewhat liberally the average values of the quoted errors of $\delta\alpha$ as 5×10^{-6} and δK_T as 200 kbar.

Figure 1 shows the data on spinel. In this case the C_p data from ROBIE *et al.* (1978) is the actually measured data at high temperatures. As pointed out by WOOD *et al.* (1986), a C_p of disorder of about 10 J/mol.K is possible in spinel. If this correction is applied to the calculated C_p, there will be a good match of the computed and experimental C_p data. In Fig. 1 the errors in $3Rn + A(T)$ are shown by vertical bars. Figure 1 demonstrates the importance of estimating the high temperature heat capacity using the present method.

Figure 2 shows the calculated C_p data on pyrope plotted against temperature. The heat capacity data (298 to 1300 K) of HASELTON (1979) are shown in the

Table 2. Coefficients for calculation of heat capacities using equation (11)

No. Minerals	k_1	k_2 (10^{-5})	k_3 (10^{-7})	A	B (10^3)
1. Mg_2SiO_4(Olivine)	-23.85	-0.3943	0.5374	-3.008	10.830
2. $MgAl_2O_4$(Spinel)	37.01	-0.8457	1.1656	-1.108	7.539
3. $MgSiO_3$(Cpx)	8.33	-0.8282	1.4941	-1.446	4.936
4. $Mg_3Al_2Si_3O_{12}$(Py)	-43.44	-0.2625	0.2294	-1.921	17.570
5. MgO(Rocksalt)	-15.87	-0.2804	0.2550	-0.230	3.861
6. SiO_2(Coesite)	19.52	-0.9914	1.7471	-0.398	0.815

* A and B are calculated from Table 1.
** k's are determined by regressing measured heat capacity data from Robie et al. (1978) and Haselton (1979).

figure. The solid line shows the calculated C_p using the experimental data between 298 and 800 K. Although the data are available up to 1300 K, we are interested in showing the effect when data are extrapolated from low temperature. The calculated C_p matches the data well to 1300 K.

Figure 3 shows that for clinoenstatite there is rather a good fit if one uses Eqn. (1) but the Berman-Brown equation overestimates C_p exceeding the limit set by Eqn. (12). Table 2 shows some of the evaluated data on heat capacity of silicates.

We conclude that Eqn. (11) should be adopted in estimating C_p. All the C_p data on silicates need a critical review and reanalysis which must be done in conjunction with data from experimental phase equilibrium and from the measurements of solid physical properties.

Acknowledgements—This work was supported by NSF grant #EAR-8516476 and by the PSC-BHE CUNY grant #4-40314. Thanks to Prof. B. J. Wood for a critical review and helpful suggestions.

Editorial handling: E. B. Watson

REFERENCES

BERMAN R. G. and BROWN T. H. (1985) Heat capacity of minerals in the system Na_2O-K_2O-CaO-MgO-FeO-Fe_2O_3-Al_2O_3-SiO_2-TiO_2-H_2O-CO_2: representation, estimation and high temperature extrapolation. *Contrib. Mineral. Petrol.* 89, 168–183.

CARMICHAEL R. S. (1982) *Handbook of Physical Properties of Rocks.* CRC Press.

DEBYE P. (1912) Zur Theorie der spezifischen Warmen. *Ann. Phys.* 39, 789–839.

EINSTEIN A. (1907) Die Plancksche Theorie der Strahlung und die Theorie der spezifischen Warmen. *Ann. Phys.* 22, 180–190.

HAAS J. L. JR AND FISHER J. R. (1976) Simultaneous evaluation and correlation of thermodynamic data. *Amer. J. Sci.* 276, 525–545.

HASELTON H. T. (1979) Calorimetry of synthetic pyrope-grossular garnets and calculated stability relations. Ph.D. dissertation, University of Chicago.

HOLLAND T. J. B. (1981) Thermodynamic analysis of simple minerals. In *Thermodynamics of Minerals and Melts* (eds. R. C. NEWTON, A. NAVROTSKY and B. J. WOOD), pp. 19–34. Springer-Verlag.

KIEFFER S. W. (1979) Thermodynamics and lattice vibrations of minerals: 1. Mineral heat capacities and their relationships to simple lattice vibrational models. *Rev. Geophys. Space Phys.* 17, 1–19.

LANE D. L. and GANGULY J. (1980) Al_2O_3 solubility in orthopyroxene in the system MgO-Al_2O_3-SiO_2: A reevaluation, and mantle geotherm. *J. Geophys. Res.* 85, 6963–6972.

MAIER C. G. and KELLEY K. K. (1932) An equation for the representation of high temperature heat content data. *Amer. Chem. Soc. J.* 54, 3242–3246.

MATSUI Y. and SYANO Y. (1968) Unit cell dimensions of some synthetic olivine group solid solutions. *Geochem. J.* 2, 51–59.

PETIT A. T. and DULONG P. L. (1819) Recherches sur quelques points important de la theorie de la chaleur. *Ann. Chim. Phys.* 10, 395–413.

ROBIE R. A., HEMINGWAY B. S. and FISHER J. R. (1978) Thermodynamic properties of minerals and related substances at 298.15 K and 1 bar (10^5 pascals) pressure and at higher temperatures. *U.S. Geol. Surv. Bull. 1452.*

SKINNER B. J. (1966) Thermal expansion. In *Handbook of Physical Constants* (ed. S. P. CLARK, JR.), pp. 75–95. Geol. Soc. Amer. Mem.

SUZUKI I. (1975) Thermal expansion of periclase and olivine and their anharmonic properties. *J. Phys. Earth* 23, 145–159.

SUZUKI I., OHTANI E. and KUMAZAMA M. (1979) Thermal expansion of γ-Mg_2SiO_4. *J. Phys. Earth* 27, 53–61.

SUZUKI I., SEYA K., TAKEI H. and SUMINO Y. (1981) Thermal expansion of fayalite, Fe_2SiO_4. *Phys. Chem. Mineral.* 7, 60–63.

SYONO Y., AKIMOTO S. and MATSUI Y. (1971) High pressure transformations in zinc silicates. *J. Solid State Chem.* 3, 369–380.

WATANABE H. (1982) Thermochemical properties of synthetic high-pressure compounds relevant to the earths mantle. In *High Pressure Research in Geophysics* (eds. S. AKIMOTO and M. H. MANGHNANI), pp. 441–464.

WOOD B. J., KIRKPATRICK R. J. and MONTEZ B. (1986) Order-disorder phenomena in $MgAl_2O_4$ spinel. *Amer. Mineral.* 71, 999–1006.

Contrib Mineral Petrol (1987) 95: 370–375

Contributions to Mineralogy and Petrology

Fluids at crustal pressures and temperatures

I. Pure species

S.K. Saxena and Y. Fei

Department of Geology, Brooklyn College, Brooklyn, NY 11210, USA
Department of Earth and Environmental Science, Graduate Center, CUNY, New York, NY 10036, USA

Abstract. The pressure-volume-temperature data of several gases (H_2, O_2, CO, CH_4, N_2 and CO_2) have been used to obtain the following corresponding states equation ($P>1$ kbar; $T>400$ K):

$$Z(\pm 0.0878)=A+BP_r+CP_r^2 \quad (21)$$

where Z is the compressibility factor, P_r reduced pressure (P/critical P), T_r reduced temperature (T/critical T) and the coefficients are given by:

$$A=1-0.5917T_r^{-2}$$
$$B=0.09122T_r^{-1}$$
$$C=1.4164\times10^{-4}T_r^{-2}-2.8349\times10^{-6}\ln T_r$$

($P>1$ kbar; $T>400$ K).

At pressures below 1 kbar, Z is given by:

$$Z(\pm 0.0761)=1+BP_r+CP_r^2 \quad (23)$$

where

$$B=0.09827T_r^{-1}-0.2709T_r^{-3}$$
$$C=0.01472T_r^{-4}-0.00103T_r^{-1.5}.$$

For water ($P>1$ kbar; $T>400$ K):

$$Z(\pm 0.0209)=A+BP+CP^2 \quad (22)$$

where

$$A=-0.7025+1.16\times10^{-3}T+99.6799T^{-1}$$
$$B=0.2143T^{-1}-3.1423\times10^{-14}T^3$$
$$C=-2.249\times10^{-6}T^{-1}-0.1459T^{-3}+2.1690\times10^{-15}T^2.$$

At pressure below 1 kbar, the equation is ($P>100$ bar; $T>673$ K):

$$Z(\pm 0.0601)=1+B'/V+C'/V^2 \quad (24)$$

where

$$B'=-2.20960T^{0.5}+3.35460\times10^{-8}T^3$$
$$C'=3.4569\times10^{-5}T^{2.5}+64.9764\ln T$$

Fugacities of the gases may be obtained by integrating the Z equations separately and combining the results as follows:

$$\int_1^P VdP=RT\left(\int_1^{1000} Z_{23}/PdP+\int_{1000}^P Z_{21}/PdP\right). \quad (26)$$

The subscript in Z denotes the equation which is to be used for calculating Z.

Introduction

Geochemists need data on phase equilibrium in the system C–H–O interacting with silicate rocks. Such data are crucial to an understanding of the stability of the gaseous species in the lithosphere and crust. The gas fugacities are also involved in monitoring the mineral compositions in metamorphic rocks. Petrologists have been well aware of their importance (e.g., Ganguly 1977; Eugster 1981, 1986; Helgeson 1981; Greenwood 1975; Walther and Wood 1986).

Although there have been number of important studies of fluid fugacities recently (e.g. Burnham et al. 1969; Holloway 1977; Kerrick and Jacobs 1981; Bottinga and Richet 1981; Halbach and Chatterjee 1982; Delany and Helgeson 1978), two aspects of the fluid studies are not much researched. First of these concerns the fugacities of a number of gases which may be part of the natural fluid mixture (e.g. H_2, O_2, CO, CH_4, N_2 etc.) and the second concerns multicomponent mixing of fluids (cf. Kerrick and Jacobs 1981; Greenwood 1973; Ryzhenko and Malinin 1971 and Mel'nik 1972, 1978). The study of these two aspects will be presented in two parts. Here, we present a review of some of the empirical equations of state used by geochemists and then equations of state for several fluids as determined in this work. A succeeding paper will deal with the multicomponent mixing models and computation of fugacities in natural mixtures.

Equations of state

The compressibility factor 'Z' may be used to express the deviation of a real gas from ideal behavior. Such deviation is strongly pressure and temperature dependent. Z may be expressed as

$$Z(P,T)=PV/RT=1+BP+CP^2+DP^3\ldots$$

or

$$Z(V,T)=1+B'/V+C'/V^2+\ldots \quad (1)$$

where the constants B, C, D, ... or B', C', D' ... etc. are called virial coefficients. For pure gases, they are functions of temperature only. It is contended that the virial equations of state are not useful at high pressures, especially at pressures near and above the critical pressure, even when a great number of constants are used. In the critical region, the whole series fails to converge. However, we note that the polynominal form of Eq. (1) could be used for generating an equation empirically, applicable particularly at high pressure-temperature ranges under consideration here.

Many equations of state, determined empirically, have been proposed in literature (e.g., Holloway 1977; Bottinga and Richet 1981; Halbach and Chatterjee 1982; Kerrick and Jacobs 1981). Historically, the most important is the van der Waals equation of state

$$(P+a/V^2)(V-b)=RT \tag{2}$$

where the term a/V^2 is called the internal or cohesive pressure and the term 'b' is called the covolume. The cohesive pressure resulting from the attractive force is responsible for the negative deviation from the ideal behavior. The larger 'a' is, the larger the cohesive pressure. A gas modeled with the hard sphere potential without attraction has a volume of 'a' equal to zero.

The term 'b' is a measure of the intermolecular distance at which mutual repulsion will become non-negligible. For a pair of molecules, 'b' is $4/3\pi d^3$, where 'd' is the distance between the centers of the molecules at the instant of collision. The covolume per molecule is $2/3\pi d^3$ and thus for Avogadro's number of molecules,

$$b=2/3\pi N d^3. \tag{3a}$$

For a hard sphere model $d=2\sigma$, and therefore,

$$b=2/3\pi N(2\sigma)^3 \tag{3b}$$

where σ denotes the radius of the molecule. At relatively high temperatures with the average translational energy becoming large, the violent collisions between molecules may result in shortening the distance between the centers of two molecules at the moment of collision: $d<2\sigma$. The particles become deformable – soft spheres which makes 'b' temperature dependent.

The van der Waals equation has not been successful in quantitatively reproducing the observed $P-V-T$ relationships. The Redlich-Kwong equation

$$P=RT/(V-b)-a/(V(V+b)T^{1/2}) \tag{4}$$

has generally been more successful in this regard. Holloway (1977) used the model of de Santis et al. (1974) and showed that if 'a' is considered as a function of temperature, the pressure computation from Eq. (4) is greatly improved.

Kerrick and Jacobs (1981) and Bottinga and Richet (1981) reviewed the modifications used for improving the Redlich-Kwong equation for modeling $P-V-T$ relationship for CO_2. Tourét and Bottinga (1979) derived the following forms of 'a' and 'b' (Eq. 4):

$$a=a_1(r^3-r^6)+a_2 \tag{5}$$

with $r=a_3/V$ and,

$$b=(\ln(V/a_3)+b_1)/b_2 \tag{6}$$

where a_1, a_2, a_3, b_1 and b_2 are adjustable parameters. Bottinga and Richet (1981) used these relations and found excellent fits to a number of observational data on CO_2.

Kerrick and Jacobs (1981) adopted the Carnahan-Starling modification of Eq. (4), such that 'a' was considered as a function of 'V' and T as follows:

$$a=c+d/V+e/V^2 \tag{7}$$

where each of c, d and e were fitted with a polynomial in T of the form

$$c=c_1+c_2T+c_3T^2. \tag{8}$$

Halbach and Chatterjee (1982) considered 'a' and 'b' as functions of T and P respectively. Their formulations are:

$$a(T)=a_1+a_2T+a_3T^{-1} \tag{9}$$

$$b(P)=(1+b_1P+b_2P^2+b_3P^3)/(b_4+b_5P+b_6P^2). \tag{10}$$

By considering 'b' as a function of P, they found that several sets of observations of H_2O not used by previous workers and some shock-wave data at high pressures (Rice and Walsh 1957) could be fitted excellently.

The modified Redlich-Kwong models as proposed by the geochemists do provide us with a means to calculate the $P-V-T$ relationship for H_2O and CO_2 and a point of diminishing returns should be considered to have been reached in regard to any further modifications. The surprising success of the Redlich-Kwong model and its derivatives is marred by the difficulty of understanding why it works. Some interesting physical insight was provided by Kerrick and Jacobs (1981). A second problem with the Redlich-Kwong formulation is the difficulty in computational algorithm (see Bottinga and Richet 1981).

The law of corresponding states

Although the Redlich-Kwong formulations have been used both for H_2O and CO_2, it is necessary to make a distinction between the two fluids. H_2O, as compared to CO_2, has properties strongly dependent on the electrostatic forces. Ross and Ree (1980) showed that CO_2 is much more like Ar, N_2, O_2 and CH_4 in its intermolecular potential. It is, therefore, likely that CO_2 and other more spherical species can be modeled with a simpler modification of the van der Waals formulation than the modified Redlich-Kwong model. This is certainly true at very high pressures and temperatures as revealed in the works of Ross and Ree (1980), who found it possible to apply the corresponding states' principle to several gases. The applicability of the law is governed by the following considerations (Ross and Ree 1980): a) The translational motion must be classical; b) The molecules must be spherically symmetric; c) The vibrational and electronic energy levels are constants; d) The intermolecular potential is given by an expression of the form:

$$\varepsilon(r)=U(r/r^*)$$

where ε and r^* are the characteristic energy and length scales respectively and U is a universal function.

The principle of corresponding states may be expressed as

$$f(P_r, T_r, V_r)=0 \tag{11}$$

where, P_r, T_r and V_r are reduced pressure (P/P_c), reduced temperature (T/T_c) and reduced volume (V/V_c), with the subscript denoting the critical value of the variable. According to Eq. (11), there exists a universal function which is valid for all substances or in other words all gases exhibit the same deviation from ideal behavior at the same P_r, T_r and V_r. We may also express the principle as

$$Z = PV/RT = f(P_r, T_r). \tag{12}$$

The molecular basis of Eq. (12) lies in the fact that the intermolecular potential curves for many different molecules have the same general shape determined by the intermolecular potential ϕ_{ik} and the distance 'r'.

In view of Ross and Ree's (1980) success in modeling the gases at very high pressure and success of Mel'nik (1972) in modeling CO and CH_4 at moderate pressures, we decided to apply the principle of corresponding states to gases (other than H_2O) at crustal temperatures and pressures.

Data

The data on CO_2 are the same as used by Bottinga and Richet (1981), namely Shmonov and Shmulovich (1974), Jüza et al. (1965), Michels et al. (1935), Kennedy and Holser (1966), Tsiklis et al. (1971) and Vukalovich et al. (1963). Many of these data were also used by Ryzhenko and Volkov (1971). The latter authors also reviewed data on other gases, which are all included here. In addition, data on CO to a pressure of 10 kbar are available in Robertson and Babb (1970). The equation of state for H_2O has been discussed by Burnham et al. (1969), Holloway (1977), Delany and Helgeson (1978) and Halbach and Chatterjee (1982). The data on water have been reviewed by Halbach and Chatterjee (1982) (Schmidt 1979; Tanishita et al. 1976; Hilbert 1979; Burnham et al. 1969). In addition, there is the data of Khodakovsky et al. (1981).

The virial equations

We shall also make use of the principle of corresponding states in formulating the virial equations of state for several gases such as H_2, N_2, CO, O_2, CH_4 and CO_2. If a single equation in P_r and T_r can be fitted to all the combined data on the gases, fugacities for several gases can be computed to high pressures.

The data on compressibility factor, Z, reduced pressure, P_r, and reduced temperature, T_r, of all gases was processed employing the new version of the SPSS (1985) technique. Stepwise multiple regression analysis was performed with the following equation of state formulation:

$$Z = 1 + B(T)\,P + C(T)\,P^2 + D(T)\,P^3 + \ldots \tag{13}$$

where, $B(T)$, $C(T)$, etc. are coefficients considered to be functions of temperature only. The pressure coefficients were considered to follow a polynomial behavior in reduced temperature, e.g., for $B(T)$, we have,

$$B(T) = [b_1 T_r + b_2 T_r^{-1} + b_3 T_r^{-2} + \ldots]. \tag{14}$$

Equations of state for pure fluids

The corresponding states equation for all gases (H_2, N_2, O_2, CO, CH_4 and CO_2) except water is determined to be

$$Z(\pm 0.1639) = 1 + BP_r + CP_r^2 + DP_r^3 \tag{15}$$

where

$$B = 9.835 \times 10^{-2} T_r^{-1} - 4.213 \times 10^{-2} T_r^{-2}$$
$$C = -6.2658 \times 10^{-8} T_r^2 - 3.4225 \times 10^{-6} \ln T_r + 2.7142 \times 10^{-4} T_r^{-3}$$
$$D = -5.4923 \times 10^{-7} T_r^{-2} + 1.488 \times 10^{-11} T_r^3.$$

The equation yields progressively worse results below 1 kbar as pressure decreases to 1 bar. The following equation may be used for calculating 'Z' below 1 kbar:

$$Z(\pm 0.0500) = 1 + BP_r + CP_r^2 + DP_r^3 \tag{16}$$

where

$$B = 0.11427\,T_r^{-1} - 0.16142\,T_r^{-2} - 0.25012\,T_r^{-3} - 1.4033 \times 10^{-7} T_r^3$$
$$C = 13.665 \times 10^{-2} T_r^{-3}$$
$$D = -9.548 \times 10^{-4} T_r^{-3}.$$

The standard error of 'Z' listed above is given by

$$\text{Standard Error} = (\Sigma (Y - Y')^2/(N - F))^{1/2} \tag{17}$$

where Y is the observed value, Y' the estimated value, N the total number of samples and F the number of parameters.

Following the same statistical procedure, the $Z-P-T$ equation was determined for water with all the data as used by Halbach and Chatterjee (1982) and including Khodakovsky et al. (1981). The equation is as follows:

$$Z(\pm 0.3308) = 1 + BP + CP^2 + DP^3 \tag{18}$$

where

$$B = -0.39821 \times 10^{-4}$$
$$C = 0.33409 \times 10^{-4} T^{-1}$$
$$D = -0.17023 \times 10^{-8} T^{-1}.$$

The large error in 'Z' is due to misfits at low pressures and temperatures. If the data below 500 bar and 573 K is excluded, the error is reduced to +0.15. The virial equation when used with volume as a variable yields somewhat better results with Z given by:

$$Z(\pm 0.17195) = 1 + B'/V + C'/V^2 + \ldots \tag{19}$$

where

$$B' = -0.2245 \times 10^9 T^{-2.5} + 0.1592 \times 10^{-7} T^3$$
$$C' = -24.8253\,T^{0.5}$$
$$D' = 0$$
$$E' = 223.065\,T + 0.1877 \times 10^9 T^{-1}.$$

It is important to note that the equation proposed here for CO_2 is not suitable for modeling the behavior of CO_2 or other gases at low pressure and temperature range including the critical region and the region close to the liquid-vapor phase boundary. For H_2O, Halbach and Chatterjee (1982) have succeeded in modeling the low $P-V-T$ behavior using a form of Redlich-Kwong equation. Bottinga and

Richet's (1981) and Kerrick and Jacobs' (1981) models for CO_2 would also work better in the low $P-T$ range than the present virial equation. For the $P-V-T$ region around the triple point and upto a pressure of 500 bars, the equation derived by Bender (1970) should be used.

Non-virial equations

During the course of this study, it became apparent that the precision of the fit of the data could not be improved by choosing different temperature dependent functions for the virial coefficients or increasing their number. However, we did note that if the following equation is used:

$$Z = A + BP + CP^2 + \ldots \quad (20)$$

where the constant A is a function of temperature, the precision improved very significantly. Errors could be further reduced by fitting the data at and below 1 kbar of pressure separately from the data at and above 1 kbar. The results are as follows:

For the corresponding states equation:

$$Z(\pm 0.0878) = A + BP_r + CP_r^2 \quad (21)$$

where

$$A = 1 - 0.5917\,T_r^{-2}$$
$$B = 0.09122\,T_r^{-1}$$
$$C = -1.4164 \times 10^{-4}\,T_r^{-2} - 2.8349 \times 10^{-6} \ln T_r$$

($P > 1$ kbar; $T > 400$ K).

For water:

$$Z(\pm 0.0209) = A + BP + CP^2 \quad (22)$$

where

$$B = -0.7025 + 1.16 \times 10^{-3}\,T + 99.6799\,T^{-1}$$
$$B = 0.2143\,T^{-1} - 3.1423 \times 10^{-1.5}\,T^{3}$$
$$C = -2.249 \times 10^{-6}\,T^{-1} - 0.1459\,T^{-3} + 2.1690 \times 10^{-1.5}\,T^{2}$$

($P > 1$ kbar; $T > 400$ K).

The pressure range below 1 kbar is covered by the following equations in which the term A is not necessary. For corresponding states:

$$Z(\pm 0.0761) = 1 + BP_r + CP_r^2 \quad (23)$$

where

$$B = 0.09827\,T_r^{-1} - 0.2709\,T_r^{-3}$$
$$C = 0.01472\,T_r^{-4} - 0.00103\,T_r^{-1.5}.$$

For water, the date are better fitted with volume as a variable rather than pressure. The opposite is true with the data at high pressures. The equation is:

$$Z(\pm 0.0601) = 1 + B'/V + C'/V^2 \quad (24)$$

where

$$B' = -2.20960\,T^{0.5} + 3.35460 \times 10^{-4}\,T^{3}$$
$$C' = 3.4569 \times 10^{-5}\,T^{2.5} + 64.9764 \ln T$$

Comparison of results

The lower standard errors of Z indicate that the $P-V-T$ data are better reproduced by the non-virial equation than by the virial. Since the errors in Z do not reveal the magnitude of the errors in volume directly, we have plotted in various figures molar volumes from different experiments and models against the volumes computed from the non-virial equations of this study. The gases H_2O, CO_2, CO and CH_4 were chosen because of the availability of their data over a broad range of pressure.

Figure 1 shows the isobaric volume data for CO_2 plotted against temperature. The correspondence with volume calculated with the equation of Bottinga and Richet (1981) is shown to be very close. The same is true with volume data calculated using the equation of Kerrick and Jacobs (1981). Table 1 compares some results following the method of Bottinga and Richet (1981, Table 3). We note that the results from the virial Eq. (15) are almost as good as those using the Bottinga-Richet equation. The results from the non-virial equations are somewhat off for CO_2 inspite of the fact that there is a reduction in the errors of Z from 0.1639 (Eq. 15) to 0.0878 (Eq. 21). It must be remembered that both these equations are for the corresponding states involving data on gases other than CO_2. The present equations fail totally at temperatures below 273 K.

Figure 2 shows the $P-V-T$ data comparison on methane. The calculated volume data are compared with those calculated by Mel'nik (1978). An excellent match is found. Jacobs and Kerrick's (1981) calculated data (not shown) are also closely similar and lie within the square except at high pressure (10 kbar) where the Kerrick-Jacobs data are a maximum of 5% higher in volume than the other two.

Figure 3 shows the $P-V-T$ data comparison for CO. In this case, the calculated data of Mel'nik (1978) shows consistently higher volumes than the volumes from the present results. Note that although the experimental data of Robertson and Babb (1970) covers the pressure range from

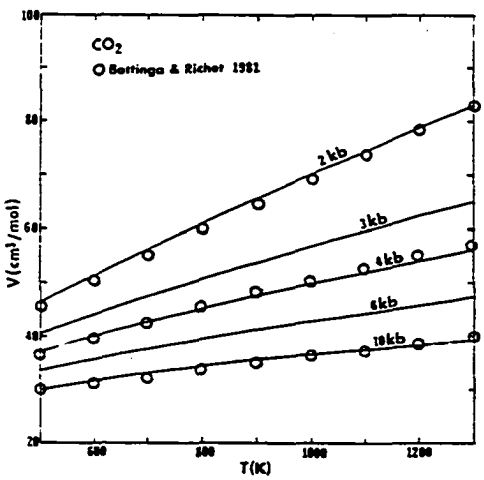

Fig. 1. Comparison of $P-V-T$ data on molar volume of CO_2. *Solid lines* data from this study; *circles* data calculated using the equation of Bottinga and Richet (1981)

Table 1. Comparisons between observed and predicted Z for CO_2 as evaluated with different equations of state

P	T °C	Z (observed)	$Z1$	$Z2$	$Z3$	$Z4$
7,903	100	7.0936	7.0433	7.0408	7.6046	7.0499
6,080	100	6.2664	6.0884	6.2094	6.6133	6.1836
7,093	200	5.8397	5.8536	6.0334	6.2073	5.7796
6,080	200	5.2002	5.1265	5.3237	5.4257	5.0988
7,093	300	5.0218	5.0921	5.2747	5.3024	4.9828
6,080	300	4.5034	4.4957	4.6664	4.6580	4.4265

Z1 Virial Eq. (31) from this study
Z2 Non-virial Eq. (37) from this study
Z3 Holloway's (1977) equation as quoted in Bottinga and Richet (1981)
Z4 Bottinga and Richet's (1981) Eq. (4) and (5) The original source of data as in Bottinga and Richet (1981)

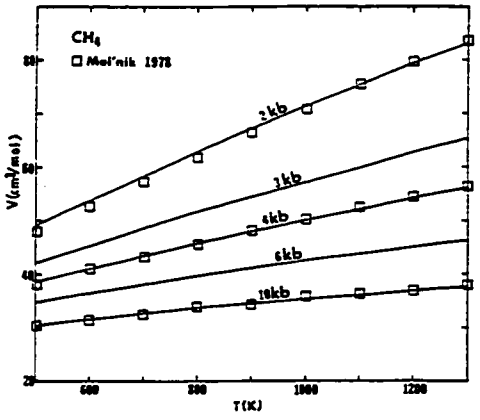

Fig. 2. Comparison of $P-V-T$ data on molar volume of methane. *Solid lines* data from this study; *squares* data from Mel'nik (1978); the experimental data and the calculated data of Jacobs and Kerrick (1981) lie within the area of the square except the latter data are about 5% high at 10 kbar

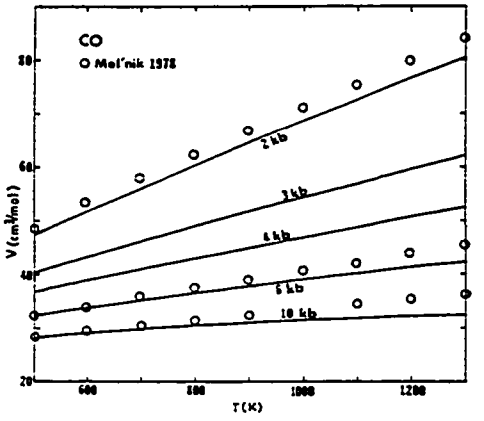

Fig. 3. Comparison of $P-V-T$ data on molar volume of CO. The calculated data of this study (*solid lines*) lie below the data calculated by Mel'nik (1978). See text for discussion

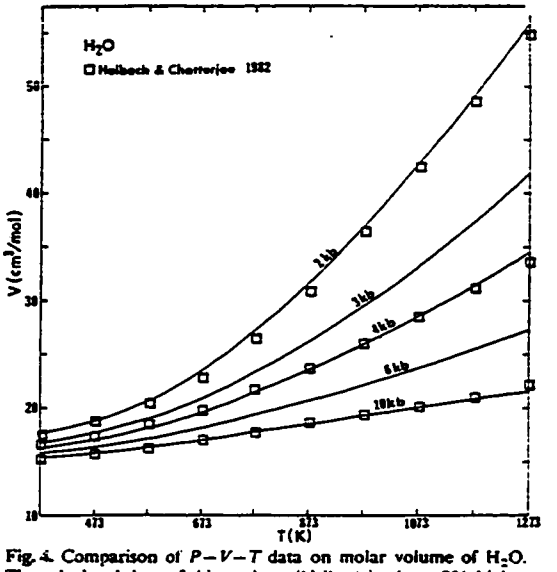

Fig. 4. Comparison of $P-V-T$ data on molar volume of H_2O. The calculated data of this study (*solid lines*) is about 2% higher than the data of Burnham et al. (1969) and Halbach and Chatterjee (1982). The differences decrease with increasing pressure

1 bar to 8 kbar, the maximium temperature reached is only 300° C. Therefore it is more desirable to base extrapolation with the corresponding states Eq. (21) than with Mel'nik's (1978)

Figure 4 shows a comparison of the $P-V-T$ data for water. The squares include the data of Halbach and Chatterjee (1982) and of Burnham et al. (1969), except at high pressure (10 kbar) and temperature (800–1000° C). The use of Eq. (22) for water leads to about 2% overestimation of volume at 2 kbar compared to the data of Halbach and Chatterjee (1982) but the difference decreases with increasing pressure and practically vanishes above 5 kbar.

Computation of pure fluid fugacities

The non-virial equations because of their greater precision in reproducing the $P-V-T$ data may be chosen to compute the pure fluid fugacity and the Gibbs free energy of formation at a certain pressure and temperature ($G_f(P, T)$).

For example, to calculate the $G_f(P, T)$ for CO_2, we may use the equations

$$G_f(P, T) = G^0_f(1, T) + \int_1^P V dP \quad (25)$$

where

$$\int_1^P V dP = RT\left(\int_1^{1000} Z_{23}/P dP + \int_{1000}^P Z_{21}/P dP \right). \quad (26)$$

The subscript in Z denotes the equation which is to be used for calculating Z. For the gases with the corresponding states equation, it is necessary to either use P_r and T_r or change Eq. (21) from P_r and T_r to one in P and T for each gas.

Conclusions

It is possible to use a corresponding states equation for a number of non-polar gases. The $P-V-T$ relation is computed with precision for use in phase equilibrium calculations. The reproducibility of the $P-V-T$ relation for most gases is excellent above a pressure of 1 kbar and a temperature of 400 K. For water equations of state similar in form to that of the corresponding states may be obtained. These equations of state are considerably simplified with fewer terms than most other equations and therefore may be useful in modeling multicomponent mixtures.

Acknowledgements. Thanks are due to Y. Bottinga for a critical review. Financial support was provided by NSF (grant #EAR-8516476) and City University (PSC-BHE #6-65191).

References

Bender E (1970) Equations of state exactly representing the phase behavior of pure substances. Am Soc Mech Engineers. Symposium Thermophys Properties, 5th, Proc 227–235

Bottinga, Y, Richet P (1981) High pressure and temperature equation of state and calculation of the thermodynamic properties of gaseous carbon dioxide. Am J Sci 281:615–660

Burnham CW, Holloway JR, Davis NE (1969) The specific volume of water in the range 10-8,900 bars, 20° to 900° C. Am J Sci 267A:70–95

Delany JM, Helgeson HC (1978) Calculation of the thermodynamic consequences of dehydration in subducting oceanic crust to 100 kb and >800 C. Am J Sci 278:638–686

De Santis R, Breedveld GJF, Prausnitz JM (1974) Thermodynamic properties of aqueous gas mixtures at advanced pressures. Ind Eng Chem Proc Dev 13:374–377

Eugster HP (1981) Metamorphic solutions and reactions. In: Wickman FE, Rickard DT (eds) Chemistry and Geochemistry of Solutions at High Temperatures and Pressures. Pergamon Press, New York. Phys Chem Earth 13/14, 461–507

Eugster HP (1986) Minerals in hot water. Am Mineral 71:655–673

Ganguly J (1977) Compositional variables and chemical equilibrium in metamorphism. In: Saxena SK, Bhattacharji S (eds) Energetics of geological processes. Springer, Berlin Heidelberg New York, pp 230–284

Greenwood HJ (1973) Thermodynamic properties of gaseous mixtures of H_2O and CO_2 between 450 and 800° C and 0 to 500 bars. Am J Sci 273:561–571

Greenwood HJ (1975) Buffering of pore fluids by metamorphic reactions. Am J Sci 275:573–593

Halbach H, Chatterjee ND (1982) An empirical Redlich-Kwong-type equation of state for water to 1,000° C and 200 kbar. Contrib Mineral Petrol 79:337–345

Helgeson HC (1981) Prediction of the thermodynamic properties of electrolytes at high pressures and temperatures. In: Rickard D, Wickman F (eds) Chemistry and geochemistry of solutions at high temperatures and pressures. Pergamon Press, New York. Phys Chem Earth 13/14:133–177

Hilbert R (1979) PVT-Daten von Wasser und von wässrigen Natriumchlorid-Lösungen bis 873 K, 4,000 Bar und 25 Gewichtsprozent NaCl. Hochschulverlag, Freiburg, S 212

Holloway JR (1977) Fugacity and activity of molecular species in supercritical fluids. In: Fraser DG (ed) Thermodynamics in geology. Reidel, Dordrecht-Holland, pp 161–181

Jacobs GK, Kerrick DM (1981) Methane: an equation of state with application to the ternary system $H_2O-CO_2-CH_4$. Geochim Cosmochim Acta 45:607–614

Jüza J, Kmonicek V, Sifner O (1965) Measurements of the specific volume of CO_2 at 700–4,000 bars and 50–475° C. Physica 31:1735–1744

Kennedy GC, Holser W (1966) Pressure-volume-temperature and phase relations of water and carbon dioxide. Geol Soc Mem 97:374–383

Kerrick DM, Jacobs GK (1981) A modified Redlich-Kwong equation for H_2O, CO_2, and H_2O-CO_2 mixtures at elevated pressures and temperatures. Am J Sci 281:735–767

Khodakovsky IL, Dorofeyeva VA, Melenikova GL, Geranin AV, Ry'zhenko BN (1981) Thermodynamic parameters of liquid water at 0–300° C and pressures upto 10,000 bar. Geokhimiya 2:208–220

Mel'nik YP (1972) Thermodynamic parameters of compressed gases and metamorphic reactions involving water and carbon dioxide. Geokhimiya 6:654–662

Mel'nik YP (1978) Thermodynamic properties of carbon monoxide and methane at high temperatures and pressures – a new correlation based on the principle of corresponding states. Geokhimiya 11:1677–1691

Michels A, Michels C, Wouters H (1935) Isotherms of CO_2 between 70 and 300 atm (amagat densities 250–600). R Soc London Proc A153:214–224

Rice MH, Walsh JM (1957) Equation of state of water to 250 kilobars. J Chem Phys 26:824–830

Robertson SL, Babb SE Jr (1970) Isotherms of carbon monoxide to 10 kbar and 300°C. J Chem Phys 53:1094–1097

Ross M, Ree FH (1980) Repulsive forces of simple molecules and mixtures at high density and temperature. J Chem Phys 73:6146–6152

Ryzhenko BN, Volkov VP (1971) Fugacity coefficients of some gases in a broad range of temperatures and pressures. Geokhimiya 7:760–773

Ryzhenko BN, Malinin SD (1971) The fugacity rule for the systems CO_2-CH_4, CO_2-N_2, and CO_2-H_2. Geokhimiya 8:899–913

Schmidt E (1979) Properties of water and steam in SI-units. Springer, Berlin Heidelberg New York, p 190

Shmonov VM, Shmulovich KI (1974) Molal volumes and equations of state of CO_2 at temperatures from 100 to 1,000° C and pressures from 2,000 to 10,000 bars. Akad Nauk SSSR Doklady 217:205–209

SPSS (1985) Statistical package for the social sciences. McGraw-Hill, NY

Tanishita I, Watanabe K, Kijima J, Ishii H, Oguchi K, Uematsu M (1976) Experimental study of the p, V, T properties of water in the range 323.15 to 773.15 K and pressures upto 200 MPa. J Chem Thermodyn 8:1–20

Touret J, Bottinga Y (1979) Equation d' etat pour le CO_2; application aux inclusions carboniques. Bull Mineral 102:577–583

Tsiklis DS, Linshits LR, Tsimmerman SA (1971) Measurement and calculation of molar volume of CO_2 at high pressure and temperature. Teplofiz Svoistva Veshchestv Mater 3:130–136

Vukalovich MP, Altunin VV, Timoshenko NI (1963) Specific volume of CO_2 at high pressure *abd* temperature. Teploenergetika 10:92–93

Walther JV, Wood BJ (1986) (eds), Fluid-rock interactions during metamorphism. (Adv Phys Geochem, vol 5), Springer, Berlin Heidelberg New York, p 211

Received July 18, 1986 / Accepted January 12, 1987

Geochimica et Cosmochimica Acta Vol. 51, pp. 783–791

0016-7037/87/$3.00+.00

High pressure and high temperature fluid fugacities

S. K. SAXENA and Y. FEI

Department of Geology, Brooklyn College, Brooklyn, NY 11210, U.S.A. and Department of Earth and Environmental Science, Graduate Center, CUNY, New York, NY 10036, U.S.A.

(*Received May* 20, 1986; *accepted in revised form December* 24, 1986)

Abstract—High-temperature and high-pressure shock-wave data on fluids (pure species) have been combined with low-temperature and low-pressure data to generate a "corresponding state" equation in the virial format in reduced pressure and temperature for many species. The equation is then modified to obtain a similar equation of state for H_2O. The fugacities of the pure species in the C-H-O system can be calculated to a temperature of 3000 K and to a pressure of 1 megabar. However, dissociation of the pure species may invalidate the data over certain pressure-temperature ranges.

INTRODUCTION

IT IS IMPORTANT to obtain data on high pressure and temperature gas fugacities for the study of geochemical processes in planetary crusts and mantles. Experimentally determined volume data on compressed fluids is generally for temperatures lower than 1073.15 K, usually close to 298.15 K, with the static pressure usually less than 10 kbar (see Fig. 1). Shock wave measurements of fluid compressibility, however, extend to higher pressure and temperatures. Shock wave data reported by RICE and WALSH (1957) on water and by Nellis and coworkers (MITCHELL and NELLIS, 1982; NELLIS and MITCHELL, 1980) on many different gases may be used to study the pressure-volume-temperature relationships. The purpose of this paper is to synthesize the available shock-wave data and generate empirical equations of state that are also consistent with the low-pressure data. The emphasis is on formulating equations that can be used to compute the Gibbs free energy of formation of a fluid at a given pressure and temperature for computation of equilibrium phase diagrams.

REVIEW OF EQUATIONS OF STATE

Many attempts have been made to model the equation of state for fluids, particularly for water (JÚZA, 1961; TODHEIDE, 1972; HOLLOWAY, 1977; KERRICK and JACOBS, 1981; HALBACH and CHATTERJEE, 1982; HELGESON and KIRKHAM, 1974; DELANY and HELGESON, 1978) and for CO_2 (KERRICK and JACOBS, 1981; BOTTINGA and RICHET, 1981). Following HOLLOWAY (1977), KERRICK and JACOBS (1981), HALBACH and CHATTERJEE (1982) and BOTTINGA and RICHET (1981) used modifications to the Redlich-Kwong equation to compute the P-V-T gas properties. These formulations unfortunately cannot be used to fit the shock wave data.

Van der Waals' equation of state uses the terms $RT/(V-b)$ and a/V^2 as representing the repulsive and attractive intermolecular interactions respectively. A two parameter formulation of the interactions was presented by REDLICH and KWONG (1949) in the following equation of state:

$$P = RT/(V-b) - a/[V(V+b)T^{1/2}] \quad (1)$$

where a and b are constants that are different for different gases. HOLLOWAY (1977) used Eqn. (1) for H_2O considering b as a constant and varying a as a function of temperature only. KERRICK and JACOBS (1981) found it necessary to express a as a function of T and V and to formulate the repulsion term using CARNAHAN and STARLING's (1972) hard-sphere model. HALBACH and CHATTERJEE (1982) extended the pressure range of the equation of state for water with the following expressions for a and b:

$$a(T) = a_1 + a_2T + a_3T^{-1} \quad (a_2 < 0) \quad (2)$$

$$b(P) = (1 + b_1P + b_2P^2 + b_3P^3)/(b_4 + b_5P + b_6P^2)$$

$$(b_3 < 0). \quad (3)$$

Halbach and Chatterjee succeeded in extending the applicability of the equation from the critical point to nearly 200 Kbar and at temperatures up to 1273.15 K.

For CO_2, TOURÉT and BOTTINGA (1979) used

$$a = a_1[(a_3/V)^3 - (a_3/V)^6] + a_2 \quad (4)$$

and

$$b = [\ln(V/a_3) + b_1]/b_2. \quad (5)$$

BOTTINGA and RICHET (1981) published CO_2 data to a pressure of 50 Kbar and to a temperature of 2100 K.

CORRESPONDING STATE EQUATIONS FOR SOME GASES

The shock wave measurements on liquids form an important data set for obtaining fluid fugacities at pressures existing in the earth's mantle and core. Nellis and coworkers (see review, NELLIS, 1984) have made such measurements on many fluids including Ar, N_2, D_2, He, Xe, CO, H_2O and CH_4. Ross and others (*e.g.*, ROSS, 1979; ROSS and REE, 1980; ROSS *et al.*, 1983) have used these data to obtain Hugoniot relationships which link the thermodynamic state (P_H, E_H, V_H) attained behind the shock front with the initial state (P_0, E_0, V_0) (P = pressure, E = internal energy, V = volume). The Rankine-Hugoniot relation is

$$E_H = E_0 + 0.5(P_H + P_0)(V_0 - V). \quad (6)$$

In these studies, internal energy and pressure calculations have been performed by taking suitable derivatives of the Helmholtz free energy equation given by (see, *e.g.*, ROSS *et al.*, 1983):

$$A = 2.5N\kappa T + N\{0.5h\nu + \kappa T \ln[1 - \exp(-\beta h\nu)]\} + A_{PE} + N\kappa T \ln \rho + \text{const.} \quad (7)$$

where T = absolute temperature, ρ = the number den-

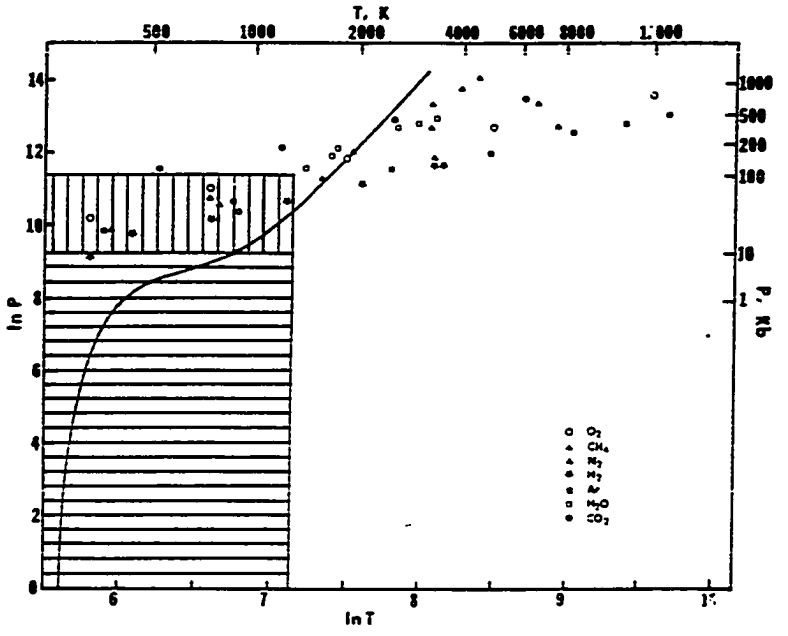

FIG. 1. Compressibility data on various species. The box with horizontal lines represents the pressure-temperature range of experimental data on water generated at static pressures by BURNHAM *et al.* (1969). The box with vertical lines represents the extended *P-T* range through the works of JUZA (1961) and TÖDHEIDE (1972). Further extension of pressure range to 200 Kbar was achieved by HALBACH and CHATTERJEE (1981). The various symbols represent shock-wave and Hugoniot data discussed by ROSS and REE (1980), RICE and WALSH (1957) and as reviewed in NELLIS (1984). For CO_2 (not shown) BOTTINGA and RICHET (1981) have generated data to 50 Kbar and 2100 K. The solid curve represents a probable geothermal gradient in the earth's mantle (data from STACEY, 1977).

sity, and $\beta = 1/\kappa T$. The first term is due to the kinetic energies of translation and rotation; the second term, with the bracket, represents the free energy of a vibrating molecule with frequency $h\nu/\kappa$. The term A_{PE} is the intermolecular potential contribution evaluated from fluid variational theory (ROSS, 1979).

$$A_{PE} = AF_{HS}(\eta) + (\rho N/2)\int dr\phi(r)g_{HS}(r,\eta) + A_{QM} \quad (8)$$

where $\eta = \Pi d^3\rho/6$, $AF_{HS}(\eta)$ is the reference excess free energy, $g_{HS}(r, \eta)$ is the hard-sphere radial distribution function, and $\phi(r)$ is a pair potential. According to ROSS (1979) $\phi(r)$ is realistically given by:

$$\phi(r) = \xi/(\alpha-6)\{6\exp[\alpha(1-r/r^*)] - \alpha(r^*/r)^6\} \quad (9)$$

where ξ and r^* are the characteristic energy and length scales respectively and α is derived from the quantum mechanical *ab initio* calculations.

Using the relationships reviewed above, ROSS and REE (1980) applied the "law of corresponding states" to the high pressure behavior of fluids. They argued that the following assumptions underlying a rigorous statistical mechanical derivation of the corresponding states theory are reasonable. These are a) the translational motion is classical, b) the molecules are spherically symmetric and c) the vibrational and electronic levels are constants. A fourth assumption, that the intermolecular potential is given by an expression of the form given in Eqn. (8) with α, ξ/κ and r^* determined from the corresponding states theory, was tested using the shock wave data for Ar, Xe, N_2, O_2, CO_2 and CH_4. ROSS and REE (1980) found that the calculated Hugoniots of Xe, N_2, O_2 and CO_2 were in surprisingly good agreement with experiments up to several hundreds of kilobars. The failure of CH_4 and CO to obey the theory at high pressure was due to their thermal decomposition. The assumption c) is not true for oxygen which has a number of low lying electronic states. For oxygen, ROSS and REE (1980) made the appropriate correction for the electron thermal excitation in computing the Hugoniot.

The success of ROSS and REE'S (1980) model prompted us to consider the use of a single equation for a number of gases. The method adopted here combines high-pressure and high-temperature shock wave data with the low-pressure (<10 Kbar) and low-temperature (<1273.15 K) experimental *P-V-T* data. All available data could not be fitted with any of the empirical equations reviewed above. Different types of modifications of the Redlich-Kwong equation are required to fit *P-V-T* data on different gases. For example, for water (HALBACH and CHATTERJEE, 1982) the parameters a and b are complicated functions of T and P respectively, but for CO_2, (BOTTINGA and RICHET, 1981) a and b are independent of P or T. We, therefore,

adopted a polynomial equation in reduced pressure and reduced temperature that has the same form as the virial equation of state:

$$PV/RT = A + BP + CP^2 + DP^3 + \cdots \quad (10)$$

where A, B, C and D are coefficients that are dependent on temperature only. While such polynomial constants, obtained through regression analysis of the P-V-T data, are useful in computation of fugacities, they may not yield much insight into the nature of the repulsive and attractive molecular interactions. In Eqn. (10), V is expressed explicitly in P, which facilitates the computation of the VdP integral.

The procedure adopted in determining the polynomial is as follows. It was considered that each coefficient in Eqn. (10) is a complex function of reduced temperature ($T_r = T/T_c$). Several terms, logarithmic and exponential, are included as variables and the coefficients determined from the multiple regression analysis of the $Z(=PV/RT) - P_r - T_r$ data on Ar, Xe, N_2, O_2, CO, CO_2, CH_4 and H_2. H_2O and NH_3 are not included because these gases are substantially different in interatomic potentials (Ross and Ree, 1980). Hydrogen also should have been excluded for a similar reason. However, it was found that its inclusion introduced no significant errors in the calculation of fugacities of other species and the hydrogen fugacity could be calculated with an average error of 7.7% in the compressibility factor. Since we wish to use the corresponding states theory and use a single equation over a wide range of pressure and temperature (not covered by the P-V-T data on a single species), it is essential that the same equation should be used for hydrogen. Percent errors in the Z data for other species are: CH_4: 2.98, N_2: 1.28, Ar: 4.7, O_2: 0.7 and CO_2: 1.23.

The low-P and low-T volume data used to obtain the equation have been reviewed by Ryzhenko and Volkov (1971), Mel'nik (1972) and Bottinga and Richet (1981). The data on CO_2 are the same as used by Bottinga and Richet (1981). In addition to these data, data for CO to a pressure of 10 kbar (Robertson and Babb, 1970) were also considered.

The equation in T_r and P_r for $Z(=PV/RT)$ is:

$$Z(\pm 0.1790) = A + BP_r + CP_r^2 + DP_r^3$$

where

$$A = 2.0614 - 2.2351T_r^{-2} - 0.39411 \ln T_r$$

$$B = 5.5125E - 2T_r^{-1} + 3.9344E - 2T_r^{-2}$$

$$C = -1.8935E - 6T_r^{-1} - 1.1092E - 5T_r^{-2} - 2.1892E - 5T_r^{-3}$$

$$D = 5.0527E - 11T_r^{-1} - 6.3033E - 21T_r^3. \quad (11)$$

The standard deviation of Z is shown in brackets. Note that Eqn. (11) does not result in the $PV = RT$ relationship at 1 bar and therefore is not strictly a virial equation of state.

Table 1 compares observed Z values from the Hugoniots with calculated values from Eqn. (11). Z values in Table 1 may be transformed to $V(P, T)$ by first changing the coefficients using the appropriate critical pressure and temperature and then using the relation $V = ZRT/P$. Because the major goal of this study was an estimation of P-V-T data at high pressure and temperature, calculated values at low pressure (*i.e.*, less than 2 Kbar) may be uncertain. Data for hydrogen has been included in Table 1 but as pointed out by Ross and Ree (1980), the potential for hydrogen is much softer than that of the other gases. Z values for hydro-

Table 1: Calculation of fluid compressibility using equation (11).

T K	P Kb	Z(Obs.)	Z(Calc.)	T K	P Kb	Z(Obs.)	Z(Calc.)
O_2(T_c=154.8 P_c=50.8)				H_2(T_c=33.1 P_c=13.0)			
330	26	17.058	17.429	266	9.67	6.122	6.515
749	59	15.159	15.079	431	15.73	5.707	6.124
1823	133	12.286	12.376	722	25.63	5.124	5.569
4883	315	9.311	9.376	1222	41.66	4.511	4.945
14367	806	6.748	6.443	2014	66.88	3.994	4.365
25601	1341	5.670	5.696	3246	107.20	3.575	3.816
				3462	114.54	3.526	3.744
CH_4(T_c=190.7 P_c=46.4)							
				Ar(T_c=151.0 P_c=48.6)			
384	19	14.878	15.354				
728	46	16.477	16.763	374	18	11.577	11.409
1912	159	17.004	17.747	860	41	10.322	9.937
3268	294	16.123	16.788	2510	100	7.607	7.416
6528	600	14.040	14.192	4570	161	6.356	6.124
3626	622	24.759	23.638	8610	266	5.202	4.869
3906	844	25.162	26.195	11960	345	4.684	4.254
4438	1196	32.317	32.106	16730	450	3.891	3.659
N_2(T_c=126.2 P_c=33.9)				CO_2(T_c=304.2 P_c=73.9)			
783	39	11.982	11.778	513	98	45.950	45.967
1573	75	10.323	10.286	1167	184	34.136	33.877
3293	147	8.593	8.642	2594	349	25.892	25.750
7554	305	6.801	6.622	6071	686	19.029	18.643

Note: All data from Ross and Ree (1980) and as reviewed in Ross et al. (1983). For a discussion of the data on hydrogen, which has a softer potential than that of the other gases, see text.

gen, therefore, are not as well reproduced as are Z values for other gases. Note, however, that the 7.7% error for hydrogen is well within acceptable limits generally considered in the formulation of an equation of state from experimental P-V-T data.

Fugacity coefficients may be calculated from the relation

$$RT \ln \gamma = \int_{P_0}^{P} V dP - RT \ln P + RT \ln f(P_0, T). \quad (12)$$

To calculate fugacity coefficients of CO_2, we set P_0 = 5 Kbar. An equation for CO_2 fugacity at 5 Kbar that is compatible with the data of BOTTINGA and RICHET (1981) is:

$$RT \ln f(5\,\text{Kb}, T) = 1000(-40.468 + 0.06702T + 8.3481 \ln T). \quad (13)$$

Fugacity coefficients from equations of KERRICK and JACOBS (1981) for CO_2 match those calculated from Eqns. (11) and (13) nearly perfectly to 20 Kbar.

EQUATION OF STATE FOR H_2O

It is possible to fit the P-V-T data on water with an equation of the same form as Eqn. (11). Such a procedure, however, led to larger errors in the results than the procedure described below. We considered the corresponding states Eqn. (11) as the reference equation of state. Deviations from such an equation may be considered to arise due to the non-spherical character of the water molecule. Therefore, the corresponding states equation was also used to fit P-V-T relations for H_2O. The experimental P-V-T data on water are the same as used by HALBACH and CHATTERJEE (1982) (SCHMIDT, 1979; TANISHITA *et al.*, 1976; HILBERT, 1979; BURNHAM *et al.*, 1969) and the recent data of KHODAKOVSKY *et al.* (1982). The experimental data were used to calculate ΔZ (Z observed $-$ Z calculated with Eqn. 11), and these values were regressed following the same procedure as discussed in the previous section. The terms in equation for ΔZ were then added to the terms in Eqn. (11) to obtain the following equation for water (with a low pressure limit of 2 Kbar):

$$Z(\pm 0.2214) = A + BP_r + CP_r^2 + DP_r^3$$

where

$$A = 1.4937 - 1.8626T_r^{-2} + 0.80003T_r^{-3} - 0.3941 \ln T_r$$

$$B = 4.2410E - 2T_r^{-1} + 2.4097E - 2T_r^{-2} - 8.9634E - 3T_r^{-3}$$

$$C = -9.016E - 7T_r^{-1} - 6.1345E - 5T_r^{-2} + 2.2380E - 5T_r^{-3} + 5.2335E - 7 \ln T_r$$

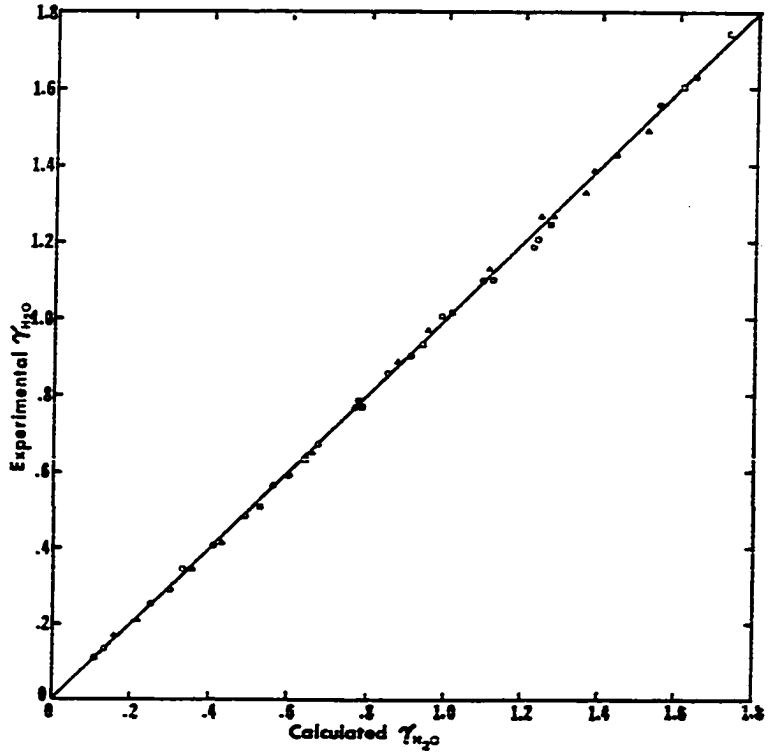

FIG. 2. Comparison of the calculated fugacity of water with that of BURNHAM *et al.* (1969) in the pressure range of 5 to 10 Kbar and the temperature range 293.15 to 1073.15 K. The data are plotted at 5 (solid circle), 6 (open circle), 7 (solid triangle), 8 (open triangle), 9 (solid square) and 10 (open square) Kbar between 473.15 and 1073.15 K at intervals of 200 K.

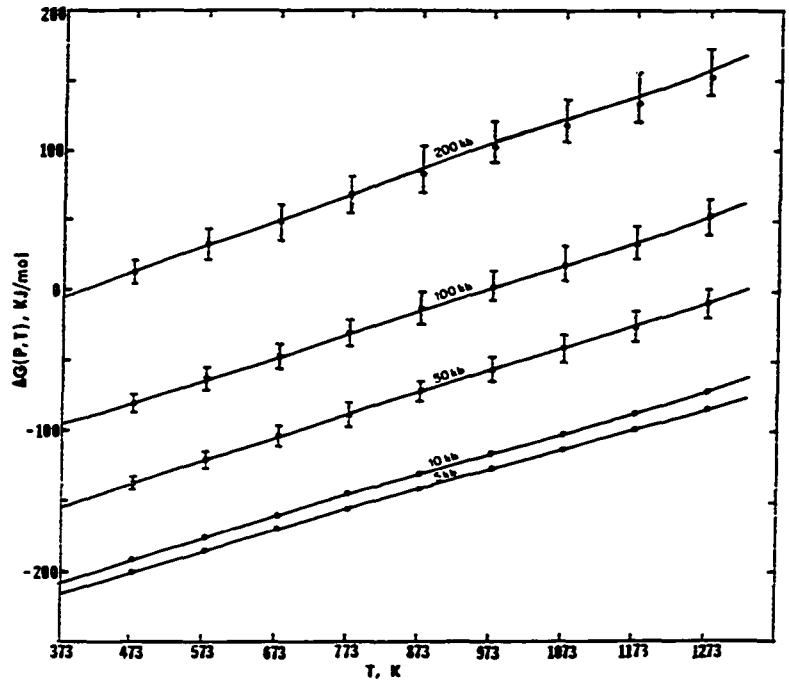

FIG. 3. Comparison of observed and computed data on the Gibbs free energy of formation of water. ΔG_f^0 as computed in this study falls on the curve (solid line). The error bars (representing two standard deviations) denote the statistical errors in Z as determined in this study. The solid circles represent the data of HALBACH and CHATTERJEE (1982). At 5 and 10 Kbar, the errors are negligible and match between the data sets is excellent.

$$D = -7.6707E-9T_r^{-1} + 4.1108E-8T_r^{-2} - 1.4798E-8T_r^{-3} - 6.3033E-21T_r^3. \quad (14)$$

$\Delta G_f^0(P, T)$ for water may be calculated from:

$$\Delta G_f^0(P, T) = \Delta G_f^0(1, T) + RT \ln f \quad (15)$$

where $\Delta G_f^0(1, T)$ is from ROBIE *et al.* (1978) and

$$RT \ln f = \int_{5\,\mathrm{Kb}}^{P} V dP + RT \ln f(5\,\mathrm{Kb}, T). \quad (16)$$

An expression for water fugacity at 5 Kbar that reproduces both the data of BURNHAM *et al.* (1969) and HALBACH and CHATTERJEE (1982) is:

$$RT \ln f(5\,\mathrm{Kb}, T) = 1000(-130.517 + 0.06497T + 19.4831 \ln T). \quad (17)$$

DISCUSSION

General

Figure 2 compares calculated and experimentally determined fugacity coefficients for water between 5 to 10 Kbar. The experimental data are from BURNHAM *et al.* (1969).

Figure 3 shows that $\Delta G_f^0(P, T)$ calculated from Eqns. (14) to (17) match very well values calculated by HALBACH and CHATTERJEE (1982) to a pressure of about 50 Kbar. The errors shown are calculated from the standard error in Z with each bar representing two standard deviations.

Figure 4 compares the high pressure volume data from shock-wave measurements with volumes calculated using Eqns. (11) and (14). The agreement is excellent in most cases.

As shown in Table 1 and Figs. 2 to 4, the polynomial expressions (11) and (14) reproduce most experimental data well. The low-pressure limit for H_2O is 5 Kbar and 5 Kbar for CO_2. Extrapolation of the data to high pressure requires some discussion. The range of pressure and temperature covered by experimental data along a possible geothermal gradient, is close to 1 Mbar and 3000 K (Fig. 1). Because experimental data extend to 15000 K, extrapolation to temperatures higher than 3000 K is probably not a problem. Extrapolation to pressures higher than 1 Mbar, however, may not be reliable. There is, however, a question of the stability of the fluid species H_2O as discussed below.

As described by NELLIS *et al.* (1984), the fluid compressibility is measured using shock-waves generated by the impact of planar projectiles onto planar target specimens. Gas guns are used to produce impact velocities of 2 and 8 Km per second. The shocked matter is generally in thermal equilibrium owing to the high densities and temperatures. Unfortunately, the technique does not permit the unambiguous recognition

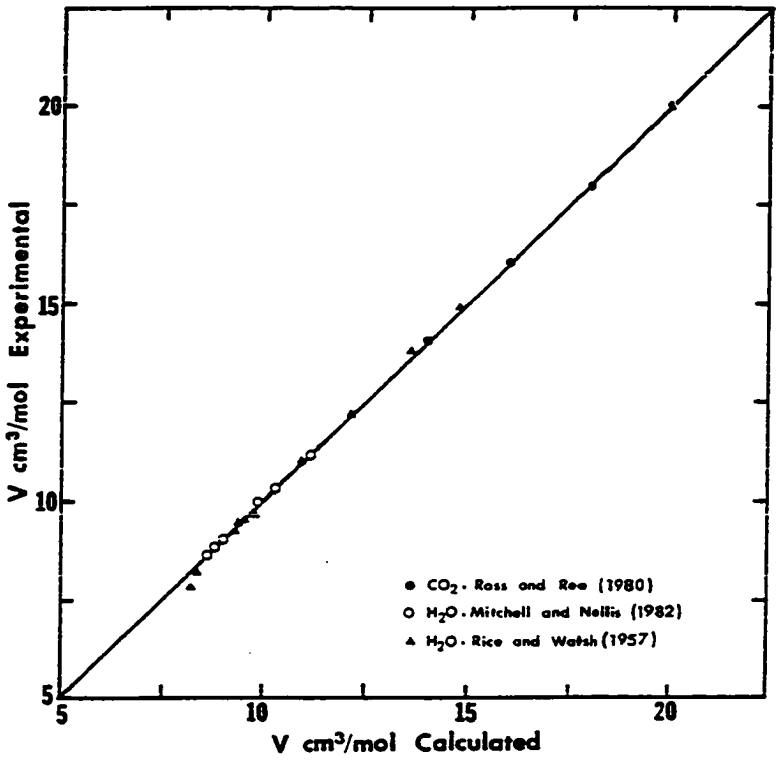

FIG. 4. Comparison of the calculated volume with the shock-wave data for CO_2 and H_2O. The range of pressure and temperature covered are: CO_2: P = 98 to 686 Kbar, T = 513 to 6071 K; H_2O: P = 10 to 410 Kbar, T = 327 to 3400 K.

of chemical reactions caused by instability of the phase. By studying the fit of the calculated Hugoniots of Xe, N_2, O_2, CO_2, CH_4 and CO, ROSS and REE (1980) concluded that N_2, CH_4 and CO may thermally decompose above pressures of 300, 230 and 150 Kbar respectively. HAMMAN (1981) plotted the shock-velocity *vs.* density of water from many different sources to pressures of 1200 Kbar and found a distinct break in the slope around 170 Kbar. HAMMAN (1981) finds that between shock densities of 1.6 and 1.9 g cm^{-3} and at a temperature of 1000°C or more, water transforms from a virtually unionized state into one in which it is fully dissociated into hydrogen and hydroxyl ions. However, this conflicts with the data of MITCHELL and NELLIS (1982) who found no evidence of dissociation.

The shock-data for water used in this study are from RICE and WALSH (1957) and MITCHELL and NELLIS (1982). The data of RICE and WALSH (1957) are based on the assumption that the derivative $(\partial H/\partial V)_p$ which is equal to $C_p/(\partial V/\partial T)_p$ is independent of temperature and that C_p is independent of pressure above 25 Kbar. HAMMAN (1981) argued that these assumptions may have resulted in overestimation of shock temperatures that is indicated by the mismatching of the data with those of JŪZA (1966), COWPERTHWAITE and SHAW (1970) and BAKANOVA *et al.* (1975). From a comparison of the results of the latter two with those of RICE and WALSH (1957), we corrected the temperatures in the data of RICE and WALSH (1957) before using them to determine Eqn. (14).

Discussion of CO_2

As emphasized earlier, the results of this study are not meant to replace the equations of state proposed by BOTTINGA and RICHET (1981), KERRICK and JACOBS (1981) and those proposed for water by KERRICK and JACOBS (1981), DELANY and HELGESON (1978) and HALBACH and CHATTERJEE (1982). BOTTINGA and RICHET's (1981) equation for CO_2 applies to the pressure range 1 bar to nearly 50 Kbar. The present work is aimed at computing fugacities in the pressure range of 5 Kbar to several hundred Kbar and this is achieved with one corresponding states equation for many different fluid species. Because our results are based on the shock-wave data on fluids not used by Bottinga and Richet, it is likely that the fugacity calculated by the two sets of equations in the overlapping pressure range (5 to 50 Kbar) may differ to some extent. As shown by ROSS and REE (1980), the very high pressure data on CO_2 is rather simply modeled with an exponential-6 potential function. To investigate the differences between predictions of the two equations of state, we have employed the following reactions from which

fugacity of CO_2 may be calculated from the experimental phase equilibrium data as discussed by HASELTON *et al.* (1977) and BOTTINGA and RICHET (1981):

$$MgCO_3 = MgO + CO_2 \quad (a)$$

$$MgCO_3 + SiO_2 = MgSiO_3 + CO_2 \quad (b)$$

$$MgCO_3 + MgSiO_3 = Mg_2SiO_4 + CO_2 \quad (c)$$

$$CaCO_3 + SiO_2 = CaSiO_3 + CO_2 \quad (d)$$

$$MgCO_3 + TiO_2 = MgTiO_3 + CO_2. \quad (e)$$

The thermochemical data used in calculating $RT\ln f$ for CO_2 are listed in Table 2. GORDON and GREENWOOD (1970) found that the thermochemical data on magnesite, periclase and CO_2 (similar to those in ROBIE *et al.*, 1978) are compatible with HARKER and TUTTLE's (1955) experimental phase equilibrium data on reaction (a) at 1 bar in the temperature range of 800 to 1200 K. Using the 1 bar phase equilibrium data, we have calculated ΔH^0_{298} and ΔS^0_{298} for magnesite which are -1105580 (± 4000) J/mol and 70.77 (± 4.5) J/mol/K, respectively. Calculated $RT\ln f$ for CO_2 using data in Table 2 are listed in columns 4 and 5 of Table 3. Note that using ΔG^0_f of magnesite from ROBIE *et al.* (1978) or from the new data set is not critical to evaluation of the equations of state of CO_2.

The difference between the 'experimental' $RT\ln f$ of CO_2 and the calculated values are listed in the last two columns in Table 3. Even the largest of these errors should be considered as within the combined errors due to a) errors in thermochemical data for the solids, b) experimental errors (see HASELTON *et al.*, 1978) and c) the statistical errors from the equation of state (Eqn. 11). Table 3 shows that for the reactions (a), (b) and (c), the errors in ΔG^0_f for CO_2 calculated in this study vary systematically with P and T (except at 5 Kbar). However, these errors are rather small as may be shown by calculating the error in equilibrium P which, for example for reaction (a) at 1800 K and 22 Kbar, is less than 1.5 Kbar. Similarly, the largest of errors resulting from the use of Bottinga and Richet's data, *e.g.* for reaction (b) at 1800 K and 43.3 Kbar, is about 4 Kbar.

Table 2. Thermodynamic data

Phases	V_o cm^3/mol	a_0 10^4	a_1 10^8	a_2	K_o Mb	K_o'
$CaSiO_3$	40.08	0.1391	2.5440	0.1282	1.00	4.00
MgO*	11.25	0.3681	0.9283	-0.7445	1.60	4.56
$Mg_{.5}SiO_2$*	21.84	0.3052	0.8504	-0.5040	1.29	4.88
$MgSiO_3$*	31.27	0.1391	2.5440	0.1282	1.00	4.00
TiO_2**	18.82	0.2072	0.9750	-0.0931	2.15	6.91
$MgCO_3$**	28.02	0.0000	5.6580	0.0000	1.10	4.00
$CaCO_3$**	36.93	0.0000	5.5440	0.0000	0.72	4.00
$MgTiO_3$	30.86	0.1391	2.5440	0.1282	1.00	4.00
SiO_2(Qz)*	22.69	0.3100	2.6780	0.0000	0.37	6.40
SiO_2(Coe)*	20.64	0.0543	0.8315	-0.0605	0.96	8.40

Phases	ΔH^o_{298} KJ/mol	ΔS^o_{298} J/molK	$C_p = a + bT + cT^{-2} + dT^2 + fT^{-1/2}$ (J/molK) a	$b(10^{-3})$	$c(10^5)$	$d(10^{-6})$	$f(10^2)$
CO_2	- 393.51	213.79	87.82	- 2.644	7.064	0	- 9.989
$CaSiO_3$	-1628.65	87.45	107.10	17.480	-22.965	0	0
MgO	- 601.49	26.94	65.21	- 1.270	- 4.619	0	- 3.872
$Mg_{.5}SiO_2$	-1087.18	47.06	113.99	1.707	- 4.470	0	- 8.723
$MgSiO_3$***	-1546.29	66.27	188.76	- 5.332	0.004	0	-18.129
TiO_2	- 944.75	50.29	63.08	11.307	- 9.862	0	- 5.616
$MgCO_3$	-1105.58	70.77	81.12	52.254	-18.320	0	0
$CaCO_3$	-1207.37	91.71	99.72	26.920	-21.576	0	0
$MgTiO_3$	-1572.77	74.56	61.64	37.673	-43.444	- 3.588	11.759
SiO_2(Qz)	- 910.70	41.46	44.60	37.754	-10.018	0	0
SiO_2(Coe)*	- 907.77	38.73	233.06	-77.765	26.036	19.24	-33.753

NOTE: $a(T) = a_0 + a_1T + a_2T^{-2}$

$V = V_o\exp[\int_{298}^{P}a(T)dT][1 + K_o'P/K_o]^{-1/K_o'}$

* See Fei and Saxena (1986). ** Data from Carmichael (1982).
*** Entropy and heat capacity from Haselton (1979) and enthalpy from Brousse et al. (1984). All other data from Robie et al. (1978).

Table 3. Comparison of RTlnf(P,T) for CO_2 derived from experimental equilibrium data with that calculated from equations of state.

T K	P Kbar	RTlnf(P,T) J/mol Exp.	This Work	B & R	D1	D2
Reaction: $MgCO_3 = MgO + CO_2$						
1298	5.0	108650	106474	106500	2176	2150
1278	7.0	109170	114298	114400	-5128	-5230
1373	10.0	128423	133478	135400	-5055	-6977
1600	16.3	172143	173049	178400	- 906	-6257
1700	19.2	191286	190222	197600	1064	-6314
1800	22.0	210049	206829	216300	3220	-6251
Reaction: $MgCO_3 + MgSiO_3 = Mg_2SiO_4 + CO_2$						
1200	16.1	137162	139804	142900	-2642	-5738
1300	20.6	159247	161349	166600	-2100	-7353
1400	25.2	181343	182614	190300	-1271	-8957
1500	29.8	203310	203461	213600	- 151	-10290
1600	34.3	225008	223731	236600	1277	-11590
1700	38.8	246618	243760	259400	2858	-12782
1800	43.3	268160	263590	282200	4570	-14040
Reaction: $MgCO_3 + SiO_2 = MgSiO_3 + CO_2$						
1400	35.5	216973	209689	220500	7284	-3527
1500	43.8	246577	238936	253500	7641	-6923
Reaction: $MgCO_3 + TiO_2 = MgSiO_3 + CO_2$						
1200	12.4	132065	133807	130400	-1742	1665
1300	16.7	154523	156799	153800	-2276	723
1400	21.0	176839	179723	177000	-2884	- 161
1500	25.3	199016	202616	199800	-3600	- 784
1600	29.6	221057	225478	222300	-4421	-1243
1700	33.8	242940	248150	244700	-5210	-1760
Reaction: $CaCO_3 + SiO_2 = CaSiO_3 + CO_2$						
1200	7.6	111878	110841	110800	1037	1078
1300	10.6	132907	129931	131300	2976	1607
1400	13.6	153876	148171	151100	5705	2776
1500	16.6	174801	165887	170600	8914	4201
1600	19.5	195496	182940	189900	12556	5596
1700	22.4	216383	199746	209100	16637	7283

B & R = Bottinga and Richet (1981). D1 and D2 are the differences in RTlnf(P,T) between the experimental and this work and between the experimental and the data of Bottinga and Richet, respectively.

For reactions (d) and (e), the calculated $RT \ln f$ data for CO_2 show negative and positive deviations, respectively. Since the pressure and temperature ranges of the two reactions overlap, the errors are probably largely due to errors in the thermochemical data of phases other than CO_2.

On the basis of the available data, our equations estimate ΔG_f^0 of CO_2 in the pressure range of 5 to 50 Kbar with an accuracy comparable to those of BOTTINGA and RICHET (1981).

Acknowledgements—Our thanks are due to Marvin Ross of the Lawrence Livermore Laboratory for several useful discussions. The manuscript style was greatly improved by suggestions from John Ferry. The research has been supported by a NSF grant (EAR #8415800) and by a PSC-BHE grant (#6-65191) from the City University of New York.

Editorial handling: J. M. Ferry

REFERENCES

BAKANOVA A. A., ZUBAREV V. N., SUTULOV YU. N. and TRUNIN R. F. (1975) Thermodynamic properties of water at high pressures and temperatures. *Sov. Phys. JETP* 41, 544–548.

BOTTINGA Y. and RICHET P. (1981) High pressure and temperature equation of state and calculation of the thermodynamic properties. *Amer. J. Sci.* 281, 620–659.

BROUSSE C., NEWTON R. C. and KLEPPA O. J. (1984) Enthalpy of formation of forsterite, enstatite, akermanite, monticellite and merwinite at 1073 K determined by alkali borate solution calorimetry. *Geochim. Cosmochim. Acta* 48, 1081–1088.

BURNHAM C. W., HOLLOWAY J. R. and DAVIS N. F. (1969) Thermodynamic properties of water to 1000°C and 10.000 bars. *Geol. Soc. Amer. Spec. Pap. 132*, 96 p.

CARNAHAN N. F. and STARLING K. E. (1972) Intermolecular repulsions and the equation of state for fluids. *Amer. Inst. Chem. Eng.* 18, 1184–1189.

CARMICHAEL R. S. (1982) *Handbook of Physical Properties of Rocks*. CRC Press. 138 p.

COWPERTHWAITE M. and SHAW R. (1970) $C_v(T)$ equation of state for liquids: Calculation of shock temperature of carbon tetrachloride, nitromethane, and water in the 100 Kbar region. *J. Chem. Phys.* 53, 555–560.

DELANY J. M. and HELGESON H. C. (1978) Calculation of the thermodynamic consequences of dehydration in subducting oceanic crust to 100 kb and >800°C. *Amer. J. Sci.* 278, 638–686.

FEI Y. and SAXENA S. K. (1986) A thermochemical data base for phase equilibria in the system Fe-Mg-Si-O at high pressure and temperature. *Phys. Chem. Minerals* 13, 311–324.

GORDON T. M. and GREENWOOD H. J. (1970) The reaction: dolomite + quartz + water = talc + calcite + carbon dioxide. *Amer. J. Sci.* 268, 225–242.

HALBACH H. and CHATTERJEE N. D. (1982) An empirical

Redlich-Kwong type equation of state for water to 1000°C and 200 Kbar. *Contrib. Mineral. Petrol.* 79, 337–345.

HAMANN S. D. (1981) Properties of electrolyte solutions at high pressures and temperatures. In *Physics and Chemistry of the Earth* (eds. D. T. RICKARD and F. E. WICKMAN), Vol. 13, pp. 89–112. Oxford.

HARKER R. I. and TUTTLE O. F. (1955) Studies in the system CaO-MgO-CO_2. Pt. 1. The thermal dissociation of calcite, dolomite and magnesite. *Amer. J. Sci.* 253, 209–224.

HASELTON H. T. JR. (1979) Calorimetry of synthetic pyrope-grossular garnets and calculated stability relations. Ph.D. Dissertation, Univ. of Chicago.

HASELTON H. T. JR., SHARP W. E. and NEWTON R. C. (1977) Decarbonation reactions and derived CO_2 fugacities at high pressures and temperatures. *EOS* 58, 1242.

HASELTON H. T. JR., SHARP W. E. and NEWTON R. C. (1978) CO_2 fugacity at high temperatures and pressures from experimental decarbonation reactions. *Geophys. Res. Lett.* 5, 753–756.

HELGESON H. C. and KIRKHAM D. H. (1974) Theoretical prediction of the thermodynamic behavior of aqueous electrolytes at high pressures and temperatures: 1. Summary of the thermodynamic/electrostatic properties of the solvent. *Amer. J. Sci.* 274, 1089–1198.

HILBERT R. (1979) *PVT-Daten von Wasser und von Wassrigen Natriumchlorid-Loungen bis 873 K, 4.000 bar und 25 Gewichts-prozent NaCl.* Hochschulverlag. 212 p.

HOLLOWAY J. R. (1977) Fugacity and activity of molecular species in super-critical fluids. In *Thermodynamics in Geology* (ed. D. G. FRASER), pp. 161–181. Dordrecht-Holland.

JOZA J. (1961) An equation of state for water and steam, steam tables in the critical region and in the range 1.000 to 100.000 bars. *Rozpravy Csekoslovenske Akademia VED Rada Technikych VED Prag.* 76, 3–121.

JOZA J. (1966) An equation of state for water and steam. *Rozpravy Csekoslovenske Akademia VED Rada Technikych ved rocnik 76, sesik* 1: Praha Academia, pp. 142.

KERRICK D. M. and JACOBS G. K. (1981) A modified Redlich-Kwong equation for H_2O, CO_2 and H_2O-CO_2 mixtures at elevated pressures and temperatures. *Amer. J. Sci.* 281, 735–767.

KHODAKOVSKY I. L., DOROFEYEVA V. A., MELNIKOVA G. L., GERANIN A. V. and RYZHENKO B. N. (1982) Thermodynamic parameters of liquid water at 0–300 C and pressures up to 10.000 bar. *Geokhimiya* 2, 208–220.

MEL'NIK YU. P. (1972) Thermodynamic parameters of compressed gases and metamorphic reactions involving water and carbon dioxide. *Geokhimiya* 6, 654–662.

MITCHELL A. C. and NELLIS W. J. (1982) Equation of state and electrical conductivity of water and ammonia shocked to the 100 GPa (1 Mbar) pressure range. *J. Chem. Phys.* 76, 6273–6281.

NELLIS W. J. (1984) Shocked fluids at high densities and temperatures. In *Shock Waves in Condensed Matter—1983* (eds. J. R. ESAY, R. A. GRAHAM and G. K. STRAUB), pp. 31–40. Elsevier.

NELLIS W. J. and MITCHELL A. C. (1980) Shock compression of liquid argon, nitrogen, and oxygen to 90 GPa (900 Kbar). *J. Chem. Phys.* 73, 6137–6145.

NELLIS W. J., HOLMES N. C., MITCHELL A. C., TRAINOR R. J., GOVERNO G. K., ROSS M. and YOUNG D. A. (1984) Shock compression of liquid helium to 56 GPa (560 Kbar). *Phys. Rev. Lett.* 53, 1248–1250.

REDLICH O. and KWONG J. N. S. (1949) On the thermodynamics of solutions. *Chem. Rev.* 44, 233–244.

RICE M. H. and WALSH J. M. (1957) Equation of state of water to 250 kilobars. *J. Chem. Phys.* 26, 824–830.

ROBERTSON S. L. and BABB S. E. JR. (1970) Isotherms of carbon monoxide to 10 kbar and 300 C. *J. Chem. Phys.* 53, 1094–1097.

ROBIE R. A., HEMINGWAY B. S. and FISHER J. R. (1978) Thermodynamic properties of minerals and related substances at 298.15 K and 1 bar (10^5 pascals) pressure and at high temperatures. *U.S. Geol. Surv. Bull. 1452.*

ROSS M. (1979) A high-density fluid-perturbation theory based on an inverse 12th-power hard-sphere reference system. *J. Chem. Phys.* 71, 1567–1571.

ROSS M. and REE F. H. (1980) Repulsive forces of simple molecules and mixtures at high density and temperature. *J. Chem. Phys.* 73, 6146–6152.

RYZHENKO B. N. and VOLKOV V. P. (1971) Fugacity coefficients of some gases in a broad range of temperatures and pressures. *Geokhimiya* 7, 760–773.

SCHMIDT E. (1979) *Properties of Water and Steam in SI-units.* Springer-Verlag. 190 p.

STACEY F. D. (1977) *Physics of the Earth.* John Wiley, New York. 414 p.

TANISHITA I., WATANABE K., KIJIMA J., ISHII H., OGUCHI K. and UEMATSU M. (1976) Experimental study of the p, V, T properties of water for temperatures in the range 323.15 to 773.15 K and pressures up to 200 M. Pa. *J. Chem. Thermodynamics* 8, 1–20.

TODHEIDE K. (1972) Water at high temperatures and pressures. In *Water* (ed. F. FRANKS), Vol. 1, pp. 463–514. Plenum Press.

TOURÉT J. and BOTTINGA Y. (1979) Equation d'etat pour le CO_2: application aux inclusions carboniques. *Bull. Minéral.* 102, 577–583.

Geochimica et Cosmochimica Acta Vol. 52, pp. 1195–1196

0016-7037/88/$3.00 + .00

The pressure-volume-temperature equation of hydrogen

S. K. SAXENA and Y. FEI
Department of Geology, Brooklyn College, Brooklyn, NY 11210, U.S.A.

(*Received October* 21, 1987; *accepted in revised form February* 11, 1988)

Abstract—Since hydrogen has a substantially different interatomic potential from that of the other gases in the C-H-O system, a corresponding states equation is not appropriate for representing its pressure-volume-temperature behavior. An independent polynomial in pressure and temperature for hydrogen is proposed, which is useful over a wide pressure and temperature range.

INTRODUCTION

THE DATA ON fugacity of hydrogen in a fluid mixture are important to geochemists in considering natural oxidation reactions and monitoring conditions in phase equilibrium experiments. The experimental data on the pressure-volume-temperature (P-V-T) relationship for hydrogen at high pressure and temperature are rather limited. This short paper is an attempt to use the available data on hydrogen to a maximum advantage by combining the low P-V-T data with those obtained from shock wave measurements. The note also improves the equations for hydrogen as proposed by us on the basis of corresponding states theory (SAXENA and FEI, 1987a,b).

There are several important data and equations of state for solid hydrogen at low temperatures and very high pressures (*e.g.*, SHIMIZU *et al.*, 1981, and VAN STRAATEN *et al.*, 1982). These data are not considered here; while the data cover a useful range of P-T for the outer planets (*e.g.* Jupiter), the region is inaccessible geologically. Their inclusion will require a more complex form of the equation than we propose to use for the high P-T data.

Recently SAXENA and FEI (1987a,b) proposed an equation of state using reduced pressure and temperature as variables for a number of gases (H_2, O_2, CO, CH_4, N_2 and CO_2). ROSS and REE (1980) in modeling the interatomic potentials of these gases from shock wave experiments demonstrated in accordance with theory that the interatomic potential of H_2 was different from that of the remaining gases. The similarity of the potential permits the use of corresponding states theory for modeling O_2, CO, CH_4, N_2 and CO_2. SAXENA and FEI (1987a,b) included hydrogen in the model because of the importance of this species and because of the limited P-V-T data on hydrogen. It was considered that the P-V-T behavior of hydrogen, albeit with some larger errors, could be modeled with support from the data on other fluids. At present there are two such equations available for hydrogen, the first based on data on the fluids at low pressures (<10 kbar, SAXENA and FEI, 1987a) and the second based on all of those data and the shock wave data (SAXENA and FEI, 1987b). We recently noted that the first equation is useful only to a pressure of about 4 kbar and the second only above 6 kbar. However, in view of the difference in interatomic potential of hydrogen from that of the other species, it may be preferable to separate hydrogen from the rest. Unfortunately the experimental P-V-T data on hydrogen are few and an independent equation of state for hydrogen must be used with caution.

METHOD OF CALCULATION

The data on hydrogen (all data as used by RYZHENKO and VOLKOV, 1971, SHAW and WONES, 1964, and the experimental data of PRESNALL, 1969, and the shock wave data as discussed by ROSS and REE, 1980, and ROSS *et al.*, 1983) were processed with nonlinear programming technique as used by JAMES and ROOS (1975). The following equation relating the compressibility parameter $Z(PV/RT)$ with P and T was adopted (see discussion in SAXENA and FEI, 1987b):

$$Z = a + bP_r + cP_r^2 + dP_r^3$$

where the coefficients are given by

$$a = a_0 + a_1T_r^{-1} + a_2T_r^{-2} + a_3 \ln T_r$$

and similarly for the other coefficients b, c and d. P_r and T_r represent, respectively, reduced pressure (P/P_c, P_c = 13) and reduced temperature (T/T_c, T_c = 33.1). Although the reduced variables are not necessary, we have retained them for computational convenience to match with the other equations presented previously (SAXENA and FEI, 1987a,b).

RESULTS AND DISCUSSION

The coefficients in the P-V-T equation for hydrogen as determined through the minimization technique are:

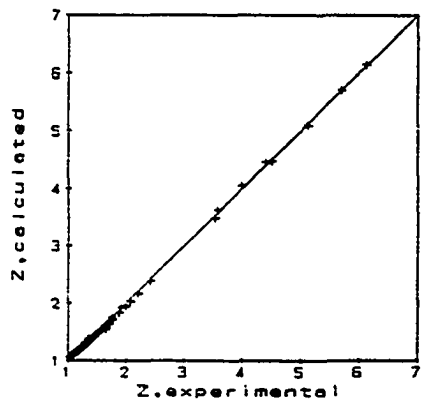

FIG. 1. A plot of the compressibility factor Z as calculated from the proposed equation *vs.* the experimentally determined Z.

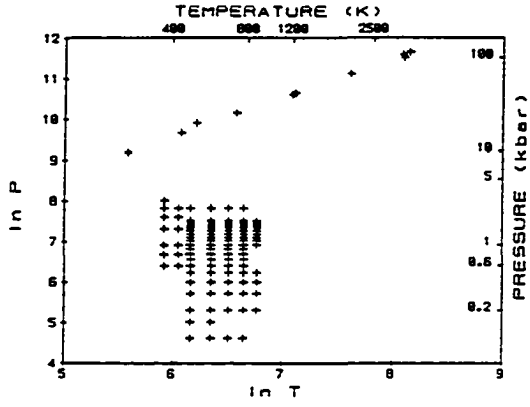

FIG. 2. A plot of P *vs.* T on a logarithmic scale to show the range of experimental data used in the formulation of the equation for hydrogen. The data are the same as used previously by RYZHENKO and VOLKOV (1971) and SHAW and WONES (1964). In addition the data of PRESNALL (1969) are included. The shock wave data are from ROSS and REE (1980).

i	0	1	2	3
a_i	1.6688	−2.0759	−9.6173	−0.1694
b_i	−2.0410E-3	7.9230E-2	5.4295E-2	4.0887E-4
c_i	−2.1693E-7	1.7406E-6	−2.1885E-4	5.0897E-β8
d_i	−7.1635E-12	1.6197E-10	−4.8181E-9	0.0000

The standard deviation for the fit is 0.0253.

Figure 1 shows a comparison of the observed Z with the Z calculated from the equation. Figure 2 shows the pressure and temperature range of the data used in formulating the equation. The equation should be most reliable within the P-T range of the data as shown in the figure. The equation on P-V-T for hydrogen may be used with the other equations on H_2O, CO_2, CH_4, CO and O_2 discussed in SAXENA and FEI (1987a,b) for calculating fugacities of species in the C-H-O system.

Acknowledgements—We thank Dr. H. K. Mao for a thoughtful review. The work was supported by grants from NSF (EAR#8516476) and PSC-BHE CUNY (6-67211).

Editorial handling: D. M. Shaw

REFERENCES

JAMES F. and ROOS M. (1975) Minuit: a system for function minimization. *Computer Physics Comm.* **10**, 343–367.

PRESNALL D. C. (1969) Pressure-volume-temperature measurements on hydrogen from 200° to 600° and up to 1800 atmosphere. *J. Geophys. Res.* **74**, 6026–6033.

ROSS M. and REE F. H. (1980) Repulsive forces of simple molecules and mixtures at high density and temperature. *J. Chem. Phys.* **73**, 6146–6152.

ROSS M., REE F. H. and YOUNG D. A. (1983) The equation of state of molecular hydrogen at very high density. *J. Chem. Phys.* **79**, 1487–1494.

RYZHENKO B. N. and VOLKOV V. P. (1971) Fugacity coefficients of some gases in a broad range of temperatures and pressures. *Geokhimiya* **7**, 760–773.

SAXENA S. K. and FEI Y. (1987a) Fluids at crustal pressures and temperatures. I. Pure species. *Contrib. Mineral. Petrol.* **95**, 370–375.

SAXENA S. K. and FEI Y. (1987b) High pressure and high temperature fluid fugacities. *Geochim. Cosmochim. Acta* **51**, 783–791.

SHAW H. R. and WONES D. R. (1964) Fugacity coefficients for hydrogen gas between 0 and 1000 C for pressures to 3000 atm. *Amer. J. Sci.* **262**, 918–929.

SHIMIZU H., BRODY E. M., MAO H. K. and BELL P. M. (1981) Brillouin measurements of solid n-H_2 and n-D_2 to 200 kbar at room temperature. *Phys. Rev. Lett.* **47**, 128–131.

STRAATEN J. VAN, WIJNGAARDEN R. J. and SILVERA I. F. (1982) Low-temperature equation of state of molecular hydrogen and deuterium to 0.37 Mbar: implications for metallic hydrogen. *Phys. Rev. Lett.* **48**, 97–100.

Geochimica et Cosmochimica Acta Vol. 52, pp. 505–512
© Pergamon Journals Ltd. 1988. Printed in U.S.A.

0016-7037/88/$3.00 + .00

Fluid mixtures in the C-H-O system at high pressure and temperature

S. K. SAXENA and Y. FEI

Department of Geology, Brooklyn College, Brooklyn, NY 11210, U.S.A. and Department of Earth and Environmental Sciences, Graduate School, CUNY, New York, NY 10036, U.S.A.

(*Received May* 15, 1987; *accepted in revised form November* 23, 1987)

Abstract—Interaction energy parameters (W_{ij}) for polar-polar and polar-nonpolar mixtures of gases (H_2, O_2, CO_2, H_2O, CO and CH_4) have been calculated using the Kihara and Stockmayer potentials, respectively. Using the mixing rules of averaging for dimensional properties and of geometric mean for potential parameters, W_{ij} data are calculated for binary mixtures. The interaction parameters are used with the van Laar solution model and are found to reproduce the experimental binary mixing data well. The mixing model has been tested against experimental phase equilibrium data on solid-fluid reactions. Examples of some applications in the systems Mg-Si-O-H, Fe-O and C-H-O are presented.

INTRODUCTION

MULTICOMPONENT FLUIDS in the system C-H-O are important constituents of the Earth's crust and possibly of the upper mantle. KERRICK and JACOBS (1981) used a hard sphere modified Redlich-Kwong equation (HSMRK) for modeling the pressure-volume-temperature relations for the pure species CO_2 and H_2O and used empirical rules for combining the HSMRK coefficients to calculate fluid fugacities of species in mixtures. KERRICK and JACOBS (1981) model successfully reproduce most of the experimental *P-V-T* data on mixtures of H_2O-CO_2 (*e.g.* CHOU and WILLIAMS, 1979; EGGLER and BURNHAM, 1978; EGGLER and KADIK, 1979; FRANCK and TODHEIDE, 1959; GEHRIG *et al.*, 1979; GREENWOOD, 1973; JACOBS and KERRICK, 1981; ZIEGENBEIN and JOHANNES, 1974; SHMULOVICH *et al.*, 1982).

HALBACH and CHATTERJEE (1982) considered some additional data for water and proposed a different modification of the Redlich-Kwong model. Their equation is applicable over a range of pressure and temperature which is broader than the range covered by the Kerrick-Jacobs equation. For CO_2, the Redlich-Kwong model was similarly modified by BOTTINGA and RICHET (1981). In order to use the mixing rules as proposed by KERRICK and JACOBS (1981), the functional dependence of the coefficients of the Redlich-Kwong equation of state for all species must be the same. In this regard, the Halbach-Chatterjee and Bottinga-Richet equations are not compatible. A further complication is added if the *P-V-T* relation of one or more of the pure species (*e.g.* CO, CH_4, H_2 and O_2) has been modeled using a non-Redlich-Kwong formulation. Virial equations of state have been used commonly in chemical literature. Recently, Ross and others (*e.g.* ROSS, 1979; ROSS and REE, 1980) have used corresponding states formulation for several gases. For computational convenience, SAXENA and FEI (1987) found it desirable to use equations of state which are explicit in pressure and not in volume.

Although KERRICK and JACOBS' (1981) mixing model is quite successful in reproducing the existing experimental data, the mixing rules are empirical and it is necessary to use the coefficients for the pure species. This study is based on an entirely different approach to modeling the mixing properties. In this approach, it is not required to use the same coefficients as have been used in modeling the *P-V-T* relations of the pure species. Success of such an approach could permit one to select and combine the best available equations for the pure species including those discussed by HELGESON (1981) for water.

MIXING MODEL

Selection of pure potentials

GUGGENHEIM (1952) defined the regular solution energy parameter W_{12} as the energy of the mixing reaction of a 1-1 pair with a 2-2 pair as:

$$W_{12} = z[\Gamma_{12} - \tfrac{1}{2}(\Gamma_{11} + \Gamma_{22})] \quad (1)$$

where Γ_{11}, Γ_{22} and Γ_{12} are comparable to the intermolecular potentials respectively for a 1-1, 2-2 and 1-2 pairs, z is the coordination number (PRAUSNITZ *et al.*, 1986, p. 295). For a simple nonpolar molecule, GUGGENHEIM (1952) suggested that Γ_{ij} may be calculated from:

$$\Gamma_{ij} = 4\epsilon[(\sigma/r)^{12} - (\sigma/r)^{6}] \quad (2)$$

where σ is the distance at which the repulsive and attractive terms in the energy just cancel each other, ϵ is characteristic energy and r is length scale which may be related to characteristic volume (V) by $(4/3)\Pi r^3 = V/N_A$, where N_A is Avogadro's number. GUGGENHEIM (1952) has given examples of calculation of the second virial coefficient from Eqn. (2) and an excellent fit is obtained by Lennard-Jones and by Keesom potentials (quoted in GUGGENHEIM, 1952, pp. 161–163, Fig. 8.3) for several nonpolar gases.

In Eqn. (2) we have used the Lennard-Jones' (LJ) potential, which is one of the most used two-parameter potentials for small nonpolar molecules. The LJ potential model permits interpenetration of two molecules completely, provided that they have enough energy. The molecules consist of point centers surrounded by "soft" electron clouds. Kihara (see PRAUSNITZ *et al.*, 1986) proposed a model in which the point center is replaced by impenetrable (hard) core. According to such a model:

$$\Gamma = 4\epsilon\{[(\sigma - 2a)/(r - 2a)]^{12} - [(\sigma - 2a)/(r - 2a)]^{6}\} \quad \text{for } r > 2a \quad (3)$$

where a ($=a^*\sigma/(2 + 2a^*)$) is the radius of the spherical molecular core. Since it is a three-parameter function, Kihara's potential is quite successful in fitting thermodynamic data for a large number of nonpolar fluids. PRAUSNITZ *et al.* (1986) have discussed specific cases in which the LJ potential succeeded only partly while the Kihara potential succeeded totally.

For polar molecules, such as water, the potential energy is a function not only of intermolecular separation but also of relative orientation. For such potentials, Stockmayer potential model (see PRAUSNITZ *et al.*, 1986) has been rather successful. This potential is:

$$\Gamma = 4\epsilon[(\sigma/r)^{12} - (\sigma/r)^{6}] - \mu^2/r^3\zeta_4(\theta_1, \theta_2, \theta_3). \quad (4)$$

The collision diameter σ is the intermolecular distance where the potential energy due to forces other than dipole-dipole forces becomes equal to zero. The last term in Eqn. (4) is characteristic of a dipole-dipole interaction with μ as the dipole moment and ζ_θ a known function of the angles θ_1, θ_2 and θ_3 which determine the relative orientation of the two dipoles. As discussed by PRAUSNITZ *et al.* (1986), with rising temperatures, the orientations become random and at moderate to high temperatures, the last term in Eqn. (4) becomes $-\frac{2}{3}\mu_i^2\mu_j^2/(r^6kT)$ where k is Boltzmann's constant and T is absolute temperature. According to TIEN and LIENHARD (1971, p. 264), Keesom's model of a rigid spherical molecule containing a dipole is

$$f(r, \theta_1, \theta_2, \phi_2 - \phi_1) = -\mu^2/r^3 b(\theta_1, \theta_2, \phi_2 - \phi_1) \quad (5)$$

where θ and ϕ refer to the four angles defining the relative orientations of the two dipoles (see PRAUSNITZ *et al.*, 1986, p. 51 for an illustration) and b is a factor is given by

$$b = 2\cos\theta_1\cos\theta_2 - \sin\theta_1\sin\theta_2\cos(\phi_2 - \phi_1). \quad (6)$$

Stockmayer (in TIEN and LIENHARD, 1971) improved upon it by combining it with the relatively short range Lennard-Jones potentials as follows:

$$\Gamma = 4\epsilon[(\sigma/r)^{12} - (\sigma/r)^6] - \mu^2/r^3. \quad (7)$$

The second term was found by averaging $\mu^2 b/r^3$. Note, however, that PRAUSNITZ *et al.* (1986) have preferred to combine with the Γ term in its explicit form.

In this work the only polar species are water and CO. The latter has a very small dipole moment and it has been ignored. For water, there is no significant difference if we use either Eqn. (4) or Eqn. (7) to calculate Γ. In addition to dipole moments, certain molecules may show multipoles. CO_2 which has no dipole moment does have a significant quadrupole moment. Such effects have not been taken into account in this study.

PRAUSNITZ (pers. commun., 1987) pointed out two other possible problems in using the model being proposed here. The Stockmayer potential is not valid at small r because the dipole-dipole term corresponds to an r that is large relative to the charge separation of the dipole. For mixing of H_2O-CO_2, this is not a problem at low pressures but if the data are to be used at very high pressures, corresponding to the Earth's mantle, we do not know how the potential will be affected. A second problem concerns the mixing of unequal size molecules. GUGGENHEIM's (1952) interchange energy parameter is strictly valid to mixtures with components of the same size. If the unlike molecules differ significantly in size or shape, the molecular arrangement in the mixture may be significantly different from that for the pure liquids. This would give rise to a nonideal entropy of mixing. In the simple model being used here, the excess entropy of mixing contribution cannot be included. We shall take note of this weakness in the model when comparing the observed and calculated solution properties.

Mixing rules

The mixing rules used, in this study, have little theoretical basis but have proven very useful for many binary mixtures as discussed in several books (*e.g.* GUGGENHEIM, 1952; TIEN and LIENHARD, 1971; PRAUSNITZ *et al.*, 1986). The mixing rules are:

$$r_{12} = \tfrac{1}{2}(r_{11} + r_{22}) \quad (8)$$

$$\sigma_{12} = \tfrac{1}{2}(\sigma_{11} + \sigma_{22}) \quad (9)$$

$$\epsilon_{12} = (\epsilon_{11}\epsilon_{22})^{1/2} \quad (10)$$

where the subscript 11, 22 and 12 denote, respectively, the 1-1, 2-2 and 1-2 pairs. The rules are most appropriate for mixtures with species of equal size. Similarly, the dimensionless dipole moment μ^* can be expressed as a geometric mean:

$$\mu^*_{12} = (\mu^*_{11}\mu^*_{22})^{1/2} \quad (11)$$

which when substituted in Eqns. (3) or (4) yield the potential for non-polar pairs and thereafter by substituting in (1), the solution interaction parameter W_{12}.

For a pair of polar (1)-nonpolar (2) molecules, as discussed by TIEN and LIENHARD (1971), we have:

$$\sigma_{12} = \tfrac{1}{2}(\sigma_{11} + \sigma_{22})\xi^{-1/6} \quad \text{and} \quad \epsilon_{12} = (\epsilon_{11}\epsilon_{22})^{1/2} \quad (12)$$

where

$$\xi = 1 + \tfrac{1}{4}\alpha^*_{22}\mu^{*2}_{11}(\epsilon_{11}/\epsilon_{22})^{1/2} \quad (13)$$

and where, in turn:

$$\mu^*_{11} = \mu_{11}/(\epsilon_{11}\sigma^3_{11})^{1/2} \quad (14)$$

and α^*_{22} is the polarizability (α) of the nonpolar molecule divided by σ^3.

Solution model

Once the basic interaction energy parameter W_{12} is calculated, a solution models available, *e.g.* quasi-chemical, Wilson, NRTL, UNI- of a solution, such as activity of a component. We have many binary solution models available, e.g. quasi-chemical, Wilson, NRTL, UNIQUAC (see ACREE, 1984; PRAUSNITZ *et al.*, 1986). After extensive exploration of the various models, we found that a simple modification of the van Laar equation, yields a good reproduction of the experimental mixing data on H_2O and CO_2. According to the van Laar equation, which is simplified Wohl's equation in which three and higher body interactions have been neglected, the excess free energy of mixing G^{ex} is given by:

$$G^{ex} = RT(2a_{12}X_1X_2q_1q_2)/(X_1q_1 + X_2q_2) \quad (15)$$

where $2a_{12}$ is equal to W_{12} and q_1 and q_2 are effective volumes, or cross sections of the molecules: q_i is a measure of the "sphere of influence" of molecule i in the solution and X_i is the mole fraction of the molecule i. In calculating W_{12} (Eqn. 1), we use the empirically established value of 10 for the coordination number (PRAUSNITZ *et al.*, 1986, p. 294). First principle calculation of q is not available. Empirically, it has been established (see PRAUSNITZ *et al.*, 1986) that for nonpolar molecules of similar shape, the ratio of the q's is the same as the ratio of the pure-component fluid molar volumes. Although water is polar, we assumed that the W_{12} as estimated for a polar-nonpolar pair will take care of this effect. For the activity-coefficients (γ), we have:

$$\ln\gamma_1 = q_1W_{12}/(1 + q_1X_1/q_2X_2)^2 \quad (16)$$

and

$$\ln\gamma_2 = q_2W_{12}/(1 - q_2X_2/q_1X_1)^2. \quad (17)$$

In the model of this study we have adopted:

$$q_1/q_2 = V_1/V_2 \quad (18)$$

and

$$q_1 + q_2 = 1 \quad (19)$$

where V_1 and V_2 are, respectively, molar volumes of molecules 1 and 2.

The model involves one empirical parameter ($q_1 + q_2$) (not counting the mixing rules and q_1/q_2, which have been widely used in chemical applications) and is very convenient for computation of component activities in both binary and multicomponent solution. The activity coefficient in a ternary solution (with components 1, 2 and 3) is given by:

$$\ln\gamma_1 = \frac{X_2^2A_{12}\left(\frac{A_{21}}{A_{12}}\right)^2 + X_3^2A_{13}\left(\frac{A_{31}}{A_{13}}\right)^2 + X_2X_3\frac{A_{21}A_{31}}{A_{12}A_{13}}\left(A_{12} + A_{13} - A_{32}\frac{A_{13}}{A_{31}}\right)}{\left(X_1 + X_2\frac{A_{21}}{A_{12}} + X_3\frac{A_{31}}{A_{13}}\right)^2}$$

where

$$A_{12} = q_1W_{12} \quad A_{21} = q_2W_{12}$$

$$A_{13} = q_1W_{13} \quad A_{31} = q_3W_{13}$$

$$A_{23} = q_2W_{23} \quad A_{32} = q_3W_{23}. \quad (20)$$

For γ_2, we may use Eqn. (20) by changing the subscripts 1 with 2, 2 with 3 and 3 with 1. Similarly, for γ_3 exchange 1 with 3, 2 with 1 and 3 with 2. A multicomponent model may be generated similarly

Table 1. Parameters for the interaction energy calculation

	a*	σ(Å)	ε/k(K)	μ*(Debye)	α(Å³)	References
1. H_2O	-	2.650	380.00	1.85	-	Tien & Lienhard (1971)
2. CO_2	0.615	3.760	424.16	-	2.65	Prausnitz et al.(1986)
3. CH_4	0.283	3.565	227.13	-	2.60	Prausnitz et al.(1986)
4. CO	-	3.760	100.20	0.10	1.95	Tien & Lienhard (1971)
5. O_2	0.308	3.109	194.30	-	1.60	Prausnitz et al.(1986)
6. H_2	-	2.960	36.70	-	0.79	Tien & Lienhard (1971)

or we may prefer to use the computationally convenient multicomponent Kohler formulation:

$$(RT\ln\gamma_i)_{12\ldots N} = \sum_j (X_i + X_j)(1 - f_i - f_j)(\Delta G_{ij}^{ex})^* - \sum_{jk} (X_j + X_k)(f_j + f_k)(\Delta G_{jk}^{ex})^* + \sum_j (f_i + f_j)(RT\ln\gamma_i)_{ij}^* \quad (i \neq j \neq k) \quad (21)$$

where f_i and f_j are weighted mole fractions using weighting factors based on the excess properties of the binary systems, X_i and X_j are the mole fractions in the multicomponent system and the binary functions are denoted by an asterisk.

RESULTS AND DISCUSSION

Fugacities

The data on the energy parameters used in calculating W_{ij} are listed in Table 1 and some of the computed values of W_{ij} for H_2O-CO_2 are shown in Fig. 1. The volumes of the pure compounds were determined from the P-V-T relationships discussed previously (SAXENA and FEI, 1987):

It is possible to use the Redlich-Kwong equations of KERRICK and JACOBS (1981) or of HALBACH and CHATTERJEE (1982) and BOTTINGA and RICHET (1981) instead of the equations proposed by SAXENA and FEI (1987). Since the volumes are functions of pressure and temperature, the W_{ij} are also functions of pressure and temperature. The W_{ij}'s for non-polar-non-polar mixing are negligible.

Figure 2 shows the activity-composition relation for CO_2-H_2O at 500°C and 2 kbar. The experimental data of SHMULOVICH *et al.* (1982) and the model generated curves are shown for comparison. Figure 3 shows the same relations at 400°C and 2 kbar. The experimental data do not match the computed activity-composition relations. SHMULOVICH *et al.* (1982) and KERRICK and JACOBS (1981), who used the Redlich-Kwong and the hard-sphere Redlich-Kwong models, respectively, also faced this problem. The experimental data in Fig. 3 seem to show that a symmetric model for the solution would fit better at low temperatures. This is contrary to the binary H_2O-CO_2 relationships at low temperatures as reviewed by BOWERS and HELGESON (1983). In Fig. 3, the model curve (dashed line) generated by KERRICK and JACOBS (1981) is shown for comparison. Figures 4 and 5 show activity-composition relations at 500 and 800°C, respectively. The Kerrick-Jacobs model yields comparable results. Figure 6 shows the activity-composition relation in CH_4-H_2O. These are closely similar to those of H_2O-CO_2.

Test of the models

It is important to show that the results can be used in reproducing experimental phase equilibrium relations in sys-

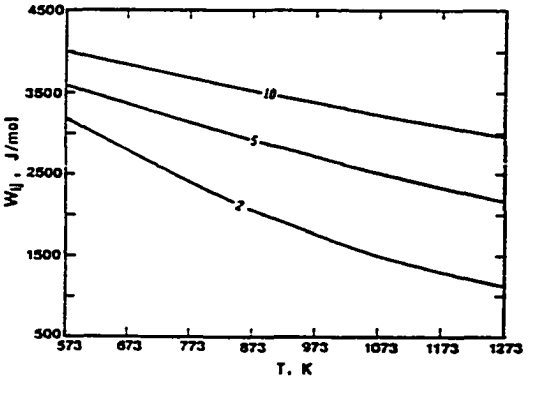

FIG. 1. The temperature dependence of the binary interaction parameter W_{ij} for CO_2-H_2. This parameter is used with the van Laar equation to calculate mixing properties of the binary fluids. See text for explanation.

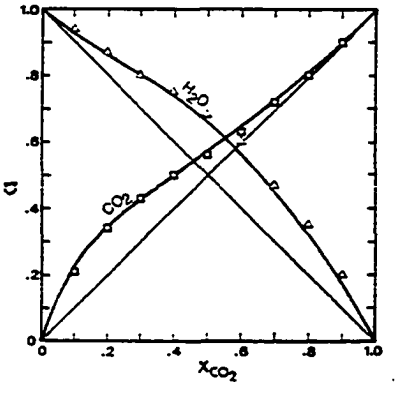

FIG. 2. Activity-composition relation in the binary H_2O-CO_2 fluid at 500°C and 2 kbar. The experimental data (open triangles for H_2 and squares for CO_2) are from SHMULOVICH *et al.* (1982). The solid curves are calculated with the van Laar model with W_{ij} as shown in Fig. 1.

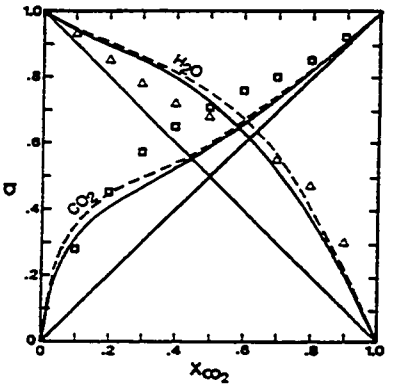

FIG. 3. Activity-composition relation in the binary H_2O-CO_2 fluid at 400°C and 2 kbar (solid curves). The fit of the calculated activities to the experimental data is poor. This misfit problem also occurs with the HSMRK model of KERRICK and JACOBS (1981) (dashed curves). See text for discussion.

tems involving multicomponent fluids. We have computed phase relations in systems that attest both to our models of pure species as discussed in Part 1, and of the mixtures. Thermochemical data used in the calculations are listed in Table 2. Calcite is considered as a solid solution of $CaCO_3$ and $MgCO_3$; the W_{ij} based on data from GOLDSMITH and NEWTON (1969) is:

$$W_{Ca\text{-}Mg} = 11175(\pm 278) + 11.67(\pm 0.41)T - 0.132(\pm 0.008)P \quad \text{(J/mol.)}.$$

For wustite solid solution, the components are FeO (1) and $FeO_{1.5}$ (2) with $W_{12} = -7229$ and $W_{21} = -2142$ (J/mol) (data from FEI and SAXENA, 1986).

Figure 7 shows the equilibrium pressures and temperatures for the reaction:

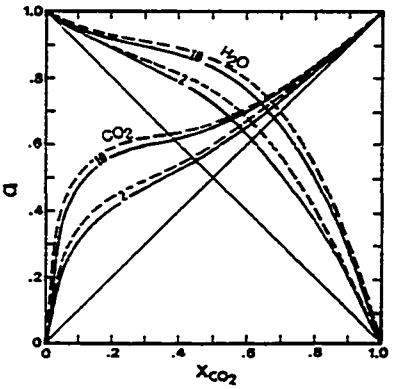

FIG. 4. Comparison of the activity-composition relations in the binary H_2O-CO_2 fluid at 500°C at pressures of 2 and 10 kbar calculated with the model of this work (solid line) and with the HSMRK model of KERRICK and JACOBS (1981) (dashed lines).

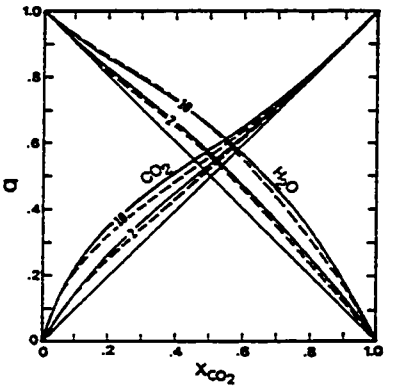

FIG. 5. Activity-composition relations as in Fig. 4 at 800°C.

calcite + quartz = wollastonite + CO_2

as a function of X_{CO_2} in H_2O-CO_2 fluids. The calculated curves (solid curves) fit most of the experimental data well. One discrepancy is in the equilibrium temperature at 6 kbar and at $X_{CO_2} = 0.86$ (open square, KERRICK and JACOBS, 1981), which is about 30°C lower than required by JACOBS and KERRICK's (1981) data.

Figure 8 shows the equilibrium pressures and temperatures for the reaction:

3 dolomite + 4 quartz + H_2O = talc + 3 calcite + 3 CO_2.

The experimental data are from METZ and PUHAN (1970, 1971) and were discussed by JACOBS and KERRICK (1981). The open circles represent experiments that were started far from equilibrium in H_2O-rich fluid progressing to the reported composition. These points, therefore, represent one side of the pressure bracket. The solid circles represent the runs that were overstepped by changing the temperature of the run after a duration of time. The solid curves are calculated from

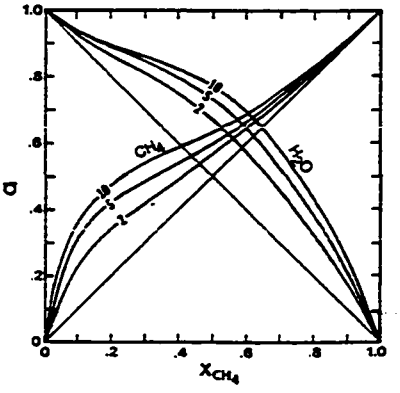

FIG. 6. Activity-composition relations in the binary CH_4-H_2O calculated from the model of this study at 500°C and at pressures of 2, 5 and 10 kbar.

Table 2. Thermochemical data for phases used in this study

Name / Formula	V_o(cm^3/mol)	ΔH_{298}(J/mol) a	b	S_{298}(J/mol.K) c	N d	f
1.Water	-	-2.418140E+05		188.830	1	
H_2O		7.368	2.7468E-2	-2.2316E-5	-4.8117E-6	3.6174E+2
2.Carbon dioxide	-	-3.935100E+05		213.790	1	
CO_2		87.820	-2.6442E-3	7.0641E-5	0.0000E+0	-9.9886E+2
3.Oxygen	-	0.000000E+00		205.150	1	
O_2		48.318	-6.9132E-4	4.9923E-5	0.0000E+0	-4.2066E+2
4.Graphite	5.298	0.000000E+00		5.740	1	
C		63.160	-1.1468E-2	7.4807E-5	1.8079E-6	-1.0323E+3
5.Iron	7.150	0.000000E+00		27.280	7	
Fe(bcc)		28.175	-7.3180E-3	-2.8950E+5	2.5040E-5	0.0000E+0
(800 0.00)		-263.454	2.5580E-1	6.1920E-7	0.0000E+0	0.0000E+0
(1000 0.00)		-641.905	6.9630E-1	0.0000E+0	0.0000E+0	0.0000E+0
(1042 0.00)		1946.250	-1.7870E+0	0.0000E+0	0.0000E+0	0.0000E+0
(1060 0.00)		-561.932	3.3410E-1	2.9120E-8	0.0000E+0	0.0000E+0
(1184 899.60)		23.991	8.3600E-3	0.0000E+0	0.0000E+0	0.0000E+0
(1665 836.80)		24.636	9.9035E-3	0.0000E+0	0.0000E+0	0.0000E+0
6.Wustite(1)	15.970	-3.809000E+05		54.900	3	
$FeO_{1.5}$		44.399	4.4413E-2	-4.5513E+5	0.0000E+0	0.0000E+0
(955 334.70)		-70.121	7.2534E-2	7.8182E-7	0.0000E+0	0.0000E+0
(1250 0.00)		-211.265	1.4374E-1	1.5417E+8	0.0000E+0	0.0000E+0
7.Wustite(2)	12.250	-2.672700E+05		57.590	1	
FeO		67.352	3.7580E-3	3.1570E+5	0.0000E+0	-3.8167E+2
8.Calcite	36.934	-1.207370E+06		91.713	1	
$CaCO_3$		99.715	2.6920E-2	-2.1576E+6	0.0000E+0	0.0000E+0
9.Magnesite	29.000	-1.113111E+06		65.690	1	
$MgCO_3$		77.906	5.7740E-2	-1.7405E+6	0.0000E+0	0.0000E+0
10.Magnetite	44.524	-1.115548E+06		150.648	3	
Fe_3O_4		73.556	2.2662E-1	1.0087E+6	0.0000E+0	0.0000E+0
(848 391.00)		-9.710	9.7404E-2	1.2512E+8	0.0000E+0	0.0000E+0
(1300 0.00)		-193.057	1.9288E-1	2.2679E+8	0.0000E+0	0.0000E+0
11.Hematite	30.274	-8.247820E+05		87.400	3	
Fe_2O_3		88.797	8.8825E-2	-9.1026E+5	0.0000E+0	0.0000E+0
(955 334.70)		-140.241	1.4507E-1	1.5636E+8	0.0000E+0	0.0000E+0
(1250 0.00)		-422.530	2.8748E-1	3.0834E+8	0.0000E+0	0.0000E+0
12.Quartz	22.690	-9.107000E+05		41.460	2	
SiO_2		44.603	3.7754E-2	-1.0018E+6	0.0000E+0	0.0000E+0
(848 499.00)		58.928	1.0031E-2	0.0000E+0	0.0000E+0	0.0000E+0
13.Dolomite	64.390	-2.327800E+06		155.180	1	
$CaMg(CO_3)_2$		547.880	-1.6759E-1	2.8400E+6	7.7076E-5	-6.5479E+3
14.Wollastonite	39.930	-1.634766E+06		81.028	1	
$CaSiO_3$		161.996	-8.6980E-4	-7.0935E+5	0.0000E+0	-1.1448E+3
15.Enstatite	31.276	-1.546290E+06		66.270	1	
$MgSiO_3$		188.755	-5.3315E-3	4.3250E+2	0.0000E+0	-1.8129E+3
16.Anthophyllite	264.460	-1.210385E+07		501.684	1	
$Mg_7Si_8O_{22}(OH)_2$		1354.287	0.0000E+0	-8.6718E+6	0.0000E+0	-1.0273E+4
17.Talc	136.250	-5.903900E+06		257.327	1	
$Mg_3Si_4O_{10}(OH)_2$		(see notes)				

Notes for Table 2

For each phase there are two or more lines of data. The first line contains enthalpy at 298.15 K (ΔH), entropy of the phase at 298.15 K (S), and number of heat capacity expressions (N). The second line contains the chemical formula and the heat capacity coefficients a,b,c,d, and f in the expression: $C_p = a + bT + cT^{-2} + dT^2 + fT^{-.5}$

If there is a phase transformation, the third and additional lines (one for each transformation) contain temperature and enthalpy of transformation (within the bracket) and the heat capacity coefficients. In all cases, except for anthophyllite and talc, the temperature range for the heat capacity is valid for the calculations.

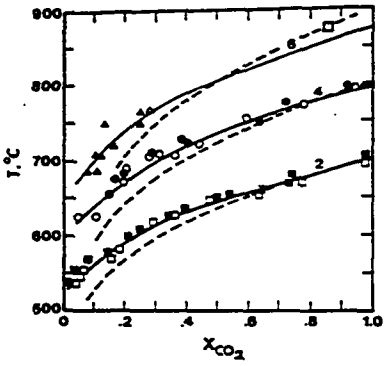

FIG. 7. Equilibrium pressures and temperatures for the reaction calcite + quartz = wollastonite + CO_2 in H_2O-CO_2 calculated from the thermochemical data in Table 2 and the fluid model of this study (solid curves). Experimental data: ZIEGENBEIN and JOHANNES (1974), KERRICK and JACOBS (1981). Open symbols: calcite + quartz are stable; Solid symbols: wollastonite is stable. Numbers indicate the pressures (in kbar). The dashed lines show the reaction curve calculated for ideal mixing of H_2O-CO_2.

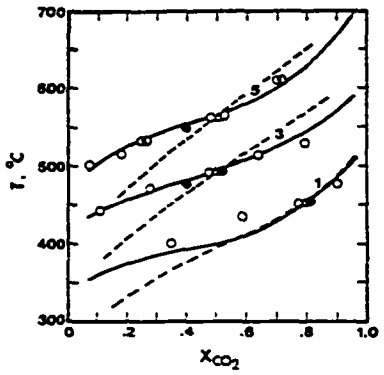

FIG. 8. Calculated equilibrium pressures and temperatures for the reaction: 3 dolomite + 4 quartz + H_2O = talc + 3 calcite + 3 CO_2. All symbols (solid and open) represent experimental data of METZ and PUHAN (1970, 1971); the open circles denote the P-T-X condition beyond which no reaction occurred. The solid circles represent temperature overstepping experiments. The triangles represent occurrence of both products and reactants. Numbers indicate the pressures (in kbar). See text for discussion.

the fluid models of this study. Note that the calculations show both the validity of the fluid models as well as their consistency with the thermochemical data listed in Table 2.

Applications

The theory and data presented in the previous sections are sufficient to permit phase equilibrium computation in the C-H-O system. To do this we choose the equations of state for the pure fluids (*e.g.* SAXENA and FEI, 1987), calculate the W_{ij} from Eqns. (1) to (7) (data in Table 1) and Eqns. (8) to (14), and compute activity coefficients from Eqns. (16) to (21). To simplify the procedure, we have calculated W_{ij} as a function of P and T for the three non-ideal binary mixtures (H_2, CO_2 and CH_4 each with water) as follows:

$$W_{CO_2\text{-}H_2O} = 10(4702 - 4.288T + 1.143 \times 10^{-3}T^2 + 0.1739P) \quad (22)$$

$$W_{CH_4\text{-}H_2O} = 10(5020 - 4.682T + 1.275 \times 10^{-3}T^2 + 0.1693P) \quad (23)$$

$$W_{H_2\text{-}H_2O} = 10(5745 - 5.628T + 1.586 \times 10^{-3}T^2 + 0.1829P) \quad (24)$$

For the activity-coefficients (γ), we use Eqns. (16) to (19). The P and T applicability of these equations is limited to a high pressure of 10 kbar and a temperature of 1200°C.

Figure 9 shows the effect of changing the fluid composition (by adding CO_2 to water) on the equilibrium pressure and temperature for the reaction:

anthophyllite = enstatite + quartz + water.

At a pressure of 5 kbar, the temperature of anthophyllite break-down changes from 560°C for nearly anhydrous con-

---

References:

1,2,3,4,8,9,12,13,14 (Robie et al., 1978); 5 (Barin and Knacke, 1978); 6,7 (discussed in Fei and Saxena, 1986); 10,11 (Haas, pers. com. 1984, see also Fei and Saxena, 1986) 15 (S and C_p from Haselton, 1979, ΔH from Brousse et al., 1984); 16,17 (C_p from Krupka et al.,1985, ΔH and S estimated by Chatterjee, 1987). The heat capacity expressions for anthophyllite and talc have been redetermined from the data of Krupka et al.,(1985) to be consistent with the high temperature constraints on C_p as discussed by Holland (1981), Berman and Brown (1985) and Fei and Saxena (1987). The C_p expression for talc is:

$$C_p = 681.233 - 5.6715\times10^{3}T^{-.5} - 8.3277\times10^{9}T^{-3}$$

The data in the system Fe-Mg-Si-O as listed above has been tested for internal consistency by Fei and Saxena (1986). However all the data taken together have not been tested. A great care is necessary in using data from different sources. It is not unlikely that some of the fits of the calculated curves are coincidental.

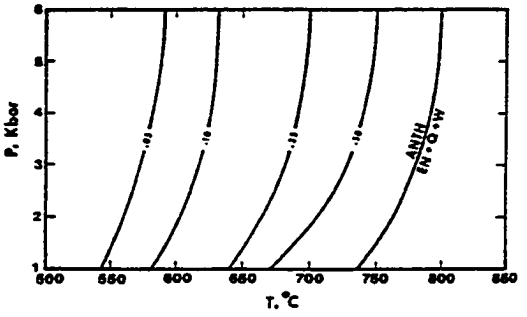

FIG. 9. Calculated equilibrium for the reaction: anthophyllite = enstatite + quartz + H_2O. The shift in equilibrium is shown as a function of changing fluid composition of the binary H_2O-CO_2 fluid; the numbers on the curves represent the equilibrium mole fraction of H_2O.

ditions to 800°C when the water pressure is equal to the total pressure. The thermochemical data of anthophyllite (heat capacity from KRUPKA *et al.*, 1985, and estimated enthalpy from CHATTERJEE, 1987) fit in the experimental phase equilibrium of the assemblage anthophyllite, enstatite and quartz as discussed by DAY *et al.* (1985).

An example of a multicomponent phase equilibrium in the C-H-O system is given in Table 3, which shows a gas phase composition in equilibrium with graphite.

Table 4 shows another example of a computation in the Mg-Si-C-H-O system at 5 kbar and 700°C. The method of Gibbs free energy minimization (ERIKSSON, 1975; SAXENA and ERIKSSON, 1985) has been used here to illustrate the power of such computational techniques. All possible phases expected to form in the system are included in the calculation, except those for which there are no thermochemical data (chrysotile and antigorite). Only six major gas species are included. Activities of solids, even if not formed, may be computed as a help in estimating the temperature of their formation; in the example, enstatite will form if temperature is increased and talc if decreased. Actual moles of various species are given so that other useful data such as heats of reactions may be calculated. The information on molar composition of the gases is useful in mass and heat transfer studies.

Table 3. Multicomponent fluid phase equilibrium in water + graphite at a temperature of 800 °C and a pressure of 5 kbar(Initial amount 100 moles of water and 20 moles of graphite).

Species	Equilibrium moles	Equilibrium pressure(bar)	Fugacity (bar)
H_2O	83.66	4146.97	4276.29
CO_2	7.94	393.64	663.66
CH_4	7.53	373.15	652.99
CO	0.46	22.63	37.60
O_2	3.94E-19	1.95E-17	3.55E-17
H_2	1.28	63.61	106.09
C(graphite)	4.07	-	-

Table 4. Phase equilibrium in the Mg-Si-C-H-O system at 5 kbar & 700 °C

Phases	Input (moles)	Equilibrium amount(moles)	Equilibrium pressure(bar)	Fugacity(bar) or activity
Gases				
H_2O	100.0	99.32	4533.9	4596.7
CO_2	0.0	9.74	444.6	938.6
CH_4	0.0	0.18	8.1	19.9
CO	0.0	0.08	3.8	8.0
O_2	10.0	1.72E-20	7.9E-19	1.9E-18
H_2	1.0	2.11E-01	9.6	20.5
Solids				
$MgSi_{1/2}O_2$	0.0	22.22	-	1.000
$MgSiO_3$(Cpx)	0.0	0.00	-	0.818
$MgSiO_3$(Opx)	0.0	0.00	-	0.919
$Mg_7Si_8O_{22}(OH)_2$	0.0	1.11	-	1.000
$MgCO_3$	0.0	0.00	-	0.128
MgO	30.0	0.00	-	0.028
SiO_2(Quartz)	20.0	0.00	-	0.526
$Mg(OH)_2$	0.0	0.00	-	0.028
C(Graphite)	10.0	0.00	-	0.272
$Mg_3Si_4O_{10}(OH)_2$	0.0	0.00	-	0.962

Acknowledgements—We thank J. M. Prausnitz for helpful suggestions. H. J. Greenwood and I.-Ming Chou's critical reviews were of great help in the revision. H. C. Helgeson and J. Ganguly provided useful comments. Financial support was provided by a N.S.F. grant (EAR8516476) and a CUNY PSC-BHE grant (6-66315).

Editorial handling: J. H. Weare

REFERENCES

ACREE W. E. JR. (1984) *Thermodynamics Properties of Nonelectrolyte Solutions*. Academic Press, New York, 308p.

BARIN I. and KNACKE O. (1978) *Thermochemical Properties of Inorganic Substances*. Springer-Verlag, New York, 861p.

BERMAN R. G. and BROWN T. H. (1985) Heat capacity of minerals in the system Na_2O-K_2O-CaO-MgO-FeO-Fe_2O_3-Al_2O_3-SiO_2-TiO_2-H_2O-CO_2: Representation, estimation and high temperature extrapolation. *Contrib. Mineral. Petrol.* **89**, 168–183.

BOTTINGA Y. and RICHET P. (1981) High pressure and temperature equation of state and calculation of the thermodynamic properties of gaseous carbon dioxide. *Amer. J. Sci.* **281**, 615–660.

BOWERS T. S. and HELGESON H. C. (1983) Calculation of the thermodynamic and geochemical consequences of non-ideal mixing in the system H_2O-CO_2-NaCl on phase relations in geologic systems: Equation of state for H_2O-CO_2-NaCl fluids at high pressures and temperatures. *Geochim. Cosmochim. Acta* **47**, 1247–1275.

BROUSSE C., NEWTON R. C. and KLEPPA O. J. (1984) Enthalpy of formation of forsterite, enstatite, akermanite, monticellite and merwinite at 1073 K determined by alkali borate solution calorimetry. *Geochim. Cosmochim. Acta* **48**, 1081–1088.

CHATTERJEE N. (1987) Phase equilibria in crustal rocks. Ph.D. dissertation, City University of New York.

CHOU I. and WILLIAMS R. J. (1979) The activity of H_2O in supercritical fluids: H_2O-CO_2 at 600°C and 700°C at elevated pressures. *Lunar Planet. Sci. Conf. 10th.* 201–203.

DAY H. W., CHERNOSKY J. V. and KUMIN H. J. (1985) Equilibria in the system MgO-SiO_2-H_2O: A thermodynamic analysis. *Amer. Mineral.* **70**, 237–248.

EGGLER D. H. and BURNHAM C. W. (1978) Activity of H_2O in diopside and CO_2-H_2O vapor to 20 kilobars, 600–1400°C. *Geol. Soc. Amer. Abstr.* **10**, 395.

EGGLER D. H. and KADIK A. H. (1979) The system $NaAlSi_3O_8$-H_2O-CO_2 to 20 kbar pressure: I. Compositional and thermodynamic relations of liquids and vapors coexisting with albite. *Amer. Mineral.* **64**, 1036–1048.

ERIKSSON G. (1975) Thermodynamic studies of high temperature equilibria. XII. SOLGASMIX, a computer program for calculation of equilibrium compositions in multiphase systems. *Chem. Scr.* **8**, 100–103.

FEI Y. and SAXENA S. K. (1986) A thermochemical data base for phase equilibria in the system Fe-Mg-Si-O at high pressure and temperature. *Phys. Chem. Minerals* **13**, 311–324.

FEI Y. and SAXENA S. K. (1987) An equation for the heat capacity of solids. *Geochim. Geochim. Acta* **51**, 251–254.

FRANCK E. U. and TODHEIDE K. (1959) Thermische Eigenschaften überkritischer Mischungen von Kohlendioxyd und Wasser bis zu 750°C und 2000 atm. *Z. Phys. Chemie, Neue Folge* **22**, 232–245.

GEHRIG M., LENTZ H. and FRANCK E. U. (1979) Thermodynamic properties of water-carbon dioxide-sodium chloride mixtures at high temperatures and pressures. In *High-Pressure Science and Technology* (eds. K. D. TIMMERHAUS and M. S. BARBER), pp. 534–542. Plenum Press, New York.

GOLDSMITH J. R. and NEWTON R. C. (1969) *P-T-X* relations in the system $CaCO_3$-$MgCO_3$ at high temperatures and pressures. *Amer. J. Sci.* **267A**, 160–190.

GREENWOOD H. J. (1973) Thermodynamic properties of gaseous mixtures of H_2O-CO_2 between 450°C and 800°C and 0 to 500 bars. *Amer. J. Sci.* **273**, 561–571.

GUGGENHEIM E. A. (1952) *Mixtures*. Clarendon Press, Oxford, 365p.

HALBACH H. and CHATTERJEE N. D. (1982) An empirical Redlich-Kwong-type equation of state for water to 1000°C and 200 kbar. *Contrib. Mineral. Petrol.* **79**, 337–345.

HASELTON H. T. (1979) Calorimetry of synthetic pyrope-grossular garnets and calculated stability relations. Ph.D. dissertation, Univ. of Chicago.

HELGESON H. C. (1981) Prediction of the thermodynamic properties of electrolytes at high pressures and temperatures. In *Chemistry and Geochemistry of Solutions at High Temperatures and Pressures: Physics and Chemistry of the Earth* (eds. D. RICKARD and F. WICKMAN), Vol. 13/14, pp. 133–177. Pergamon Press, New York.

HOLLAND T. J. B. (1981) Thermodynamic analysis of simple minerals. In *Thermodynamics of Minerals and Melts* (eds. R. C. NEWTON, A. NAVROTSKY and B. J. WOOD), pp. 19–34. Springer-Verlag, New York.

JACOBS G. K. and KERRICK D. M. (1981) Methane: an equation of state with application to the ternary system H_2O-CO_2-CH_4. *Geochim. Cosmochim. Acta* **45**, 607–614.

KERRICK D. M. and JACOBS G. K. (1981) A modified Redlich-Kwong equation for H_2O, CO_2, and H_2O-CO_2 mixtures at elevated pressures and temperatures. *Amer. J. Sci.* **281**, 735–767.

KRUPKA K. M., HEMINGWAY B. S., ROBIE R. A. and KERRICK D. M. (1985) High-temperature heat capacities and derived thermodynamic properties of anthophyllite, diopside, dolomite, enstatite, bronzite, talc, tremolite, and wollastonite. *Amer. Mineral.* **70**, 261–271.

METZ P. and PUHAN D. (1970) Experimentelle Untersuchung der Metamorphose von kieselig dolomitischen Sedimenten. I. Die Gleichgewichtsdaten der Reaktion 3 Dolomit + 4 Quartz + H_2O = Talc + 3 Calcit + $3CO_2$ für die Gesamtgasdruke von 1000, 3000 und 5000 bar. *Contrib. Mineral. Petrol.* **26**, 302–314.

METZ P. and PUHAN D. (1971) Korrektur zur Arbeite "Experimentelle Untersuchung der Metamorphose von kieselig dolomitischen Sedimenten. I. Die Gleichgewichtsdaten der Reaktion 3 Dolomit + 4 Quartz + H_2O = Talc + 3 Calcit + $3CO_2$ für die Gesamtgasdruke von 1000, 3000 und 5000 bar." *Contrib. Mineral. Petrol.* **31**, 169–170.

PRAUSNITZ J. M., LICHTENTHALER R. N. and DE AZEVEDO E. G. (1986) *Molecular Thermodynamics of Fluid-Phase Equilibria*. Prentice-Hall, New York, 600p.

ROBIE R. A., HEMINGWAY B. S. and FISHER J. R. (1978) Thermodynamic properties of minerals and related substances at 298.15 K and 1 bar (10^5 pascals) pressure and at higher temperatures. *U.S. Geol. Survey Bull. 1452*.

ROSS M. (1979) A high-density fluid-perturbation theory base on an inverse 12th-power hard-sphere reference system. *J. Chem. Phys.* **71**, 1567–1571.

ROSS M. and REE F. H. (1980) Repulsive forces of simple molecules and mixtures at high density and temperature. *J. Chem. Phys.* **73**, 6146–6152.

SAXENA S. K. and ERIKSSON G. E. (1985) Anhydrous phase equilibria in Earth's upper mantle. *J. Petrol.* **26**, 378–390.

SAXENA S. K. and FEI Y. (1987) Fluids at crustal pressure and temperatures. I. Pure species. *Contrib. Mineral. Petrol.* **95**, 370–375.

SHMULOVICH K. I., SHMONOV V. M. and ZHARIKOV V. A. (1982) The thermodynamics of supercritical fluid systems. In *Advances in Physical Geochemistry* (ed. S. K. SAXENA), Vol. 2, pp. 172–190. Springer-Verlag, New York.

TIEN C. L. and LIENHARD J. H. (1971) *Statistical Thermodynamics*. Holt, Rinehart & Winston, New York, 397p.

ZIEGENBEIN P. and JOHANNES W. (1974) CO_2 Aktivitäten in überkritischen CO_2-H_2O Mischungen: Experimentelle bestimmte Abweichung von der idealen Mischbarkeit. *Fortschrifte der Mineral.* **58**, 142–144.

GEOLOGICAL NOTES

PHASE EQUILIBRIUM IN A SYSTEM OF CHONDRITIC COMPOSITION: IMPLICATIONS FOR EARLY MANTLE-FLUID COMPOSITIONS[1]

S. K. SAXENA AND Y. FEI
Department of Geology, Brooklyn College, Brooklyn, NY 11210
Department of Earth and Environmental Sciences, Graduate School, CUNY, NY 10036

ABSTRACT

The chemical composition of the fluid that could exist in the Si-Mg-Fe-C-H-O system has been calculated at various pressure and temperature conditions in a growing mantle of carbonaceous chondritic composition. The results show that the fluid in such a primitive mantle was dominantly methane, with subordinate amounts (<10% by volume) of hydrogen and water. Such a composition is stable over a broad range of pressure and temperature. The phase equilibrium assemblage consisting of olivine, pyroxene, graphite or diamond, and iron is an appropriate model composition of the present earth in its undifferentiated form. The possibility that primitive mantle fluids were dominated by methane requires a reconsideration of the composition of the core and the role of methane in understanding the process of differentiation and evolution of the mantle.

INTRODUCTION

At present, the composition of the earth's atmosphere is partially the result of over 4 b.y. of evolution of the planet's interior. This evolutionary process involves dynamic activities which are forming the earth's crust and mantle and shaping its mountains and oceans. The present distribution of the earth's mass into core, mantle, crust and a hydrosphere may be the result of such activities operating in an initially homogeneous planet (accreting cold, e.g., Ringwood 1979) or in an initially heterogeneously assembled planet (Turekian and Clark 1975; Saxena and Eriksson 1983). In either case there is agreement that fluids have played a very important role in differentiating the earth's interior and in forming its hydrosphere and atmosphere.

The conclusions of several geochemists (e.g., Holland 1984; Safronov and Vitjazev 1986; Wetherill 1980; Ringwood 1979) on the processes leading to the formation of the earth are as follows. The earth formed by the accumulation of preassembled materials. If the planet was created in one stage (cold accretion) with a system composition resembling carbonaceous chondrites, a very large quantity of volatiles must have evolved either during or immediately after accretion, which for physical reasons is difficult to accept. Many comparisons of rare gas compositions of the meteorites with the earth's mantle and atmosphere are available. Manuel's (1978) data on Xe and Kr show that these gases are depleted significantly in the atmosphere relative to the carbonaceous chondrites. If the earth had assembled, not in one stage but through many intermediate steps (e.g., Wetherill 1976), the present volatile inventory of the earth could find acceptable explanations.

Although we are not certain what proportion of volatiles (relative to carbonaceous chondrites) was incorporated into the growing earth, it is certain that significant amounts of gases were somehow trapped in the condensed parts of the growing planet. By comparing isotopic ratios (e.g., $^3He/^4He$) of escaping volcanic gases, xenolith diamonds, and volcanic glasses with that of the atmosphere (Craig et al. 1975; Jenkins et al. 1978; Kurz et al. 1975; Ozima and Zashu 1983), Holland (1984) concluded that the major portion of the rare gases, and of other volatiles as well, was trapped directly together with the solids in infalling objects. This conclusion is important since it permits us to consider solid-fluid phase equilibrium relations during the accumulation and growth history of the earth, which may have taken as long as 10^8 years (Safranov and Vitjazev 1986; Wetherill 1980), providing sufficient time for equilib-

[1] Manuscript received November 16, 1987; accepted May 28, 1988.

[JOURNAL OF GEOLOGY, 1988, vol. 96, p. 601–607]

0022-1376/88/9605-0008$1.00

rium processes to operate locally. During the growth of the planet, the chondritic and other types of meteoritic components (including metallic Fe-Ni and organics) were certainly among the materials that fell on the surface.

One of Holland's (1984) conclusions is that after the initial loss of part of the volatiles to an early atmosphere during accretion, volatiles have been added gradually to the atmosphere and hydrosphere by degassing of the earth's interior. This provides the motivation for computing phase equilibrium relations in a primitive mantle composition involving C-H-O fluids. Some of our current concepts of the mantle composition and its oxidation state are described below.

The question whether the earth's primitive mantle equilibrated with metallic Fe has been in the forefront of planetary chemistry (Ringwood 1979; Brett 1984). The enigma is associated with some of the observed distributions of the siderophile elements such as Ni, Co, Ir, and Au which are not as depleted in the peridotite silicates (Jaqoutz et al. 1979) as they would be if equilibrium with Fe was established. Another aspect of this problem is that if silicates and Fe were equilibrated in the presence of C-H-O fluids, the oxygen fugacity of the mantle would have a well defined value. A succeeding question is whether such an oxygen fugacity is consistent with other observations on mantle minerals. According to Ringwood (1979), Fe^{3-}/Fe^{2-} ratios of fresh oceanic basaltic glasses and of unaltered primary mantle minerals (from xenoliths and peridotites) could be consistent with a Fe^{3-}/Fe^{2-} ratio of 0.05 to 0.1 for primary pyrolite; those equilibrated with metallic iron at high temperature are lower by an order of magnitude. The recent results of Christie et al. (1986) indicate a very low Fe^{3-}/Fe^{2-} ratio in the MORB (mid oceanic ridge basalt) glasses. Ringwood (1979) concluded that if the mantle had equilibrated with metallic iron, the volatiles degassing from the mantle would be dominated by CO and H_2 rather than CO_2 and H_2O. He further considered the total redox state of the Earth to be such that it may be possible for oxygen to be dissolved in iron and form the core of an appropriate density. More recently, Ringwood (1987) proposed that oxygen is indeed the most likely element dissolved in the Fe-Ni core.

There are relatively few experimental studies of petrological systems involving fluids (see Woermann and Rosenhauer 1985). Most such studies have been confined to a maximum pressure of 40 kbar in simple systems with one-component or binary fluids. It is, therefore, important to study fluid phase-solid phase equilibrium relations of a model mantle by using pressure-volume-temperature (P-V-T) models of fluids and thermochemical data on solid phases. The P-V-T relations appropriate for the fluids in the C-H-O system have been modeled by Saxena and Fei (1987*a*, 1987*b*) from the available experimental data [static low pressure (e.g., Burnham et al. 1969) and high pressure shock wave data (e.g., Ross and Ree 1980)]. With the availability of thermochemical data on the Fe-Mg-Si-O system (see Fei and Saxena 1986; Berman et al. 1986) and the P-V-T relations in the C-H-O system (Saxena and Fei 1987*a*, 1987*b*), it is possible to compute relevant phase equilibrium data. However, at present we are restricted in our ability to compute phase equilibrium relations in systems involving melts. Therefore this study is confined to calculation of sub-solidus phase equilibrium. The elements Mg, Fe, Si, C, O, and H make up over 95% of the mantle. Solid phases with Al, Ca, Na, and K constitute a very small proportion of the chondritic assemblage and do not affect the fluid composition significantly. The presence of S in the gas would modify the fluid composition: however, the sulfur content of the carbonaceous chondrite is about one-tenth of the oxygen content, and it will be distributed between FeS and H_2S.

Recent studies of the oxidation state of the shallow parts of the mantle have been conducted by Mattioli and Wood (1986) and Eggler (1983) using thermobarometric methods, and by Arculus and Delano (1981) and Ulmer et al. (1986) using experimental measurement of intrinsic fO_2 in minerals. These studies have produced contradictory results. The thermobarometric results favor an oxidized upper mantle; the fO_2 intrinsic measurements indicate a rather reduced fluid composition. The uncertainties of the two methods have been subject to extensive discussions (Wood and Virgo 1987; Arculus and Kersting 1987). This study does not contribute directly to the problem except insofar as it provides a set of

initial mantle conditions on the composition of fluids in an undifferentiated primitive meteorite, which might eventually help us understand the nature of the present mantle fluids.

THERMODYNAMIC DATA

Formulation of the thermodynamic equations of equilibrium are given in Fei and Saxena (1986). The heat capacity expression used is that of Fei and Saxena (1987).

The pressure-temperature dependence of molar volume is best modeled through the use of the Birch-Murnaghan equation (see Jeanloz and Knittle 1986). This $V(P, T)$ equation does not include the temperature dependence of the bulk modulus. Such data are available for very few substances. It is expected that in computing ΔG, such effects will largely be cancelled.

The pressure-volume-temperature data of several gases (H_2, O_2, CO, CH_4, N_2, and CO_2) were used by Saxena and Fei (1987*a*) to obtain *P-V-T* equations for fluids. The equation for hydrogen was subsequently modified (Saxena and Fei 1988*b*). These equations are valid over restricted ranges of pressures and temperatures as specified in Saxena and Fei (1987*a*, 1988*b*) and have been used in this study. The equations are not suitable for calculations at low pressure (<1 kbar) and temperatures (<500 K); for such calculations other models (e.g., Bowers and Helgeson 1983) should be used.

The data on solution parameters and the method of calculating the mixing properties of fluids are given in Saxena and Fei (1988*a*). The *P* and *T* applicability of the mixing calculations have been tested to a high pressure of 10 kbar and a temperature of 1200°C. In this range, the computed deviations from ideal mixing using the models of Kerrick and Jacobs (1981) and Jacobs and Kerrick (1981) are closely similar to those calculated by Saxena and Fei (1988*b*). At pressures and temperatures above this range, the model is only applicable to the range specified for the pure species (see fig. 9 Saxena and Fei 1987*b*). Here too the behavior of the interaction potential W_{ij} at high pressures is not well understood.

The thermodynamic data on 23 species used in the computational work are listed in table 1 available from *The Journal of Geology* free of charge upon request.

The data on thermal expansion and bulk modulus are the same as used by Fei and Saxena (1986). For hydrous phases such data are not available. For solid solutions the data are: olivine (Wood and Kleppa 1981), orthopyroxene (Chatillon-Colinet et al. 1983) and wustite (Fei and Saxena 1986). Other minerals are considered as ideal. We have used sets of data for enstatite and forsterite (Fei and Saxena 1986; Saxena and Chatterjee 1986) which are different from some other sets (e.g., Berman et al. 1986); the effect of differences in data sets is discussed later in this work. The method of free energy minimization is used in the computation of phase equilibrium (Eriksson 1985; Saxena and Eriksson 1983).

PHASE RELATIONS IN A CHONDRITIC COMPOSITION

Our evaluated thermochemical data permit us to compute phase equilibrium relations in the system Fe-Mg-Si-C-H-O for model primitive earth chemistries and physical conditions. Table 2 shows computed phase equilibrium data for a system of chondritic composition; the elemental composition for Si, Fe, Mg, and C is from Wasson (1974) to which various amounts of water is added. We have calculated equilibrium compositions for many different contents of water; the one displayed in table 2 is for a fixed water content of 16.2 moles. This particular result is selected because the composition of olivine closely matches the observed composition in the present mantle. However, as shown in figure 1, olivine may vary in composition over a wide range without affecting the conclusions presented here. Although the assumption that the olivine composition in the growing mantle was about the same as the observed composition of olivine in peridotites is not necessary. Without such an assumption, however, it will be difficult to explain the match between the distribution of iron and silicates in the core and the mantle, discussed by Ringwood (1966) and calculated from the results in table 2. The equilibrium assemblage consists of olivine, orthopyroxene, iron, and graphite or diamond. The composition of the fluid in the primitive undifferentiated mantle (i.e., in equilibrium with

TABLE 2

PHASE EQUILIBRIUM IN A CARBONACEOUS CHONDRITE

Phase	P = 10 kbar, T = 1273 K		P = 60 kbar, T = 1700 K	
	Equilib. Moles	Mole Fraction	Equilib. Moles	Mole Fraction
Fluids				
H_2O	.75	8.80E-3	3.44	.04
CO_2	5.80E-4	6.80E-6	1.20E-3	1.40E-5
CH_4	77.00	.91	76.70	.90
CO	1.40E-2	1.60E-4	2.00E-2	2.40E-4
O_2	4.16E-20	4.90E-22	2.60E-15	3.10E-17
H_2	7.24	8.50E-2	5.08	.06
Olivine				
Mg_2SiO_4	193.6	.88	384.9	.88
Fe_2SiO_4	22.5	.12	52.2	.12
Pyroxene				
$MgSiO_3$	672.6	.86	675.1	.86
$FeSiO_3$	106.2	.14	106.4	.14
Pure Phases				
Fe	738.7		741.5	
C(graphite)	622.9			
C(diamond)			623.2	

NOTE.—Input (moles): H_2O 162, MgO 60, $MgSiO_3$ 1000, C 700, Fe 900.

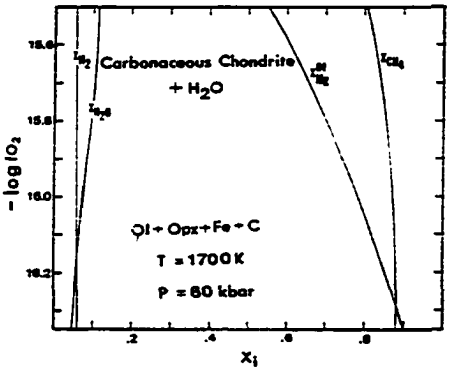

FIG. 1.—Phase equilibrium relations in a CI chondrite (composition from Wassen 1974). The fluid phase is about 90% methane and 8% hydrogen with remaining species CO, CO_2, and H_2O. The composition of olivine and pyroxene varies with water input. P = 60 kbar, T = 1700 K. QFM (quartz, fayalite and magnetite buffer) is at log fO_2 of −12.00.

Fe and C) at two different sets of P and T conditions are shown in the table. The fluid composition is dominated by methane (nearly 90%) and hydrogen (6 to 8%). Figure 1 shows that such fluid composition is possible with coexisting silicates which may vary in Fe/Mg ratio over a wide range.

TABLE 3

PHASE EQUILIBRIUM IN A CARBONACEOUS CHONDRITE WITH WATER AND CO_2

Fluid Phases	P = 60 kbar, T = 1700 K	
	Mole Fraction	Solid Phases
H_2	.10	Olivine (X_{Mg} = .67)
CO_2	7.50E-5	Pyroxene (X_{Mg} = .69)
CH_4	.85	Iron
CO	5.40E-4	Diamond
O_2	1.60E-16	
H_2	.06	

NOTE.—Input (moles): H_2O 162, CO_2 162, MgO 60, $MgSiO_3$ 1000, Fe 900, C 538.

It is interesting to examine the phase relations when the input fluid composition is not pure H_2O but a mixture of H_2O and CO_2. Table 3 shows the results of calculating phase equilibrium in a chondritic system which contains variable amounts of H_2O and CO_2. We note again that the gas phase is dominantly CH_4. The silicates, however, are more oxidized than those observed in the upper mantle samples. Diamond is a stable phase, and therefore we may further reduce the content of carbon in the system without affecting our results.

DISCUSSION AND CONCLUSIONS

The calculated mineral proportions in table 2 represent the assemblage at depth in an undifferentiated proto-earth including both the present mantle and the core. The proportion of orthopyroxene and olivine are different from those found in the upper mantle peridotite because the proportion is a function of the silica content of the system; the more silica (and the fluid) there is, the more olivine will form in a system of otherwise fixed composition. The fluids in equilibrium with the early earth remain almost unchanged with variable olivine/pyroxene ratios, however.

It may be argued that the results shown in tables 2 and 3 may change substantially if we use (a) a different set of thermochemical data and (b) a different model for fluid mixture. As discussed elsewhere (Fei and Saxena 1986; Saxena and Chatterjee 1986; Berman et al. 1986), the enthalpies of enstatite and forsterite may vary over a range of values. Similarly somewhat different sets of Fe-Mg solution parameters may be used for olivine. Fei and Saxena (1986) found it necessary to use a W/R (W = Margules interaction parameter, R = gas constant) value of -1000 J/mol to fit the distribution of Fe and Mg in coexisting minerals at high pressures (100–450 kbar). In this work, we have used a W/R value corresponding to a symmetrical model fitted to the data of Wood and Kleppa (1981). Computed results using different sets of data give almost identical results, however. Use of the data of Berman et al. (1986) for enstatite and forsterite, a negative value of W/R for the Fe-Mg olivine, or an ideal gas mixture all confirm the conclusion about methane being the dominant species.

We have considered high pressure and high temperature phase equilibrium in a system of chondritic composition; such a composition is considered important in the formation of the proto-earth. The fluid composition, therefore, refers to the time prior to the differentiation of the earth into a core and mantle and implies that the fluid in the accreting material was highly reducing permitting the formation of iron and diamonds. This conclusion is contradictory to Ringwood's (1987) hypothesis of oxygen as the light component of the core. Many light elements can dissolve in iron, and Ringwood (1979, 1987) does not make it clear why oxygen should be the preferred element. In a growing proto-earth, the oxygen fugacity would be governed by the overall composition of the fluid phase and multiple reaction equilibria. Any hypothesis on equilibrium composition of an iron-melt must involve an experimental or computational study of the entire system.

If there is any fluid in the deep mantle, it must be rich in methane. This statement does not contradict the possible occurrence of fluids of various compositions in the shallow (~150 km) mantle. Such a conclusion has an important bearing on our models of the evolutionary history of the earth. As temperatures rise in the growing mantle, iron would melt in equilibrium with carbon and a methane-dominated fluid, which would rule out any possible oxygen dissolution in the melt and oxygen as the light element in the core; carbon would be favored (cf. Sato 1978). The methane-rich fluid would affect the melting of silicates (Eggler and Baker 1982) and the formation of early magmatic bodies and planetary differentiation. Its role would be less and less important in the succeeding evolutionary stages.

The methane-dominated fluid trapped in the growing mantle would continue to influence the subsequent petrogenetic history of the mantle until it all finally escaped to the atmosphere. One argument against the involvement of methane with the upper mantle and the rocks of granulite facies is the occurrence of the CO_2-rich inclusions (see Roedder 1984 and Newton 1980, 1986). Lamb and Valley (1984) find that many of the Adirondack granulites with reduced oxide minerals were not exposed to CO_2 in high concentration at the peak metamorphic temperatures. The discussion of metamorphic fluids cannot be adequately presented here—the material is covered in two recent books (Walther and Wood 1986; Roedder 1984). As discussed by Valley et al. (1983), it is quite likely that the fluid phase becomes highly variable in composition as the mantle fluids ascend and react with the upper mantle and the lower crustal material (see discussion in Green et al. 1986).

ACKNOWLEDGMENTS.—Thanks are due to two anonymous reviewers for useful suggestions. The work was supported by a PSC-BHE CUNY grant (#6-67211) and a NSF grant (#EAR8516476).

REFERENCES CITED

ANDERS, E., and EBIHARA, M., 1982, Solar-system abundances of the elements: Geochim. Cosmochim. Acta, v. 46, p. 2363–2380.

ARCULUS, R. J., and DELANO, J. W., 1980, Implications for the primitive atmosphere of the oxidation state of the earth's upper mantle: Nature, v. 288, p. 72–74.

———, and KERSTING, A. B., 1987, Apparent paradox evident in current estimates of upper mantle redox states: EOS, v. 68, p. 443.

BARIN, I., and KNACKE, O., 1978, Thermochemical Properties of Inorganic Substances: New York, Springer-Verlag, 919 p.

BERMAN, R. G.; ENGI, M.; GREENWOOD, H. J.; and BROWN, T. H., 1986, The derivation of internally-consistent thermodynamic data by the technique of mathematical programming: a review with application to the system MgO-SiO_2-H_2O: Jour. Petrol., v. 27, p. 1331–1364.

BOTTINGA, Y., and RICHET, P., 1981, High pressure and temperature equation of state and calculation of the thermodynamic properties of gaseous carbon dioxide: Am. Jour. Sci., v. 281, p. 615–660.

BOWERS, T. S., and HELGESON, H. C., 1983, Calculation of the thermodynamic and geochemical consequences of nonideal mixing in the system H_2O-CO_2-NaCl on phase relations in geologic systems: metamorphic equilibria at high pressures and temperatures: Am. Mineral., v. 68, p. 1059–1075.

BRETT, R., 1984, Chemical equilibration of the earth's core and the upper mantle: Geochim. Cosmochim. Acta, v. 48, p. 1183–1188.

BURNHAM, C. W.; HOLLOWAY, J. R.; and DAVIS, N. F., 1969, Thermodynamic properties of water to 1,000 bars: Geol. Soc. America, Special Paper 132.

CHATILLON-COLINET, C.; KLEPPA, O. J.; NEWTON, R. C.; and PERKINS, D., 1983, Enthalpy of formation of $FeSiO_3$ at high temperature in alkali borate solution calorimetry: Geochim. Cosmochim. Acta, v. 47, p. 439–444.

CHATTERJEE, N., 1987, Evaluation of thermochemical data on Fe-Mg olivine, orthopyroxene, spinel and Ca-Fe-Mg-Al garnet: Geochim. Cosmochim. Acta, v. 51, p. 2515–2525.

CRAIG, H.; CLARKE, W. B.; and BEG, M. A., 1975, Excess ^3He in deep water on the East Pacific Rise: Earth Planet. Sci. Lett., v. 26, p. 125–132.

EGGLER, D. H., and BAKER, D. R., 1982, Reduced volatiles in the system C-O-H: implications to melting, fluid formation, and diamond genesis, *in* AKIMOTO, S., and MANGHNANI, M., eds., High Pressure Research in Geophysics: Tokyo, Center for Academic Publications, p. 237–250.

ERIKSSON, G., 1975, Quantitative equilibrium calculations in multiphase systems at high temperatures, with special reference to the roasting of chalocopyrite, $CuFeS_2$: Unpub. PhD. thesis, University of Umea, Umea, Sweden.

FEI, Y., and SAXENA, S. K., 1986, A thermochemical data base for phase equilibria in the system Fe-Mg-Si-O at high pressure and temperature: Phys. Chem. Minerals, v. 13, p. 311–324.

———, and ———, 1987, An equation for the heat capacity of solids: Geochim. Cosmochim. Acta, v. 51, p. 251–254.

GREEN, D. H.; FALLON, T. J.; and TAYLOR, W. R., 1987, Mantle-derived magmas-roles of variable source peridotite and variable C-H-O fluid compositions, *in* MYSEN, B. O., ed., Magmatic processes: physicochemical principles: Geochemical Soc. Spec. Pub. 1, p. 139–154.

GUSTAFSSON, P., 1984, A thermodynamic evaluation of the Fe-C system: TRITA-MAC, Royal Inst. Tech., Stockholm, Sweden.

HALBACH, H., and CHATTERJEE, N. D., 1982, An empirical Redlich-Kwong type equation of state for water to 1000°C and 200 Kbar: Contrib. Mineral. Petrol., v. 79, p. 337–345.

HOLLAND, H. H., 1984, Chemical Evolution of the Atmosphere and Oceans: Princeton, Princeton University Press.

JACOBS, G. K., and KERRICK, D. M., 1981, Devolatilization equilibria in H_2O-CO_2 fluids: an experimental and thermodynamic evaluation at elevated pressures and temperatures: Am. Mineral., v. 6, p. 1134–1153.

JAGOUTZ, E.; PALME, H.; BADDENHAUSEN, H.; BLUM, K.; CENDALES, M.; DREIBUS, G.; SPETTEL, B.; LORENZ, V.; and WANKE, H., 1979, The abundances of major, minor and trace elements in the earth's mantle as derived from primitive ultramafic nodules: Proc. Lunar Planet. Sci. Conf. 10th, p. 2031–2050.

JEANLOZ, R., and KNITTLE, E., 1986, Reduction of mantle and core properties to a standard state by adiabatic decompression, *in* SAXENA, S. K., ed., Chemistry and Physics of Terrestrial Planets (Advances in Phys. Geochem. vol. 6): New York, Springer-Verlag, p. 275–309.

JENKINS, W. J.; EDMONDS, J. M.; and CORLISS, J. B., 1978, Excess ^3He and ^4He in Galapagos submarine hydrothermal waters: Nature, v. 272, p. 156–158.

KERRICK, D. M., and JACOBS, G. K., 1981, A modified Redlich-Kwong equation for H_2O, CO_2, and H_2O-CO_2 mixtures at elevated pressures and temperatures: Am. Jour. Sci., v. 281, p. 735–767.

KURZ, M. D.; JENKINS, W. J.; SCHILLING, J. G.; and HART, S. R., 1975, Helium isotopic variations in the mantle beneath the central North Atlantic Ocean: Earth Planet. Sci. Lett., v. 58, p. 1–14.

LAMB, W., and VALLEY, J. W., 1984, Metamorphism of reduced granulites in low-CO_2 vapour-free environments: Nature, v. 312, p. 56–58.

MANUEL, O. K., 1978, A comparison of terrestrial and meteoric noble gases, *in* ALEXANDER, E. C., JR., and OZIMA, M., eds., Terrestrial Rare Gases: Japan, Scientific Societies Press, p. 85–91.

MATTIOLI, G. S., and WOOD, B. J., 1986, Upper mantle oxygen fugacity recorded by spinel lherzolites: Nature, v. 322, p. 626–627.

NEWTON, R. C., 1986, Fluids of granulite facies

metamorphism. *in* WALTHER, J. W., and WOOD, B. J., eds., Advances in Physical Geochemistry: New York, Springer-Verlag, v. 5, p. 36–59.

OZIMA, M., and ZASHU, S., 1983, Primitive helium in diamonds: Science, v. 219, p. 1067–1068.

RINGWOOD, A. E., 1979, Origin of the Earth and Moon: New York, Springer-Verlag.

———, 1987, Oxygen in the core: geochemical and geophysical implications: EOS, v. 68, p. 1210.

ROBIE, R. A.; HEMINGWAY, B. S.; and FISHER, J. R., 1978, Thermodynamic properties of minerals and related substances at 298.15 K and 1 bar. 10^5 pascals pressure, and at high temperatures: U.S. Geol. Surv. Bull., 1452 p.

ROSS, M., and REE, F. H., 1980, Repulsive forces of simple molecules and mixtures at high density and temperature: Jour. Chem. Phys., v. 73, p. 6146–6152.

SAFRONOV, V. S., and VITJAZEV, A. V., 1986, The origin and early evolution of the terrestrial planets, *in* SAXENA, S. K., ed., Chemistry and Physics of Terrestrial Planets (Advances in Phys. Geochem. Vol. 6): New York, Springer-Verlag, p. 1–29.

SATO, M., 1978, A possible role of carbon in characterizing the oxidation state of a planetary interior and originating a metallic core: Lunar Planet. Sci. Conf. 9th, pt. 2, p. 990–992.

SAXENA, S. K., and CHATTERJEE, N., 1986, Thermochemical data on mineral phases: the system CaO-MgO-Al_2O_3-SiO_2: Jour. Petrol., v. 27, p. 827–842.

———, and ERIKSSON, G., 1983, Theoretical computation of mineral assemblages in pyrolite and lherzolite: Jour. Petrol., v. 24, p. 538–555.

———, and FEI, Y., 1987*a*, Fluids at crustal pressures and temperatures. I. Pure species: Contrib. Mineral. Petrol., v. 95, p. 370–375.

———, and ———, 1987*b*, High pressure and high temperature fluid fugacities: Geochim. Cosmochim. Acta, v. 51, p. 783–791.

———, and ———, 1988*a*, Fluid mixtures in the C-H-O system at high pressure and temperature: Geochim. Cosmochim. Acta, in press.

———, and ———, 1988*b*, The pressure-volume-temperature equation of hydrogen: Geochim. Cosmochim. Acta, in press.

STACEY, F. D., 1977, Physics of the Earth, New York, Wiley, 414 p.

TUREKIAN, K. K., and CLARK, S. P., JR., 1975, The non-homogeneous accumulation model for terrestrial planet formation and the consequences for the atmosphere of Venus: Jour. Atmos. Sci., v. 32, p. 1257–1261.

ULMER, G. C.; MOATS, M. A.; and WEIS, D. A., 1985, Oxygen fugacity, carbon, and the mantle redox state: EOS, v. 66, p. 393.

VALLEY, J. W.; MCLELLAND, J.; ESSENE, E. J.; and LAMB, W. M., 1983, Metamorphic fluids in the deep crust: evidence from the Adirondacks: Nature, v. 301, p. 226–228.

WALTHER, J. V., and WOOD, B. J., 1986, Fluid-rock interactions during Metamorphism, New York, Springer-Verlag.

WASSON, J. T., 1974, Meteorites: New York-Heidelberg-Berlin, Springer-Verlag.

WETHERILL, G. W., 1976, The role of large bodies in the formation of the earth and moon: Proc. Lunar Science Conf., 7th, v. 3, p. 3245–3257.

———, 1980, Formation of the terrestrial planets: Ann. Rev. Astron. Astrophys., v. 18, p. 77–113.

WOERMANN, E., and ROSENHAUER, M., 1985, Fluid phases and the redox state of the Earth's mantle: extrapolations based on experimental, phase-theoretical, and petrological data: Fortschr. Mineral., v. 63, p. 263–349.

WOOD, B. J., and KLEPPA, O. J., 1981, Thermochemistry of forsterite-fayalite olivine solutions: Geochim. Cosmochim. Acta, v. 45, p. 529–534.

———, and VIRGO, D., 1987, Oxidation state of the upper mantle: ferric-ferrous ratios in coexisting minerals from spinel lherzolite: Geol. Soc. America Abs. with Prog.: v. 19, p. 896.

INTERNALLY CONSISTENT THERMODYNAMIC DATA AND EQUILIBRIUM PHASE RELATIONS IN THE SYSTEM MgO-SiO_2 AT HIGH PRESSURE AND HIGH TEMPERATURE

Yingwei Fei[1] and Surendra K. Saxena

Department of Geology, Brooklyn College, Brooklyn, NY 11210

and Department of Earth and Environmental Sciences,

Graduate School, CUNY, New York, NY 10036

Alexandra Navrotsky

Department of Geological and Geophysical Sciences,

Princeton University, Princeton, NJ 08544

Abstract

Thermochemical and thermophysical data for phases in the system MgO-SiO_2 are critically evaluated, refined and supplemented by calculating phase equilibrium relations from the available calorimetric data. Lattice vibrational models are used to further constrain the entropies and heat capacities. Phases in the data base are MgO, SiO_2 (coesite, stishovite), Mg_2SiO_4 (olivine, β-phase, spinel), and $MgSiO_3$ (pyroxene, garnet, ilmenite, and perovskite). The internally consistent data set reproduces the experimentally determined phase relations in the system at pressures to 30 GPa and to melting temperatures.

1. Present address: Geophysical Laboratory, Carnegie Institution of Washington, 2801 Upton Street, N.W., Washington, D.C. 20008.

Experimental Determination of Element Partitioning and Calculation of Phase Relations in the Mg-Fe-Si-O System at High Pressure and High Temperature

Yingwei Fei, Ho-Kwang Mao and Bjorn O. Mysen

Geophysical Laboratory, Carnegie Institution of Washington,

2801 Upton Street, N.W., Washington, D. C. 20008

Abstract

The Mg-Fe partitioning between coexisting phases, magnesiowustite (Mw) and olivine (α), Mw and β-phase, Mw and spinel (γ), and Mw and perovskite (Pv), have been determined experimentally with piston-cylinder apparatus, the multi-anvil device and the diamond-anvil cell technique at pressures between 2 and 28 GPa and temperatures between 1473 and 1773 K. The solution parameters of each solid solution were obtained by fitting the experimental data simultaneously using the Margules formulation. The optimized solution parameters (in J/mol) are $W^{Mw}_{Mg\text{-}Fe} = 16100$, $W^{Mw}_{Fe\text{-}Mg} = 26300 - 5.56T$; $W^{\alpha}_{Mg\text{-}Fe} = 4500 + 130P$, $W^{\alpha}_{Fe\text{-}Mg} = 6500 + 130P$; $W^{\beta}_{Mg\text{-}Fe} = 1000$, $W^{\beta}_{Fe\text{-}Mg} = 2000$; $W^{\gamma}_{Mg\text{-}Fe} = 3900 - 1.10T$, $W^{\gamma}_{Fe\text{-}Mg} = 3900$; and $W^{Pv}_{Mg\text{-}Fe} = 4130 - 1.37T + 110P$, $W^{Pv}_{Fe\text{-}Mg} = -4050 - 2.45T + 150P$ where P is in GPa and T in K. These parameters are consistent with solution calorimetry and phase equilibrium data.

Phase relations in the Mg-Fe-Si-O system are calculated by using the Margules solution model combined with internally consistent thermodynamic data of the pure phases. The computed phase diagrams are in good agreement with those experimentally determined. The results indicate that the depth and width of the phase transformations of olivine to β-phase and of spinel to perovskite plus magnesiowustite are compatible with the seismic observation of the 400 km and the 670 km discontinuities, respectively.

BIBLIOGRAPHY

Acree, W. E. Jr, Thermodynamics Properties of Nonelectrolyte Solutions, Academic Press, New York, 308 pp, 1984.

Ahrens, T. J., D. L. Anderson, and A. E. Ringwood, Equations of state and crystal structure of high-pressure phases of shocked silicates and oxides, Rev. Geophys., 7, 667-707, 1969.

Akaogi, M., and S. Akimoto, Pyroxene-garnet solid solution equilibria in the system $Mg_4Si_4O_{12}$-$Mg_3Al_2Si_3O_{12}$ and $Fe_4Si_4O_{12}$-$Fe_3Al_2Si_3O_{12}$ at high pressures and temperatures, Phys. Earth Planet. Inter., 15, 90-106, 1977.

Akaogi, M., E. Ito, and A. Navrotsky, The olivine-modified spinel-spinel transitions in the system Mg_2SiO_4-Fe_2SiO_4: calorimetric measurements, thermochemical calculation, and geophysical application, J. Geophys. Res., in press, 1989.

Akaogi, M., and A. Navrotsky, The quartz-coesite-stishovite transformations: New calorimetric measurements and calculation of phase diagrams, Phys. Earth Planet. Inter., 36, 124-134, 1984.

Akaogi, M., A. Navrotsky, T. Yagi, and S. Akimoto, Pyroxene-garnet transition: thermochemistry and elasticity of garnet solid solutions, and application to a pyrolite mantle, in High Pressure Research in Mineral Physics, pp. 251-260, edited by M. H. Manghnani and Y. Syono, Terra Publications, Tokyo, Japan, 1987.

Akaogi, M., N. L. Ross, P. McMillan, and A. Navrotsky, The Mg_2SiO_4 polymorphs (olivine, modified spineland spinel) thermodynamic properties from oxide melt solution calorimetry, phase relations and models of lattice vibrations, Amer. Mineral., 69, 499-512, 1984.

Akimoto, S., The system MgO-FeO-SiO_2 at high pressures and temperatures--phase equilibria and elastic properties, Tectonophysics, 13, 161-187, 1972.

Akimoto, S., High-pressure research in geophysics: past, present and future, in High Pressure Research in Mineral Physics, pp. 1-13, edited by M. H. Manghnani and Y. Syono, Terra Publications, Tokyo, Japan, 1987.

Akimoto, S., and H. Fujisawa, Olivine-spinel solid solution equilibria in the system Mg_2SiO_4-Fe_2SiO_4, J. Geophys. Res., 73, 1467-1473, 1968.

Akimoto, S., H. Fujisawa, and T. Katsura, Olivine-spinel transition in Fe_2SiO_4 and Ni_2SiO_4. J. Geophys. Res., 66, 1969-1977, 1965.

Akimoto, S., E. Komada, and I. Kushiro, Effect of pressure on the melting of olivine and spinel polymorphs of Fe_2SiO_4, J. Geophys. Res., 68, 679-686, 1967.

Akimoto, S., Y. Matsui, and Y. Syono, High pressure crystal chemistry in orthosilicates and formation of the mantle transition zone, in the Physics and Chemistry of Minerals and Rocks, edited by R. J. Strens, pp. 327-363, John Wiley, London, 1976.

Akimoto, S., and Y. Syono, High-pressure decomposition of the system $FeSiO_3$-$MgSiO_3$, Phys. Earth Planet. Inter., 3, 186-188, 1970.

Akimoto, S., T. Yagi, and K. Inoue, High temperature-high pressure phase boundaries in silicate systems using in-situ X-ray diffraction, in High-Pressure Research: Application to Geophysics, edited by M. H. Manghnani and S. Akimoto, pp. 585-602, Academic Press, New York, 1977.

Akimoto, S., T. Suzuki, T. Yagi, and O. Shimomura, Phase diagram of iron determined by high-pressure/temperature X-ray diffraction using synchrotron radiation, in High Pressure Research in Mineral Physics, pp. 149-154, edited by M. H. Manghnani and Y. Syono, Terra Publications, Tokyo, Japan, 1987.

Anderson, O. L., and K. Zou, Formulation of the thermodynamic functions for mantle minerals: MgO as an example, Phys. Chem. Minerals, in press, 1989.

Ashida, T., S. Kume, E. Ito, and A. Navrotsky, $MgSiO_3$ ilmenite: heat capacity, thermal expansivity, and enthalpy of tramsformation, Phys. Chem. Minerals, 16, 239-245, 1988.

Berman, R. G., and T. H. Brown, Heat capacity of minerals in the system Na_2O-K_2O-CaO-MgO-FeO-Fe_2O_3-Al_2O_3-SiO_2-TiO_2-H_2O-CO_2: representation, estimation and high temperature extrapolation, Contrib. Mineral. Petrol., 89, 168-183, 1985.

Berman, R. G., M. Engi, H. J. Greenwood, and T. H. Brown, Derivation of internally-consistent thermodynamic data by the technique of mathematical programming: a review with application to the system MgO-SiO_2-H_2O, J. Petrol., 27,1331-1364, 1986.

Bertrand, G. L., W. E. Acree Jr, T. Burchfield, Thermodynamical excess properties of multicomponent systems: representation and estimation from binary mixing data, J. Sol. Chem., 12, 327-340, 1983.

Bina, C. R., and B. J. Wood, The olivine-spinel transitions: experimental and thermodynamic constraints and implications for the nature of the 400 km seismic discontinuity, J. Geophys. Res., 92, 4853-4867, 1987.

Bjorkman, B., Quantitative equilibrium calculations on systems with relevance to copper melting and converting. Ph.D. Thesis, Univ. of Umea, Sweden, 1984.

Bohlen, S. R., and A. L. Boettcher, The quartz = coesite transformation: a precise determination and the effects of other components, J. Geophys. Res., 87, 7073-7078, 1982.

Bohlen, S. R., and A. L. Boettcher, Experimental investigations and geological applications of olivine-orthopyroxene geobarometry, Amer. Mineral., 66, 951-964, 1981.

Boyd, F. R., and J. L. England, Apparatus for phase-equilibrium measurements at pressures up to 50 kilobars and temperatures up to 1750 °C, J. Geophys. Res., 65, 741-748, 1960.

Boyd, F. R., and J. L. England, Effect of pressure on the melting of diopside,

$CaMgSi_2O_6$, and albite, $NaAlSi_3O_8$, in the range up to 50 kilobars, J. Geophys. Res., 68, 311-323, 1963.

Boyd, F. R., J. L. England, and B. T. C. Davis, Effect of pressure on the melting and polymorphism of enstatite, $MgSiO_3$, J. Geophys. Res., 69, 2101-2109, 1964.

Brousse, C., R. C. Newton, and O. J. Kleppa, Enthalpy of formation of forsterite, enstatite, akermanite, monticellite and merwinite at 1073 K determined by alkali boarate solution calorimetry, Geochim. Cosmochim. Acta, 48, 1081-1088, 1984.

Bundy, F. P., Pressure-temperature phase diagram of iron to 200 kbar, 900 °C, J. Appl. Phys., 36, 616-620, 1965.

Carmichael, R. S., Handbook of Physical Properties of Rocks, CRC Press, 1982.

Carmichael, I. S. E., J. Nicholls, F. J. Spera, B. J. Wood, and S. A. Nelson, High temperature properties of silicate liquids: application to the equilibration and ascent of basic magmas, Phil. Trans. R. Soc. London Ser. A, 286, 373-431, 1977.

Chatterjee, N., Evaluation of thermochemical data on Fe-Mg olivine, orthopyroxene, spinel and Ca-Fe-Mg-Al garnet, Geochim. Cosmochim. Acta, 51, 2515-2525, 1987.

Chen, C. -H., and D. C. Presnall, The system Mg_2SiO_4-SiO_2 at pressure up to 25 kilobars, Amer. Mineral., 60, 398-406, 1975.

Clark, S. P. Jr, Handbook of Physical Constants, Mem. Geol. Soc. Am., 97, 1966.

Davis, B. T. C., and J. L. England, The melting of forsterite up to 50 kbar, J. Geophys. Res., 69, 1113-1116, 1964.

Debye, P., Zur Theorie der spezifischen, Warmen. Ann. Phys., 39, 789-839, 1912.

Einstein, A., Die Plancksche Theorie der Strahlung und die Theotie der spezifischen, Warmen. Ann. Phys., 22, 180-190, 1907.

Eriksson, G., Thermodynamic studies of high temperature equilibria. XII.SOLGASMIX a computer program for calculation of equilibrium compositions in multiphase systems, Chem. Scr., 8, 100-103, 1975.

Eugster, H. P., and D. R. Wones, Stability reactions of ferruginous biotite, annite, J. Petrol., 3, 82-125, 1962.

Eriksson, G., and E. Rosen, Thermodynamic studies of high temperature equilibria. VIII. General equations for the calculation of equilibria in multiphase systems, Chemica Scripta 4, 193-194, 1973.

Fei, Y., and S. K. Saxena, A thermochemical data base for phase equilibria in the system Fe-Mg-Si-O at high pressure and temperature, Phys. Chem. Minerals, 13, 311-324, 1986.

Fei, Y., and S. K. Saxena, An equation for the heat capacity of solids, Geochim. Cosmochim. Acta, 51, 251-254, 1987.

Fei, Y., S. K. Saxena, and G. Ericksson, Some binary and ternary silicate solution models, Contrib. Mineral. Petrol., 94, 221-229, 1986.

Fei, Y., S. K. Saxena, and A. Navrotsky, Internally consistent thermodynamic data and equilibrium phase relations in the system MgO-SiO_2 at high pressure and high temperature, J. Geophys. Res., submitted, 1989.

Finger, L. W., and R. M. Hazen, Crystal structure and isothermal compression of Fe_2O_3, Cr_2O_3, and V_2O_3 to 50 kbars, J. Appl. Phys., 51, 5362-5366, 1980.

Finger, L. W., R. M. Hazen, and A. M. Hofmeister, High-pressure crystal chemistry of spinel ($MgAl_2O_4$) and magnetite (Fe_3O_4): comparisons with silicate spinels, Phys. Chem. Minerals, 13, 1986.

Fletcher, R., A new approach to variable metric algorithms, Comput. J., 13, 317-322, 1970.

Flory, P. J., Molecular configuration of polyelectrolytes, J. Chem. Phys., 21, 162-163, 1953.

Fukizawa, A., Direct determinations of phase eqilibria of geophysically important materials under high pressures and high temperature using in-situ X-ray diffraction method, Ph.D. Thesis, Univ. of Tokyo, Tokyo, 1982.

Furnish, M. D., and W. A. Bassett, Investigation of the mechanism of the olivine-spinel transition in fayalite by synchrotron radiation, J. Geophys. Res., 88, 10333-10341, 1983.

Ganguly, J., and S. K. Saxena, Mixing properties of aluminosilicate garnets: Constraints from natural and experimental data, and applications to geothermo-barometry, Am. Mineral., 69, 88-97, 1984.

Ghiorso, M. S., and I. S. E. Carmichael, A regular solution model for met-aluminous silicate liquids: applications to geothermometry, Immiscibility, and the source regions of basic magmas, Contrib. Mineral. Petrol., 71, 323-342, 1980.

Given, J. W., and D. V. Helmberger, Upper mantle structure of Northwestern Eurasia, J. Geophys. Res., 85, 7183-7194, 1980.

Goel, R. P., H. H. Kellogg, and J. Larrain, Mathematical description of the thermodynamic properties of the system iron-oxygen and iron-oxygen-silica. Metall. Trans. B., 11B, 107-117, 1980.

Grand, S. P., and D. V. Helmberger, Upper mantle shear structure of North America, Geophys. J. R. astr. Soc., 76, 399-438, 1984.

Guggenheim, E. A., Mixtures, Clarendon Press, Oxford, 365 pp., 1952.

Guillermet, A. F., and P. Gustafson, An assessment of the thermodynamic properties and the (p,T) phase diagram of iron, High Temperatures-High Pressures, 16, 591-610, 1985.

Guyot, F., M. Madon, J. Peyronneau, and J. P. Poirier, X-ray microanalysis of high-pressure/high-temperature phase synthesized from natural olivine in a diamond-anvil cell, Earth Planet. Sci. Lett., 90, 52-64, 1988.

Haas, J. L. Jr, and J. R. Fisher, Simultaneous evaluation and correlation of thermodynamic data, Am. J. Sci., 276, 525-545, 1976.

Halbach, H., and N. D. Chatterjee, The use of linear parametric programming for determination of internally consistent thermodynamic data for minerals, in High-Pressure Researches in Geoscience, edited by W. Schreyer, E. Schweizerbartsche Verlagsbuchhandlung, 475-491, 1982.

Haselton, H. T., Calorimetry of synthetic pyrope-grossular garnets and calculated stability relations, Ph.D. thesis, Univ. of Chicago, Chicago, 1979.

Hazen, R. M., and R. Jeanloz, Wustite ($Fe_{1-x}O$): A review of its defect structure and physical properties, Rev. Geophys. Space Phys., 22, 37-46, 1984.

Heinz, D. L., and R. Jeanloz, The equation of state of the gold calibration standard, J. Appl. Phys., 55(4), 885-893, 1984.

Hentschel, B., Stoichiometric FeO as metastable intermediate of the decomposition of wustite at 225 °C, Z. Naturforsch, A25, 1996-1997, 1970.

Holland, T. J. B., Thermodynamic analysis of simple minerals, in Thermodynamics of Minerals and Melts, edited by R. C. Newton, A. Navrotsky and B. J. Wood, pp. 19-34, Springer-Verlag, New York, 1981.

Huang. E., and W. A. Bassett, Rapid determination of Fe_3O_4 phase digram by synchrotron radiation, J. Geophy. Res., 91, 4697-4703, 1986.

Huang, E., W. A. Bassett, and P. Tao, Study of bcc-hcp iron phase transition by synchrotron radiation, in High Pressure Research in Mineral Physics, pp. 165-172, edited by M. H. Manghnani and Y. Syono, Terra Publications, Tokyo, Japan, 1987.

Inoue, K., Development of high temperature and high pressure x-ray diffraction apparatus with energy dispersive technique and its geophysical applications, Ph.D. thesis, Tokyo Univ., Tokyo, 1975.

Ito, E., Ultra-high pressure phase relations of the system MgO-FeO-SiO_2 and their geophysical implications, in Materials Science of the Earth's Interior, edited by I. Sunagawa, pp.387-394, Terra Publications, Tokyo, Japan, 1984.

Ito, E., and E. Takahashi, Post-spinel transformations in the system Mg_2SiO_4-Fe_2SiO_4 and some geophysical implications, J. Geophys. Res., in press, 1989.

Ito, E., E. Takahashi, and Y. Matsui, The mineralogy and chemistry of the lower mantle: an implication of the ultrahigh-pressure phase relations in the system MgO-FeO-SiO_2, Earth Planet. Sci. Lett., 67, 238-248, 1984.

Ito, E., and H. Yamada, Stability relations of silicate spinel ilmenites and perovskites, in High-Pressure Research in Geophysics. edited by S. Akimoto and M. H.

Manghnani, pp. 405-419, Cent. Acad. Pub. Japan, Japan, 1982.

Ito, H., K. Kawada, and S. Akimoto, Thermal expansion of stishovite, Phys. Earth Planet. Inter., 8, 277-281, 1974.

Ito, E., and Y. Matsui, Silicate ilmenite and the post-spinel transformations, in High-Pressure Research: Application to Geophysics, edited by M. H. Manghnani and S. Akimoto, pp. 193-208, Academic Press, New York, pp 193-208, 1977.

Ito, E., and A. Navrotsky, $MgSiO_3$ ilmenite: calorimetry, phase equilibria, and decomposition at room pressure, Amer. Mineral., 70, 1020-1026, 1985.

Jackson, I., and H. Niesler, The elasticity of periclase to 3 GPa and some geophysical implications, in High-Pressure Research in Geophysics, edited by S. Akimoto and M. H. Manghnani, pp. 93-113, Cent. Acad. Pub. Japan, Japan, 1982.

James, F., and M. Roos, MINUIT, Computer Physics Comm., 10, 343-367, 1975.

Jeanloz, R., and R. M. Hazen, Compression, nonstoichiometry and bulk viscosity of wustite, Nature, 304, 620-622, 1983.

Jeanloz, R., and E. Knittle, Reduction of mantle and core properties to a standard state by adiabatic decompression, in Chemistry and Physics of Terrestrial Planets, edited by S. K. Saxena, pp. 275-309, Springer-Verlag, New York, 1986.

Jeanloz, R., and A. B. Thompson, Phase transitions and mantle discontinuities, Rev. Geophys. Space Phys., 21, 51-74, 1983.

Kato, T., and M. Kumazawa, Melting curves of Mg_2SiO_4 and $MgSiO_3$ up to 9 GPa, in Program and Abstract, the High Pressure Conference of Japan, 198-199, 1983.

Kato, T., and M. Kumazawa, Garnet phase of $MgSiO_3$ filling the pyroxene-ilmenite gap at very high temperatures, Nature, 316, 803-804, 1985.

Kato, T., and M. Kumazawa, Melting and phase relations in the system Mg_2SiO_4-$MgSiO_3$ at 20 GPa under hydrous conditions, J. Geophys. Res., 91, 9351-9355, 1986.

Katsura, T., and E. Ito, The system Mg_2SiO_4-Fe_2SiO_4 at high pressures and temperatures: precise determination of stabilities of olivine, modified spinel and spinel, J. Geophy. Res., in press, 1989.

Kawada, K., System Mg_2SiO_4-Fe_2SiO_4 at high pressures and temperatures and the earth's interior, Ph.D. thesis, Univ. of Tokyo, Tokyo, 1977.

Kieffer, S. W., Thermodynamics and lattice vibrations of minerals: 1. Mineral heat capacities and Their relationships to simple lattice vibrational models, Rev. Geophys. Space Phys., 17, 1-19, 1979a.

Kieffer, S. W., Thermodynamics and lattice vibrations of minerals: 2. Vibrational characteristics of silicates, Rev. Geophys. Space Phys., 17, 20-34, 1979b.

Kieffer, S. W., Thermodynamics and lattice vibrations of minerals: 3. Lattice dynamics and approximation for minerals with application to simple substances and framework silicates, Rev. Geophys. Space Phys., 17, 35-59, 1979c.

Kieffer, S. W., Thermodynamics and lattice vibrations of minerals: 4. Application to chain and sheet silicates and orthosilicates, Rev. Geophys. Space Phys., 18, 862-886, 1980.

Kieffer, S. W., Thermodynamics and lattice vibrations of minerals: 5. Application to phase equilibria, Isotopic fractionation, and high-pressure thermodynamic properties, Rev. Geophys. Space Phys., 20, 827-849, 1982

Knittle, E., R. Jeanloz, and G. L. Smith, The thermal expansion of silicate perovskite and stratification of the earth's mantle, Nature, 319, 214-216, 1986.

Krupka, K. M., R. A. Robie, B. S. Hemingway, D. M. Kerrick, and J. Ito, Low-temperature heat capacities and derived thermodynamic properties of anthophyllite, diopside, enstatite, bronzite, and wollastonite, Amer. Mineral., 70, 249-260, 1985a.

Krupka, K. M., R. A. Robie, B. S. Hemingway, D. M. Kerrick, and J. Ito, High-temperature heat capacities and derived thermodynamic properties of anthophyllite, diopside, enstatite, bronzite, and wollastonite, Amer. Mineral., 70, 261-271, 1985b.

Kubaschewski, O., Iron-binary Phase Diagrams, pp. 185, Springer-Verlag, 1982.

Kudoh, Y., E. Ito, and H. Takeda, Effect of pressure on the crystal structure of perovskite-type $MgSiO_3$, Phys. Chem. Minerals, 14, 350-354, 1987.

Kushiro, I., Compositions of magmas formed by partial zone melting of the earth's upper mantle, J. Geophys. Res., 73, 619-634, 1968.

Kuskov, O. L., and O. B. Fabrichnaya, The SiO_2 polymorphs: The equations of state and thermodynamic properties of phase transformations, Phys. Chem. Minerals, 14, 58-66, 1987.

Lane, D. L., and J. Ganguly, Al_2O_3 solubility in orthopyroxene in the system MgO-Al_2O_3-SiO_2: a reevaluation, andmantle geotherm, J. Geophys. Res., 85, 6963-6972, 1980.

Lees, A. C., M. S. T. Bukowinski, and R. Jeanloz, Reflection properties of phase transition and compositional change models of the 670-km discontinuity, J. Geophys. Res., 88, 8145-8159, 1983.

Leitner, B. J., D. J. Weidner, and R. C. Liebermann, Elasticity of single-crystal pyrope and implication for garnet solid solution series, Phys. Earth Planet. Inter., 22, 111-121, 1980.

Levien, L., and C. T. Prewitt, High-pressure crystal structure and compressibility of coesite, Amer. Mineral., 66, 324-333, 1981.

Liebermann, R. C., H. Watanabe, T. Gasparik, C. T. Prewitt, and D. J.

Weidner, High pressure mineral synthesis in USSA-2000, EOS, 67, 361, 1986.

Lindsley, D. H., B. T. C. Davis, and I. D. MacGregor, Ferrosilite ($FeSiO_3$): synthesis at high pressures and temperatures, Science, 144, 73-74, 1964.

Liu, L. G., The system enstatite-pyrope at high pressures and temperatures and the earth's mantle, Earth Planet. Sci. Lett., 36, 237-245, 1977.

Liu, L. G., The equilibrium boundary of spinel = corundum + periclase: a calibration curve for pressure above 100 kbar, High Temperature-High Pressures, 12, 217-220, 1980.

McMillan, P. F., and N. L. Ross, Heat capacity calculations for Al_2O_3 corumdum and $MgSiO_3$ ilmenite, Phys. Chem. Minerals, 14, 225-234, 1987.

Maier, C. G., and K. K. Kelley, An equation for the representation of high temperature heat content data, Am. Chem. Soc. J., 54, 3242-3246, 1932.

Manghnani, M. H., L. C. Ming, J. Balogh, S. B. Qadri, E. F. Skelton, and D. Schiferl, Equation of state and phase transition studies under in situ high P-T conditions using synchrotron radiation, in Solid State Physics Under Pressure: Recent Advance with Anvil Devices, edited by S. Minomura, pp. 335-341, KTK Scientific Publishers, Tokyo, 1985.

Manghnani, M. H., L. C. Ming, and N. Nakagiri, Investigation of the α-Fe = ε-Fe phase transition by synchrotron radiation, in High Pressure Research in Mineral Physics, pp. 155-164, edited by M. H. Manghnani and Y. Syono, Terra Publications, Tokyo, Japan, 1987.

Mao, H. K., and P. M. Bell, Design and varieties of the megabar cell, Carnegie Inst. Washington Year Book, 77, 904-908, 1978.

Mao, H. K., and P. M. Bell, Disproportionation equilibrium in iron-bearing systems at pressures above 100 kbar with applications to chemistry of the earths mantle, in Energetics of Geological Processes, edited by S.K. Saxena and S. Bhattacharji, pp 236-249, Springer-Verlag, 1977.

Mao, H. K., P. M. Bell, and C. Hadidiacos, Experimental phase relations of iron to 360 kbar, 1400 °C, determined in an internally heated diamond-anvil apparatus, in High Pressure Research in Mineral Physics, pp. 135-140, edited by M. H. Manghnani and Y. Syono, Terra Publications, Tokyo, Japan, 1987.

Mao, H. K., Y. Fei, and T. Gasparik, Multi-cell sample chamber in multi-anvil apparatus - a tool for high-resolution and high-efficiency experimental studies, EOS, 70, 471, 1989.

Mao, H. K., T. Takahashi, W. A. Bassett, G. L. Kinsland, and L. Merrill, Isothermal compression of magnetite to 320 kbar and pressure-induced phase transformation, J. Geophys. Res., 79, 1165-1170, 1974.

Marumo, F., M. Isobe, and S. Akimoto, Electron density distributions in crystals for γ-Fe_2SiO_4 and γ-Co_2SiO_4, Acta Crystallography Sect., B33, 713-716, 1977.

Matsui, Y., and O. Nishizawa, Iron (II)-magnesium exchange equilibrium between olivine and calcium-free pyroxene over a temperature range 800 to 1300 °C. Bull. Soc. fr. Mineral. Crystallogr., 97, 122-130, 1974.

Nafziger, R. H., and A. Muan, Equilibrium phase compositions and thermodynamic properties of olivines and pyroxenes in the system MgO-"FeO"-SiO_2, Amer. Mineral., 52, 1364-1385, 1967.

Navrotsky, A., High pressure transitions in silicates and related compounds. Progress in Solid State Chemistry, 17, 53-86, 1987.

Navrotsky, A., Thermochemistry of perovskites, in Perovskite, A Structure of Great Interest to Geophysics and Materials Science, edited by A. Navrotsky and D. J. Weidner, Amer. Geophys. Union, Washington D. C., 1989.

Navrotsky, A., F. S. Pintchovski, and S. Akimoto, Calorimetric study of the stability of high pressure phase in the system CoO-SiO_2 and "FeO"-SiO_2 and calculation of phase diagrams in MO-SiO_2 systems, Phys. Earth Planet. Inter., 19, 275-292, 1979.

Navrotsky, A., D. Ziegler, R. Oestrike, and P. Maniar, Calorimetry of silicate melts at 1773 K: measurement of enthalpies of fusion and of mixing in the systems diopside-anorthite-albite and anorthite-forsterite, Contrib. Mineral. Petrol., 101, 122-130, 1988.

Ohtani, E., Melting relation of Fe_2SiO_4 up to 200 kbar, J. Phys. Earth, 27, 189-208, 1979.

Ohtani, E., and M. Kumazawa, Melting of forsterite Mg_2SiO_4 up to 15 GPa, Phys. Earth Planet. Inter., 27, 32-38, 1981.

Remsberg, A. R., J. N. Boland, T. Gasparik, and R. C. Liebermann, Mechanism of the olivine-spinel transformation in Co_2SiO_4, Phys. Chem. Minerals, 15, 498-506, 1988.

Renon, H., and J. M. Prausnitz, Local compositions in thermodynamic excess functions for liquid mixtures, Am. Inst. Chem. Eng. J., 14, 135-144, 1968.

Ringwood, A. E., The proxene-garnet transition in the earth's mantle, Earth Planet. Sci. Lett., 3, 255-263, 1967.

Ringwood, A. E., Composition and Petrology of the Earth's Mantle, 618pp., McGraw-Hill, New York, 1975.

Ringwood, A. E., and A. Major, The system Mg_2SiO_4-Fe_2SiO_4 at pressures and temperatures, Phys. Earth Planet. Inter., 3, 89-108, 1970.

Robie, R. A., B. S. Hemingway, and H. Takei, Heat capacities and entropies of Mg_2SiO_4, Mn_2SiO_4 and Co_2SiO_4 between 5 and 380 K, Amer. Mineral., 67, 470-482, 1982.

Robie, R. A., B. S. Hemingway, and J. R. Fisher, Thermodynamic properties of minerals and related substances at 298.15 K and 1 bar (105 pascals) pressure and at higher temperatures, U.S. Geol. Survey Bull., 1452, 1978.

Rosenhauer, M., H. K. Mao, and E. Woermann, Compressibility of $(Fe_{0.4}Mg_{0.6})O$ magnesiowustite to 264 kbar, Carnegie Inst. Washington, Year Book 75, 513-515, 1976.

Sato, Y., Equation of state of mantle minerals determined through high-pressure x-ray study, in High-pressure Research: Applications in Geophysics, edited by M. H. Manghnani and S. Akimoto, pp. 307-323. Academic Pess, New York, 1977.

Sato, Y., and S. Akimoto, Hydrostatic compression of four corundum-type compounds: α-Al_2O_3, V_2O_3, Cr_2O_3, and α-Fe_2O_3, J. Appl. Phys., 50, 5285-5291, 1979.

Sawamoto, H., Phase equilibrium of $MgSiO_3$ under high pressures and high temperatures: garnet-perovskite transformation (abstract), U.S.-Japan Seminar, High-Pressure Research: Application in Geophysics and Geochemistry, Honolulu, Hawaii, pp. 50-51, 1986a.

Sawamoto, H., Single crystal growth of the modified spinel (β) and spinel (γ) phases of $(Mg,Fe)_2SiO_4$ and some geophysical implications, Phys. Chem. Minerals, 13, 1-10, 1986b.

Sawamoto, H., Phase diagram of $MgSiO_3$ at pressures up to 24 GPa and temperatures up to 2200 K: phase stability and properties of tetragonal garnet, in High-Pressure Research in Mineral Physics, edited by M. H. Manghnani and Y. Syono, pp. 209-219, Terra Publications, Tokyo, Japan, 1987.

Sawamoto, H., D. J. Weidner, S. Sasaki, and M. Kumazawa, Single-crystal elastic properties of the modified spinel (beta) phase of Mg_2SiO_4, Science, 224, 749-751, 1984.

Saxena, S. K., Thermodynamics of Rock-forming Crystalline Solutions, Springer-Verlag, Heidelberg, 189 pp., 1973.

Saxena, S. K., Assessment of bulk modulus, thermal expansion and heat capacity of minerals, Geochim. Cosmochim. Acta, 53, in press, 1989.

Saxena, S. K., and N. Chatterjee, Thermochemical data on mineral phases: The system CaO-MgO-Al_2O_3-SiO_2, J. Petrol., 27, 827-842, 1986.

Saxena, S. K., and G. Eriksson, Anhydrous phase equilibria in Earth's upper mantle, J. Petrol., 26, 378-390, 1985.

Simons, B., Composition-lattice parameter relationship of the magnesiowustite solid solution series. Carnegie Inst. of Washington, Yearbook 79, 376-380, 1980.

Skinner, B. J., Thermal expansion of ten minerals, U.S. Geol. Surv. Prof. Paper, 450D, 109-112, 1962.

Skinner, B. J., Thermal expansion, in Handbook of Physical Constants, edited by S. P. Clark, Jr., pp. 75-95, Geol. Soc. Amer. Mem., 1966.

Smith, W. R., and R. W. Missen, Chemical Reaction Equilibrium Analysis, Wiley-Interscience, New York, pp. 365, 1982.

Soga, N., The temperature and pressure deriveratives of isotropic sound velocities of a-quartz, J. Geophys. Res., 73, 827-829, 1968.

Stacey, F. D., Physics of The Earth, Wiley, New York, 1977.

Strong, H. M., R. E. Tuft, and R. E. Hanneman, The iron fusion curve and a-g-e triple point, Met. Trans., 4, 2657-2661, 1973.

Suito, K., Phase transitions of pure Mg_2SiO_4 into a spinel structure under high pressures and temperatures, J. Phys. Earth, 20, 225-243, 1972.

Suito, K., Phase relations of pure Mg_2SiO_4 up to 200 kilobars, in High-Pressure Research: Application to Geophysics, edited by M. H. Manghnani and S. Akimoto, pp. 365-371, Academic Press, New York, 1977.

Sumino, Y., The elastic constants of Mn_2SiO_4, Fe_2SiO_4 and Co_2SiO_4 and the elastic properties of olivine group minerals at high temperature, J. Phys. Earth 27, 209-238, 1979.

Sumino, Y., O. Nishizawa, T. Goto, I. Ohno, and M. Ozima, Temperature variation of elastic constants of single-crystal forsterite between 190 and 400 K, J. Phys. Earth, 28, 273-280, 1977.

Sumino, Y., O. L. Anderson, and I. Suzuki, Temperature coefficients of elastic constants of single-crystal MgO between 80 and 1300 K, Phys. Chem. Minerals, 9, 38-42, 1983.

Sung, C. M., and R. G. Burns, Kinetics of high-pressure phase transformations: implications to the evolution of the olivine-spinel transition in the downgoing lithosphere and its consequences on the dynamics of the mantle,mTectonophysics, 31, 1-32, 1976.

Suzuki, I., Thermal expansion of periclase and olivine and their anharmonic properties, J. Phys. Earth, 23, 145-159, 1975.

Suzuki, I., E. Ohtani, and M. Kumazawa, Thermal expansion of γ-Mg_2SiO_4, J. Phys. Earth, 27, 53-61, 1979.

Suzuki, I., E. Ohtani, and M. Kumazawa, Thermal expansion of modified spinel, β-Mg_2SiO_4, J. Phys. Earth, 28, 273-280, 1980.

Suzuki, I., K. Seya, H. Takei, and Y. Sumino, Thermal expansion of fayalite, Fe_2SiO_4, Phys. Chem. Minerals, 7, 60-63, 1981.

Syono, Y., S. Akimoto, and Y. Matsui, High pressure transformations in zinc silicates, J. Solid State Chem., 3, 369-380, 1971.

Thompson, J. B. Jr, and D. R. Waldbaum, Mixing properties of sanidine crystalline solutions. III Calculation based on two-phase data, Am. Mineral., 54, 811-838, 1969.

Tomlinson, J. W., M. S. R. Heynes, and J. O. M. Bockris, The structure of liquid silicates, part 2, molar volumes and expansivities, Trans. Faraday Soc., 54, 1822-1833, 1958.

Ulmer, G. C., Research Techniques for High Pressure and High Temperature, Springer Verlag, 1971.

Watanabe, H., Thermochemical properties of synthetic high-pressure compounds relevant to the earths mantle, in High-Pressure Research in Geophysics, edited by S. Akimoto and M. H. Manghnani, pp. 411-464, Cent. Acad. Pub. Janpan, Japan, 1982. Springer-Verlag, New York, 1986.

Weaver, J. S., D. W. Chipman, and T. Takahashi, Comparison between thermochemical and phase stability data for the quartz-coesite-stishovite transformations, Amer. Mineral., 64, 604-614, 1979.

Weidner, D. J., and H. R. Carleton, Elasticity of coedite, J. Geophys. Res., 82, 1334-1346, 1977.

Weidner, D. J., H. Wang, and J. Ito, Elasticity of orthoenstatite, Phys. Earth Planet. Inter., 17, 7, 1978.

Weidner, D. J., J. D. Bass, A. E. Ringwood, and W. Sinclair, The single-crystal elastic moduli of stishovite, J. Geophys. Res., 87, 4740-4746, 1982.

Weidner, D. J., H. Sawamoto, S. Sasaki, and M. Kumazawa, Single-crystal elastic properties of the spinel phase of Mg_2SiO_4, J. Geophys. Res., 89, 7852-7860, 1984.

Weidner, D. J., and E. Ito, Elasticity of $MgSiO_3$ in the ilmenite phase, Phys. Earth Planet. Inter., 40, 65-70, 1985.

Wiggins, R. A., and D. V. Helmberger, Upper mantle structure of the western United States, J. Geophys. Res., 78, 1870, 1973.

Wilburn, D. R., W. A. Bassett, Y. Sato, and S. Akimoto, X-ray diffraction compression studies of hematite under hydrostatic, isothermal conditions, J. Geophys. Res., 83, 3509-3512, 1978.

Williams, Q., R. Jeanloz, and P. McMillan, Vibrational spectrum if $MgSiO_3$ perovskite: Zero-pressure Raman and mid-infrared spectra to 27 GPa, J. Geophys. Res., 92, 8116-8128, 1987.

Williams, Q., E. Knittle, and R. Jeanloz, Geophysical and crystal chemical significance of $(Mg,Fe)SiO_3$ perovskite, in Perovskite, A Structure of Great Interest to Geophysics and Materials Science, edited by A. Navrotsky and D. J. Weidner, Amer. Geophys. Union, Washington D.C., 1989.

Wilson, G. M., A new expression for the excess free energy of mixing, J. Am. Chem. Soc., 86, 127-130, 1964.

Wolf, G. H., and M. S.T. Bukowinski, Theoretical study of the structural

properties and equations of state of $MgSiO_3$ and $CaSiO_3$ perovskites: implications for lower mantle composition, in High-Pressure Research in Mineral Physics, edited by M. H. Manghnani and Y. Syono, pp. 313-331, Terra Publications, Tokyo, Japan, 1987.

Wood, B. J., and O. J. Kleppa, Thermochemistry of forsterite-fayalite olivine solutions. Geochim. Cosmochim. Acta, 45, 529-534, 1981.

Yagi, T., M. Akaogi, O. Shimomura, T. Suzuki, and S. Akimoto, In situ observation of the olivine-spinel phase transformation in Fe_2SiO_4 using synchrotron radiation, J. Geophy. Res., 92, 6207-6213, 1987.

Yagi, T., and S. Akimoto, Direct determination of coesite-stishovite transition by in-situ X-ray measuremnets, Tectonophys, 35, 259-270, 1976.

Yagi, T., P. M. Bell, and H. K. Mao, Phase relations in the system MgO-FeO-SiO_2 between 150 and 700 kbar at 1000 °C, Carnegi Inst. of Washington Year Book, 78, 614-618, 1979.

Yagi, T., H. K. Mao, and P. M. Bell, Structure and crystal chemistry of perovskite-type $MgSiO_3$, Phys. Chem. Minerals, 3, 97-110, 1978.

Yagi, T., H. K. Mao, and P. M. Bell, Hydrostatic compression of perovskite type $MgSiO_3$, in Advances in Physical Geochemistry, vol 2, edited by S. K. Saxena, pp. 317-326, Springer-Verlag, New York, 1982.

Yeganeh-Haeri, A., D. J. Weidner, and E. Ito, Single crystal elastic moduli of magnesium metasilicate perovskite, in Perovskite, A Structure of Great Interest to Geophysics and Materials Science, edited by A. Navrotsky and D. J. Weidner, Amer. Geophys. Union, Washington D.C., 1989.